

Alignment, Characterization and Application of Polyfluorene in Polarized Light-Emitting Devices

Dissertation
zur Erlangung des Doktorgrades
der Naturwissenschaften
(Dr. phil. nat.)

angefertigt am
Max Planck-Institut für Polymerforschung
in Mainz

vorgelegt beim Fachbereich Physik
der Johann Wolfgang Goethe-Universität
in Frankfurt am Main

von
Andreas Meisel
aus Karlsruhe

Frankfurt 2001

Alignment, Characterization and Application of Polyfluorene in Polarized Light-Emitting Devices

A thesis performed at the
Max Planck-Institute for Polymer Research in Mainz
presented by

Andreas Meisel

born in Karlsruhe

In partial fulfillment of the
requirement of the degree of
Doctor of natural sciences
(Dr. phil. nat.)
in
Solid State Physics

Submitted to the
Department of Physics
of the
University of Frankfurt/M.
2001

As thesis accepted
by the Department of Physics
of the
University of Frankfurt/M.

Dean: Prof. Dr. Werner Mäntele

Referees: Prof. Dr. Dieter Neher

Prof. Dr. Hartmut Roskos

Day of Defense: June 22, 2001

Contents

1	General Introduction	9
2	Theory	12
2.1	Electroluminescence from Conjugated Polymers	12
2.1.1	The Basic Processes in Single-Layer OLEDs	15
2.1.2	Efficiency of OLEDs	19
2.1.3	Multilayer Devices	20
2.1.4	Emission Color	21
2.1.5	Polarized Electroluminescence	22
2.2	Polymer Alignment	24
2.2.1	Quantitative Description of Molecular Orientation – Order Parameter, Polarization Ratio and Dichroic Ratio	24
2.2.2	Mechanical Alignment – Stretching and Rubbing of the Emissive Layer	25
2.2.3	Langmuir-Blodgett Deposition	26
2.2.4	Alignment on Particular Substrates	27
2.2.5	Liquid-Crystalline Polymers on top of Alignment Layers	27
3	Materials and Methods	35
3.1	Materials	35
3.1.1	Polyfluorene (PF) – Emission	35
3.1.2	Copoly(phenyleneethynylene) – Emission	43
3.1.3	Poly(phenoxyphenylimide) (PI) – Alignment	43
3.1.4	Dopants for Polyimide – Hole Transport	44
3.1.5	Dopants for the Emissive Material – Color, Efficiency and Stability	47
3.1.6	Poly(3,4-ethylenedioxythiophene) doped with Poly(styrene sulfonate) (PEDOT-PSS) – Hole Injection	47
3.2	Preparation of Isotropic LEDs	48
3.3	Preparation of Polarized LEDs	49
3.3.1	Rubbing Procedure	49
3.3.2	Annealing Setup and Procedure	50
3.4	Investigation of Optical and Electrical Properties of Materials	52
3.4.1	Recording of Electroluminescence Spectra	52
3.4.2	Determination of the Degree of Anisotropy – Polarized UV/Vis, Polarized PL, Polarized EL	53
3.4.3	Luminance and Color Coordinates	54
3.4.4	Film thickness determination	54
3.4.5	Current–Voltage and Intensity–Voltage Characteristics	54

3.5	Structure Investigations	55
3.5.1	Polarized Optical Microscopy	55
3.5.2	Low-Voltage Scanning Electron Microscopy (LVSEM)	55
3.5.3	Transmission Electron Microscopy (TEM) and Electron Diffraction	56
3.5.4	Atomic Force Microscopy (AFM)	57
3.5.5	X-Ray Diffraction	57
4	Alignment of Polymers for the Use in Polarized LEDs	58
4.1	Polyfluorene	58
4.1.1	Alignment by means of Rubbed Hole-Transporting Alignment Layers	58
4.1.2	Investigation of Alternative Alignment Concepts	60
4.1.3	Optimization of the Nature of Side-Chains	62
4.2	Alignment of Poly(phenyleneethynylene)	66
5	Morphology, Structure and Properties of Polyfluorene and Alignment Layers ...	69
5.1	Polyfluorene	69
5.1.1	Alignment Behavior of Polyfluorene	69
5.1.2	Morphology and Structure of Aligned Polyfluorene	74
5.2	Alignment Layers	84
5.2.1	Basic Effects of Doping of Alignment Layers	84
5.2.2	Variation of Hole-Transporting Materials	87
5.2.3	Influence of Doping on the Alignment and on Electroluminescence	94
5.2.4	Influence of Doping on the Morphology of Hole-Transporting Alignment Layers	95
5.2.5	Other Factors Influencing the Alignment	107
6	Electroluminescence from Polyfluorene	110
6.1	(Undoped) Polyfluorene	110
6.1.1	Optimization of the Device Architecture in Isotropic LEDs	110
6.1.2	Polarized Electroluminescence from Undoped Polyfluorene	115
6.1.3	Problems with the Use of Undoped Polyfluorene	117
6.2	Endcapped Polyfluorene	119
6.2.1	Isotropic Electroluminescence from Endcapped Polyfluorene	119
6.2.2	Polarized LEDs from Endcapped Polyfluorene	125
7	Doping of Charge-Trapping Dyes into Polyfluorene	127
7.1	Green Emissive Thiophene Dyes	127
7.1.1	Isotropic Electroluminescence	127
7.1.2	Polarized Electroluminescence	129
7.2	Red Light-Emitting Diodes Based on Dendronized Perylenes	134

7.2.1 Dendrimers and Electroluminescence	134
7.2.2 LEDs with Model Compound and Dendrimers as Active Layer	137
7.2.3 Doping of M, G1, and G2 into Polyfluorene	138
8 Summary	150
A Appendix	154
A.1 Luminous Intensity and Luminance of OLEDs	154
A.2 Chromaticity	157
A.3 Properties of Polyfluorenes with Different Side-Chain Patterns	159
Zusammenfassung	160
Abbreviations	165
Bibliography	168
List of Figures	176
List of Tables	179
List of Publications	180
List of Patents	181
Danke Schön	183
Curriculum Vitae	185

1 General Introduction

Plastics are used in almost every aspect of daily life because they provide excellent mechanical properties while being cheap to produce and easy to process. One of the characteristic features we commonly have in mind when we think of organics in materials science is, apart from flexibility and strength, their insulating nature. We make use of these material goods in applications like insulation around wires. However, there is a special class of organic materials with conjugated bonds found in the backbone that in fact display semiconducting behavior and allow for transport of charges. Moreover, in the early 1960s it was found that particular organic materials are electroluminescent under certain conditions,¹ meaning that they emit light when bipolar current is flowing. To realize this, a film of the semiconducting material is sandwiched between two electrodes. Electrons and holes are injected from the electrodes, and recombination of these charge carriers can lead to luminescence. Yet, at that time, the required voltages were in the order of 1000 V and therefore, organic semiconductors were not of great interest for applied science. This changed in the late 1980s with the capability to produce thin films with a thickness of a few hundred nanometers.

When efficient electroluminescence from small molecular organic materials was demonstrated for the first time in 1987, organics started emerging as realistic candidates for display applications.² Their fast response and high brightness was now accessible at low operating voltages. The discovery of electroluminescence from conjugated *polymers* in 1990³ finally enabled the production of displays using simple coating techniques instead of expensive and inconvenient vapor deposition of inorganic materials or of small molecule organics. Polymers are processable by the technique of spincoating – putting a droplet of polymer solution in the middle of a spinning substrate. This means that fabricating a simple light-emitting diode (LED) is accomplished simply by enclosing the resulting thin polymer film between two electrodes, one of which is transparent. A schematic picture of such a device is shown in the figure below.

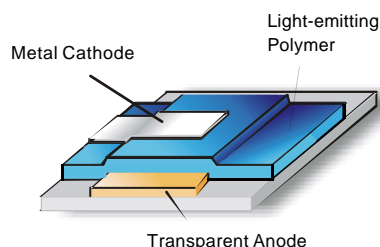


Figure 1.1. Schematic picture of a very simple LED with a polymer layer sandwiched between two electrodes.

Apart from the relative straightforwardness of fabrication, polymers offer additional advantages. They enable the homogeneous illumination of large areas, and displays can be made

as thin as one millimeter. A complete new world of applications is opened, as lightweight displays may be produced on a wide variety of flexible substrates ranging from optically-clear plastic films to reflective metal foils. This provides the ability to conform, bend or roll a display into any shape.

One of the key advantages of polymer semiconductors over their conventional solid-state inorganic counterparts is the tunability of the emissive color by structural modifications. This is very important with regards to the fabrication of full color red-green-blue (RGB) displays. Meanwhile, all colors are available from polymers, and RGB-displays with small pixel size can be realized by the use of inkjet printing technology. Furthermore, bandgap and color tuning of organic materials can be achieved not only by chemical modifications, but also by a further method. Blue light can be down-converted into green and red emission by simply doping the blue emitter with lower bandgap fluorescent dyes. For that reason, developing an efficient and stable blue polymer LED is of foremost interest.

Another attractive property of organics is the possibility for the development of order at the molecular level. This ability of organics to self-organize is very useful in the field of polarized electroluminescence. Polarized light-sources on the basis of highly ordered polymers have tremendous potential as backlight in liquid crystal displays (LCDs). They could replace the common isotropic fluorescent bulbs, which require additional sheet polarizers associated with cost, weight, and power-consuming absorptive losses.

As a result of these considerations, the central objective of this work was the realization of efficient blue electroluminescence showing a high degree of polarization. The emissive material polyfluorene was chosen, because it is among the most promising candidates for efficient blue luminescence, and several groups have demonstrated bright blue emission from polyfluorenes. A second important property of polyfluorenes is their thermotropic liquid crystallinity. It has recently been shown that polyfluorenes can be aligned in the liquid crystalline state on top of a rubbed polyimide alignment layer. As a novel concept of this work, the non-conducting polyimide was modified for hole conduction by the addition of suitable hole-transporting moieties, enabling the incorporation of such adapted alignment layers into light-emitting devices. The architecture of such a polarized LED is shown in Figure 1.2.

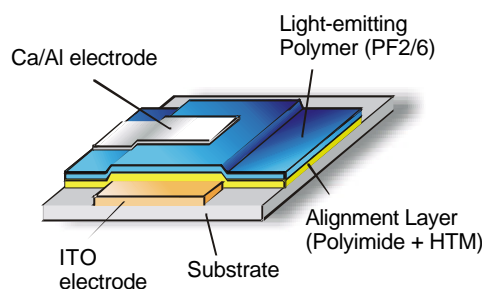


Figure 1.2. Schematic picture of a polarized LED. The emissive polymer layer is oriented on top of a rubbed hole-transporting alignment layer of polyimide, which is doped with suitable hole-transporting moieties.

Based on this approach, the essential goal of this thesis was the optimization both of the polyfluorene emissive layers and of the hole-transporting alignment layers with regards to the attainable degrees of orientation. This required the determination of the factors influencing the orientational abilities of the polymers. In this connection, polyfluorenes with various side-chain patterns were examined. To further extend the studies, the alignment properties of an alternative liquid crystalline blue-emitting material, polyphenyleneethynylene, were investigated.

To find explanations for the observed differences in the degrees of orientation, structural investigations were carried out on well-aligned layers by means of optical and electron microscopy and by electron- and X-ray diffraction. Special attention was paid to the hole-transporting alignment layers of polyimide doped with hole-transporting moieties. Layers with different concentrations of the dopant were investigated by means of AFM and SEM techniques in order to elucidate the influence of dopant concentration on the layer morphology.

The final objective of the work was the application of the acquired knowledge for the fabrication of devices with efficient, highly-polarized electroluminescence. In the course of this work, the polyfluorene layer was doped with green- and red-emitting fluorescent dyes, with the aim to optimize the efficiency, to accomplish color tuning and finally to understand the mechanisms leading to an emission contribution of guest molecules doped into a host matrix.

2 Theory

2.1 Electroluminescence from Conjugated Polymers

Absorption of energy by atoms, molecules or condensed matter can result in the emission of light. If the absorbed energy leads to the generation of excited states, i.e. if it increases the potential energy of the substance rather than its heat – as is the case for the thermal generation of light by heat radiation (incandescence) – the subsequent emission is called *luminescence*. Luminescence is observed from many inorganic and organic substances, the luminophores, and can be induced by various physical processes.

In general, excitation (1) by absorbed energy is comprised of transitions $S_{0,n} - S_{n,n'}$ followed by radiativeless transitions (2) to vibrational states of the first excited singlet state $S_{1,n'}$ and *internal conversion* (3) to the lowest level $S_{1,0}$ (the numbers in brackets correspond to the numbers in Figure 2.1). The radiative transition (4) $S_{1,0} - S_{0,n}$ from the lowest excited to the lowest ground state is denoted as *fluorescence*. This radiative transition competes with *intersystem crossing*, a non-radiative transition (5) from $S_{1,0}$ to triplet states with similar energy, followed by transitions (6) to the metastable lowest triplet state $T_{0,0}$ *. Intersystem crossing involves a change of spin states from $S = 0$ for the singlet state to $S = 1$ for the triplet. There are three different ways for de-excitation of the triplet state, the first of which is a non-radiative transition (7) to a level $S_{0,n}$ and subsequent distribution of the vibrational energy (8). The second – radiative – path is *phosphorescence*, the transition (9) to $S_{0,0}$, with a very low transient probability since the transition $T_0 \rightarrow S_0$ is forbidden in the electric-dipole approximation. The last possibility for de-excitation of the triplet state is the transition (10 + 11) from $T_{0,0}$ to the $S_{1,\sigma}$ -state by means of thermal energy, which is only possible if the energy difference between the two states is not more than some kT . In case of high excitation densities, a bimolecular interaction of two molecules in triplet state T_0 may also yield an electron in the S_1 state (*triplet-triplet-annihilation*).⁷

* Another route for de-excitation of the excited singlet state is the non-radiative inter- and intramolecular electronic excitation energy transfer via either Coulomb interaction (Förster transfer; section 7.2.3.1)⁴ or via electron exchange (Dexter transfer;⁵ this interaction is of very short range, since it requires the spatial overlap of donor and acceptor orbitals) between donor and acceptor molecules.⁶

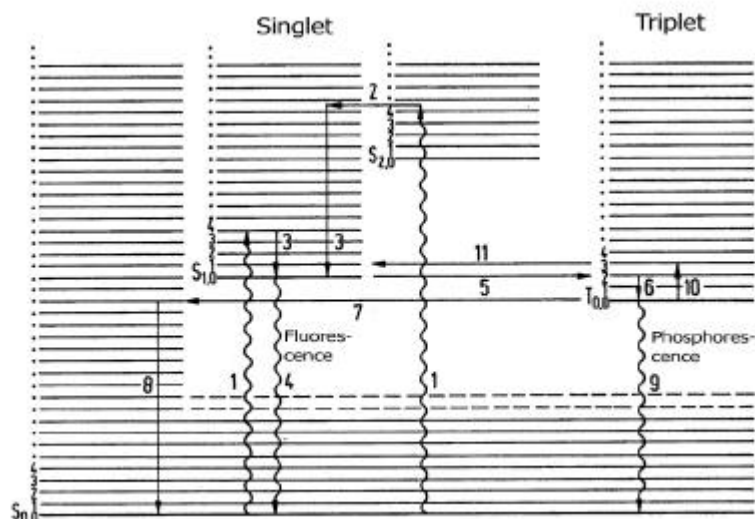


Figure 2.1. Typical energy level diagram of organic molecules. The description of the processes of excitation and de-excitation is given in the text. Taken from Bergmann-Schaefer.⁷

Depending on the way the excited state was generated, the fluorescent emission is called photoluminescence (*optical* absorption of photons), electroluminescence (*electrical* excitation resulting from the application of an electric field), chemiluminescence (due to chemical reactions), bioluminescence (owing to chemical reactions in living species), etc.⁷ The process responsible for *electroluminescence* requires (i) the injection of electrons from one electrode and of holes from the other into an inorganic or organic semiconductor, followed by (ii) the transport of electrons and holes as negative and positive *polarons*,* respectively, through the material. Besides, (iii) the capture of these oppositely charged carriers (*recombination*) and (iv) the radiative decay of the excited electron-hole state (*exciton*) which is generated by the recombination process are necessary for electroluminescence. In inorganic light-emitting diodes (LEDs) rectification and light emission are due to an electrical junction of two oppositely doped regions (*p* and *n* type) of the semiconductor. On the contrary, in organic LEDs (OLEDs) an undoped insulating organic layer is sandwiched between two metal electrodes and rectification and light emission are due to the asymmetrical nature of these electrodes. One metal has a high work-function and consistently injects holes more efficiently than electrons into the organic material – it serves as the anode –, whereas the other, low work-function metal injects only electrons into the organic layer and works as cathode.

Electroluminescence from organic crystals was first observed for anthracene in 1963,¹ but due to poor performance of the device, research was concentrated on inorganic LEDs for a long time. In 1987, Tang and VanSlyke² fabricated an OLED, using 8-hydroxyquinoline (Alq_3) as the

* Note that adding an electronic charge to an undoped polymer creates a lattice deformation. The charge and the accompanying deformation is called a polaron, and the electron polarons and hole polarons are often referred to as electrons and holes.

emissive layer, which emitted green light with reasonable performance. In 1990, the first EL from conjugated polymers was reported by Friend *et al.*³ who achieved green electroluminescence from poly(*p*-phenylene vinylene) (PPV). This opened the way towards the production of displays using simple coating techniques rather than the expensive and inconvenient vapor deposition of inorganic materials or of small molecule organics. Other advantages, apart from the ease of fabrication are that organics offer the possibility of the construction of flexible displays which could be used for such devices as roll-up screens in the future. Furthermore, they enable the homogeneous illumination of large areas, and, most importantly, the tunability of the emissive color by structural modifications. Even blue and white LEDs with high brightness and efficiency have successfully been fabricated, which is difficult and expensive to achieve by the use of inorganics, because semiconductors with large band gaps are required. Blue light is of great interest for application, since it can be converted to green or red with proper dyes (section 2.1.4).

The organic materials fulfilling the requirements for electroluminescence – the capability to accept and transport charges and to fluoresce efficiently – can be classified into (i) low-molecular weight materials, (ii) conjugated oligomers with defined chain length, and (iii) conjugated polymers. The physical mechanisms being responsible for the electroluminescence are essentially the same for all these classes of materials, while the method of film deposition substantially differs. Small molecules must be evaporated under vacuum, while the big advantage of polymers is their easy processability by the technique of spincoating. Although polymers are more prone to defects due to their higher disorder in the arrangement of the molecules, efficiency and lifetimes have been substantially enhanced during the last years, gradually approaching the values known from small molecules. Here, only the class of conjugated polymers will be discussed. An excellent review of organic electroluminescent materials in general can be found in Mitschke *et al.*⁸

Conjugated polymers are organic semiconductors characterized by a regular alternation of single and double carbon-carbon bonds in the polymer backbone, the latter giving rise to delocalized *p*-molecular orbitals along the polymeric chain. Due to the orbital overlap, the *p*-electrons are delocalized within a molecule, i.e. they can be thought of a cloud that extends along the entire conjugated chain. In this cloud the electrons are free to move along the molecule. Therefore, even though the charge density in pure undoped organics is very low, injected electrons and holes can be well transported through the conjugated material. To enable operation at low voltages, the devices must be very thin, typically in the range between 100 and

300 nm. The wavelength of the emitted light depends primarily* on the energy gap between the highest occupied molecular orbital (HOMO) and the lowest unoccupied molecular orbital (LUMO), corresponding to the valence band and conduction band of the semiconductor. For conjugated polymers, this energy gap is between 2–4 eV, so that transition frequencies can be in the visible region. As a result of the low electronic coupling between the molecules, the carriers are strongly localized on a molecule. Both charged and neutral excitations are mobile, allowing for both charge and energy transport.

The polymer chains are not conjugated along the whole chain, but instead they consist of conjugated segments only, since twists and bends in the polymer chain disrupt the p -bonds between different segments of the same polymer chain. The mean length of these conjugated segments is designated as the *conjugation length* of the polymer. The electronic structure of the polymer film is described by a distribution of electronic states which is produced by the distribution of conjugated lengths and is additionally broadened by disorder in the local arrangement of the polymer chains.

2.1.1 The Basic Processes in Single-Layer OLEDs

The basic physical processes in OLEDs are (i) the injection of charge carriers from the electrodes, (ii) the charge transport through the organic layer under an applied electric field, (iii) the formation, and (iv) the decay of excitons within the active layer.

Generally, if an external voltage is applied to the electrodes, electrons and holes are injected into the polymer. In the presence of an electric field the electrons and holes move through the active layer towards the oppositely charged electrode, approaching each other. Upon meeting, they form neutral excited states, called *excitons*, and are bound to their oppositely charged partner by a binding energy in the range of a few tenths of an electron volt for conjugated polymers.⁹ The spin wavefunction of excitons is either a singlet ($S = 0$) or triplet ($S = 1$), and as discussed in the previous section, typically only the singlet state may relax radiatively by fluorescence. However, the radiative decay from triplet excited states has been demonstrated both for molecular and for polymeric conjugated host systems doped with a phosphorescent dye^{10,11} defeating the spin-statistic argument, which had so far limited the EL efficiency (section 2.1.2) to less than one quarter of the respective PL efficiency.

* One further parameter is the exciton binding energy of excitons in the conjugated materials. However, the values of the binding energies in most conjugated polymers are still under debate and will not be discussed further in this thesis.

2.1.1.1 Charge Injection

The *injection of charge carriers* into the polymer depends on the electronic energy structure of the active layer and on the work-function of the metal electrodes (Figure 2.2). Assuming no interaction between the metal and the polymer interface, the energies $\Delta E_{h,e}$ required for hole and electron injection are according to the ideal Schottky model¹² determined by (i) the ionization potential I_p of the polymer – the energy required to remove an electron from the HOMO of the polymer into the vacuum (injection of a hole) –, (ii) the electron affinity E_a of the polymer – the energy gained from the addition of an electron to the LUMO of the polymer –, and (iii) by the work-functions $f_{a,c}$ of the anode and cathode, respectively.* The barrier to injection is determined according to the relations:

$$\begin{aligned}\Delta E_h &= I_p - f_a \\ \Delta E_e &= f_c - E_a.\end{aligned}\tag{2.1}$$

Thus, the higher the absolute values of I_p and E_a , the more difficult is the injection of holes and electrons, respectively. To inject electrons into the polymer the cathode should be an electropositive metal with a low work-function close to or slightly less than E_a , such as Al (4.3 eV), Mg (3.7 eV) or Ca (2.9 eV). For the injection of holes, the work-function of the anode should be close to or slightly lower than I_p . Since one of the electrodes must be transparent for the observation of light-emission from the layer, usually an indium tin oxide (ITO) with a work-function of ca. 4.8–5.0 eV^{13,14} is used as the anode.

* For electroluminescent organics, typical values are 5.0 eV or higher for I_p and 3.0 eV or lower for E_a (with respect to vacuum).

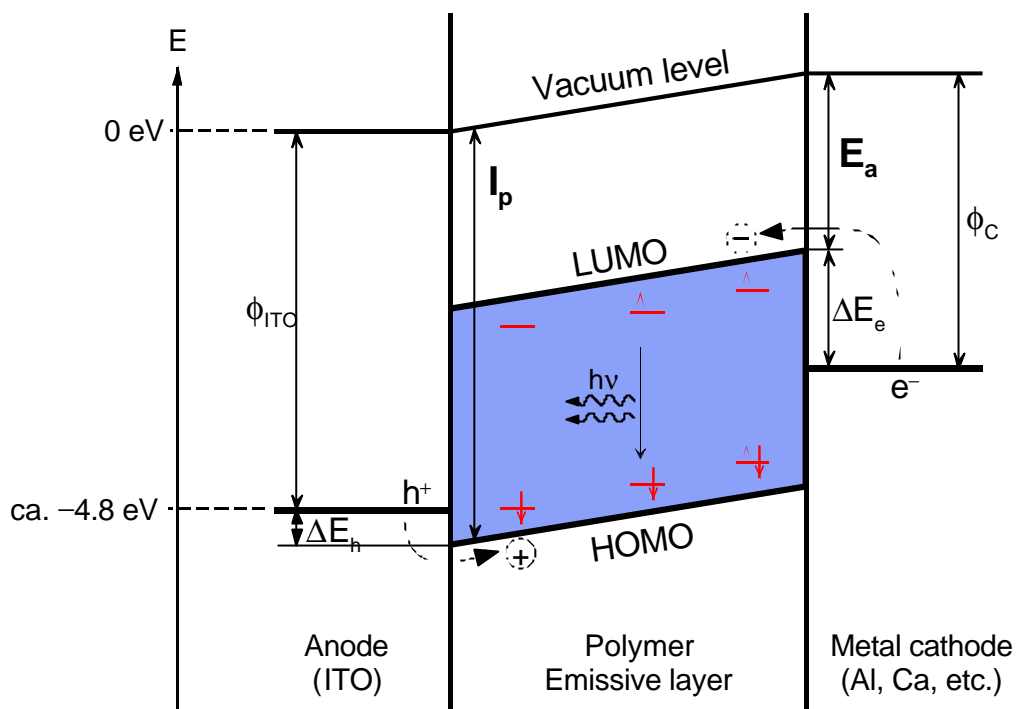


Figure 2.2. Schematic energy level diagram for a single-layer LED with structure ITO/polymer/metal cathode showing the ionization potential (I_p) and the electron affinity (E_a) of the polymer, the work-function of the ITO anode and Al cathode (ϕ_{ITO} and ϕ_C), the barriers to the injection of holes (ΔE_h) and electrons (ΔE_e), and the positive and negative polarons (h^+ and e^-).

The height of the barrier ΔE also controls the current flow within an OLED. Depending on the size of the barrier, the current through such a device is either (i) *transport-limited (ohmic)* or (ii) *injection-limited*. In the case of high barriers, the current is injection-limited, which means that the contact is not capable to provide the number of carriers required for bulk-limited charge transport. Instead, the rate at which charges are injected from the contact into the organic materials determines the current density. The Richardson-Schottky model of *thermionic emission* and the Fowler-Nordheim model of *tunneling injection* are common models which have been used to describe injection-limited currents.¹⁵⁻¹⁷ However, both models are critical to precisely describe the current characteristics observed in real OLEDs, and further improvements of the models have been introduced for example by Bässler *et al.*¹⁸⁻²⁰ and by Graupner *et al.*¹⁵

In contrast to the injection-limited case, the metal(oxide)/polymer-contact is *ohmic* if the barriers to charge injection are small. The charge carriers are easily injected into the polymer and the current flow is not limited by the injection from the contact. Instead, the contact is capable of supplying equal or more charge carriers than the sample can transport. Depending on the applied field, the injected charge carriers may accumulate and build up a space-charge region. The current is then limited by its own space-charge (*space-charge limited current (SCLC)*) which, in the extreme case, may even reduce the electric field to zero at the injecting contact. The SCLC regime is easily reached due to the rather low mobilities of the charge carriers in the

relatively disordered organic materials. Starting with Poisson's equation and the continuity equation, the equation for trap-free space-charge limited current conduction (*Child's law*) is obtained:^{18,21}

$$j_{SCLC} = \frac{9}{8} \epsilon \epsilon_0 \mu \frac{U^2}{d^3} \quad (2.2)$$

where ϵ_0 is the vacuum permittivity and U is the applied voltage. The other quantities determining the current flow are characteristics of the bulk: ϵ is the dielectric constant, μ the charge carrier mobility, and d is the thickness of the polymer.

2.1.1.2 Charge Transport and Recombination

The *charge transport* in disordered organic materials occurs via *hopping*, i.e. tunneling of carriers from one transport site to another.^{18,22-24} The disorder in organics results in a localization of the states, and charge transport occurs via tunneling between such localized states. This is in contrast to *band transport* in inorganic crystals or organic single crystals, where the free charge carriers are delocalized and move as plane waves.

Both the site distances and energies are distributed, and hopping is only possible to the nearest-neighbors. As a consequence, the mobilities in disordered organic materials are much smaller (seven to ten orders of magnitudes) than in inorganic semiconductors – typical values for conjugated polymers are in the range of 10^{-8} – 10^{-3} cm^2/Vs .²⁵ Theories based upon the assumption of hopping successfully described the charge transport in molecularly doped polymers and in organic glasses^{26,27} although there is still controversy concerning its applicability for conjugated polymers.²⁸ A more detailed treatment of the charge transport can be found in the literature.^{21,22,29}

As a result of the hopping and the low mobility, the *recombination* of electrons and holes in disordered organic materials obeys the Langevin law.^{30,31} In general, recombination is based on the concept that two oppositely charged carriers, which approach at a distance smaller than the Coulomb radius, $r_C = e^2/4\pi\epsilon\epsilon_0 kT$,* will certainly recombine. Since the Coulomb radius in organic materials is significantly smaller than the layer thickness ($r_C \sim 18$ nm at room temperature; $\epsilon = 3$), a large density of injected carriers is necessary to enable efficient recombination of the carriers. For Langevin recombination, the recombination rate is determined by the approach of the carriers under their Coulomb attraction and the formation of the excitons, and thus, increases with the mobility of the charge carriers.^{22,31,32} Due to the low mobility of charge

* The Coulomb radius is the distance at which the kinetic energy (kT) of a charge carrier equals the Coulomb attractive potential energy ($e^2/4\pi\epsilon\epsilon_0 r_C$) of the recombining counter-charge.

carriers in disordered materials, the effective recombination cross section is smaller than the Coulomb radius by a factor of ca. 3–4. This further strengthens the necessity of a high charge carrier density to ensure a high probability of exciton formation and recombination.

2.1.2 Efficiency of OLEDs

A singlet exciton, formed via the combination of a positive and negative polaron, cannot be distinguished from a singlet exciton formed by optical excitation.* Hence, the photoluminescence quantum yield h_{PL} essentially determines the efficiency of electroluminescence. An expression of the *internal EL quantum efficiency* h_{int} – i.e. the number of generated photons per injected electron – is given by:³³

$$h_{int} = h_{PL} \cdot f_s \cdot f_r \quad (2.3)$$

where f_s is the fraction of singlet state excitons formed, and f_r is the probability that charges recombine to excitons. In most organic materials, f_s equals 1/4, since due to spin statistics, three times more triplet than singlet excited states are created in the electron-hole recombination process.³⁴ The parameter f_r is determined by the process of the injection of charge carriers and reaches the maximum of unity, if the current densities for injection of electrons and of holes are equal.¹⁵ Thus, the maximum internal electroluminescence quantum efficiency in the case of an ideal electroluminescent device is 25 %:

$$h_{int}(EL_{ideal}) = 25 \%. \quad (2.4)$$

Due to refraction, not all of the photons emitted can be perceived by an external observer. Therefore, the *external quantum efficiency* h_{ext} is defined as the number of photons actually leaving the device per injected electron, and h_{ext} is diminished by the factor of $2n^2$ with respect to the internal efficiency:³⁵

$$h_{ext} = \frac{h_{int}}{2n^2} \quad (2.5)$$

where n is the refractive index of the organic layer. Using typical values of n for polyfluorene ($n \approx 1.7$),³⁶ the maximum external quantum efficiency of any EL device is ~ 4 %:

$$h_{ext}(n = 1.7) \leq 4 \%. \quad (2.6)$$

* Another fact showing the connection between photoluminescence and electroluminescence is that the spectra of PL and EL are very similar (section 3.1.1), indicating that radiative decay of the same singlet exciton is responsible for the emission in both cases.

† To achieve efficient luminescence it is necessary to have (i) a good balance of electron and hole current (every charge carrier which does not meet a counter-charge before reaching the electrode does not form an exciton and is

Since in electroluminescence electricity is directly converted into light, another important measure of the efficiency is the *power efficiency* h_{pow} which is the ratio of the emitted light power to the electrical input power (eU):

$$h_{pow} = \frac{h\nu}{eU} h_{ext} \leq h_{ext}. \quad (2.7)$$

For the calculation of the *luminous efficiency* of an electrically driven light source, the power efficiency, which is a *radiometric* quantity, is related to the selective spectral responsivity of the human eye, yielding a *photometric* quantity (see Appendix A.1). Therefore, (Equation 1.7) is multiplied by the relative luminous efficiency function $f(I)$, introduced by the 'Commission Internationale de L'Eclairage' (CIE).³⁷ (Appendix A.1, Figure A.1):

$$h_{lum} = h_{pow} \cdot f(I) \cdot K_m \quad (A.4)$$

with $K_m = 683$ lm/W for photopic vision and $K_m = 1699$ lm/W for scotopic vision.³⁸

For the calculation of the *luminance efficiency*, the obtained luminance L (see Appendix A.1) is related to the current density j in the device:

$$h_{lum} = \frac{L}{j}. \quad (2.8)$$

the unit of the luminous efficiency is candela per ampere (cd/A).

2.1.3 Multilayer Devices

Most organic semiconductors are better suited to transport holes rather than electrons, and recombination then takes place in the vicinity of the cathode. Recombination close to an electrode is generally predicted to be the case for unbalanced charge carrier concentration within the device, and the lifetime and efficiencies of the corresponding diodes are substantially decreased due to quenching effects. To overcome this problem, the recombination zone has to be shifted towards the center of the organic layer, and one approach is the fabrication of *multilayer devices*.^{25,39}

Multilayer devices usually consist of two or three polymer layers and they are typically designed so that radiative recombination primarily occurs in only one of the layers. The function of the additional layers is to serve (i) as *blocking layers*, i.e. to block charge carriers from traversing the device and reaching the other electrode without recombining, (ii) as *injection or transport layers*, i.e. enhancing either the injection or the transport of charge carriers, or (iii) as

lost to the radiative recombination process), (ii) efficient capture of electron and holes within the active layer and

alignment layers. The essential parameters for the device design and operation are the energy levels and the mobilities of holes and electrons of the respective layers.

Blocking layers provide an energy barrier to the type of charge carriers which otherwise would dominate the current flow either due to a lower injection barrier or due to higher mobility with regard to the oppositely charged carrier. Thus, they improve the balance of charge carriers and the efficiency of the device. Blocking layers produce two important effects: an accumulation of charge carriers at the blocking interface and, as a consequence of this, a change of the electric field distribution in the device structure.

Injection or transport layers have either a reduced Schottky injection barrier or an increased mobility of electrons or holes. By means of appropriate design it is possible to enhance the recombination rate by balancing the charge carrier concentration, and to move the center of recombination away from the electrodes. Moreover, the energy barriers at the interface and the strong mobility difference for the carriers increase the effective transit time of the charge carriers within the active layer leading to a high recombination probability.*

Alignment layers for the use in light-emitting devices have to be designed such that they disturb the injection of charge carriers as little as possible. Typically, alignment layers consist of rubbed polyimide, an insulator, and therefore hole-injection and -transport has to be enabled by the addition of appropriate hole-transporting materials (section 3.1.4 and 5.2).⁴⁰⁻⁴²

2.1.4 Emission Color

One major advantage of organic LEDs over their inorganic counterparts is the continuous tunability of their emissive color. The latter can simply be adjusted by modifications of the molecular structure (such as varying the aromatic rings, the substituents or the regioregularity of the polymers) or by doping with highly fluorescent dyes.^{8,43} Even highly efficient blue LEDs have successfully been realized and, as discussed above, blue emitters are of crucial interest, because red and green emission can be achieved through the doping of proper dyes via energy transfer from the blue-emitting guest to the lower band gap material host-system (chapter 7).⁴⁴⁻

46

Blue emission has been achieved from a large number of organic compounds with large HOMO-LUMO separation, and also from various conjugated polymers (e.g. poly(*p*-phenylene)

efficient formation of singlet excitons, and (iii) efficient radiative decay of singlet excitons.

* For example, by insertion of a hole-transporting layer into a device with electron-dominated current the hole current is increased. Due to the different mobilities in the two layers, the hole density changes abruptly at the interface of the two layers and it is larger in the lower mobility layer. The enhanced hole-mobility helps to concentrate holes in a region where the electron density is high and to increase the recombination rate.

(PPP)⁴⁷ or its derivatives,^{8,46} polythiophenes,^{8,48} polypyridines,⁴⁹ and from polyfluorenes),^{8,14,39,42,50-59} from conjugated polymer blends,^{39,60} from numerous copolymers with interruption in the conjugation sequence,^{39,46} and from polymers with isolated fluorophores.⁴⁶

A white organic light-emitting diode was fabricated by Kido,⁶¹ showing a voltage-dependent color change and reaching 2200 cd/m² at 16 V with a turn-on voltage of 6 V. White LEDs are useful for the application in light weight illumination devices, as backlighting for liquid crystal displays (LCDs) or for full-color displays.

2.1.5 Polarized Electroluminescence

One possible application of organic materials in the area of flat panel displays might be the use of OLEDs emitting *polarized* light as backlights for conventional LCDs. These devices still suffer from high power consumption, attributable to the necessity of polarizing the isotropic backlight – usually generated by fluorescent bulbs – with additional sheet polarizers (Figure 2.3). The removal of the light-consuming and expensive polarizer would require OLEDs with polarization ratios of up to 200:1 (depending on the specific application).⁶² However, even if the polarization ratios are insufficient for a complete elimination of the polarizer, the device efficiency can still be substantially improved due to the diminished absorption of the partly polarized light.

One approach to construct such a device is the use of organic materials which can be oriented in a specific direction, since high polarization ratios require high degrees of anisotropy in the emissive layer. Various approaches to the alignment of organic electroluminescent materials have been reported in the literature, and to date the best results were obtained from polymers.⁶² The most common methods for the alignment of polymers will be discussed in chapter 2.2.

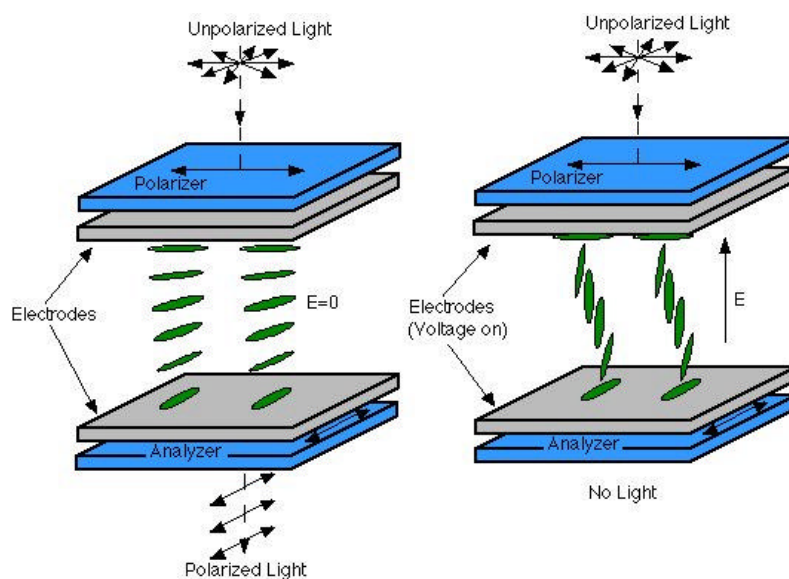


Figure 2.3. Cartoon of a conventional liquid crystal display (LCD). The combination of isotropic backlight and highly energy consuming polarizers may be replaced by an organic LED emitting *polarized* light.

For a more detailed discussion of electroluminescence from organic materials and related topics the reader is referred to very good articles given in the reference section.^{8,22,29,34,39,43,46,62-71}

2.2 Polymer Alignment

As discussed above (section 2.1.5), the application of organic materials as active materials in backlights for LCDs requires high degree of polarization of the emitted light which is achieved by a high degree of molecular alignment of the chromophores. There are numerous methods to achieve such orientation, and the most successful ones with regard to the alignment of polymers will be discussed in this section.

2.2.1 Quantitative Description of Molecular Orientation – Order Parameter, Polarization Ratio and Dichroic Ratio

The degree of molecular orientation is commonly quantified by means of the *orientational order parameter* S , a single scalar quantity describing the spread of molecule orientation about the director (overall axis of preferential orientation), with a large value of S implying a small spread. Properly speaking, this term – originating from Landau's theory of phase transitions⁷² – should be applied only to anisotropic systems that are in the thermodynamic equilibrium, but it is used in the literature for any aligned state of anisotropic molecules. Marrucci *et al.* reduced the three-dimensional problem⁷³ to its two-dimensional analogue and defined the order parameter in two dimensions by:^{74,75}

$$S \equiv 2\langle \cos^2 \mathbf{q} \rangle - 1 = \langle \cos 2\mathbf{q} \rangle = \int_0^p f(\mathbf{q}) \cos 2\mathbf{q} \, d\mathbf{q} \quad (2.9)$$

where $f(\mathbf{q})$ is the normalized distribution function of the main chain orientation, i.e. the probability of a molecule being oriented with an angle \mathbf{q} to the director ($f(\mathbf{q})$ is large around $\mathbf{q} = 0$ or \mathbf{p} and is small for $\mathbf{q} \approx \mathbf{p}/2$). This definition ensures the order parameter becomes zero in the isotropic case and unity in the fully aligned case.

By means of the order parameter of the emitters, an upper limit of the achievable *polarization ratio* P can be estimated using the following relation:

$$P \leq \frac{1+S}{1-S} \quad \text{or} \quad S \geq \frac{P-1}{P+1} \quad (2.10)$$

where the polarization ratio is defined as the ratio of the emitted light intensity parallel (I_p) and perpendicular (I_{pp}) to the molecular alignment:

$$P = \frac{I_{pl}}{I_{pp}}. \quad (2.11)$$

These inequalities are also valid when replacing the polarization ratio P by the *dichroic ratio* D yielding:

$$D \leq \frac{1+S}{1-S} \quad \text{or} \quad S \geq \frac{D-1}{D+1} \quad (2.12)$$

where the dichroic ratio is the ratio of the absorbance parallel (A_{pl}) and perpendicular (A_{pp}) to the molecular orientation:*

$$D = \frac{A_{pl}}{A_{pp}} \quad (2.13)$$

From relation (2.18) one can estimate that for a polarization ratio of $P = 20$ an order parameter of at least $S = 0.9$ is required, stressing the need for high degree of orientation.

An exact calculation of the order parameter using the measurable polarization (dichroic) ratio R is only possible with the knowledge of the angle α between the emission (absorption) dipole and the molecular symmetry axis, using the relation:⁷⁶

$$S = \frac{R-1}{R+1} (1 - 2 \cos^2 \alpha) \quad (2.14)$$

Furthermore, for an accurate calculation, anisotropic internal fields should be considered as well as surface reflection due to birefringence of the light entering or leaving the film.⁶² This difficulty is often ignored, and in order to be more exact in the following, the degree of molecular orientation will be described only in terms of the dichroic ratio D (in the case of absorption) and the polarization ratio P (in the case of emission).

2.2.2 Mechanical Alignment – Stretching and Rubbing of the Emissive Layer

Polymers can be aligned by means of a number of mechanical methods, the first of which is orientation by *stretching*. Polarized electroluminescence realized by this technique was first reported by Dyreklev *et al.* who obtained a polarization ratio of about 2 from stretch-oriented conjugated polythiophenes.⁷⁷ Although in photoluminescence, much higher polarization ratios have been reported, for example from stretch-oriented MEH-PPV (poly(2-methoxy-5-[2'-

* The physical principle underlying the dichroism is that the absorbance is proportional to the square of the cosine of the angle between the transition dipole moment vector and the electrical field vector: if the two vectors are parallel, the radiation is strongly absorbed, whereas no light is absorbed if they are perpendicular to each other.

ethylhexyloxy]-*p*-phenylene-vinylene)),⁷⁸ the method of stretch orientation has severe drawbacks. Soft materials are required for elongation which tend to relax back into an unoriented equilibrium state. This problem may be circumvented by quenching into a glassy or crystalline state after stretching from the soft state (melt or solution),⁷⁹ or by drawing a precursor during conversion.^{80,81} However, the performance of the EL device reported by Lemmer *et al.* was poor due to a large separation of 10 μm between the electrodes, yielding a polarization ratio of 8 at a voltage of 500 V. On the other hand, the implementation of stretched films into active EL configurations with the required thickness of less than 1 μm is very problematic, since the structural integrity of the films is disturbed by the high drawing ratios.

A second method of mechanical alignment is the *rubbing* of conjugated polymer films – a procedure known for two decades from the preparation of alignment layers for liquid crystals⁸² – in order to directly obtain polarized emission from the aligned chains without the need for additional alignment layers. A polarization ratio of 4 in EL was reported by Hamaguchi *et al.* from a three-layer device comprised of rubbing-aligned alkoxy-substituted PPV as the emissive layer.⁸³ Polarized emission was also obtained from rubbing a film of hexyl-dodecyl copoly(phenyleneethynylene) (PPE)⁸⁴ (section 4.2).⁸⁵ To date, the best performance of a device with a directly rubbed polymer emissive layer was achieved with a precursor PPV aligned by rubbing during conversion.⁸⁶ A polarization ratio of 12 in electroluminescence and a maximum brightness of 200 cd/m^2 at 20 V was reported. However, due to mechanical damage of the films, the stability and lifetime of such devices is problematic.

2.2.3 Langmuir-Blodgett Deposition

By means of Langmuir-Blodgett (LB) deposition, macroscopically aligned films of few nanometer thickness can be fabricated.⁸⁷ This technique consists of transferring monolayers of amphipathic molecules onto solid substrates by their dipping and raising through a monolayer floating on the surface of purified water. Polarized emission was obtained by applying the anisotropic LB technique to side-chain substituted conjugated polymers, such as substituted poly(*p*-phenylene), and polarization ratios of 3–4 were reported.⁸⁸ However, the build-up of an EL device requires up to 100 deposition cycles under precisely controlled conditions, not rendering the LB deposition compatible for large-scale production of commercial devices. Furthermore, crystallization of LB films over time is a severe problem and the polarization ratios obtained to date are not sufficient for applications.

2.2.4 Alignment on Particular Substrates

Since their initial report in 1991 alignment layers prepared by means of friction transfer technique have been shown to yield high degrees of molecular orientation.⁸⁹ Usually, such an alignment layer is fabricated by squeezing and shearing a poly(tetrafluoroethylene) (PTFE) rod on a surface, yielding a molecularly oriented ultra-thin PTFE film with the direction of orientation of the PTFE main chains matching the friction direction. Layers of friction-transferred poly(*p*-phenylene) (PPP) have also been used for alignment of epitaxially grown thiophene/phenylene co-oligomers for example, and polarization ratios of up to ~ 100 have been obtained in photoluminescence.⁹⁰ The friction transfer is a multipurpose technique, because it allows the alignment of small molecules, conventional polymers and conjugated polymers – regardless whether they are liquid crystalline or not.^{89,91-93}

Due to the insulating nature of PTFE the fabrication of electroluminescent devices is very difficult, and has only been reported until now by Chen *et al.* They made use of the rather inhomogeneous film morphology and obtained charge injection from ITO through areas of the sample which were not covered with PTFE. Polarized EL was reported both for small molecules and conjugated polymers (which were epitaxially grown on top of the oriented PTFE), and the highest anisotropy for solution-cast polymers was a polarization ratio of ~ 4 .⁹⁴

2.2.5 Liquid-Crystalline Polymers on top of Alignment Layers

2.2.5.1 Introduction into Liquid Crystalline Polymers

As implied by the name, liquid-crystalline Polymers (LCPs) combine the properties of polymers (associated with the nature of the backbone) with those of liquid crystals. The latter entails low viscosity in the liquid crystalline state and the tendency to align with the long axis of their rod-like molecules along a preferred direction, which is known as the director. However, the size of such aligned domains in LCPs is much too small (only a few micrometers – in average the directors are oriented randomly) to produce polarized light from suitable electroluminescent LCPs, unless macroscopic alignment is imposed by external action. The conventional method to achieve the required monodomains of uniform homogeneous molecular alignment in thin films is the use of additional alignment layers upon which the LCPs align when they are brought into the mesogenic – low viscous – state. The alignment of the LC molecules is preserved into the crystalline state by cooling down slowly, or into the glassy (frozen) LC state by cooling down quickly (quenching). The most common alignment layer consists of polyimide⁶²

(section 3.1.3), because polyimide has excellent alignment ability as well as thermal and chemical stability.⁹⁵ Furthermore, it is transparent for visible light and therefore fulfills another fundamental requirement for an incorporation into an LED structure. Polyimide can be aligned by rubbing with a cloth or by irradiation with UV-light. Both of these methods will be discussed in the following section after a short introduction into liquid crystalline polymers.

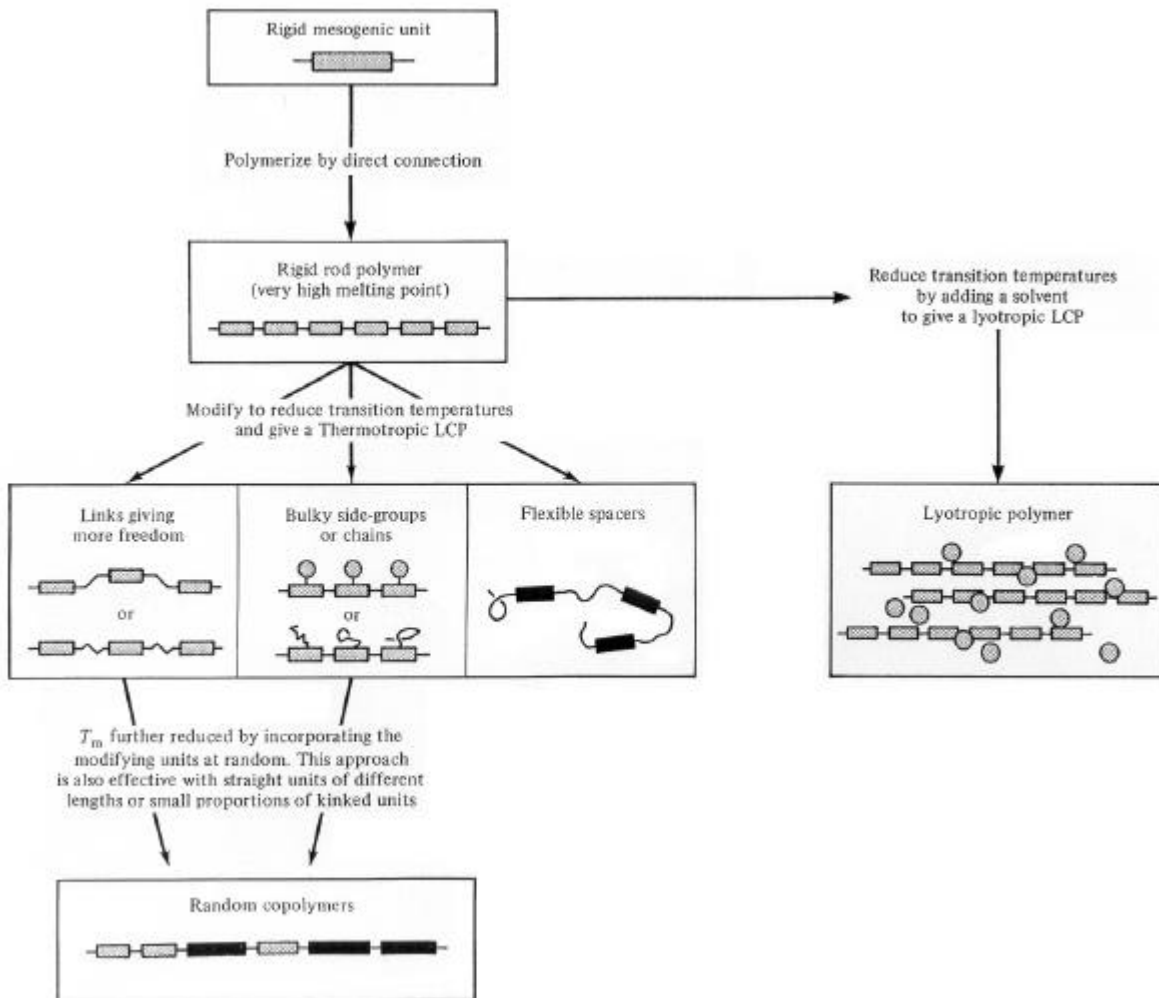


Figure 2.4. Principles of the molecular design of liquid-crystalline polymers (from Windle).⁹⁸

The prerequisite for normal flexible polymers to display liquid crystal characteristics is the incorporation of rod-like or disk-like elements (*mesogens*) into their chains. The most basic construction of an LCP is simply to link the rigid mesogenic units end-to-end and by this to form a so called (main-chain) *rigid rod polymer* (Figure 2.4).^{*} However, due to the polymerization the

^{*} Another way to polymerize rigid mesogenic units by direct connection may yield *side-chain polymers* which do only unwillingly form a liquid crystalline phase. Decoupling the mesogenic side-groups from the backbone via flexible spacers is an approach to obtain side-chain LCPs.⁹⁶ The versatility of side-chain LCPs arises because these structures can be varied in the backbone structure, in the mesogenic unit or in the spacer. Although side-chain LCPs based on a PPV backbone, where the vinylene bond was substituted with a lateral flexible spacer with a terminal cyanobiphenyl mesogenic group, showed an alignment with a dichroic ratio of 2 (on a friction-transferred alignment layer of poly(tetrafluoroethylene)),⁹⁷ no real monodomain alignment was reported from such substituted PPVs and its copolymers.

crystal melting temperatures T_m (or glass transition temperature T_g in the absence of crystallinity) increase significantly, and often the molecules tend to decompose before they melt into the liquid crystalline phase.*

Thus, shifting the crystal melting point into an accessible temperature range without destroying the mesophase stability is the central aim in the design of thermotropic LCPs. There are several approaches, all of which either have to increase the entropy change on melting DS or decrease the respective enthalpy change DH or both: At the melting point, the crystal phase is in equilibrium with the melt and hence, one can write

$$T_m = \Delta H / \Delta S. \quad (2.15)$$

For example, a stiff chain will have little additional freedom to move in the melt than in the crystal yielding small DS and high T_m , whereas a more flexible molecule will have a higher mobility in the melt and thus a higher DS and a lower melting point.

As a rule, the degree of flexibility of a chain is a decisive factor for whether it will form a mesophase or not, and a suitable parameter which describes the tendency of a polymer to show liquid crystallinity is the *persistence ratio* p i.e. the relationship between persistence length l_p and the average chain diameter d .⁹⁸

$$p = \frac{l_p}{d}. \quad (2.16)$$

The persistence length l_p is a significant parameter of a *semi-rigid* 'worm-like' chain and provides a measure of the degree of chain expansion. Suppose a freely rotating chain is centered in a Cartesian coordinate system with its first link along the y -direction. The persistence length is then the average projection of the end-to-end distance of the chain in that direction, or in other words, it is the sum of the projections of the remaining bonds in that direction.⁹⁹ Hence, it gives a measure of the memory of the direction taken by the first segment. The higher the persistence length, the straighter is the chain.

These relations originate from the modification of the theory of rigid rods to semi-rigid polymers: In their simplest form, theories describing the relationship between chemical structure and liquid crystallinity handle LC molecules as ideal rigid rods. Flory's lattice theory,¹⁰⁰ as an example, allows the prediction of main features of phase diagrams and of the onset of liquid

* In general, the range of the mesophase stability increases with polymerization, since the upper transition temperature $T_{LC@i}$ – where the liquid crystalline phase reverts to an isotropic liquid – increases faster than the melting temperature T_m .⁹⁶ However, the temperatures themselves become steadily higher so that processing becomes more and more inconvenient if thermal degradation does not prevent the mesophase from being observed at all.

crystallinity of a lyotropic* LC primarily from the knowledge of the *axial ratio* x of the (rigid) monomer rods (rod length/diameter). The description of the LC in the bulk rather than in solution is far more complicated, but it is of great interest since thermotropic LCs instead of lyotropics are used the most in technical applications. The theory of Maier-Saupe enabled the description of thermotropic rigid rods by the introduction of an anisotropic interaction without specifying the particular origin of this interaction.¹⁰¹

However, only a few macromolecules approach the ideal of a perfectly rigid rod polymer – but the assumptions concerning rigid rods can be adapted to *semi-rigid* polymers by describing them in terms of a 'worm-like chain' and further to model this chain as a series of discrete rigid rods connected together by joints which are free to move in all directions. This model equivalent to the worm is termed the *Kuhn chain* (Figure 2.5), and the length of each segment l_k of the Kuhn chain is twice the persistence length of the molecule.⁹⁸ The theory of rigid rods may be applied to worm-like molecules by simply replacing the axial ratio x of the rod molecule by the axial ratio x_k of the Kuhn segment, which is twice the persistence ratio p . A very low value of this ratio points to a very short Kuhn length (with respect to the diameter), the former indicating that the molecules are not stiff enough for displaying a mesophase. Modeling of aromatic polyester molecules revealed that liquid crystallinity is observed when the persistence ratio is not less than a critical value of ~ 6 , which was shown to be a rule applicable for LCs in general.^{99,102,103}

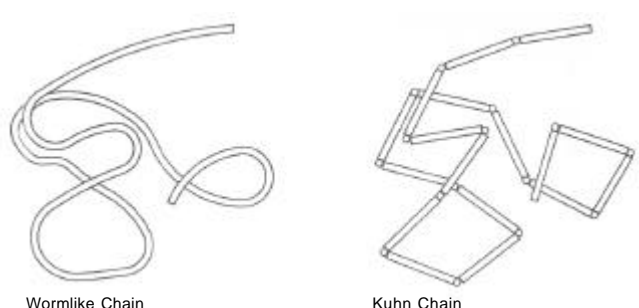


Figure 2.5. Schematic pictures of a wormlike chain and the equivalent Kuhn chain. Taken from Windle.⁹⁸

As mentioned above, increasing the flexibility of the chains is an approach to lower the transition temperatures into the LC phase. In general, the required higher flexibility can be achieved by chain modifications, such as (i) the incorporation of links between the mesogenic units giving additional freedom of rotation, (ii) the attachment of bulky side-chains or -groups, and (iii) the incorporation of flexible (non-mesogenic) spacer units between the rigid mesogenic units (rigid rod/flexible spacer polymers) (Figure 2.4).⁹⁸

* There are two different ways to induce a transition into the liquid crystalline state, (i) by variation of the concentration of rods or (ii) by variation of the temperature. If the transitions are given by concentration, the liquid crystals are called *lyotropic*, and for temperature-induced transitions they are referred to as *thermotropic*.

Here, only the chain modification by *side-chains or -groups* will be discussed, since this is the most important approach to increase flexibility and substantially reduce the melting temperature with regards to the alignment of conjugated LCPs.* The addition of non-mesogenic side-chains (such as linear or branched alkanes) to straight, rigid backbones leads to molecules which are referred to as '*hairy rods*'.^{87,106} Hairy rods with suitable side-chains reach their liquid crystalline phase at easily accessible temperatures. The longer the side-chains the lower the transition temperatures T_m and $T_{LC@i}$, because the chains act as bond solvent molecules, which reduce the anisotropic interaction between the rigid chains and therefore decrease DH . Moreover, the side-chains increase the number of conformations Z in the melt and thus, they increase $DS = k \cdot \ln Z$.¹⁰⁷

A number of the typical conjugated EL polymers, such as some substituted PPVs¹⁰⁸ or poly(phenylene-thiophene)s, are thermotropic liquid crystalline hairy rods which are originally stiff due to the extended backbone conjugation but made flexible by the introduction of suitable side-chains.¹⁰⁹ Furthermore, this type of polymers evolved as an important class with regard to alignment, because hairy-rod type polyfluorenes were shown to orient well on top of alignment layers. The example reported first was poly(9,9-dioctylfluorene) (PF8),¹¹⁰⁻¹¹² the stiffness of which is rather high indicated by a Kuhn length of ~ 17 nm[†] and a large persistence ratio of ~ 21.5 .¹¹⁴ In addition, the polymers being the central emissive materials for this work, poly(9,9-bis(2-ethylhexyl)fluorene-2,7-diyl) (PF2/6) and its derivatives, are also hairy-rod molecules which are slightly bulkier than PF8 due to branched rather than linear side-chains. These polyfluorenes show transition temperatures well below decomposition as well as very good alignment properties (next section and 3.1.1, 4.1, and 5.1).^{41,42,85} Although polyfluorenes are the only class of hairy rods which until now have been reported to successfully align on alignment layers,⁶² it is very probable that other examples will follow.

2.2.5.2 Rubbing-aligned Polyimide

By far the most common procedure for obtaining highly aligned samples of low-molecular weight or polymer thermotropic liquid crystals (LCs) is the use of polyimide which has been unidirectionally rubbed by a cloth as an alignment layer (section 3.3.1). Afterwards, the alignment of the LCs into monodomains is accomplished by heating them into the LC phase, followed by rapid cooling for preservation of the emerging order. This technique does not only re-

* Although segmented conjugated LCPs with a rigid rod/flexible spacer-backbone structure were successfully aligned in monodomains,^{104,105} the achieved polarization ratios were considerably lower than in hairy-rods as discussed below. This is due to the relatively short mesogenic units. Moreover, rigid rod/flexible spacer-LCPs suffer from limited charge transport due to the breaking of their backbone conjugation.⁶²

† Poly(phenyleneethynylene) which is expected to be 'infinitely' stiff was shown to have a Kuhn length of ~ 30 nm.¹¹³

sult in high degrees of anisotropy, but it is also suitable for mass production and for large area treatment. The first example of monodomain alignment of fully conjugated LCPs by means of rubbing-aligned polyimide was the orientation of a poly(9,9-dioctylfluorene) (PF8) by Grell *et al.*¹¹⁰

Polyimide is an insulator, however, and unlike in the case of an application in a standard LCD cell, the alignment layer in an electroluminescent device needs to be capable of transporting holes from the anode into the emissive layer. This problem was solved in our group by doping the polyimide with suitable hole-transporting materials. Lim *et al.* have reported on hole conducting layers based on polyimide filled with 50 wt.% triphenylamine (TPD), which they have used in conjunction with Alq₃ to fabricate EL devices, but not as alignment layers.¹¹⁵ After thermal conversion and rubbing, our doped* layer was suited to hole-transport *and* to align poly(9,9-bis(2-ethylhexyl)fluorene-2,7-diyl) (PF2/6) yielding highly polarized EL emission (section 3.1.4 and chapter 6).⁴¹ Comparable results were also obtained with PF8 on top of a similarly doped alignment layer of polyimide.¹¹¹ More recently, it was shown that a rubbed layer of precursor-route PPV can replace the doped polyimide and may serve as hole-injecting alignment layer as well, on top of which PF8 was successfully oriented into monodomains.¹¹²

Although rubbing is the technique most widely used to align polyimide, the alignment mechanism is still not understood at the molecular level. At present, it is commonly recognized that alignment of the polyimide chains parallel to the rubbing direction takes place, and that alignment of a bulk LC on top of rubbed polyimide is due to this molecular alignment rather than to microgrooves created by rubbing.¹¹⁶⁻¹²³ There are two different theories about the origin of the molecular orientation within the polyimide layer: mainly thermal¹²⁴ and mainly mechanical¹²⁰ effects. The first model involves frictional heating between the rubbing fibers and the rigid polyimide layer. The local increase in temperature dT as a result of rubbing is thought to be in the range of up to 230 °C, and therefore large enough to heat the polyimide near or above its glass transition temperature T_g , at which point the polyimide can be easily aligned. The other model supposes dT to lie between 40 and 170 °C only and hence, not sufficient to reach T_g . This view suggests that the polyimide molecules are aligned by the direct mechanical force applied by the rubbing fibers rather than by frictional heating. Kim *et al.* propose a combination of the thermal and mechanical mechanisms to be responsible for the polyimide alignment.⁵⁰ They calculated a temperature increase during rubbing well above the glass transition temperature and they found that higher temperatures generally led to enhanced anisotropies.

* In the following, the term 'doping' will be used to describe the addition of a low-molecular weight compound to the polymer layer. This follows a commonly used convention in the literature. It does not imply that the polymer is 'electrically doped', which would require a charge transfer between the polymer and the dopant.

In any case, the rubbing is believed to induce a polarity in the surface layer, and alignment of an overlying LC is due to van der Waals forces between the polar groups and the LC molecules.¹¹⁷ Actually, X-ray scattering measurements showed unambiguously that only the chains in the near-surface region (< 5 nm) are oriented and act as template in aligning LC molecules, whereas the bulk of the polyimide still exhibits an isotropic orientation of the polymer chains.¹²⁵ To be more precise, the oriented polyimide molecules induce an anisotropic molecular orientation of the first LC monolayer via intermolecular van der Waals-interaction which then propagates into the bulk of the LC through elastic interaction among the LC molecules.^{123,126,127} The liquid crystalline order thus grows epitaxially. The molecules both of polyimide and of the surface LC layer orient on average along the rubbing direction and they are tilted up from the surface. The molecular order of the LC film was found to be higher than the one of the underlying polyimide. This can be explained by assuming that an LC molecule in the first monolayer (in contact with the polyimide) orients parallel to the average orientation of *several* (~ 8) monomer units of polyimide close to the LC molecule rather than only to the direction of the *nearest* single monomer unit. This enhances the order of the LC molecules since the surface in-plane order for the first LC monolayer was shown to increase with the number of polyimide monomer units the LC interacts with.¹²⁷

2.2.5.3 Photo-aligned Polyimide

Although rubbing of polyimide is still the current method of choice for the fabrication of alignment layers, alignment by means of photochemical reactions under polarized UV irradiation becomes gradually more attractive, because this technique overcomes the problems of electrostatic charging and mechanical damage created by the rubbing procedure.

In general, three different photochemical interactions may yield photoalignment:¹²⁸ crosslinking, *trans/cis* isomerization, and photodissoziation – but only the latter two are applicable to polyimide and will be discussed here.

It was shown that polymers doped with azo dyes may give homogeneous alignment when exposed to polarized UV light, because the azo dyes undergo photoinduced isomerization from the *trans*-isomer to the *cis*-isomer (UV exposure) and vice versa (visible light exposure), resulting in the maximum number density of azo molecules being located perpendicular to the vector of the incident light, **E**. This procedure was also applied to polyimide as a matrix for the alignment layer,¹²⁹ but the alignment achieved was thermally not stable and disappeared completely upon heating the samples above 50 °C. Other problems with regards to device applications are the photochemical instability of azo dyes and the fact that the alignment layers with such dopants are colored rather than fully transparent.

Photoalignment of polyimide may also be achieved by exposure to linearly polarized UV light due to anisotropic photodissociation of photosensitive chemical imide bonds parallel to its polarization.¹³⁰ Homogeneous alignment is observed in the direction perpendicular to the polarization of the incident light,^{128,131} because the number of unbroken polyimide chains in that direction is higher. On absorption of the UV light, weak bonds in the polyimide were shown to be disrupted and to form radicals, which then take part in oxidation reactions. However, also in the case of these photodissoziated layers, the temperature stability of the obtained alignment is rather low due to the relaxation of residual polymers segments upon heating to higher temperatures. This problem was partly solved by Kim *et al.* who achieved much better performance and stability when the UV irradiation was done during the imidization of the precursor at elevated temperatures.¹³²

Apart from the problem of insufficient temperature stability, the polar anchoring energy (the strength to fix the director of the LC at the interface along the anchoring direction) of photoaligned polyimide layers is up to 10 times lower compared to their rubbed counterparts, attributed in part to the lowering of the surface energy by decomposition. Up to now, the reported degrees of alignment in the polyimide layer as well as of the LC on top are still substantially lower when achieved by photoalignment rather than by rubbing.¹²⁸ Furthermore, the electrical performance may be affected by the UV light, and negative charges were shown to be created in the films due to formation of carboxylic acid.¹³³ These problems explain why photoaligned polyimide alignment layers have not been applied to OLEDs so far.*

* The first report of an incorporation of a photoaligned alignment layers into an EL device was given by Contoret *et al.* only very recently. They used a coumarin-based photoalignment layer, doped with a hole transporter, to macroscopically orient a light-emitting fluorene-based LC of low-molecular weight, which was subsequently crosslinked to form a nematic network, and obtained an EL polarization ratio of 11.¹³⁴

3 Materials and Methods

3.1 Materials

3.1.1 Polyfluorene (PF) – Emission

As mentioned in the previous chapters, a central objective of this work was the realization of polarized electroluminescence from blue-emitting polymers. In a first place, this of course required the search for an emissive material fulfilling the necessary prerequisites. Fluorene-based compounds offer a number of advantages making them very attractive for the use in electroluminescence applications, and several reports have demonstrated bright blue emission from polyfluorene (PF) homopolymers.^{51,53,55} Poly(fluorene-2,7-diyl)s have pairs of phenylene rings locked into a coplanar arrangement by the C-9 atom. Linear or branched alkyl- or ethylene oxide-substituents attached to C-9 have been shown to provide good solubility in conventional organic solvents without affecting the conjugation along the polymer backbone. This is an important advantage over poly(*p*-phenylene)s where the steric demand of solubilizing groups has the drawback of forcing the phenylene groups out of conjugation. A typical structure of a 9,9-dialkylfluorene homopolymer is shown in Figure 3.1 and sketched in Figure 3.2. As implied by their name, all polyfluorenes display extremely high fluorescence efficiencies¹³⁵⁻¹³⁷ both in solution and in solid state, with emission wavelengths predominantly in the blue region. Their absorption spectra are broad and featureless while photoluminescence spectra show well-defined vibronic structures (Figure 3.5). Via copolymerization, the band gap and energy levels can be readily adjusted over the whole visible range.¹³⁸⁻¹⁴⁰

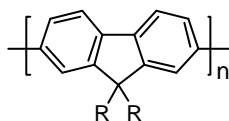


Figure 3.1. Structure of substituted polyfluorene homopolymer.

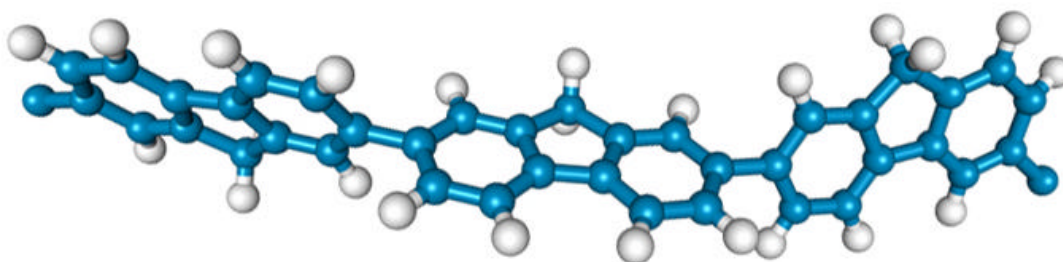


Figure 3.2. Three-dimensional model of polyfluorene.

Another important feature of polyfluorenes is their thermotropic liquid-crystallinity, which was the main reason to choose them as emissive polymers for this work. At temperatures above the melting point – but well below those for thermal decomposition – they display liquid crystalline (LC) phases, which allows to align the molecules of these polymers in monodomains by means of suitable alignment layers, such as rubbed polyimide (section 4.1).^{56,110,114} By using hole-transporting alignment layers, LEDs emitting polarized light with high polarization ratios have been fabricated.^{42,85,112,141,142}

Concerning the charge transport properties, cyclic voltammetric data of polyfluorene films indicate an ionization potential of approximately $I_p = 5.8\text{--}5.9\text{ eV}$ ^{14,42} causing a high barrier to hole injection from ITO ($I_p \sim 4.8\text{--}5.0\text{ eV}$).^{13,14} Due to the lower barrier to electron injection from a Ca cathode, which is expected to be in the range of 0.2 eV ^{42,143} to 0.8 eV ,¹⁴ fluorene polymers are believed to have electrons as the majority carriers.^{52,143} This is in contrast to the better known poly(phenylenevinylene) (PPV) and related materials, which are characterized by holes being the majority charge carriers.¹⁴⁴ Therefore, the performance of polyfluorene-based devices can be remarkably improved when appropriate polymeric hole-transporting layers are additionally incorporated.^{55,143}

3.1.1.1 Non-encapped Poly(9,9-dialkylfluorene-2,7-diyl)s

In the following, the synthesis and main characteristics of poly(9,9-dialkylfluorene-2,7-diyl)s are described, with emphasis on polyfluorene with branched *ethylhexyl* side-chains, since these types of polymers appeared to have very good alignment properties (section 4.1 and 5.1).^{41,85,142} All polyfluorenes were synthesized by Heinz-Georg Nothofer at the MPI for Polymer Research, Mainz. Details of the synthesis are described elsewhere.¹⁴⁵

The molecular weights M_n of the resulting polymers range between 30 000 g/mol and 200 000 g/mol (PS standard) depending upon the length of the alkyl-substituents, which designate the solubility and other physicochemical properties of the product. Alkyl-chains containing 6-10 carbon atoms are favorable, various substitution patterns are shown in Figure 3.3. Some of the essential properties of these different types of polyfluorenes are summarized in Appendix A.3 (Table A.2).

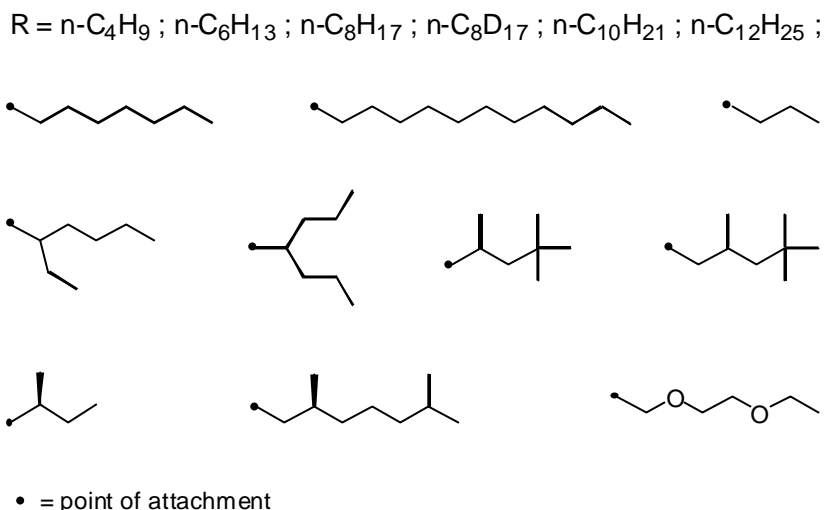


Figure 3.3. Various substitution patterns for the synthesis of polyfluorenes. See also Appendix B, Table B.1 for an overview over essential properties of some of these polyfluorenes.

Thermotropic LC-phases of such alkyl-substituted polyfluorenes can be observed in a temperature range between 100 and 250 °C, depending on the molecular weight and on the substitution pattern. As an example, Figure 3.4 depicts the calorimetric characterization of a sample of poly(9,9-bis(2-ethylhexyl)fluorene-2,7-diyl) (PF2/6) ($M_n = 127\,000$, $M_w = 210\,000$). The transitions at 167 °C on heating (curve a) and at 132 °C on cooling (curve b) correspond to melting and crystallization in the sample, respectively. For a sample quenched from 200 °C to room temperature, the identical transition is observed (curve c). Above the transition point, PF2/6 shows a birefringent, fluid phase, i.e. liquid crystallinity (section 2.2.5.1). The high enthalpies of these transitions demonstrate a substantial difference between crystalline and LC structures of PF2/6.

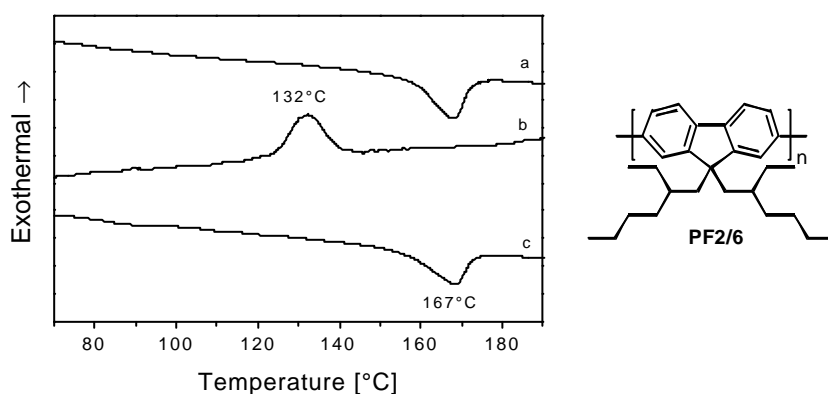


Figure 3.4. Calorimetric characterization of a film of PF2/6, spincoated from toluene. (a) heating scan (10 °C/min), (b) cooling scan of the sample (10 °C/min), (c) heating scan for a sample, which was quickly quenched from 200 °C.

Figure 3.5 shows the UV/Vis absorption and photoluminescence spectra of PF2/6 in solution and in solid state. In solution, all presented polyfluorenes exhibit similar absorption and

photoluminescence spectra, since the substitution pattern does not affect the main chain conformation, with an absorption maximum located between 383 and 389 nm and two emission maxima at about 415 nm and 440 nm.

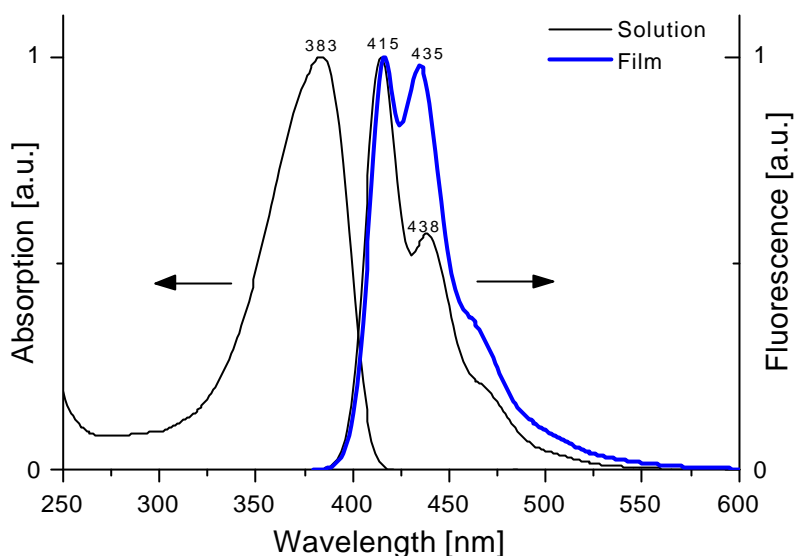


Figure 3.5. UV/Vis absorption and photoluminescence spectra of PF2/6 in solution (CHCl_3 ; thin line) and in solid state (thick line).

However, in the solid state, the absorption and emission characteristics substantially vary for the different types of polyfluorenes and they cannot be generalized. Although all polyfluorene homopolymers are characterized by inherent blue excitonic emission bands due to vibronic coupling¹⁴⁶ at approximately 425 and 448 nm, they show an additional broad band in the low-wavelength region (500–530 nm), which strongly varies both in strength and in position. This emission contribution is assigned to interchain interactions, which do form in films of conjugated polymers, such as aggregates and excimers.

As implied by the name, interchain states imply that p -electron density is shared between multiple chromophores – either in the same or from different polymer chains¹⁴⁷ – and this delocalization of the excited-state wave function lowers the energy of this state relative to a single-chain exciton, so that interchain luminescence is red-shifted relative to the standard exciton emission. The most predominant interchain species are aggregates and excimers,¹⁴⁷⁻¹⁴⁹ and studies of polyfluorene derivatives (but also of other conjugated polymers, for example of ladder-type poly(*para*-phenylene)¹⁵⁰) showed strong evidence for aggregate formation in films.¹¹⁴ However, the strength of such interchain interactions appears to depend on a variety of factors, such as the nature of the side-chains,¹⁵¹ on the molecular weight and molecular weight distribution,⁵³ on steric hindrance effects,¹⁵² on the chemical nature of the solvents and the concentration of the polymer in solution,¹⁴⁷ on certain physicochemical treatment conditions,¹⁵³ or on degradation effects.¹⁴⁸ The resulting differing intensities of such interchain interactions explain

the varying strength of the red-shifted emission contribution to the emission spectrum for the different polyfluorenes.

We show in section 6.2, that endcapping the polyfluorene with hole-transporting materials is a successful approach to effectively suppress the red-shifted emission contribution in electroluminescence. The chemical and electronic properties of such endcapped polyfluorene are discussed in the following paragraph.

3.1.1.2 Endcapped Poly(diethylhexyl)fluorene

As mentioned above, the endcapping of the polyfluorene main chain with low-molecular weight hole-transporting moieties suppressed the mentioned long-wavelength emission tail and pronounce the blue excitonic emission bands representing the inherent characteristics of polyfluorene. We will show in section 6.2, that this concept furthermore substantially improved the device performance with regards to efficiency, brightness and color stability and enabled the realization of highly polarized LEDs.

We investigated two types of endcapped polyfluorenes, the chemical structures of which are shown in Figure 3.6. Two different endcappers and different monomer/endcapper feed ratios were used. The synthesis of the PF homopolymer was similar to the one for the non-endcapped PF, with the only difference that the required amount of the endcapping reagent bis(4-methylphenyl)(4-bromophenyl)amine or (4'-bromo-biphenyl-4-yl)-naphthalen-2-ylphenyl-amine (obtained from SynTec GmbH, Wolfen, Germany¹⁵⁴) was added to the reaction mixture in the very beginning. By increasing the amount of the monofunctional endcapping reagent in the reaction mixture the molecular weight of the final product decreased significantly (Table 3.1). This indicates that the endcappers are indeed chemically attached to the polymer chains, which can be further confirmed by ¹H/¹³C-NMR analysis.

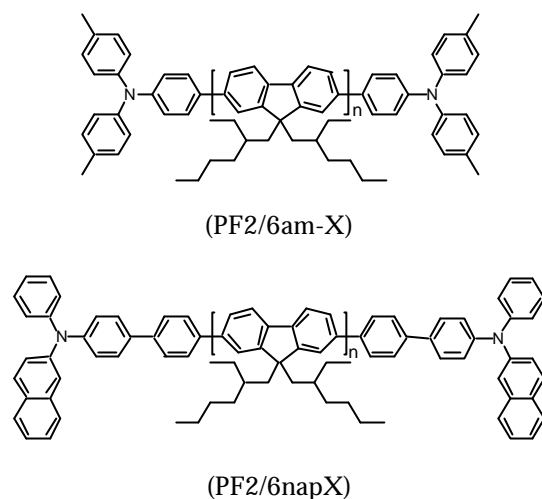


Figure 3.6. Chemical structures of poly(9,9-bis(2-ethylhexyl)fluorene-2,7-diyl) endcapped with bis(4-methylphenyl)phenylamine (PF2/6am-X) and with (N-(biphenyl-4-yl)-N-naphth-2-yl-N-phenylamine) PF2/6napX, respectively.

Table 3.1. Molecular weights of the polyfluorenes shown in Figure 3.6 for different monomer feed ratios. Also given are the endcapper concentrations as determined from $^1\text{H-NMR}$ data (integral of signals from methylprotons of endcappers divided by integral of all side-chain protons) and the melting temperatures T_m of the crystalline-LC transition as determined from DSC (2nd heating, heating rate 10 K/min).

Polymer	Monomer/Endcapper Feed Ratio [mol/mol]	M_n (GPC) [g/mol]	M_w/M_n (GPC)	Concentration of end groups from NMR [mol%]	T_m [$^{\circ}\text{C}$]
PF2/6am0	100:0	122 000	2.0	0.0	169
PF2/6am2	98:2	103 000	1.4	1.8	163
PF2/6am4	96:4	48 000	1.6	3.0	152
PF2/6am9	91:9	12 000	2.6	8.3	135 [†]
PF2/6nap3	97:3	59 000	1.5	/*	151
PF2/6nap9	91:9	12 000	2.6	/*	130 [†]

* not determined

[†] melting peak only appears in first heating scan

For all PF2/6am-X* compounds, the endcapper concentration determined by $^1\text{H-NMR}$ (Table 3.1) is slightly smaller than the monomer feed ratio, which indicates different reactivities of the bifunctional dibromofluorene derivative and the monofunctional bromotriarylamine endcapper during the reductive coupling reaction. Chain termination via debromination is expected to compete with the attachment of the triarylamine endcapper in particular for lower endcapper concentrations.

* The X denotes the content of the endcapper in mol% with respect to the PF2/6 monomer.

The electronic properties of the two materials were determined from cyclic voltammetry (CV) of the polymers in solution (Figure 3.7). It is well established that the ionization potential I_p and the electron affinity E_a – and thus, the HOMO and LUMO energies – can be related to the oxidation and reduction potentials, which are measured by CV.^{14,155} However, the values correlating the oxidation and reduction potentials to the absolute energies with respect to the vacuum level are still under discussion. In the following, we will use an offset of 4.4 eV between the electrochemical scale with the Ag/AgCl reference electrode and the vacuum level, as proposed by Janietz *et al.*,¹⁴ although other values have been also applied.¹⁵⁵

The CVs of the endcapped polymers exhibited dominant signals related to the oxidation ($E_{ox}^0 = 1.08$ V vs. Ag/AgCl) and reduction (partly irreversible peak at $E_{red}^0 = -1.9$ V) of the PF backbone itself, which occurred at potentials almost identical to those for the non-endcapped PF. Slightly larger onset potentials ($E_{ox} = 1.4$ V, $E_{red} = -2.28$ V vs. Ag/AgCl) were reported for CV investigations on thin films of poly(di-octylfluorene) (PF8).¹⁴ We attribute this discrepancy to the effect that redox reactions on thin films generally occur at higher oxidation and reduction potentials compared with investigations on the same compounds in solution.¹⁵⁶ Using the values obtained for the films, Janietz *et al.* estimated molecular orbital levels of polyfluorene of ~ 5.8 eV for the HOMO and ~ 2.1 eV for the LUMO. However, we believe that the corresponding HOMO-LUMO gap of ~ 3.7 eV and the barrier to electron injection from the Cathode of ~ 0.8 eV might be too large. By scanning tunneling spectroscopy measurements, Alvarado *et al.*¹⁵⁷ determined a HOMO-LUMO gap of 3.2 ± 0.1 eV for PF8, which is also in good agreement to the value of 3.0 eV, as obtained from our measurements in solution. Taking these numbers into account, we regard a LUMO energy level of polyfluorene of ~ 2.6 eV as more realistic.

In addition to the redox processes on the PF *main chain*, separate signals for the oxidation of the *end-groups* (at $E_{ox}^0 = 0.68$ V for PF2/6am-X and $E_{ox}^0 = 0.80$ V for PF2/6napX, respectively) are observed. For comparison, the oxidation potential of tris(p-tolyl-amine (TTA), a model for the end-groups in PF2/6am-X, is $E_{ox}^0 = 0.67$ V. This reveals that the attached end-groups act as independent electroactive moieties and constitute *hole traps* within the PF-matrix.

On the other hand, there is no indication for a reduction of the endcapper below the reduction potential of PF. This is further illustrated in the energy diagram in the inset of Figure 3.7. Despite the larger electronic π -system, the naphthyl system is more difficult to oxidize ($DE = 120$ mV), which indicates the stronger electron-donating power of the tolyl groups and is consistent with similar observations for N,N,N',N'-tetrakis(4-tolyl)-benzidine and its mononaphthyl derivatives (N,N'-di(naphthalene-1-yl)-N,N'-diphenyl-benzidine ($DE = 50$ mV).

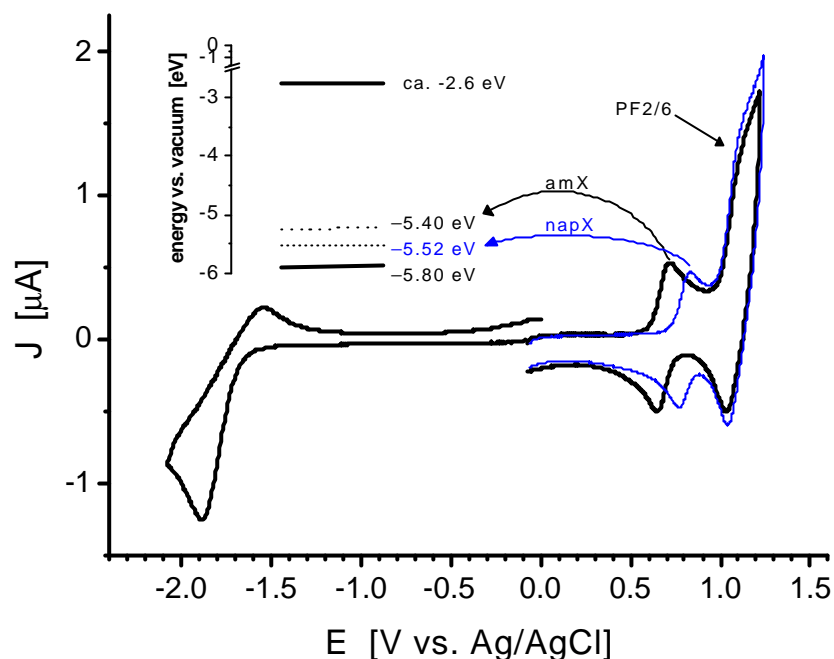


Figure 3.7. Cyclic voltammograms recorded at scan rate of 100 mV/s for PF2/6am9 (thick line) and PF2/6nap9 (thin line) in $\text{CH}_2\text{Cl}_2/\text{TBAPF}_6$ solution. The reduction curve was almost identical in both cases (only one is shown). Inset: Energy diagram for orbital levels. Starting from a HOMO level of ~ 5.8 eV for the pure PF2/6, as determined for films of pure PF8,¹⁴ the numbers for the endcappers were estimated according to the observed differences in the signals with respect to the pure PF2/6. The value of the LUMO level was calculated assuming a HOMO-LUMO gap of 3.2 eV, according to Alvarado *et al.*¹⁵⁷

3.1.1.3 Polyfluorene Copolymer

A copolymer of polyfluorene containing 90 % ethylhexyl side-chains and 10% of chiral substituents with a methyloctyl side-chains was also used in this study. The number average molecular weight was about 173 000 g/mol and the polydispersity was $PD = 1.66$. The transition temperature from crystalline to liquid crystalline state was at approximately 149 °C. The chemical structure of this copolymer is shown in the Figure below.

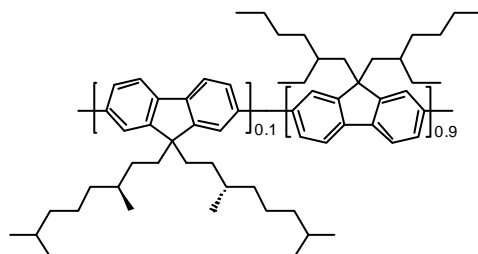


Figure 3.8. Chemical structure of poly(2,7-(9,9-bis(2-ethylhexyl))co-(9,9-bis((3S)-3,7-dimethyloctyl))fluorene) (PF8/1/1C2/6).

Furthermore, a second polyfluorene copolymer with 50 % butyl- and 50 % dodecyl side-chains was investigated. The number average molecular weight was ~ 129 000 g/mol with a

polydispersity of 1.65. The phase transition to the mesophase was observed at $T_{C@LC} \sim 152$ °C. Figure 3.9 shows the chemical structure of this polymer.

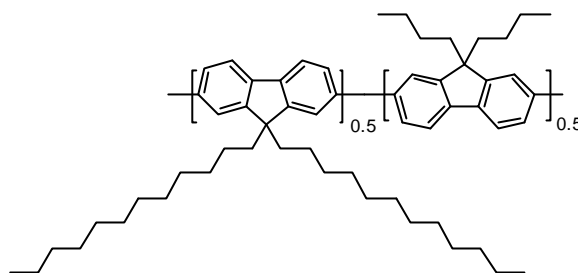


Figure 3.9. Chemical structure of poly(2,7-(9,9-bis(2-butyl))co-(9,9-bis(dodecyl))fluorene) (PF4C12).

3.1.2 Copoly(phenyleneethynylene)

Hexyl-dodecyl copoly(phenyleneethynylene)^{158,159} (PPE; Figure 3.10) was used as emissive layer in devices where polarized emission was obtained by directly rubbing the active film in the crystalline state rather than by aligning it in the LC state on alignment layers (section 4.2).⁸⁵

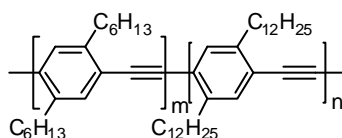


Figure 3.10. Chemical structure of hexyl-dodecyl copoly(phenyleneethynylene) (PPE).

3.1.3 Poly(phenoxyphenylimide) (PI) – Alignment

For the alignment of the liquid crystalline polyfluorene layers, we have used alignment layers on the base of rubbed polyimide. For the usage in polarized EL devices, the polyimide had additionally been filled with various hole-conducting materials. Whether doped or not, all the alignment layers, which are described in this work were made starting from a commercial polyamic ester precursor (Merck KG, Darmstadt, Kit 'ZLI 2650') which was thermally converted into a high T_g , inert poly(phenoxyphenyl-imide) (PI). The chemical structure of PI is shown in Figure 3.11.

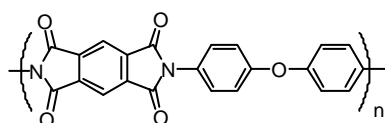


Figure 3.11. Chemical structure of poly(phenoxyphenylimide) (PI).

Unless stated otherwise, the alignment layers were fabricated by spincoating the PI precursor (or PI precursor/HTM blends) at a total solid content of 30 g/L in the ZLI 2650 kit solvent at approximately 2000 rpm for 50 s. After a 15 min softbake at 80 °C, the precursor was converted at 270–300 °C for 1 hour under rotary pump vacuum, yielding a layer thickness in the range between 40 and 50 nm.

3.1.4 Dopants for Polyimide – Hole Transport

3.1.4.1 Low-Molecular Weight Compounds

Several hole-transporting materials (HTM) have been used to fabricate hole-transporting alignment layers with high glass transition temperatures, and they have been compared with each other concerning the attainable EL device performance and degree of alignment (section 5.2.2.1).

The first one was a starburst-type amine, 4,4',4''-tris(1-naphthyl)-N-phenyl-amino)-triphenylamine (ST 638), which had a melting point of 250 °C and according to cyclovoltammetric data (Figure 3.13) a very low oxidation potential of ca. $E_{ox}^0 = 0.31$ V (vs. SCE, $\text{CH}_2\text{Cl}_2/\text{ClO}_4$). This corresponds to an ionization potential of approximately $I_p \approx 4.7$ eV,* when assuming an offset of 4.4 eV between the electrochemical scale with the Ag/AgCl reference electrode and the vacuum level.¹⁴ The next hole-transporting material, 1,1-bis-(4-bis(4-methylphenyl)-amino-phenyl)-cyclohexane (ST 755) had a relatively low melting point of 186 °C and an ionization potential of $I_p \approx 5.2$ eV, whereas 4,4'-bis{N-(1-naphthyl)-N-phenylamino}-biphenyl (ST 16-7) did not melt before 273 °C and the ionization potential was ca. 5.1 eV. The last one was N,N'-diphenyl-N,N'-bis(4'-(N,N-bis(naphth-1-yl)-amino)-biphenyl-4-yl)-benzidine (ST 1163), which is comparable to the better known triphenylamine derivative (TPTE).¹⁶⁰ and has a melting point of MP ~ 200 °C and $E_{ox}^0 = 0.77$ V yielding an ionization potential of $I_p \sim 5.2$ eV. All these materials were obtained from SynTec GmbH, Wolfen,¹⁵⁴ and the chemical structures are shown in Figure 3.12.

* As mentioned in section 3.1.1.2, the values, which relate the oxidation potential measured by CV to the ionization potential, are still under discussion. We estimate the values to compare between the different hole-transporting materials rather than to give exact numbers.

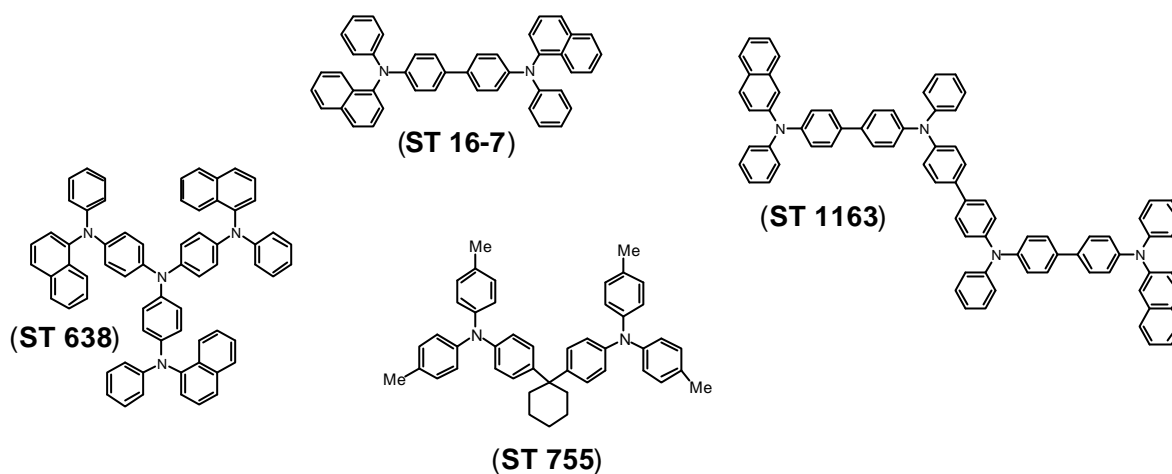


Figure 3.12. Chemical structures of four different hole-transporting materials, 4,4',4''-tris(1-naphthyl)-N-phenylamino-triphenylamine (ST 638), 4,4'-bis{N-(1-naphthyl)-N-phenylamino}-biphenyl (ST 16-7), 1,1-bis-(4-bis(4-methyl-phenyl)-amino-phenyl)-cyclohexane (ST 755), and N,N'-diphenyl-N,N'-bis(4'-(N,N-bis(naphth-1-yl)-amino)-biphenyl-4-yl)-benzidine (ST 1163).

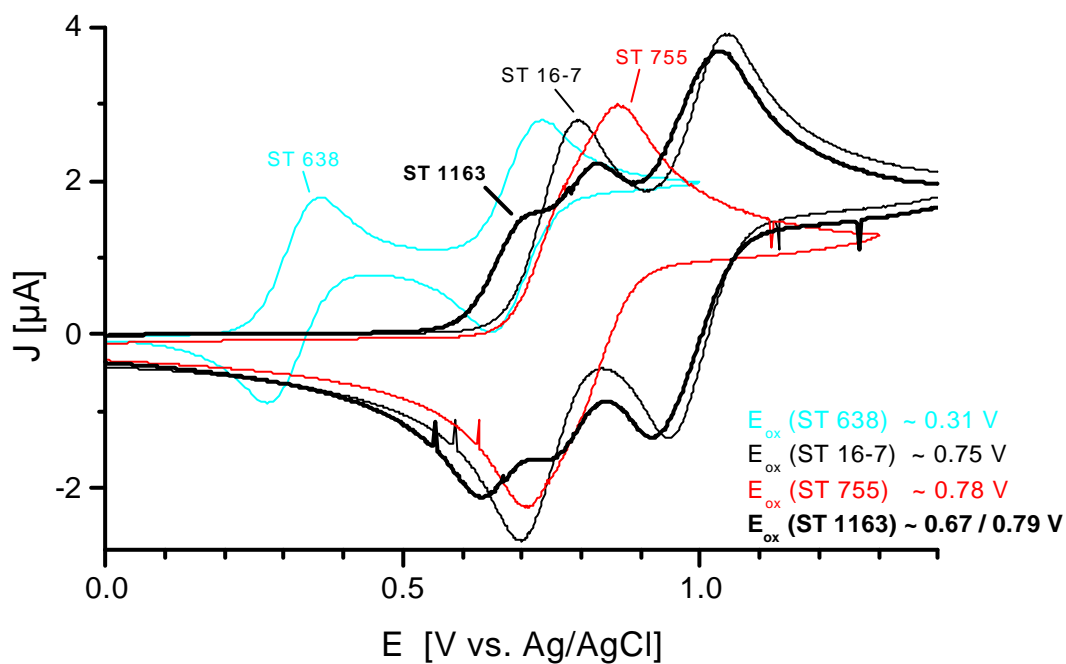


Figure 3.13. Cyclic voltammograms recorded at scan rate of 100 mV/s for ST 638, ST 16-7, ST 755 and 1163 in $\text{CH}_2\text{Cl}_2/\text{ClO}_4$ solution.

3.1.4.2 Polymer Compounds

3.1.4.2.1 Poly(triphenylamine)s and Comparable Compounds

Using low-molecular weight hole-transporting materials as dopant for polyimide can imply the problem of phase-separation. This may negatively affect the alignment power of the HTAL and substantially decrease the attainable degrees of alignment. An approach to overcome this problem is the replacement of the low-molecular compounds by *polymers*.

We considered polymers on the base of triphenylamine derivatives as promising candidates for polymer-HTMs. Triphenylamine derivatives, such as (N,N'-biphenyl-N,N'-bis-(3-methylphenyl)-[1,1'-biphenyl]-4,4'-diamine) (TPD; Figure 3.14), as low-molecular weight compounds have been shown to be a suitable material for HTMs.¹⁶¹⁻¹⁶³ We investigated poly-TPD (triphenyldiamine), poly-NPD (naphthyl phenylamino-biphenyl) and poly-TPD with an additional (CH₂)₆-spacer unit in the main chain (p-HeO-TPD).

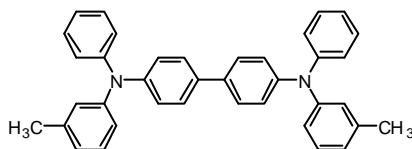


Figure 3.14. Chemical structure of N,N'-biphenyl-N,N'-bis-(3-methylphenyl)-[1,1'-biphenyl]-4,4'-diamine (TPD).

3.1.4.2.2 Poly(aniline)

Polyaniline (PAni) is known to be highly conductive when being doped with functionalized protonic acids like camphorsulfonic acid (CSA).^{164,165} We blended PAni-CSA with polyimide at different concentrations to arrive at hole-conducting alignment layers after conversion, similar to the ones reported for the low-molecular weight compounds. The structure of PAni-CSA is shown in Figure 3.15. The results obtained with such layers are described in section 5.2.2.2.2.

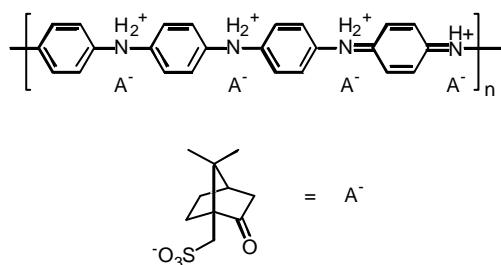


Figure 3.15. Chemical structure of PAni-CSA.

3.1.5 Dopants for the Emissive Material – Color, Efficiency and Stability

As mentioned in section 2.1.4 blue light can be down-converted into green and red by doping a blue emissive material with lower band gap materials. This is of interest with regards to the realization of full color red-green-blue displays. It was shown that doping a small amount of a fluorescent dye into an OLED can significantly change the color of luminescence.^{166,167} Furthermore, such doping may have beneficial effect on the color stability and device efficiency.¹⁶⁸ To realize green emission, we doped polyfluorene with the low-molecular weight fluorescent thiophene dye S2_3 shown in Figure 3.16. This dye is a green emitter with photoluminescence peaking at 527 nm (not shown) and with absorption spectra as plotted in Figure 7.1. The corresponding results are discussed in section 7.1.

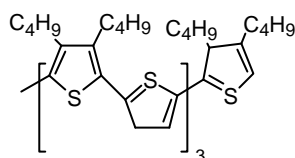


Figure 3.16. Chemical structure of the thiophene dye S2_3.

3.1.6 Poly(3,4-ethylenedioxythiophene) doped with Poly(styrene sulfonate) (PEDOT-PSS) – Hole Injection

Poly(3,4-ethylenedioxythiophene) (PEDOT) doped with poly(styrene sulfonic acid) (PSS) was used as hole-injection layer between the ITO anode and the light-emitting layer in isotropic LEDs (Figure 3.17). The ITO/PEDOT-PSS bilayer anode is known to have a remarkably higher work function (~ 5.2 eV) than ITO (4.8–5.0 eV), and due to the resulting lower barrier height at the anode/polymer interface the hole-injection is significantly improved. Using PEDOT-PSS between the ITO and the emissive polymer has shown to yield a dramatic increase in device efficiency and lifetime as well as a reduction of both the turn-on and the operating voltage.^{13,14} PEDOT-PSS was obtained under its commercial name, BAYTRON P, from Bayer-AG. A detailed review of PEDOT is given in Groenendaal *et al.*¹⁶⁹

PEDOT-PSS is not stable at temperatures higher than 200 °C, and therefore, it was only used in isotropic devices in this work. It could not be applied in our devices for *polarized* light emission, since the latter include hole-transporting alignment layers based on PI, which require thermal conversion at ~ 300 °C (see section 3.3).

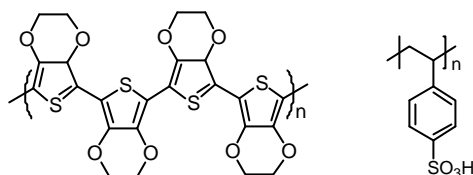


Figure 3.17. Chemical structures of poly(3,4-ethylenedioxythiophene) (PEDOT, left) and poly(styrene sulfonic acid) (PSS, right).

3.2 Preparation of Isotropic LEDs

Generally, for all the light-emitting diodes described in this work, the device architecture was a metal(oxide)/polymer/metal structure employing indium tin oxide (ITO) as a transparent anode and aluminum or calcium as the cathode. Depending on the respective purpose, additional layers with different functions were used below or above the polymer emissive layer.

For the fabrication, glass substrates patterned with 100 nm ITO electrodes (Balzers) have been cleaned subsequently in ultrasonic baths of acetone, ionic detergent water solution, ultrapure water (MilliQ unit from Waters) and isopropanol. After drying, a 20–30 nm hole-injection layer of polyethylenedioxythiophene doped with poly(styrene sulfonate) (PEDOT-PSS, see section 3.1.4) was spincoated on top. The films were dried in vacuum for 6 h at room temperature. All the different emitting materials were spincoated from toluene on top to get a final thickness of the emissive layer of approximately 70–90 nm. When necessary, the solutions were filtered immediately before spincoating in order to optimize the homogeneity of the films. After drying overnight under vacuum at room temperature, the top electrode was deposited by thermal evaporation at a pressure of $\sim 6 \times 10^{-6}$ mbar. If not otherwise stated, the cathode consisted of a 20 nm Ca layer covered with a 100 nm Al protection layer, the evaporation rate was 7 Å/s for Ca and 5 Å/s for Al. In case of optimized devices, a LiF layer was used between the emissive layer and the Ca cathode, the thickness of this additional film was 8 Å and the evaporation rate was 1 Å/s. Such additional layers were shown to substantially improve the device efficiency,¹⁷⁰ which is often attributed to an enhancement of electron injection. However, the function of these layers are not unambiguously clear yet. Hole-only devices were single-layer devices with the respective film sandwiched between ITO and a 50 nm gold top-electrode evaporated at a rate of 1 Å/s. The overlap between the two electrodes resulted in device areas of 5 mm². A scheme of an isotropic LED is shown in Figure 6.1.

3.3 Preparation of Polarized LEDs

The main difference between isotropic and polarized LEDs is that the latter require the usage of an additional alignment layer below the emissive layer (Figure 6.6). For all the devices described in this work, that layer consisted of polyimide (PI, section 3.1.3) doped with different hole-transporting materials. A second difference is the replacement of PEDOT-PSS as hole-injection material, since its temperature stability is insufficient to withstand the temperatures required for polyimide conversion. Instead, a layer of a hole-transporting material (HTM) was used to yield a stepwise barrier for hole-injection (see section 5.2.2).

The polarized devices were fabricated starting with a thin layer (20 nm) of an HTM spin-coated from Liquicoat solution (Merck-ZLI 2650 kit solvent) at a concentration of 15 g/l onto ITO covered glass substrates. Then, the hole-transporting alignment layer was prepared by spincoating a mixture of the PI precursor (section 3.1.3) and an HTM at varying concentrations and a total solid content of 30 g/l in Liquicoat at 1900 rpm for 50 s. After a 15 min softbake at 80 °C, the PI precursor was converted to PI at 250-300 °C for 1 hour under rotary pump vacuum. The film thickness after conversion was between 40 and 50 nm. Thereafter, the doped PI layer was unidirectionally rubbed as described in the following subsection. Films of the respective emissive material were spun from a toluene solution onto the rubbed PI alignment layers to obtain a layer thickness of approximately 80 nm. To induce monodomain alignment, the samples were annealed according to the procedure explained below.

The procedure of electrode deposition was the same as for the isotropic LEDs. Similar to the isotropic LEDs, a LiF layer as described above was used as additional layer between the cathode and the aligned emissive layer in order to enhance the device efficiency.

3.3.1 Rubbing Procedure

Rubbing of the samples was done by means of a rubbing machine from E.H.C. Co., Ltd., Japan. The rotating cylinder (diameter of 70 mm) was covered with a rayon cloth (Yoshikawa Chemical Co., YA-25-N, average fiber diameter 15 μm , average fiber length 2.5 mm, and average fiber density 1040 cm^{-2}) and rotated at maximum speed of 23 revolutions/s. The samples were unidirectionally passed twice under the cylinder at a translating speed of 2.2 mm/s. These parameters ensure a relatively high velocity of the rubbing cloth relative to the sample of approximately 510 cm/s. Zero rubbing strength is defined as the condition where sample and rubbing cloth are osculating and for higher rubbing strengths the distance of rubbing fiber and sample was reduced, thereby deforming the pile of the cloth. The bending depth of the cloth fi-

bers due to contact pressure¹⁷¹ was approximately 0.8 mm. For defined surrounding conditions, the rubbing machine was placed in a fume-hood and rubbing was done under a constant nitrogen flow.

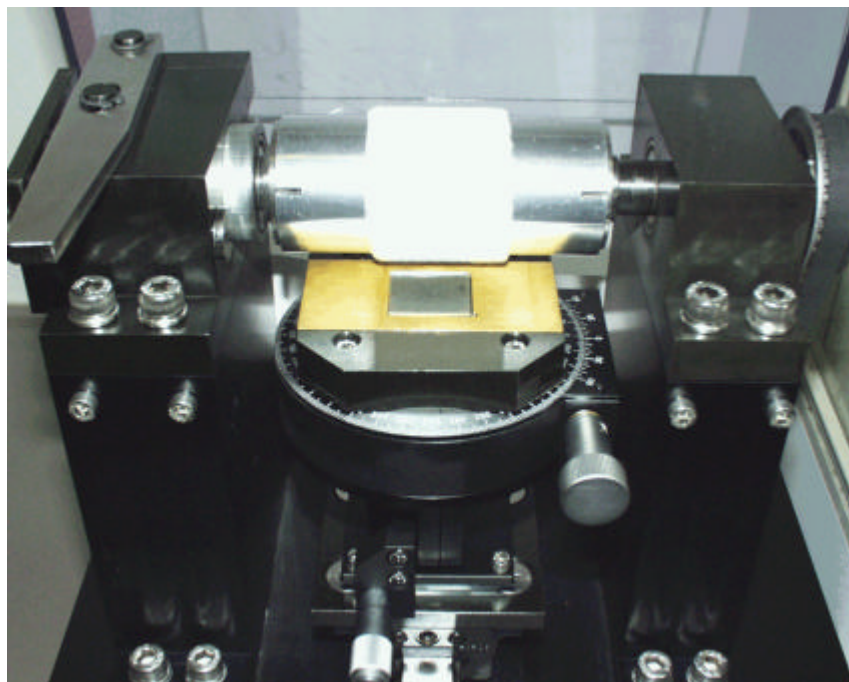


Figure 3.18. Picture of the rubbing machine.

Due to attrition effects, each rubbing cloth was changed after treatment of about 50 samples. The cloth was fixed with spray mount onto the rubbing cylinder guaranteeing homogeneous attachment. Thereby, the preferential direction of the rubbing fibers was chosen to be in line with the moving direction of the sample.

The effect of variation of these parameters and of the type of rubbing cloth (and also of attrition) on the alignment and on the morphology of the rubbed layers is described in section 5.2.5.

3.3.2 Annealing Setup and Procedure

Annealing was done in a home-built setup, which allowed for the defined control of the annealing procedure. An evacuable glass cover was equipped with a brass hot-table on which the samples were laid upon horizontally. After evacuation, the system was filled by means of a modulating valve with a defined amount of an inert gas of choice. The hot-table was directly heated through heating cartridges yielding a heating rate of the samples of more than 60 K/min. This high rate and the resulting large contact area between samples and hot-stage effectively shortened the total time the samples had to stay under high temperatures in order to achieve alignment.

A PT-100 temperature controller directly connected to one of the samples enabled the measurement of the exact sample temperature, and via a pressure sensor, the pressure of the annealing atmosphere was monitored during annealing. The glass tube allowed the illumination of the samples with an UV-lamp and by observation with a polarizer the *in-situ control* of the alignment. The cooling procedure was fastened by a constant gas flow induced by feeding of nitrogen through the modulating valve and simultaneous pumping with a rotary pump.

By way of this annealing system, the samples were heated under a 0.1 bar argon-atmosphere into the liquid crystalline state and after duration of approximately 10 minutes at constant temperature they were cooled down to room temperature at a rate of approximately 5 K/min. Although alignment can also be achieved in vacuum, the results are more reproducible when the annealing is done under 0.1 bar argon atmosphere. This is attributed to the better control of the temperature at the sample surface.

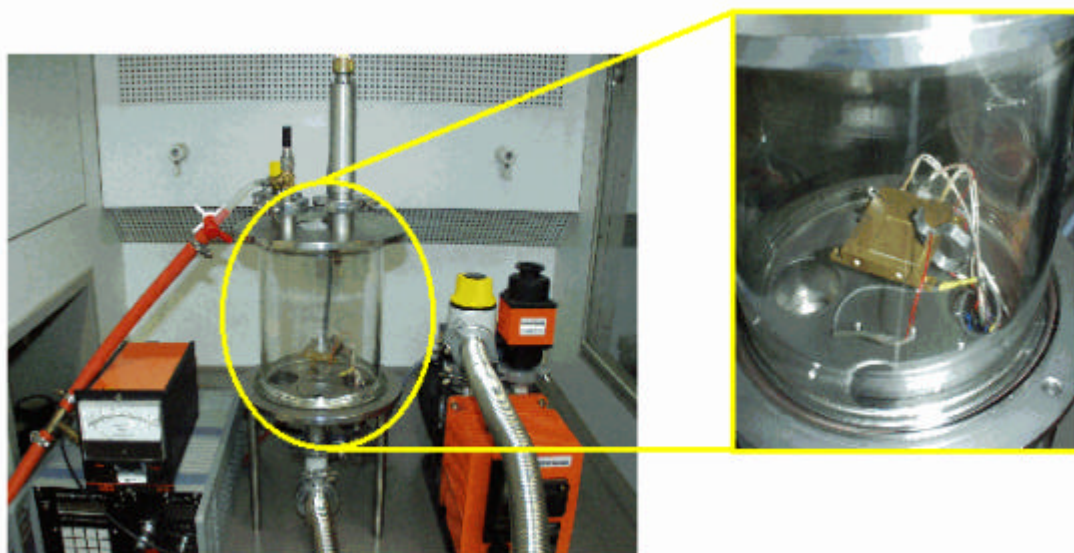


Figure 3.19. Picture of the annealing setup with a heating table under a glass cover, which can be evacuated and re-filled with a gas at choice.

3.4 Investigation of Optical and Electrical Properties of Materials

3.4.1 Recording of Electroluminescence Spectra

Electroluminescence spectra were recorded using the computer-controlled setup shown in Figure 3.20. The light emitted from the LED in the evacuated sample chamber is focused via an achromatic lens into the entrance-slit of a digital triple-grating spectrograph (Model 1235 from EG&G Princeton Applied Research), and detected by a photomultiplier (Model R928P from Products for Research, Inc.), in combination with a discriminator with fast time-resolution (Model 1182 from EG&G Princeton Applied Research). The generated output signal is evaluated by a computer, which also controls the Keithley 236 source measure unit to bias the devices.

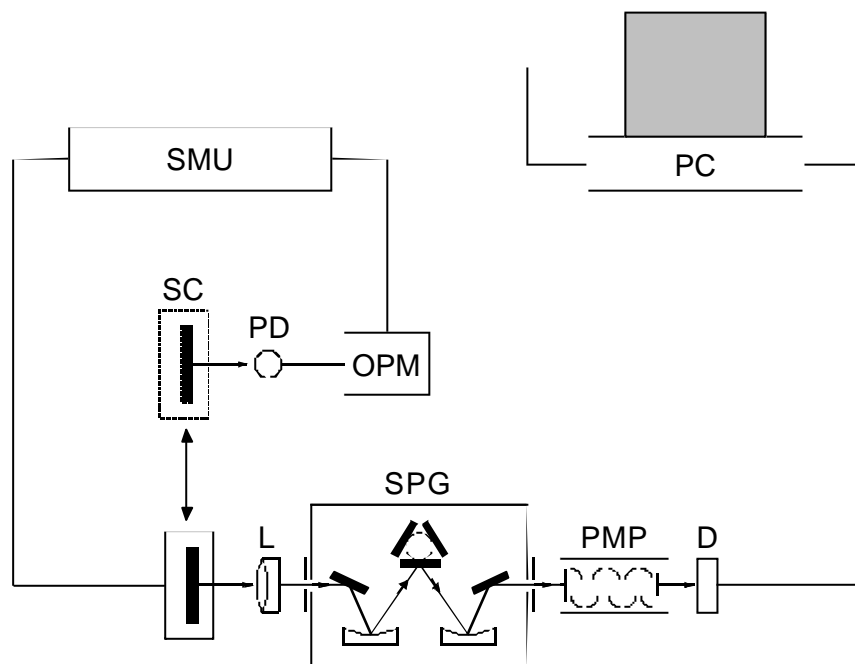


Figure 3.20. Computer-controlled setup for recording electroluminescence spectra with sample chamber (SC), achromatic lens (L), digital triple-grating spectrograph (SPG), photomultiplier (PMP), discriminator (D), and source measure unit (SMU). Alternatively, the setup can also be used for measuring the intensity of the electroluminescent devices at a wavelength of choice by means of the photodiode (PD) connected to the computer-controlled optical power meter (OPM) (section 3.4.5).

3.4.2 Determination of the Degree of Anisotropy – Polarized UV/Vis, Polarized PL, Polarized EL

The degree of anisotropy is described in terms of the dichroic ratio D in absorption and in terms of the polarization ratio P in emission. The determination of D has been carried out by means of polarized UV/Vis spectroscopy, and the ratios of P were deduced from polarized PL and EL spectroscopy, respectively.

Polarized absorption spectra were recorded with a Perkin-Elmer Lambda 9 UV/Vis spectrometer with a Glan-Thompson polarizer inserted into the sample beam. For each layer to be measured the spectra were recorded with light polarized parallel and perpendicular, respectively, to the direction of alignment. All spectra were corrected for the transmission of the substrates and of all additional present layers, and the polarization bias of the spectrometer was taken into account. To determine the dichroic ratios, the baselines of the spectra parallel and perpendicular to the rubbing were adjusted to similar height of the baselines in the region between 450–500 nm, followed by measuring the respective peak heights.

Polarized photoluminescence spectra were recorded with a SPEX Fluorolog 2 (F212) spectrometer, which was equipped with double monochromators for excitation and emission. The excitation wavelength was 380 nm and the light beam was incident to the film side of the samples. The detection was done at 90° with respect to the excitation light and 30° with respect to the surface normal. The polarization of the excitation was always parallel to the chain alignment of the samples. The spectra were recorded with analyzer position of 0° and 90° versus the excitation. The measurements were performed by Achmad Zen at the MPI for Polymer Research, Mainz.

Polarized electroluminescence spectra were obtained by inserting a Glan-Thompson polarizer parallel and perpendicular, respectively, between the electroluminescent device and the spectrograph described above. From the two resulting spectra, both the peak polarization ratio and the integral polarization ratio were determined, such that the polarization bias of the monochromator was always taken into account.

To eliminate errors resulting from inaccurate positioning of the polarizer, the polarization ratio was also determined by recording the electroluminescence intensity at fixed wavelength while constantly rotating the polarizer. From the maxima and minima of the resulting sine curve, both the polarization ratio at the respective wavelength and the time-stability of the polarization can be obtained. The device characterization was carried out in an evacuated sample chamber.

3.4.3 Luminance and Color Coordinates

The luminance and color coordinates in electroluminescence were measured by means of a Minolta Chroma Meter CS-100, a tristimulus colorimeter for non-contact measurements of light sources or reflective surfaces.

3.4.4 Film thickness determination

The film thickness was determined with a Tencor Alpha 200 surface profiler. A scratch was made into the respective layer and the resulting step profile was measured. The maximum resolution of the profile meter itself was 5 nm, but this value depends severely on the film quality and homogeneity.

For critical samples, the measurements were done on a computerized, highly sensitive KLA-Tencor P-10 surface profiler with the ability to measure micro-roughness with a nominal resolution of up to 1 Å over short distances.

3.4.5 Current–Voltage and Intensity–Voltage Characteristics

Current–voltage characteristics were recorded with a Keithley 236 source measure unit with a sensitivity of 10^{-13} A, and the internal voltage source of the electrometer was used to bias the devices. The intensity of the electroluminescent devices at a wavelength of choice was recorded simultaneously to the current measurements, using a Newport photodiode NP818-UV, which was connected to a Newport 835 Picowatt digital optical power meter (Figure 3.20). All measurements and recordings have been controlled by a computer, and the device characterization was carried out in an evacuated sample chamber.

3.5 Structure Investigations

Besides of the conclusions drawn from the UV/Vis absorption spectra, and from the spectra of PL and EL measurements, investigation of the structure and morphology of the samples were done by means of the following techniques.

3.5.1 Polarized Optical Microscopy

Polarized optical microscopy was performed on a Zeiss Axioskop 50. By means of polarization microscopy the degree of anisotropy may be determined by turning the samples between crossed polarizers. In case of high orientational order, a complete extinction is observed at every 90° stage rotation interval indicating the molecular director being parallel to one of the polarizers.

3.5.2 Low-Voltage Scanning Electron Microscopy (LVSEM)

All measurements were done with a LEO 1530 Field Emission Scanning Microscope with GEMINI field emission column for optimized resolution especially at low-voltage operation.¹⁷² The influence of the concentration of hole-transporting alignment layers in polyimide on the morphology was investigated in detail by means of low-voltage scanning electron microscopy, and therefore, this technique will be shortly explained (see section 5.2.4).

Electron microscopy is comparable to conventional light microscopy except that electrons rather than photons are used for image generation. Electrons are accelerated up to almost speed of light. Due to the high kinetic energy, the wavelength of the electrons is much smaller and the attainable resolution much higher than in the case of visible light. The electron beam is guided by magnetic rather than by 'normal' optical lenses and diffraction is due to the Lorentz force.

Scanning electron microscopy (SEM) is a powerful and generally applicable electron microscopic approach for the study of surfaces. In contrast to transmission electron microscopy (TEM) where investigations are restricted to replicas of surfaces, in particular fracture surfaces, SEM can be applied for samples of higher thickness. However, conventional electron microscopy methods are difficult to apply to polymers, and few techniques can be employed to produce contrast so that addressing fine surface details or determining the bulk microstructure is problematic. In general, polymers are vulnerable to beam-induced radiation damage and as non-conductors, they charge severely under the electron radiation. The accumulation of negative

charge results in the rejection of the electron probe in successive scans, since the incoming electrons do not drain away faster than they are supplied, as it is the case with conducting samples. The problems of charging and limited resolution can partly be solved by TEM, but the investigation of surface morphology is very difficult with TEM and the problem of beam-damage remains. Furthermore, TEM requires careful preparation of undeformed, ultrathin samples.

An efficient way to overcome these difficulties is the investigation of polymers by means of a field-emission gun source, high-resolution low-voltage scanning electron microscope (LVSEM). The image resolution is comparable to TEM, and information of high quality can be obtained from uncoated samples, even from those which could hardly be prepared for TEM. By adjusting the voltage the penetration depth of the electron probe can be varied. Thus, under favorable conditions information on both surface topography and composition as a function of depth can be acquired. The field-emission gun yields very high brightness and the electron probe can be focused down to the size of few nanometers while still maintaining enough intensity for sufficient signal levels. Due to the high probe intensity the signals are sufficient at very low accelerating voltages ($< 1\text{--}2$ kV), resulting in (i) higher resolution, (ii) insignificant beam damage of the samples, and (iii) the possibility to investigate the samples without conducting coating-films for elimination of beam-induced charging. Detailed descriptions of scanning electron microscopy can be found in the literature.¹⁷³⁻¹⁷⁶ All measurements were done in cooperation with Gunnar Glaser at the MPI for Polymer Research, Mainz.

3.5.3 Transmission Electron Microscopy (TEM) and Electron Diffraction

For all transmission electron microscope (TEM) observations, both the polyfluorene film and the underlying polyimide layer were floated off the supporting glass slide onto a water surface and transferred to 600 mesh copper grids. The films were examined in a LEO 912 TEM without carbon supporting film.¹⁷² In order to suppress inelastic scattering of energy losses exceeding 20 eV in case of electron diffraction and elastic darkfield imaging, an electron energy loss spectrometer was used which was integrated in the column of the TEM.

Electron diffraction patterns were recorded on photographic Ilford PAN F film and calibrated with TiCl_3 powder. The diffraction patterns were evaluated after tenfold magnification in a darkroom magnifier. The measurements were performed by Dr. Günter Lieser at the MPI for Polymer Research, Mainz.

3.5.4 Atomic Force Microscopy (AFM)

Atomic force microscopy (AFM) was done on a Digital Instruments Nanoscope IIIa multi-mode AFM.¹⁷⁷ The scanning was performed in tapping mode, with non-contact Cantilever NSC-12 from Silicon-MDT.¹⁷⁸ The measurements were recorded by Volker Scheumann at the Max Planck-Institute for Polymer Research in Mainz. The principles of atomic force microscopy will not be discussed in detail here, and the reader is referred to the literature. For example, an introduction into the application of AFM for the imaging of polymers was given by Sheiko.¹⁷⁹

3.5.5 X-Ray Diffraction

X-ray fiber diagrams were recorded in a vacuum flat film camera (Huber, Germany). The measurements were done by Michael Steiert at the Max Planck-Institute for Polymer Research in Mainz. The fibers were drawn from liquid crystalline polyfluorene melt (175 °C) and annealed at 175 °C for 4 h and 24 h, respectively.

4 Alignment of Polymers for the Use in Polarized LEDs

4.1 Polyfluorene

4.1.1 Alignment by means of Rubbed Hole-Transporting Alignment Layers

In the previous chapters we learned that the key issues towards the realization of blue polarized electroluminescence from polymers are, besides of a blue emissive polymer, the ability to (i) align this material into monodomains and (ii) to incorporate the aligned polymer into a light-emitting device structure.

One of the most promising materials with regards to these prerequisites is polyfluorene, which is described thoroughly in section 3.1.1. This is a blue emitting polymer with highly satisfying EL performance^{51,53,55} belonging to the class of thermotropic liquid crystalline polymers (LCPs). The latter are known to have the potential for aligning well on top of suitable alignment layers, as discussed in section 2.2.5. As mentioned in section 2.2.5, the alignment of thermotropic LCPs on top of alignment layers is in general accomplished by annealing of the material into the LC state and by subsequently 'freezing' the alignment into the crystalline or glassy state by rapid cooling. The primary requirements for the alignment in liquid crystalline state are (α) low viscosity in the mesophase and (β) low transition temperatures well below any transition temperature in the alignment layer.

In the case of polyfluorenes, the use of alignment layers is particularly promising – a finding explicable by the temperature-dependent X-ray powder diffraction shown in Figure 4.1. In the crystalline state at temperatures of $T = 30\text{ }^\circ\text{C}$ and $T = 50\text{ }^\circ\text{C}$, strong and sharp Bragg peaks are observed at $2q = 6.15^\circ$ and $2q = 10.7^\circ$. Here, the first value corresponds to the distance between adjacent polymer chains, which is approximately 14 \AA , while the second peak is related to the projected monomer length unit of $\sim 8\text{ \AA}$.¹⁸⁰ On the contrary, in the liquid crystalline state at $T > 160\text{ }^\circ\text{C}$, the respective peaks are substantially broadened, and the peak attributed to the distance between chains almost disappears. These features reveal a high dissimilarity between the crystalline and liquid crystalline state. While the former is characterized by a defined distance between the molecules, the latter shows a substantially lower degree of interchain order, pointing to an increased conformational freedom. The higher degree of disorder is also visible from the increase in the bandwidth of the second peak, indicating a smaller correlation length.

The observed substantial difference between the crystalline and liquid crystalline states indicates that the viscosity in the mesophase is quite small, satisfying condition (α). Also prerequisite (β) for alignment of polyfluorene in the LC state is fulfilled, since the polymers enter the mesogenic phase at easily accessible temperatures.

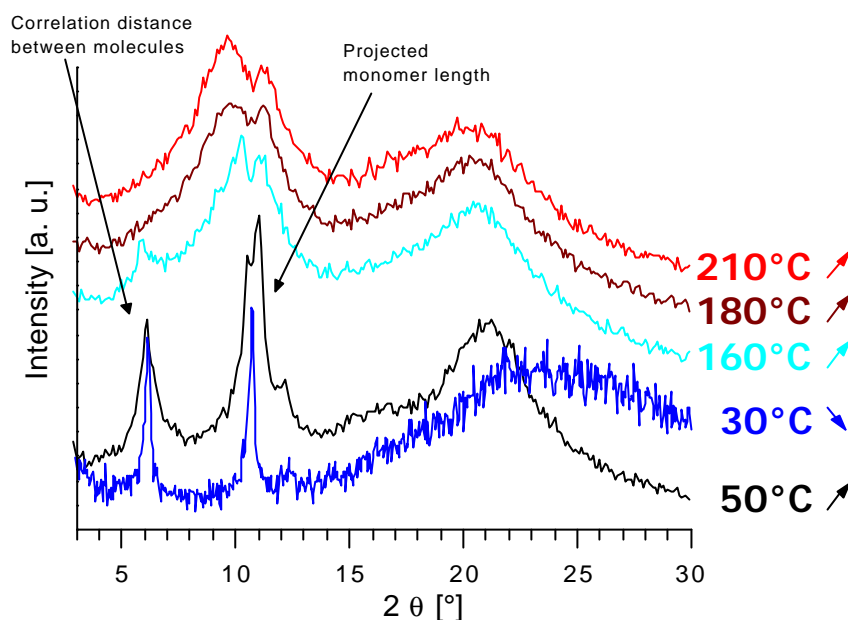


Figure 4.1. Temperature-dependent powder X-ray diffraction of poly(9,9-bis(2-ethylhexyl)fluorene-2,7-diyl). The arrows behind the temperature values correspond to heating (arrow up) and cooling (arrow down), respectively.

The first monodomain-alignment of polyfluorene was reported by Grell *et al.* who oriented poly(9,9-dioctylfluorene) (PF8) on top of alignment layers of rubbed polyimide.¹¹⁰ However, despite of the high suitability of rubbed polyimide as alignment layer, it does –when incorporated into typical LED structures as shown in Figure 1.2 – not allow for the required charge transport due to its insulating nature. Therefore, this approach does not fulfill condition (ii).

That problem was solved in our group by blending the polyimide with appropriate hole-transporting materials (HTMs) as described in section 3.1.4 and 5.2.⁴¹ By this approach, the ability of pure polyimide to yield transparent alignment layers of high chemical, mechanical and thermal stability⁹⁵ was combined with the capacity of the dopants for charge-transport. The extension of plain alignment layers to *hole-transporting* alignment layers (HTALs) with satisfactory charge transport characteristics (section 5.2) enabled the usage of polyimide within LEDs for the first time. We confirmed that charge transport via percolation is established at concentrations low enough not to suffer from the problem of phase-separation. Simultaneously, the doping does not noticeably affect the alignment strength known from pure polyimide as long as the dopant concentration is moderate (see following section). Moreover, the HTMs of choice are thermally stable up to temperatures of more than 300 °C, which is sufficient to withstand the temperatures required to convert the PI precursor. A typical homopolyfluorene, e.g.

poly(9,9-bis(2-ethylhexyl)fluorene-2,7-diyl) (PF2/6), is liquid crystalline at temperatures of ~ 167 °C, as shown in section 3.1.1.1 and Figure 4.1.

The incorporation of such rubbed HTALs of doped polyimide into light-emitting device structures and the successive alignment of polyfluorene on top turned out to be a successful concept for the realization of highly polarized blue electroluminescence. Dichroic ratios in excess of 16 and polarization ratios of more than 21 were obtained from such polarized LEDs. A comprehensive analysis of the corresponding devices is presented in chapter 6. Their fabrication was done according to the procedure explained in section 3.3.

4.1.2 Investigation of Alternative Alignment Concepts

In order to determine the best technique for the alignment of polyfluorene we also tested whether there are alternatives to (i) the rubbing and/or (ii) to the usage of the originally insulating polyimide.

Alignment of the polyimide by other means than by rubbing could avoid the problems of electrostatic charging and mechanical damage of the films, which may negatively affect the device performance.¹²⁸ Therefore, we examined layers of polyimide, which had been aligned by linearly polarized UV-light. As discussed in section 2.2.5.3, the temperature stability of photoaligned polyimide layers in general was problematic until now, and the layers used here were only stable up to temperatures of ~ 140 °C. For that reason, they could only be used for selected polyfluorenes with transition temperatures well below. Using e.g. a poly(9,9-bis(2-ethylhexyl)fluorene-2,7-diyl) endcapped with 9 mol% of bis(4-methylphenyl)phenylamine, which has a transition temperature of $T_m \sim 135$ °C, dichroic ratios in the range of 9 were obtained by means of photoaligned polyimide. However, compared to dichroic ratios of ~ 20 , which had been achieved with similar polyfluorenes on top of *rubbed* polyimide, the degree of alignment achievable by rubbing rather than by photoalignment is more than doubled (Figure 4.2). Apart from that, the majority of the polyfluorenes reach the LC phase at temperatures above 140 °C, and therefore, the doping and successive incorporation of such photoaligned polyimide into light-emitting devices was not examined.

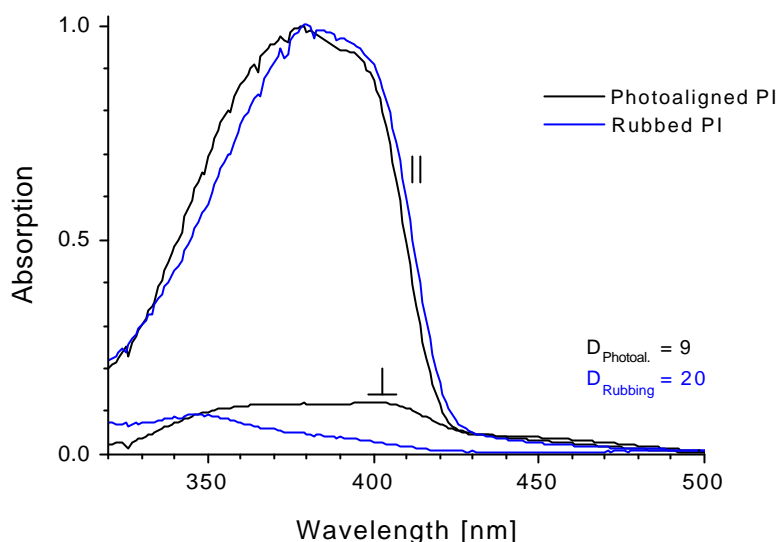


Figure 4.2. Polarized absorption spectra of poly(9,9-bis(2-ethylhexyl)fluorene-2,7-diyl) endcapped with bis(4-methylphenyl)phenylamine, aligned on *photoaligned* PI and on *rubbed* PI, respectively (on top of glass substrates). The spectra are recorded with polarization parallel and perpendicular to the direction of rubbing. The numbers given in the figure correspond to the dichroic ratio D .

The need for doping with charge-transporting materials and the concomitant problem of phase-separation could possibly be circumvented by replacing the aligning matrix of insulating polyimide by an inherently conductive material. Therefore, we investigated the alignment strength both of rubbed PEDOT-PSS^{13,169} (section 3.1.6) and of various rubbed derivatives of cross-linkable N,N' -bis(3-tolyl)- N,N' -diphenyl-benzidine (TPD)¹⁸¹ all common as hole-conducting materials.

The alignment of polyfluorene was tried on top of such rubbed layers, with sample configuration and preparation similar to the experiments with rubbed polyimide. However, no measurable degrees of alignment were achieved by means of these rubbed hole-transporting layers – neither with rubbed PEDOT-PSS nor with rubbed TPD-derivatives. One possible reason for this could be that the PEDOT-PSS layers themselves are aligned, but that the alignment ability is not sufficient to orient the liquid crystalline polymer on top. On the other hand, the PEDOT-PSS layers might not exhibit any preferential alignment after rubbing, which can be explained by an only weak correlation between neighboring chains or an amorphous structure.

Apart from the methods described above, which all included the use of hole-transporting alignment layers, it was tested whether there are also substantially different methods allowing for the orientation of polyfluorene within an LED structure. As discussed in section 2.2.2, alignment is also conceivable by directly rubbing the emissive layer itself – this would avoid the need of any additional alignment layer from the beginning. Applying the direct rubbing technique to various kinds of polyfluorene did not yield any degrees of alignment, however. This is in contrast to other conjugated polymers, such as poly(phenyleneethynylene)s (PPEs), which are described below. An explanation of this is given in section 4.2.

Attempts to further enhance a given orientation of polyfluorene (after the alignment on top of rubbed HTALs) by a subsequent treatment with another alignment technique were not effective. Polyfluorene spincoated on top of a rubbed HTAL was exposed to the magnetic field of a 7 Tesla NMR magnet, since magnetic fields can induce high degrees of order.⁸⁷ (Attempts to align polyfluorene solely by the magnetic field, without the use of an alignment layer, did not yield any alignment.) The dichroic ratio resulting from this treatment was ca. 16, identical to samples without additional magnetic field influence. This demonstrates that in the case of polyfluorene even strong magnetic fields do not affect the alignment properties of the material.

Likewise, the subsequent rubbing of polyfluorene, which had been aligned on top of rubbed polyimide, did not further increase the degree of alignment. Instead, mechanical damage of the films and a concurrent decrease of the orientational order were observed.

Concluding these investigations, it was shown that the usage of hole-transporting alignment layers of rubbed polyimide upon which the emissive material aligns when being annealed into the liquid crystalline state is not only a successful, but also the only method until now to induce monodomain alignment of polyfluorene. Other techniques of polymer alignment presented in chapter 2.2 were shown not to be appropriate for polyfluorenes.

4.1.3 Optimization of the Nature of Side-Chains

The nature of the side-chains of a liquid crystalline polymer has a major impact on the characteristics of the material, e.g. on the solubility and on the phase transition temperatures.¹⁸² To investigate their influence on the alignment behavior, polyfluorenes with different types of alkyl side-chains (Figure 4.3) were aligned on top of rubbed polyimide layers and evaluated with respect to the achieved degrees of alignment. Not only the length of the chains was varied, but also linear side-chains were compared with branched ones. In addition, a combination of side-chains was studied by means of the copolymers PF8/1/1/C2/6 and PF4C12. For convenience, the essential properties of these polyfluorenes are summarized in Table A.3, Appendix A.3.

Our investigations started off from poly(dioctylfluorene) PF8 ($M_n = 150\,000$ g/mol, $PD = 2.0$), which is a polymer with good solubility and easily accessible transition temperature for melting of ~ 174 °C. Furthermore, this type of polyfluorene is known for good alignment properties since the first report of its monodomain alignment by Grell *et al.*¹¹⁰ As can be seen from Figure 4.4, PF8 was aligned on top of rubbed polyimide showing a dichroic ratio of $D = 9$, consistent with numbers reported in the literature.¹¹¹

The figure also shows that the highest degree of order was obtained from PF2/6. The dichroic ratio, $D = 16$, was almost doubled compared to PF8. PF2/6 is substituted with ethylhexyl side-chains, having the same number of carbon atoms as the octyl-substituents in PF8, but in branched conformation. The transition temperature of 167 °C is even lower than the one of PF8.

The slightly shorter but symmetric propylpentyl side-chains of PF3/5 yielded a dichroic ratio of 12, which is higher than the ratio obtained for the linear octyl and lower than for the branched ethylhexyl chains. The molecular weight of this polymer was $M_n = 32\,000$ g/mol with a polydispersity of $PD = 1.84$. Due to the bulky structure of the side-chains, the transition temperature was with 195 °C significantly higher than that of PF2/6.

The negative effect of increasing the side-chain length on the degree of alignment has further been established in the case of the copolymers PF8/1/1C2/6 ($M_n = 173\,000$ g/mol, $PD = 1.66$) and PF4C12 ($M_n = 129\,000$ g/mol, $PD = 1.65$). For the former, a content of only 10 % dimethyloctyl side-chains reduced the dichroic ratio from 16, which had been obtained for the pure ethylhexyl polyfluorene, to a value of $D = 13$. In the presence of extremely long side-chains, almost no alignment was obtained. For the copolymer PF4C12, which contains long dodecyl side-chains at a content of 50 % (softening temperature of ~ 152 °C), the dichroic ratio D was 3, only.

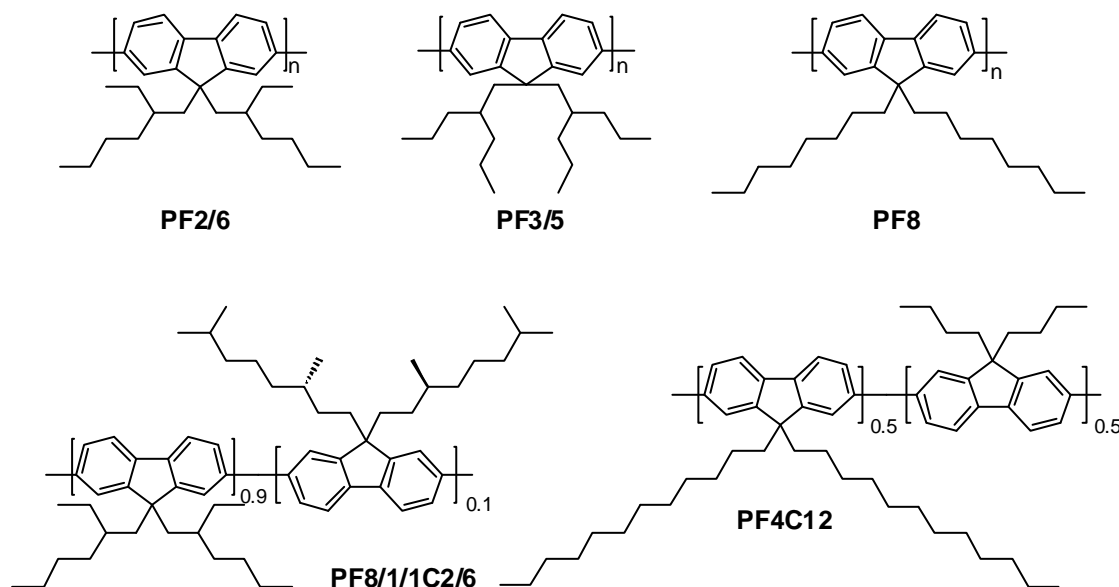


Figure 4.3. Chemical structures of poly(9,9-bis(2-ethylhexyl)fluorene-2,7-diyl) (PF2/6), poly(9,9-bis(2-propylpentyl)fluorene) (PF3/5), poly(9,9-bis(2-octyl)fluorene) (PF8), poly(2,7-(9,9-bis(2-butyl))co-(9,9-bis(dodecyl))fluorene) (PF4C12), and poly(2,7-(9,9-bis(2-ethylhexyl))co-(9,9-bis((3S)-3,7-dimethyloctyl))fluorene) (PF8/1/1C2/6).

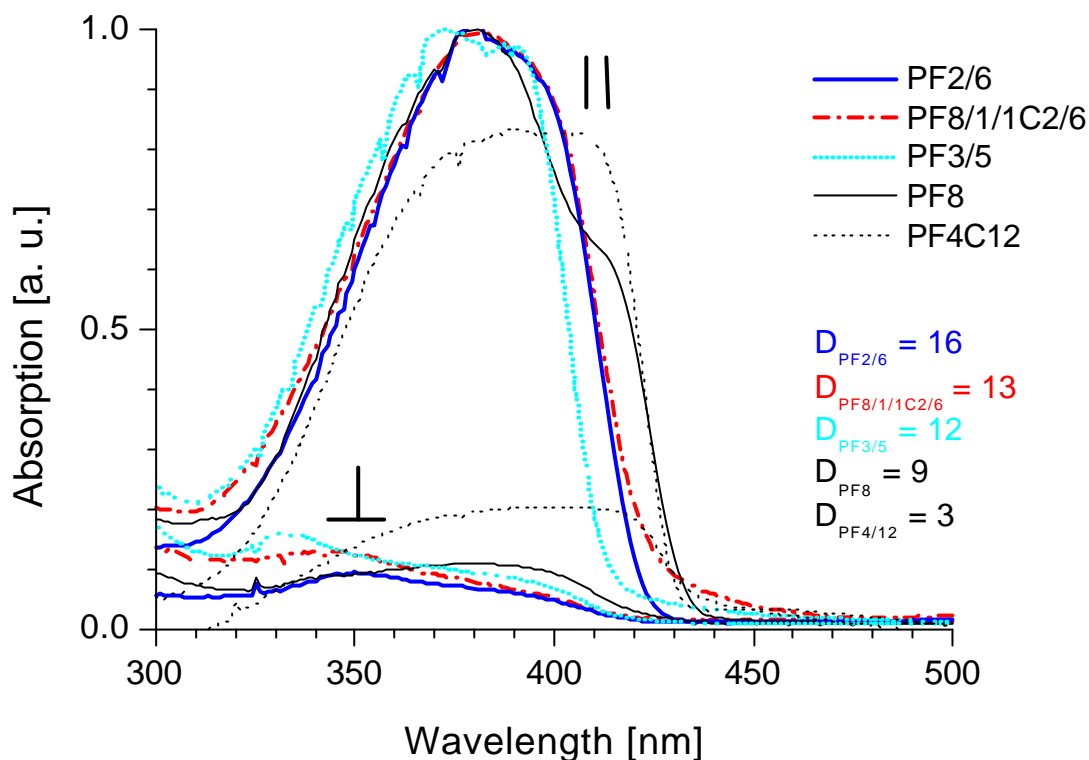


Figure 4.4. Polarized absorption spectra of polyfluorenes with different alkyl side-chains (shown in Figure 4.3) aligned on rubbed PI (on glass substrates). The numbers given in the figure correspond to the dichroic ratio D .

The variation of the nature of side-chains within polyfluorene clearly suggests that branched ethylhexyl chains are by far most favorable in connection with attainable degrees of alignment. Furthermore, the transition temperatures of PF2/6 are in a convenient region. This result is fully consistent with the theory of liquid crystalline polymers. As discussed in section 2.2.5.1, longer side-chains increase the solubility and flexibility of the polymer, the latter resulting in lower transition temperatures for melting and isotropization, respectively.¹⁸² However, the length and shape of the side-chains do also determine the diameter of the polymer (without affecting the persistence length) and hence the persistence ratio p (persistence length l_k /diameter d) (Equation 2.16). The achievable order parameter of a liquid crystalline polymer increases with increasing persistence ratio,¹⁸³ and thus the characteristics of the side-chains also crucially influence the alignment behavior of the material.

The phase transition temperatures of PF8 showed that straight side-chains with eight carbon atoms along the chain yield polymers with appropriate processing properties – in contrast to PF3/5 with shorter chains, resulting in high transition temperatures. However, the dichroic ratio of PF8 was rather moderate, $D = 9$, and opened room for optimization.

A successful approach was the replacement of the linear octyl side-chains by branched ones containing the same number of carbon atoms. The lower overall length of the side-chain leads to a lower effective diameter of the polymer molecule, whereas the Kuhn length of the molecule should not be affected. As a result, the persistence ratio of PF2/6 is noticeably increased, ex-

plaining the substantially higher order parameters compared to PF8. Moreover, the nature of the side-chains is such that the transition temperature is still in an easily accessible region, in contrast to PF3/5. Here, the chains are slightly shorter, but they also possess a more bulky structure than in the ethylhexyl chains in PF2/6. Therefore, the overall diameter of this polymer might be slightly larger and the persistence ratio lower than of PF2/6. Consequently, the dichroic ratio of PF3/5 is higher than for PF8, but lower than for PF2/6. However, a direct comparison of the dichroic ratios is critical, since the transition temperature of this polymer is larger than those of PF2/6 and PF8, and annealing has to be performed at considerably higher temperatures.

The very long dodecyl side-chains within PF4C12 obviously disturb the alignment properties significantly. This can be understood by considering the shape of the absorption spectra of the different polymers shown in Figure 4.4. With increasing length of the side-chains, the spectra display a shoulder between 420 and 440 nm. As demonstrated by Grell *et al.*, a strong correlation exists between the optical properties in absorption and the degree of local order.¹⁵³ These authors attributed the additional absorption peak to a planarization of the polymer conformation, and in case of PF8, a planar zigzag conformation was suggested for the well-ordered state. According to this, the polyfluorenes with very long side-chains apparently adopt a board-like planar structure, which goes along with an increased interchain interactions (*p-p*-stacking) unfavorable for alignment, explaining the observed decrease of orientation. These assumptions are consistent with studies by Teetsov *et al.* who established the effect of the alkyl side-chain length on the polymer interchain interactions in isotropic solid samples. They compared polyfluorenes containing short hexyl and long dodecyl side-chains, respectively. In the case of the long substituents, these authors also observed red-shifted fluorescence spectra, which they attributed to pronounced interpolymer aggregation.^{182,184} In chapter 5, the influence of the polymer structure on the alignment behavior will be further discussed.

4.2 Alignment of Poly(phenyleneethynylene)

In the previous section, we examined the influence of the chemical structure on the alignment behavior by comparing various polyfluorenes with different side-chain patterns. To extend these investigations, our aim was to study the orientational ability of another blue-emitting conjugated polymer, namely hexyl-dodecyl copoly(phenyleneethynylene) (PPE)⁸⁴ (Figure 4.5).

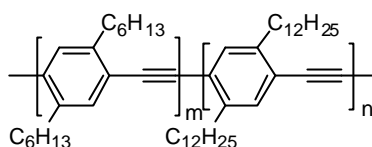


Figure 4.5. Chemical structure of hexyl-dodecyl copoly(phenyleneethynylene) (PPE).

In general, poly(phenyleneethynylene)s are known as rigid polymers¹¹³ with a strictly linear conformation, and similar to polyfluorene, PPE was shown to be a thermotropic liquid crystalline polymer.¹⁵⁸ This suggested to attempt the alignment of this polymer in the liquid crystalline state on top of rubbed polyimide layers.

However, in contrast to polyfluorene, no alignment was obtained. This finding can be understood by evaluating the differential scanning calorimetry (DSC) traces of PPE (Figure 4.6). The clearly defined transitions during the heating/cooling cycles correspond to isotropisation (190 °C) and LC phase formation (~170 °C),¹⁵⁸ respectively, as viewed by polarizing microscopy. Contrary, the enthalpy of the crystalline/LC phase transition at ~110 °C is evidently too low to be detected by DSC. This reveals high similarity between the two phases. Thus, even in the liquid crystalline state, PPE resembles its crystalline form, which is characterized by extremely high stiffness.^{113,114} These observations are supported by studies of the optical properties of films of PPE at different temperatures (not shown here). Both in the crystalline and liquid crystalline state, the spectra displayed a sharp peak at 440 nm (see also Figure 4.7). Along with the discussion in the previous section, this peak points to a planar, board-like backbone conformation,¹⁵⁹ which is not favorable for orientation on alignment layers. Therefore, it may be well understood that PPE could not be aligned on top of rubbed polyimide layers.

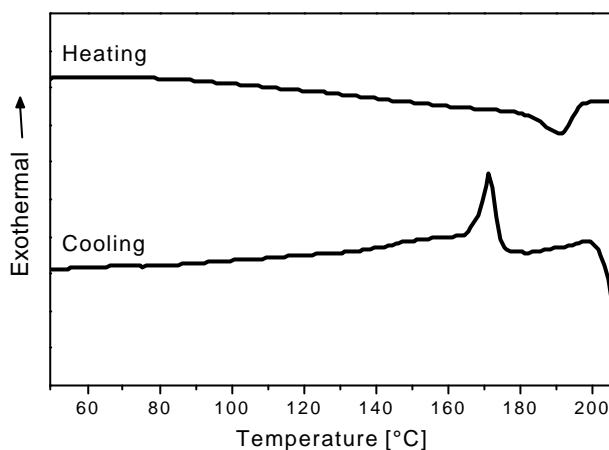


Figure 4.6. DSC-traces of hexyl-dodecyl copoly(phenyleneethynylene) (PPE).

However, in section 2.2.2 we stated that PPE can be aligned by direct rubbing of the PPE layer itself. We showed that in contrast to the semi-rigid polyfluorene, the applied rubbing force can be well transformed to the rigid polymer backbone and high degree of alignment of the molecules can be induced. The direct rubbing of 150 nm thick crystalline layers of PPE with a smooth cloth led to a dichroic ratio of 12 at the absorption peak of 439 nm (Figure 4.7). When viewed by polarizing microscopy the directly rubbed films of PPE can be seen to consist of highly oriented crystallites (Figure 4.8).

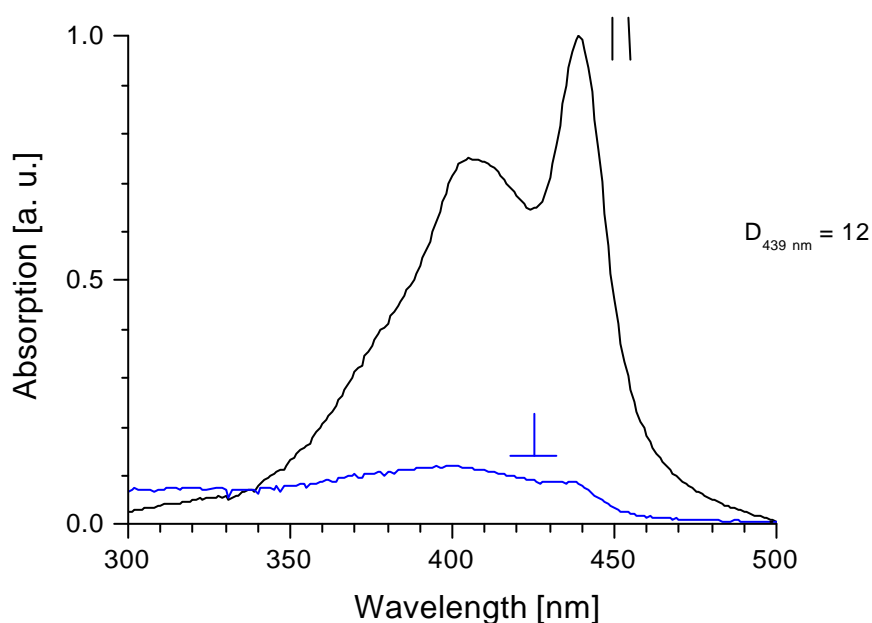


Figure 4.7. Polarized absorption spectra of PPE aligned by direct rubbing. The spectra are recorded with polarization parallel and perpendicular, respectively, to the direction of rubbing.

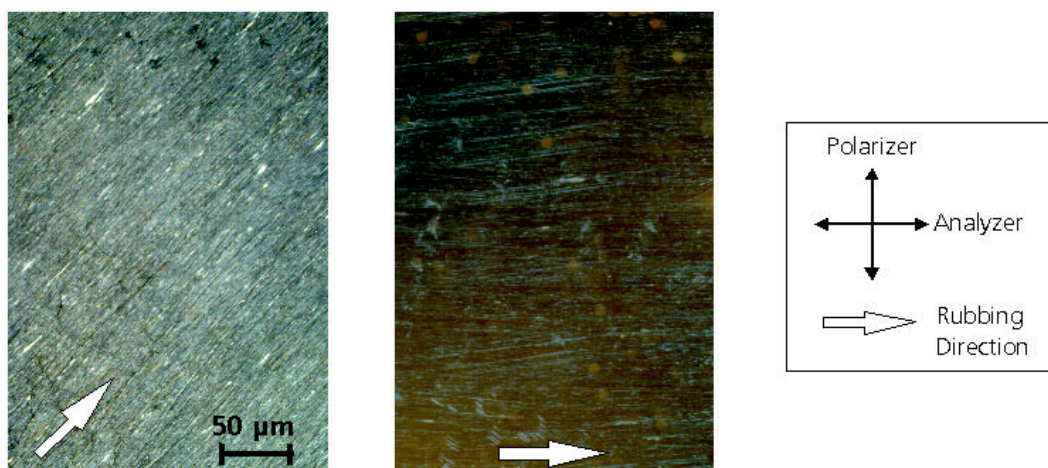


Figure 4.8. Directly rubbed films of PPE viewed under the polarization microscope (crossed polarizers, the arrow corresponds to the rubbing direction).

A polarized light emitting diode with rubbed PPE as emissive layer was successfully realized.⁸⁵ It was necessary to control the uniformity of the film thickness and to prevent erosion of the polymer from the substrate during rubbing. As discussed in section 2.2.2, this is a general problem of mechanical alignment by the direct rubbing technique. Covering the rubbed polymer with a 20 nm thick Li-surfactant layer helped to prevent electrical shorts due to mechanical destruction and additionally improved the injection of electrons. The hole-injection from the ITO into the polymer, which is characterized by a HOMO level of 5.8–6.3 eV²²⁷ was facilitated by a PEDOT-PSS layer between the anode and PPE. By this, a polarized LED with the structure ITO/PEDOT-PSS/PPE/Li-surfactant/Al could be fabricated.

However, the mechanical damage of the film was still severe and resulted in a relatively short lifetime of the device. Furthermore, the achieved dichroic ratios were still substantially lower than the ones obtained from the alignment of polyfluorenes in the liquid crystalline state. For these reasons, these devices – although being of scientific interest – will not be further discussed in this work.

Concluding the results of this chapter, we found that in case of polyfluorene, the only technique to obtain high degrees of orientation was the alignment in the liquid crystalline state on top of suitable alignment layers. Furthermore, comparison of polyfluorenes with different side-chain patterns revealed that the highest degrees of orientation were obtained for PF2/6 with ethylhexyl substituents. As an alternative to polyfluorenes, the alignment behavior of PPE was investigated, showing that orientation could only be induced in the crystalline state by direct rubbing rather than in the LC state on top of alignment layers. However, the results for PPE were not comparable with the ones obtained for PF2/6, and therefore, only the latter polymer will be discussed in the following.

5 Morphology, Structure and Properties of Polyfluorene and Alignment Layers

In the following chapter we present detailed information on the morphology and on the structure of the two essential layers required for polarized electroluminescence. On the one hand, it was of fundamental interest to find explanations for the differences observed for PF2/6 and PF8 concerning the alignment behavior and the absorption characteristics, which are attributed to the polymer conformation. On the other hand, the studies concerned the hole-transporting alignment layers based on doped polyimide. The respective layers were investigated by means of optical and electron microscopy, and by electron- and X-ray diffraction.

5.1 Polyfluorene

5.1.1 Alignment Behavior of Polyfluorene

We found that for polyfluorenes with a given side-chain pattern, the primary factor influencing the alignment behavior is their molecular weights.

In principal, the molecular weight determines the phase transition temperatures for melting and isotropization.⁹⁹ Therefore, studies of polyfluorenes with different molecular weights were carried out with the aim of shifting the transition temperatures into easily accessible regions. We confirmed that lower molecular weights result in a decrease of the transition temperature, which allows for a reduction of the annealing temperatures during the alignment procedure. This has a positive effect on the device performance, since the latter suffers severely from high temperatures.⁸ However, apart from its effect on the thermal behavior, the molecular weight was shown to crucially determine also the alignment ability of the polymers.

To study the correlation between these two factors in detail, poly(9,9-bis(2-ethylhexyl)fluorene-2,7-diyl) (PF2/6) was fractionated into five portions of different molecular weights with low polydispersity (*PD*). The aforementioned decrease of the melting temperatures with decreasing molecular weights becomes apparent from the DSC traces of the fractions, which are shown in Figure 5.1. Comparing the peak positions of the transition from crystalline to liquid crystalline state reveals a remarkable shift of 10 K from 174 °C for the fraction with the highest number average molecular weight of $M_n \sim 373\,000$ g/mol to 164 °C for the fraction with the lowest molecular weight of $\sim 62\,000$ g/mol (Table 5.1).

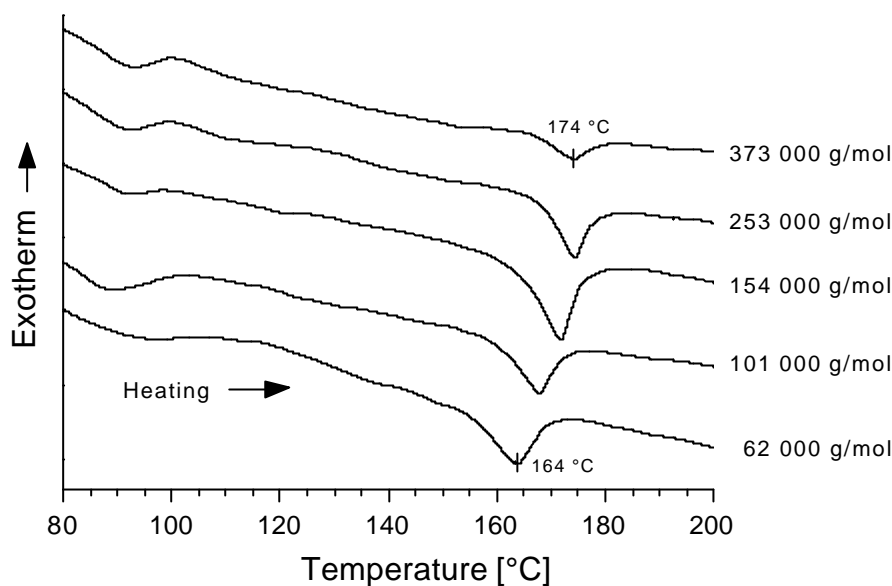


Figure 5.1. DSC-traces of poly(9,9-bis(2-ethylhexyl)fluorene-2,7-diyl) (PF2/6) fractionated into portions of different molecular weights and low polydispersity (first heating scan). The molecular weights given in the figure correspond to the number average molecular weight M_n .

In order to compare the dependence of the alignment behavior on the molecular weight, material of each fraction was annealed on top of rubbed polyimide and investigated by means of polarized absorption spectroscopy as well as by electron diffraction. As shown in Table 5.1, the alignment of polyfluorene is aggravated with increasing molecular weight, until at a certain point, no macroscopic orientation is achievable at all. The data that was obtained from polarized absorption spectroscopy, demonstrates that an upper limit for macroscopic alignment is in the range of $M_n \sim 100\,000$ g/mol. The corresponding dichroic ratio was ~ 16 , and with the lower molecular weight of $\sim 60\,000$ g/mol, a slightly higher ratio of $D \sim 17$ was obtained. Conversely, annealing the fractions with $M_n \sim 150\,000$ g/mol resulted in a dichroic ratio as low as ~ 2 , and molecular weights exceeding this value did not yield any measurable degree of macroscopic alignment.

Analysis of the electron diffraction patterns clarifies the observed behavior. As shown in Figure 5.2, the samples with number average molecular weight below $100\,000$ g/mol (lowest row in the figure) display distinct features indicating the high degree of alignment. In particular, the confinement of the arced meridian reflections, which represent the molecular orientation⁹⁶ establishes a very narrow orientational distribution and high degree of order. Especially the pattern of the sample with $M_n = 101\,000$ g/mol shows the sharp reflections, which are typical for highly oriented PF2/6¹⁸⁰ and which are discussed more thoroughly in the following section. The opposite is the case for the samples, which did not show any measurable macroscopic alignment (middle and upper row). The meridian reflection is much broader and difficult to observe, especially in the case of the samples with M_n of $373\,000$ g/mol and $154\,000$ g/mol, respectively. The samples are not completely isotropic, visible from the somewhat arced meridian

reflections in the pattern of the sample with M_n of 253 000 g/mol. This indicates molecular orientation on a local scale (the spot size in the electron diffraction experiments was ca. 2.7 μm in diameter). However, comparison with the polarized absorption spectra, which averages the molecular orientation across an array of ca. 5 mm^2 , shows that the alignment layers do not induce any preferential orientation in layers of high molecular weight fractions.

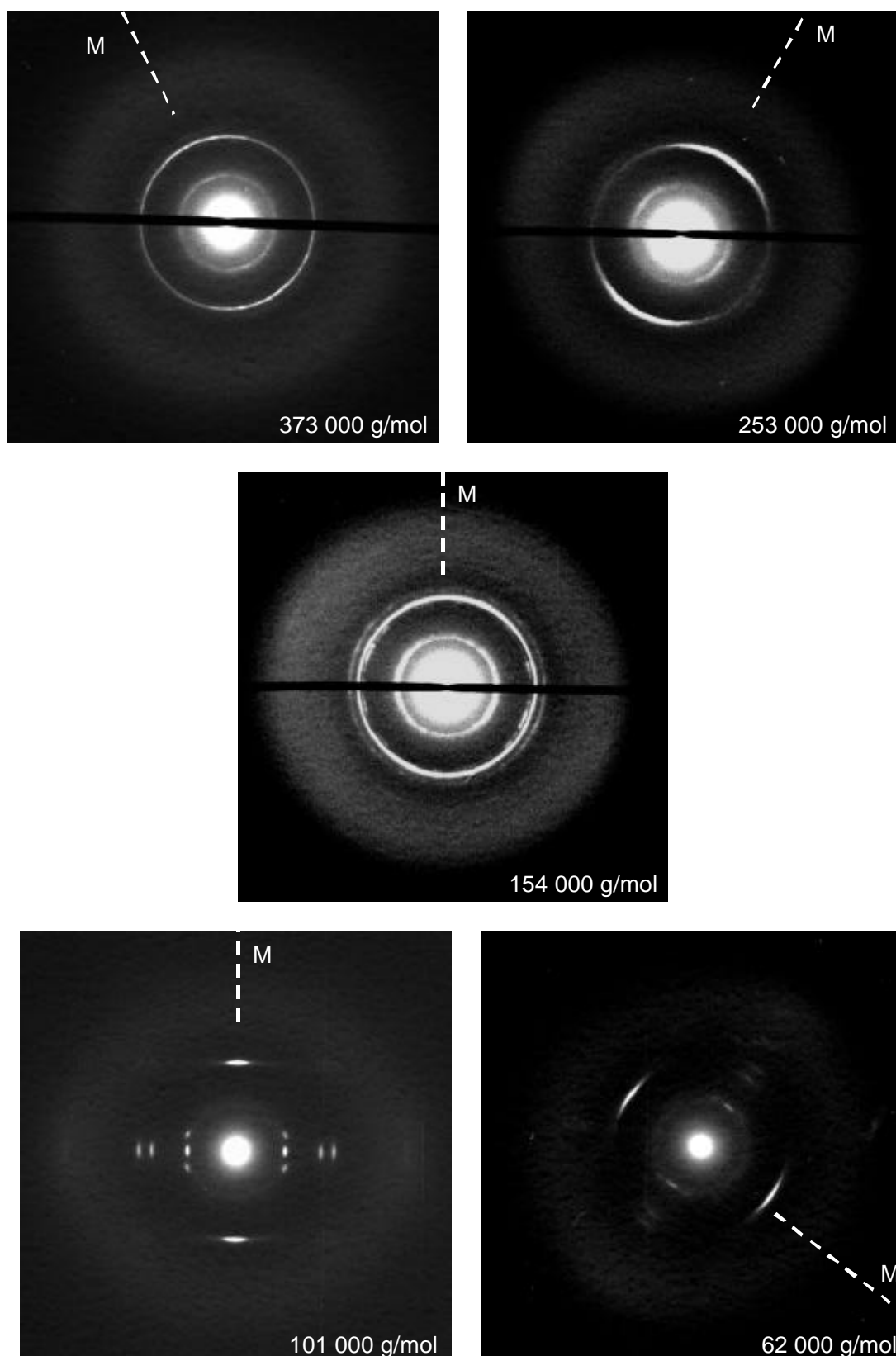


Figure 5.2. Electron diffraction patterns of different fractions of poly(9,9-bis(2-ethylhexyl)fluorene-2,7-diyl) (PF2/6) with varying molecular weight, which were oriented on top of rubbed polyimide. The patterns correspond to circular areas of the respective samples of 2.7 μm in diameter. The numbers given in the pictures correspond to the number average molecular weight M_n of the respective fraction. The dotted lines marked with 'M' correspond to the respective meridian direction.

The finding that the electron diffraction patterns of the samples with M_n of 101 000 g/mol and 253 000 g/mol show higher degree of order than the respective sample of next lower molecular weight can be explained by experimental restrictions. First, the patterns do not represent the whole area of the respective samples, but only a circular area of 2.7 μm in diameter, and the order recorded within these areas might deviate from the average macroscopic order. Furthermore, in the case of long exposure times during the measurement, very weak reflections may be overemphasized in relation to the stronger peaks, leading to diminished contrast and less distinct patterns.

Table 5.1. Influence of the molecular weight on the phase transition temperatures (determined from DSC-traces) and on the dichroic ratios D (determined from polarized absorption spectroscopy), respectively. The values are compared for plain poly(9,9-bis(2-ethylhexyl)fluorene-2,7-diyl) (PF2/6) and for different fractions with low polydispersity (PD) of PF2/6, respectively. The fractions were obtained from the batch of PF2/6, which is marked with a star. In addition, the respective values are also shown for the endcapped PF2/6am-X discussed in chapter 6, and the percentage given in the table corresponds to the endcapper/monomer feed ratio in mol%.

		M_n [g/mol]	M_w [g/mol]	PD	$T_{C@LC}$ [°C]	D
Fractionated PF2/6		373 000	455 000	1.22	174	1
		253 000	308 000	1.22	174	1
		154 000	212 000	1.38	172	2
		101 000	165 000	1.63	168	16
		62 000	138 000	2.22	164	17
Plain PF2/6		195 000	320 000	1.66	~172	10
		127 000	210 000	1.65	169	13
		111 000	247 000	2.22	169	~15*
		106 000	233 000	2.19	167	16
Endcapped PF2/6	2 %	103 000	146 000	1.41	165	>20
	4 %	48 000	75 000	1.55	157	>20
	9 %	12 000	31 000	2.57	135	>20

As shown in Table 5.1, high dichroic ratios of ~ 10 were achieved also for materials with $M_n \sim 200\,000$ g/mol, a molecular weight which is almost twice the value stated above as upper limit for alignment ability. This discrepancy is attributed to the higher polydispersity of the material, guaranteeing that also a relevant number of molecules with lower molecular weight are present. The results obtained for the fractions with narrow molecular weight distribution clearly indicate that it is exclusively the portions of low-molecular weight, which are accountable for the alignment.

Concluding from the findings described above, a low value of the molecular weight has a positive influence both on the transition temperature and on the alignment behavior of the respective polymer. However, from another point of view there exists a lower limit for reducing the molecular weight. Samples of very low-molecular weight form unstable films with high tendency to dewetting. Below a certain value, the characteristics of the material approach the ones of low-molecular weight compounds, which lack of the film forming properties of polymers. As a result, the EL performance is negatively affected. Thus, for optimized device performance the molecular weight should be low enough to yield low transition temperatures and high alignment ability, but sufficiently high to ensure good film quality of the samples. Further optimization of molecular weights of polyfluorene via the approach of endcapping, which is described in section 6.2 revealed that molecular weights of $M_n \sim 50\,000$ g/mol produced the best results – allowing for high alignment capability and convenient transition temperatures well below 160 °C, very good film forming properties, and very good EL performance.

5.1.2 Morphology and Structure of Aligned Polyfluorene

As mentioned above, high degrees of macroscopic order are observed after the alignment of films of PF2/6 on top of rubbed polyimide alignment layers. As shown in Figure 4.4, typical dichroic ratios at the absorption peak at 381 nm reach values between 15 and 17. The large difference between the absorption parallel and perpendicular to the rubbing direction points to a narrow orientational distribution and high degree of molecular alignment with the director. These findings are confirmed when viewing samples of oriented PF2/6 in the optical microscope between crossed polarizers. Figure 5.3 shows micrographs corresponding in size to the area of a typical light emitting diode of 0.05 cm². A complete extinction all over the films was observed at every 90° of stage rotation, when the direction of rubbing was exactly parallel to one of the polarizers. Apart from high orientation, these observations reveal a high degree of homogeneity and confirm the monodomain alignment of the oriented layers.

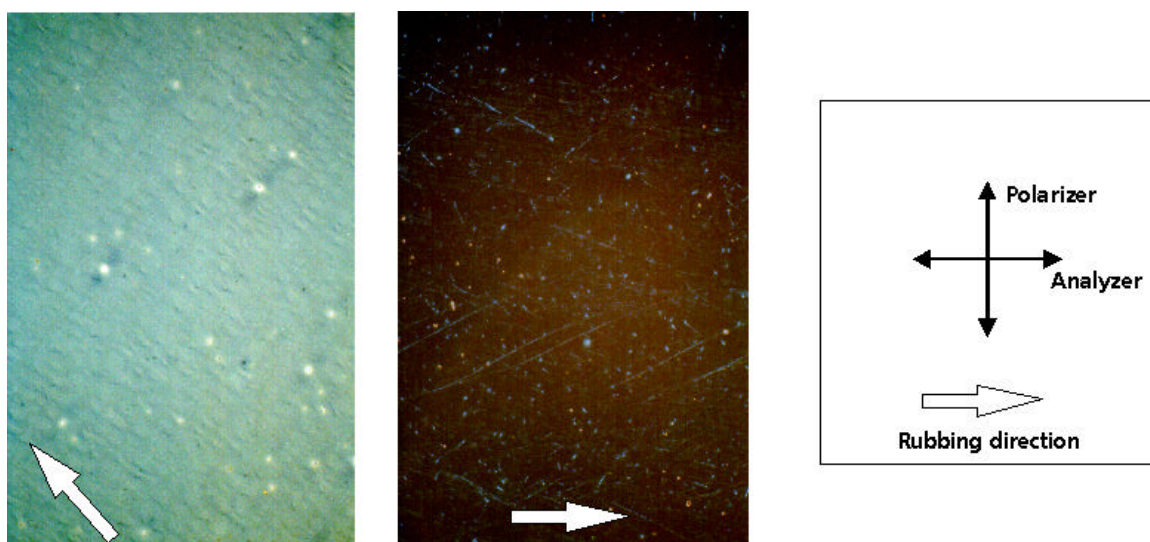


Figure 5.3. A film of PF2/6, which was aligned on top of a rubbed hole-transporting alignment layer of polyimide molecularly doped with ST 638, viewed in a polarization microscope (crossed polarizers, the arrows in the pictures correspond to the rubbing direction).

After considering the macroscopic alignment of PF2/6, several questions remained to be clarified. Of foremost interest was to find an explanation for the finding that the degrees of orientation attained for PF2/6 were considerably higher than for PF8. As described in section 4.1.3, the dichroism barely exceeded 10 for PF8,¹¹¹ whereas $D > 15$ had been achieved for PF2/6. Another important question addressed the observed differences in the absorption spectra of PF2/6 and PF8. As mentioned above, the spectrum of well-ordered PF8 displayed a sharp peak at 437 nm, which has been assigned by Grell *et al.*¹⁸⁵ to a planar zigzag conformation (2_1 helix) of the oriented polymer. This peak was not observed in the spectrum of PF2/6. In search of possible answers to these problems, studies on the conformation and packing of PF2/6 were carried out. Films of highly oriented PF2/6 were investigated by means of optical microscopy, by transmission electron microscopy (TEM) and by electron diffraction.¹⁸⁰ The work described in the following section was done in collaboration with Dr. Günter Lieser, who worked at the Max Planck-Institute for Polymer Research in Mainz.

5.1.2.1 Morphology of Aligned Polyfluorene

To learn about the morphology of aligned polyfluorene films, we first examined TEM darkfield images of highly oriented PF2/6, as shown in Figure 5.4. The aligned films were prepared by spincoating PF2/6 on top of rubbed polyimide alignment layers and by subsequent annealing at 175 °C for 2 hours under inert atmosphere. The final film thickness of the layers was 30 nm for polyimide and 20 nm for PF2/6, respectively.

The films are polycrystalline at room temperature. In the darkfield micrograph from elastic scattered electrons (Figure a), we observe bright bands (attributed to well-ordered areas), which

are interrupted by relatively long black stripes crossing perpendicular to the direction of rubbing. The lateral extension of the bright bands exceeds the bandwidth between the stripes by far. These features are common for hairy-rod molecules and they can be explained in close analogy to partially crystallized polymers.¹⁸⁶ Accordingly, the bright bands are read as ordered lamellae, whereas the black stripes correspond to disordered areas interrupting these ordered regions. In general, we believe that the lamellae are formed in an early stage during the annealing. In the very beginning, the hairy-rod polymers are in an anisotropic melt and start to adopt parallel orientation. With increasing dwell time during the stay in the liquid crystalline state, the lamellae gradually take shape. Inside of the lamellae the chains are oriented more or less perpendicular to the lamella surface. The lamella thickness strongly depends on the chain length,¹⁸⁶ and due to the chain length distribution (molecular weight distribution) of the polymer the surface of the lamellae in this stage is rough. However, in a later stage of annealing, the molecules inside the lamellae domains start to segregate with regards to their chain lengths and the shorter chains get expelled toward the lamellae ends. The structure of the lamellae becomes more regular and wedge-shaped. This demixing of chains in previously investigated lyotropic and thermotropic samples was associated with annihilation of disclinations in the director fields of the liquid crystals. In the case of PF2/6 the oriented polyimide substrate prevents the formation of similar singularities or accelerates their annihilation. The unique and homogeneous orientation of PF2/6 over large areas is favored by 'graphoepitaxy',¹⁸⁷ the oriented growth on structured surface patterns.¹⁸⁰

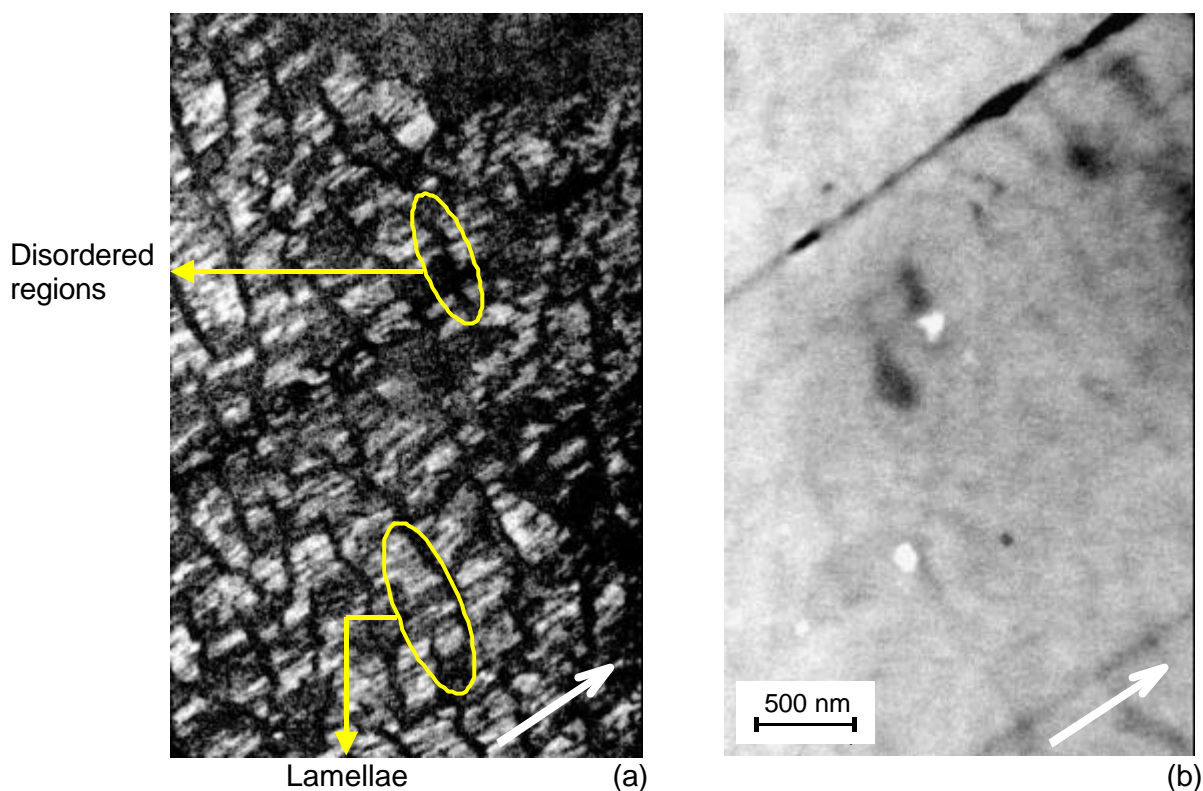


Figure 5.4. Electron micrographs of an oriented PF2/6 film. (a) dark field image in the light of the 00.5 reflection; (b) mass thickness distribution in the same area by an inelastic darkfield image at an electron energy loss of 100 eV. The white arrow corresponds to the direction of rubbing, and the scale is the same for both pictures.

The micrograph in Figure 5.4a shows that the current sample indeed passed through both of the two mentioned stages of annealing. The ordered lamellae, which were formed in the mesophase and fixed by the subsequent crystallization during cooling to the ambient are clearly visible as the bright band-like domains. The annealing time of 2 hours obviously was sufficient to reach the second stage of annealing, during which the chains segregate according to their lengths, rendering the lamellae wedge-shaped. In the thicker parts of the lamellae, the degree of polymerization of the respective chains is ~ 300 , whereas in the ends of the wedges this number is reduced to < 100 , in agreement to molecular weight measurements. In the regions outside of the lamellae, which are imaged in the darkfield as the black lines, the end groups of the main chains are concentrated. The end groups and the residual disorder as a result of the chain length distribution prevent the formation of crystalline order and thus explain the disorder within these interlamellar regions.

From the significant disturbance of the film continuity, which is seen in the elastic darkfield image one might presume that the films are also disrupted by the disordered interlamellar areas. However, electron microscopy with inelastic scattered electrons reveals that this is not the case. By this technique, the mass distribution of the film is emphasized. The darkfield image shown in Figure 5.4b demonstrates the relative uniformity of the films. The few lines perpendicular to

the direction of rubbing, which are darker than the image on average correspond to the inter-lamellar disordered regions also seen in the elastic darkfield image.

The observed pronounced formation of ordered lamellae and demixing of chains according to their lengths with prolonged stay in the mesophase might suggest that the degree of *macroscopic* alignment and the homogeneity of the films could also be enhanced by further increasing the annealing time. In order to investigate the validity of this speculation, samples annealed for different amounts of time were compared with regards to the obtained alignment and morphology.

Figure 5.5 shows polarized optical micrographs of two samples of PF2/6 on top of rubbed polyimide, which had been annealed for 1 hour and 4 hours, respectively. In comparison to the sample annealed for 1 hour, the polycrystalline morphology of the film treated for 4 hours was characterized by highly pronounced boundaries between the oriented crystallites. With values between 30 and 50 nm, the height of these edges even reached the range of the film thickness. Moreover, it turned out that for both of the samples the dichroic ratios was $D > 20$ and thus, the maximum achievable degree of macroscopic alignment was attained already by the short thermal treatment.

These findings were supported by experimental observations as well as by temperature dependent X-ray diffraction patterns of fibers with different thermal histories. When watching the films under UV light with a polarizer during the annealing procedure, it was observed that macroscopic alignment occurs within the first minute after passing the transition temperature without being further enhanced by longer annealing times. Looking at the behavior of corresponding fibers of PF2/6, we found that annealing for 3 minutes even yielded essentially the same degree of alignment as it was obtained by annealing for 1 hour (Figure 5.6).

Keeping in mind that the performance of LEDs suffers from the exposure to high temperatures, the time of annealing should be kept as short as possible. However, we regarded duration in the range of 12 to 15 minutes as optimum annealing time – definitely ensuring macroscopic alignment but also enabling a certain degree of further arrangement of the chains within the formed lamellae.

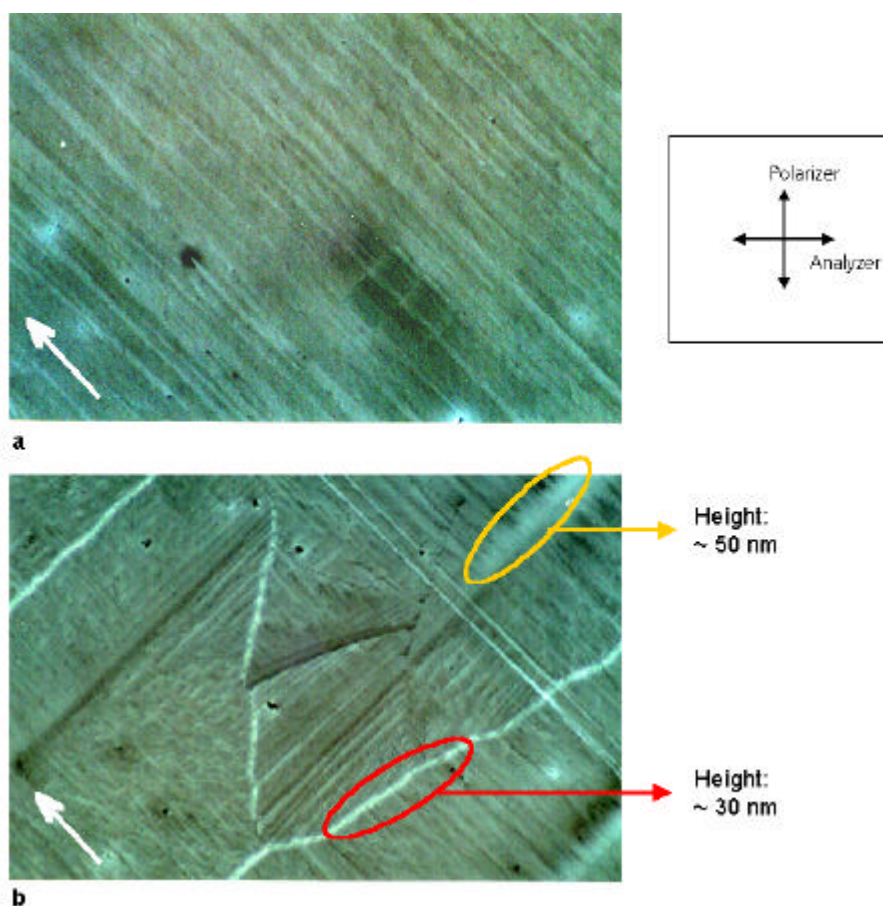


Figure 5.5. Polarized optical micrographs of PF2/6 films (thickness 90 nm) on top of rubbed polyimide alignment layers. The time of annealing at a temperature of $\sim 175^\circ\text{C}$ was 1 hour (a) and 4 hours (b), respectively. The white arrow in the picture corresponds to the direction of rubbing. Both of the two samples showed a dichroic ratio of $D > 20$.

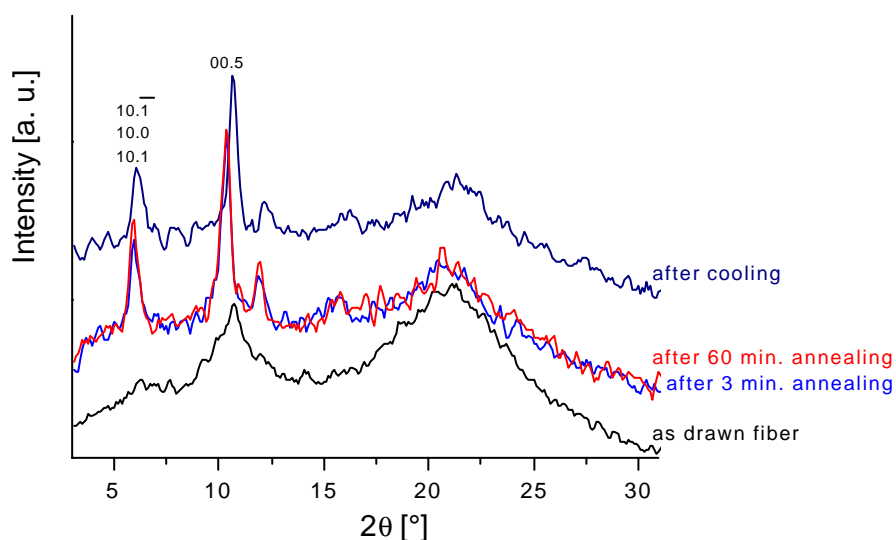


Figure 5.6. Temperature dependent X-ray diffraction pattern of fibers of PF2/6 with varying history of treatment.

In synthesis, we found that the morphology of oriented PF2/6 is characterized by highly ordered lamellae, which are interrupted by disordered regions. With prolonged stay in the liquid crystalline stage, a segregation of the wormlike molecules with respect to their chain lengths

takes place while the formation of the ordered lamellae proceeds. The shorter chains are pushed towards the lamellae ends and the lamellae thus become wedge-shaped. Within the disordered interlamellar areas, the end groups of the chains are assembled preferentially. Comparing annealing times of 1 hour and of 4 hours with respect to the achievable macroscopic alignment showed that longer times did not yield any further enhancement but rather stimulated the formation of boundaries between the crystallites. Since macroscopic alignment was observed to appear shortly after passing the melting temperature, the time of annealing found as optimum for EL applications was in the range of 12 to 15 minutes. This time guarantees macroscopic alignment and also a certain degree of chain arrangement in the lamellae, but simultaneously keeps the exposure to elevated temperatures relatively short.

5.1.2.2 Structure of Aligned Polyfluorene Layers

Electron diffraction opens a way to reveal the structure of highly aligned polyfluorene layers. Figure 5.7 shows an electron diffraction pattern of a PF2/6 film corresponding to the samples investigated by TEM and discussed in the previous section.

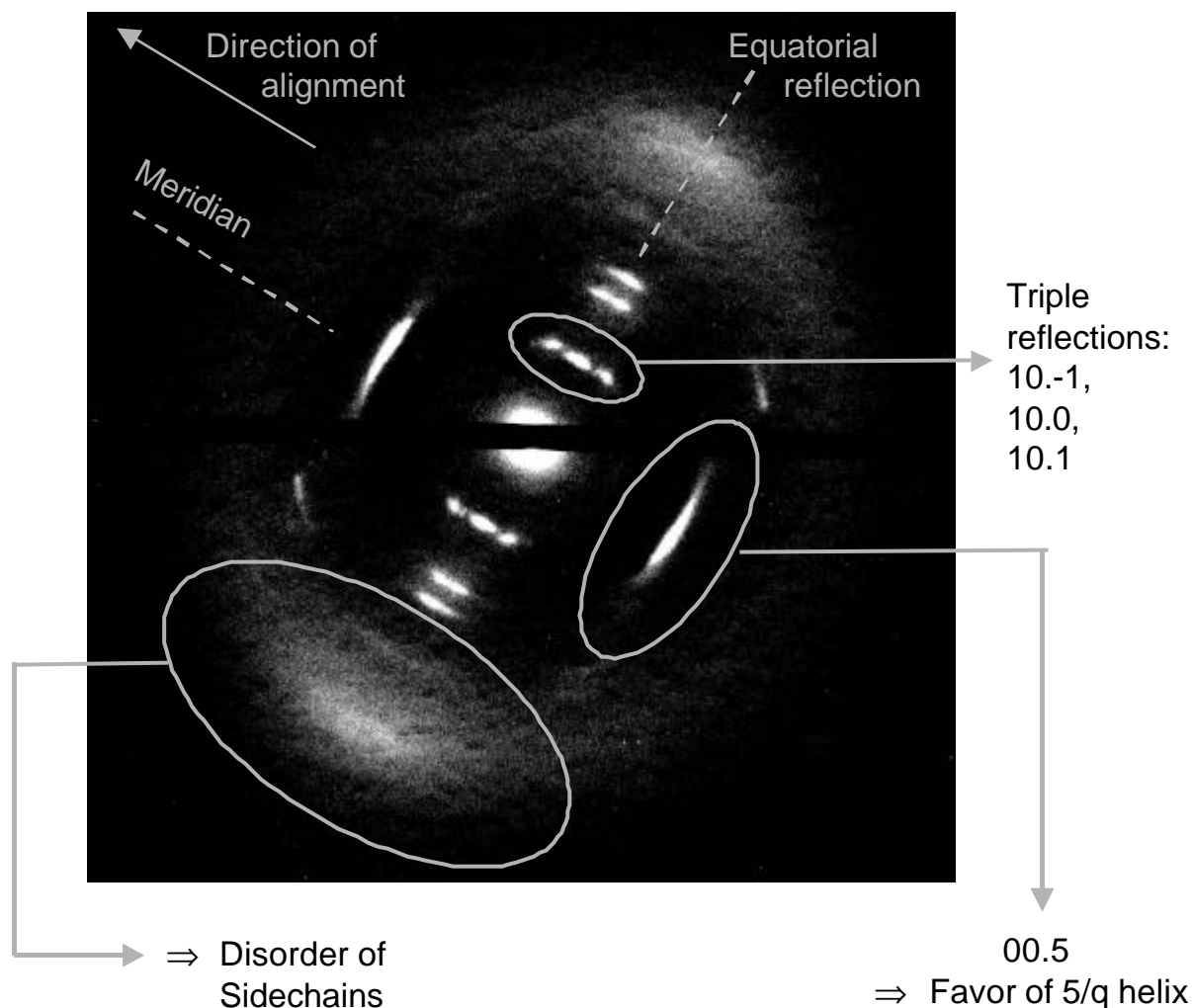


Figure 5.7. Electron diffraction pattern of PF2/6 oriented on top of rubbed polyimide from a circular area of 2.7 μm in diameter. The meridian and the equatorial directions are sketched as dotted lines. Also marked are the most predominant features of the pattern: the first triple reflections in equatorial direction, the arced reflections in the meridional direction representing the molecular direction, and the halo with sampling on the equator corresponding to the disorder of the aliphatic sidechains.

One of the most prominent features of the pattern is the strong confinement of the meridional reflections and their sickle-like shape. This is evidence for a narrow orientational distribution of the main chain orientation⁹⁶ and thus confirms the very high degree of molecular alignment (the dichroic ratio of the current sample was 15). That innermost meridional reflection is the 00.5 reflection and we observed that in the meridional direction, only reflections with Miller index $\ell = 5n$ (n integer) are visible. One can show that this favors a $5/q$ helix for the backbone conformation of the present polyfluorene (5 monomers perform q turns within a helix; see Figure 5.8).¹⁸⁰ From the diffraction data alone, the first choice of the q -parameter of the helix

would be $q = 1$. However, molecular modeling based on ab initio molecular orbital (MO) calculations have been carried out by Oda *et al.* with the aim to obtain independent information on the chain geometry and conformation.¹⁸⁸ Founded on the observed packing of the individual polyfluorene chains, these calculations give preference to $q = 2$ rather than to a 5/1 helix.



Figure 5.8. Molecular Modeling of oligo(25)-fluorene with $5/q$ helix. (Up): $q = 1$; (Down): $q = 2$. Structures are based on RHF/6-31G calculations of bi- and terfluorene. Ethylhexyl side chains were replaced by hydrogen.

The reflections in Figure 5.2 in the equatorial direction exhibit a sequence, which is characteristic for a unit cell of the hexagonal family. The striking triple of reflections in that direction corresponds to the reflections with the indices $\ell = \pm 1$ (10.-1 / 10.0 / 10.1) and define a first layer line. Concluding from the reflections of several electron diffraction patterns, the following preliminary data for the corresponding hexagonal unit cell of aligned PF2/6 were determined:

$$\begin{aligned} a = b = 16.7 \text{ \AA} & & \mathbf{a} = \mathbf{b} = 90^\circ \\ c = 40.4 \text{ \AA} & & \mathbf{g} = 120^\circ \end{aligned} \quad (5.1)$$

The texture of the film is fiber-like, which is confirmed by the invariance of the patterns upon rotating the sample around the molecular axis. This direction in real space corresponds to the direction of the meridian reflection in reciprocal space, implying orthogonality between the fiber axis and hexagonal base plane.

All electron diffraction patterns of the film are fully consistent to X-ray diagrams of fibers, which had been drawn from the melt and annealed in the liquid crystalline state (not shown here).

The diffuse halo with sampling in the equatorial direction is attributed to the disorder of the aliphatic side-chains, which surround the wormlike backbone of the main chain. This flexible and disordered side-chain shell around each individual polymer renders the viscosity in the solid state very low, explaining the much higher degrees of alignment obtained with these class of polyfluorenes in comparison to PF8 or poly(phenyleneethynylene) (PPE). PPE is a representative of the class of board-like systems,⁸⁷ which are a counterpart to the class of hairy-rods. The experiments discussed in section 4.2 as well as vague calculations suggest that these board-like

systems form smectic lamellar LC phases, in which the rotation around the triple bond is restricted. The conjugated backbone is characterized by a planar arrangement, and the polymer thus displays a sheet-like geometry with high stiffness and excessive viscosity even in the liquid crystalline state. PF8 with linear side chains might just present a mixed-character between hairy-rods and board-like systems, in which the bent monomer unit in conjunction with the rotational potential of the backbone favors a cylindrical *helical* conformation, while the linear side chains induce a *planar zigzag* backbone conformation in the solid state under certain conditions. This mixed characteristics could explain the observed lower degree of orientation of PF8 on alignment layers compared to PF2/6.

Concluding the structure investigations by means of electron diffraction, we showed that the individual polymer chains of PF2/6 have a cylindrical shape with hexagonal packing, in conjunction with a backbone conformation of almost linear structure of a 5/2-helix. The worm-like backbone is surrounded by a cylindrical shell of disordered side-chains, and the concomitant low viscosity explains the enhanced alignment behavior of PF2/6 in comparison to PF8 or PPE.

5.2 Alignment Layers

5.2.1 Basic Effects of Doping of Alignment Layers

As mentioned above, the alignment of the liquid crystalline polyfluorene emissive layers was accomplished by using alignment layers based on rubbed polyimide (PI). We also learned that in order to enable the utilization of these originally insulating alignment layers within polarized EL devices, the polyimide has been additionally doped with various hole-transporting materials (HTMs). In the following, the main characteristics of these doped alignment layers will be discussed.

We studied the influence of doping on the alignment properties of the layers. At first, we confirmed that doping of polyimide layers did not generally affect the mechanical stability of the polyimide, which is required for its alignment strength. Investigations of the layer morphology, which will be discussed in section 5.2.4, showed that at moderate filler contents the resulting blend films displayed no obvious signs of degradation or phase-separation after conversion. For such reasonable concentrations, the mechanical stability known for the pristine polyimide layers was not altered by the addition of the hole-transporting moieties, which guaranteed that the doped films were not noticeably affected by the rubbing procedure. As a consequence, the alignment abilities of the doped layers were comparable to those of pure rubbed polyimide layers. We also confirmed the stability of the doped layers by comparing the hole-transporting properties of the layers before and after the rubbing treatment, and established that the difference was almost negligible.

The charge injection and charge transport characteristics of the hole-transporting alignment layers (HTALs) are illustrated in Figure 5.9, exemplary using 4,4',4''-tris(1-naphthyl)-N-phenylamino-triphenylamine (ST 638) as HTM (section 3.1.4.1). In the upper graph, the current density is plotted versus the applied voltage for devices of the structure ITO/(PI+ ST 638)/Al at different filler contents. The positive effect of the doping on the charge transport characteristics was already noticed at dopant concentrations of 5 wt.% only, increasing the current density by more than one order of magnitude in comparison to the pure polyimide films. The increase was almost three orders of magnitude when the filler concentrations reached values of 17 wt.%. For concentrations exceeding this value, a further rise in the dopant content only yielded weak increase in current density, suggesting percolation-type¹⁸⁹ threshold of conductivity for films of filler contents of 17 wt.% and more. Details of the influence of dopant concentration on the device performance are discussed in section 5.2.3.

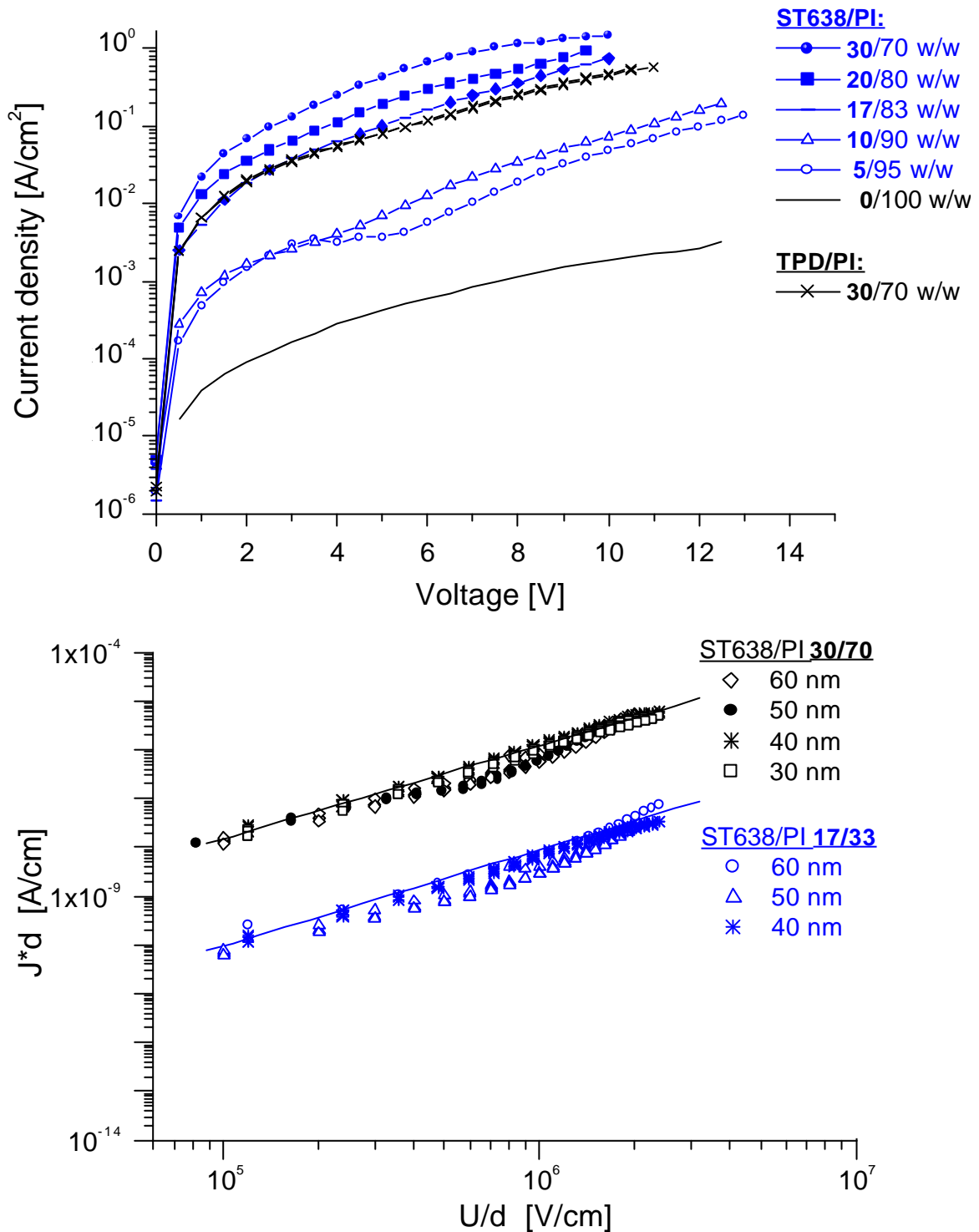


Figure 5.9. (Up): Current density–voltage characteristics for polyimide films with different content of ST638 filler. For comparison, the film characteristic of polyimide doped with 30 wt.% TPD is shown as well. Within the error of measurement, all films were 50 nm thick. (Down): Current density–electric field characteristics of 17%ST638/83%PI and 30%ST638/70%PI films of different thickness d in the representation $J \cdot d$ versus the electric field E . The straight lines correspond to linear fits to the data of $d = 40$ nm.

The half-wave oxidation potential of ST 638 is $E_{ox}^0 = 310$ mV vs. Ag/AgCl (section 3.1.4.1), which corresponds to an ionization potential of approximately $I_p \approx 5.1$ eV, when an offset of 4.8 eV between the electrochemical scale with the Ag/AgCl reference electrode and the

vacuum level is assumed.^{155,190} Thus, the HOMO level of the doped polyimide layers is very close to the ionization potential of ITO (4.8–5.0 eV),^{13,14} and the contact between the two layers is ohmic. The small barrier to hole-injection from the ITO into the polymer layer causes the current to be transport-limited (section 2.1.1.1). In the lower graph of Figure 5.9, we see that the j - V characteristics for 30%ST 638/70%PI films of different thickness d are virtually identical if plotted as $\log(j \cdot d)$ versus $\log E$. According to Child's law for space-charge limited currents (Equation 2.3), this confirms the expected space-charge limited conduction. Giebeler *et al.*¹⁹¹ have reported similar results for pure, glassy films of a material closely related to ST 638. The currents found here are on the same order of magnitude. Using Equation (2.3) and a dielectric constant of $\epsilon = 3$, the effective mobility of holes can be estimated to be in the range of $\mu_{17\%} \sim 3 \cdot 10^{-8} \text{ cm}^2/\text{Vs}$ for filler concentration of 17 wt.% and $\mu_{30\%} \sim 0.5\text{--}1 \cdot 10^{-5} \text{ cm}^2/\text{Vs}$ for contents of 30 wt.%. The slight deviations from the SCLC fits, which are observed in the plots, might point to a weak dependence of the hole drift mobilities on the electric field.

We have studied the j - V characteristics of converted films, which had been additionally flushed with toluene following conversion, and confirmed that the electrical properties were not considerably changed. This means that it is possible to spincoat an EL active layer from toluene on top without losing the hole-transporting properties of the alignment layer. This opens the way towards the fabrication of polarized light-emitting devices.

Details of the performance of such polarized EL devices will be more thoroughly discussed in the next chapter, and further information to the device structure and fabrication is given in chapter 3. At this point, only the characteristics of the hole-transporting alignment layers will be examined. We confirmed that they yielded highly satisfying device performance when incorporated into electroluminescent devices. In Figure 5.10 we compare the intensity–voltage characteristics of devices with *doped*, *undoped* and *without* additional polyimide alignment layer between the ITO anode and an 80 nm emissive layer of PF2/6. While devices with the pure polyimide layers did not produce any significant light output even at very high voltages ($< 5 \text{ cd/m}^2$ at 25 V), the devices containing the HTALs reached high light intensities of 200 cd/m^2 at reasonable voltages of 20 V, with a light turn on voltage of $\sim 15 \text{ V}$ – without any further layer optimization. The doped alignment layers indeed facilitated hole injection, which was evident from the comparison with the monolayer devices of PF2/6 without any additional alignment layer. In the latter case, the barrier to injection of holes from the ITO was very large due to the high HOMO level of PF2/6 ($\sim 5.9 \text{ eV}$). The maximum light intensities obtained from the monolayer LEDs were considerably lower and, moreover, the voltages required to get a certain light output were up to 7 V higher than in the case of the double-layer devices.

These results demonstrate that polyimide films can be modified for hole conduction by the addition of suitable hole-transporting moieties at moderate concentration. Only the doping en-

abled the incorporation of alignment layers into polarized light-emitting devices, which will be described in section 6. Before, we will focus on the optimization of the hole-transporting alignment layers with respect to EL applications.

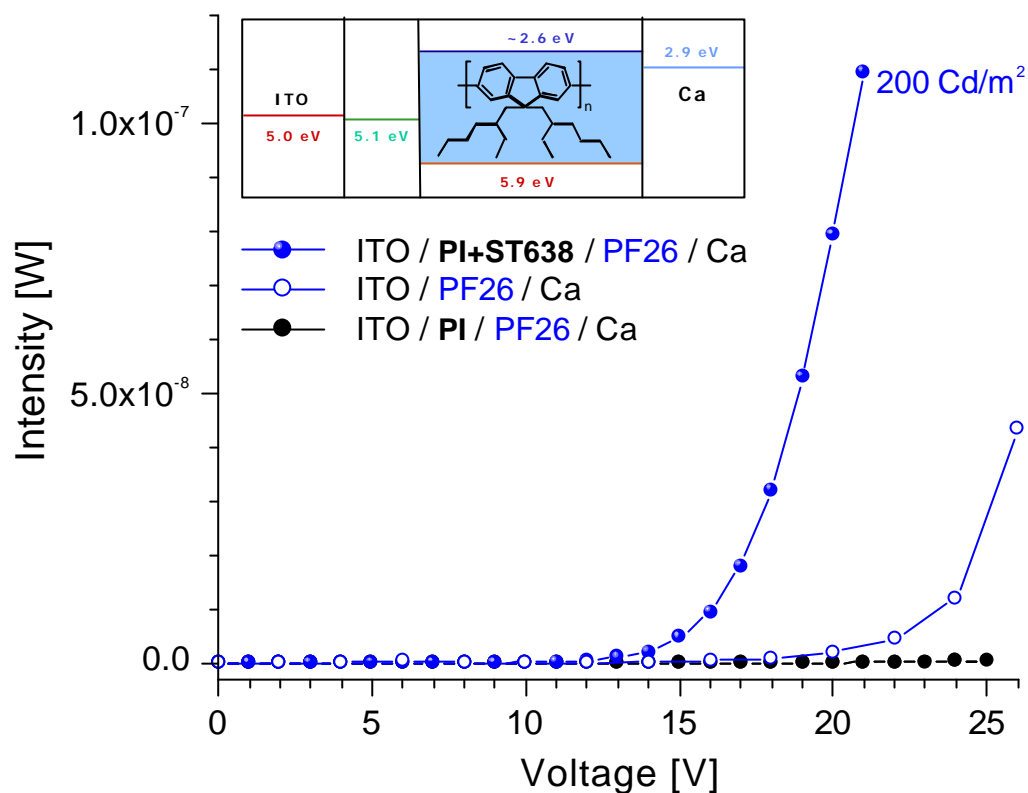


Figure 5.10. Intensity–voltage characteristics of devices with *doped*, *pristine* and *without* alignment layer of polyimide between the ITO anode and an 80 nm thick emissive layer of PF2/6. In case of doping, ST 638 was used as hole-transporting material. The inset shows the layer arrangement with schematic energy level diagram of the device, which contained the hole-transporting alignment layer.

5.2.2 Variation of Hole-Transporting Materials

5.2.2.1 Low-Molecular Weight Compounds and Their Combination

In the previous section we demonstrated by the comparison of PF2/6-monolayer LEDs and double-layer devices containing an HTAL, that the introduction of an additional layer reduced the barrier to hole-injection from the anode side and enhanced the device performance (Figure 5.10). In general, such a reduction of the barrier height is in part the motivation for multilayer devices (section 2.1.3). However, the low HOMO level of ST 638 of ~ 5.1 eV causes only the barrier from the ITO side to be low, whereas the barrier to the emissive layer remains very large with up to 0.8 eV. Therefore, the idea was to incorporate a further layer between the ITO and

the alignment layer, realizing stepwise barriers of lower heights between the ITO and the emissive polyfluorene layer.

The appropriate HOMO level of the additional layer was adjusted by means of various low-molecular weight hole-transporting materials with high glass transition temperature, similar to ST 638, but with different oxidation potentials and electronic properties. Besides of ST 638, three other low-molecular weight compounds were investigated: 4,4'-bis{N-(1-naphthyl)-N-phenylamino-biphenyl} (ST 16-7; $I_p \sim 5.5$ eV), 1,1-Bis-(4-bis(4-methyl-phenyl)-amino-phenyl)-cyclohexane (ST 755; $I_p \sim 5.6$ eV), and N,N'-Diphenyl-N,N'-bis(4'-(N,N-bis(naphth-1-yl)-amino)-biphenyl-4-yl)-benzidine (ST 1163; $I_p \sim 5.6$ eV). The chemical structures and cyclic voltammograms of these materials are shown in section 3.1.4.1.

Several sets of combinations of these HTMs were compared with respect to the attainable device performance and the degree of alignment. At first, the two HTMs ST 755 and ST 16-7 were investigated in various combinations with ST 638. Therefore, isotropic devices were fabricated with two different hole-transporting layers (hole-transporting bilayer structure) covered by PF2/6 as active layer. A schematic picture of that device configuration is sketched in the inset of Figure 5.11, and details to the device fabrication are given in section 3.3 and 6. Towards the anode side, only ST 638 was used as hole-transporting material, since the cyclovoltammetry data of ST 16-7 and ST 755 suggested an injection limited rather than an ohmic contact with the ITO (section 2.1.1.1).¹⁹² The content of the HTMs within the respective blends with polyimide was always 20 wt.%. Since only the upper of the two HTLs was to serve as alignment layer, the lower one did not necessarily require polyimide as component. Consequently, the layer configuration of a pure ST 638 layer spincoated on top of the ITO and covered with a hole-transporting layer of doped polyimide was also tested.

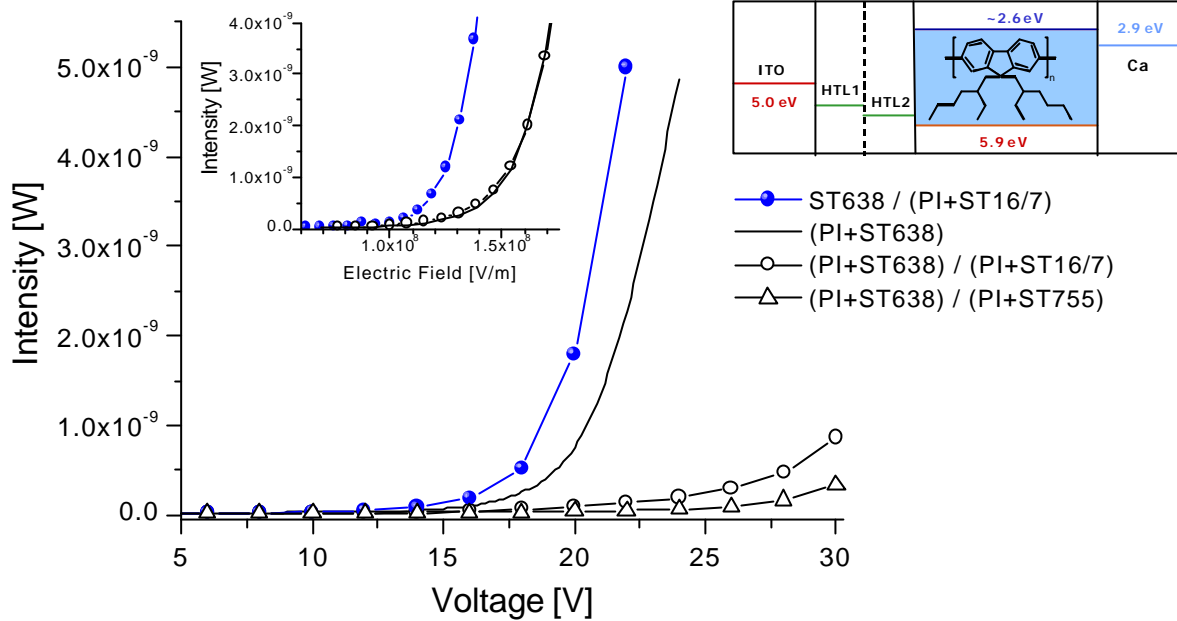


Figure 5.11. Intensity–voltage characteristics for isotropic diodes with PF2/6 emitting layer and different combinations of HTMs (HTM:PI 20:80). In the inset, the intensity is plotted versus the electric field. Also sketched is the layer arrangement with schematic energy level diagram of the device with the structure ST 638/(PI+ ST 16-7), which showed the best performance.

Figure 5.11 shows the intensity–voltage characteristics of the (isotropic) devices under investigation. The results confirmed the positive effect of a hole-transporting bilayer structure on the device performance, attributed to the reduction of the barrier to hole-injection into the emissive layer. The current density and the onset voltage for devices comprising a bilayer structure consisting of a 30 nm hole-injection layer of pure ST 638 covered with a 40 nm HTAL of (PI+ 20%ST 16-7) were comparable to those for devices with a single 40 nm thick HTAL of the blend of (PI+ 17% ST 638). Taking into account the larger overall thickness of the devices with a bilayer HTL structure, emission is observed at lower electric fields, which guarantees higher stability (inset of Figure 5.11). However, it turned out that a bilayer HTL structure was only of advantage if the first HTL below the actual alignment layer consisted of the pure hole-transporting material without polyimide. The combination of two PI-layers doped with two different HTMs did not improve the diode characteristics.

Based on these results for devices with *isotropic* emitting layer, different combinations of HTMs and HTL structures were investigated in devices with *aligned* PF2/6 emitting layer, i.e. with polarized emission (section 6.1.2). Also in this case, the combination of a pure HTL covered by the doped HTAL yielded the best performance. In comparison to the other dopants, the degree of alignment was the highest when ST 16-7 was used as HTM in the alignment layer. While the electroluminescence of an LED with the bilayer HTL structure ST 638 / (PI+ ST 638) showed a polarization ratio of 15, this ratio was 21, when ST 16-7 was blended into the polyimide. The luminance of these devices typically was 100 cd/m² at 18 V.¹⁴²

In a next step, the hole-transporting bilayer structure was further optimized by the usage of ST 1163 as HTM. We found that the device performance was by far the best when using ST 1163, both as pure hole-injection layer and as dopant for the polyimide in the HTAL. Compared to ST 638, the maximum intensity was almost one order of magnitude larger and the light onset voltage was remarkably lower when doping the polyimide with ST 1163, as shown in Figure 5.12.* This finding suggests that the reason for the improved device performance is not primarily a stepwise barrier between the respective layers. We believe that the positive effect of the bilayer HTL structure is rather due to an increased concentration of HTMs in the lower regions of the doped alignment layer. Since the two layers of the HTL bilayer structure are spincoated from the same solvent, the interface between the two layers is probably graded rather than sharp. A certain amount of HTMs might enter the polyimide blend from the pure HT layer and increase the concentration in the vicinity of the interface, yet without reaching the uppermost zone of the alignment layer. In section 5.2.4 we show that an homogeneous increase of the HTM concentration by higher filler contents in the blend can affect the alignment properties of the layer. Raising the concentration by the bilayer HTL structure, however, can shift the hole-injection towards the emissive layer, without causing this decrease in alignment ability. Thus, it seems to be a gradual rather than a stepwise change of the concentration of the hole-transporting molecules in combination with a gradual change in the HOMO level position towards the emissive layer, which reduces the effective barrier to the HOMO of polyfluorene and further improves the hole-injection.

The enhancement of the performance when using ST 1163 is attributed to its electronic properties. We established that the first shoulder in the cyclic voltammogram shown in Figure 3.13 already corresponds to the first oxidation potential of ST 1163, which is located at ~ 0.66 eV. In connection with PF2/6, the respective HOMO level of ~ 5.4 – 5.5 eV obviously guarantees the best possible injection characteristics among all the tested HTMs.

* The ST 1163 injection layer was 40 nm instead of ~ 20 nm, and the HTAL was 60 nm instead of 40–50 nm thick.

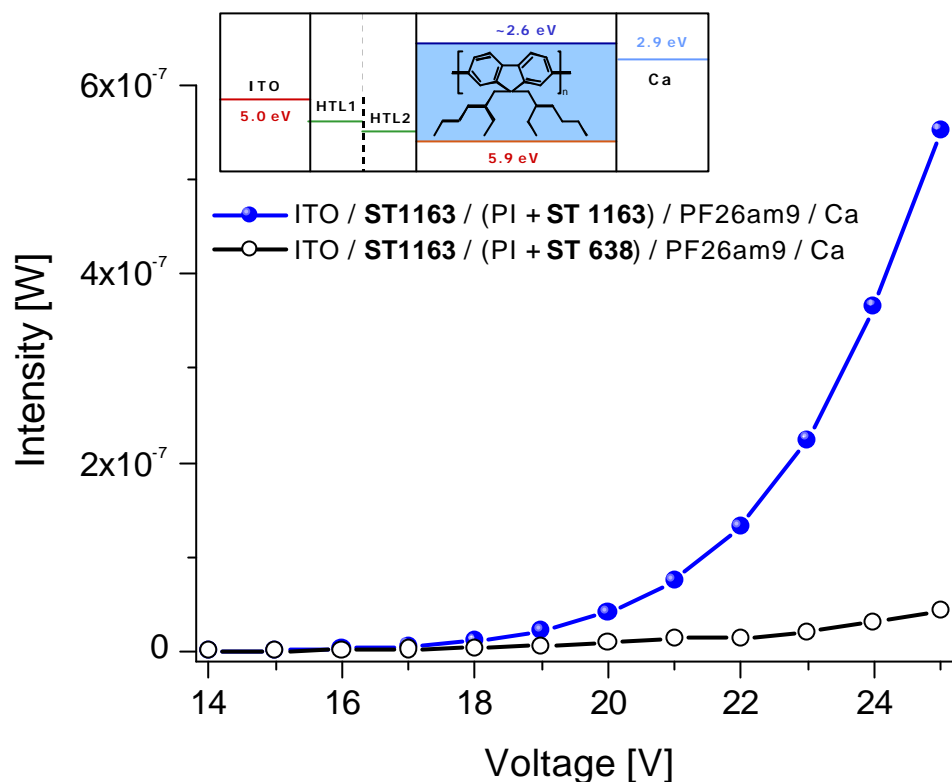


Figure 5.12. Intensity–voltage curves for diodes with HTALs of PI blended with 21 wt.% of ST 638 and ST 1163, respectively. The emissive layer was PF2/6am9 (section 6.2). Note the higher onset voltages compared to the previously shown data of typically 7.5–8 V, which is due to a higher layer thickness (see footnote).

5.2.2.2 Polymer Compounds as Hole-Transporting Materials

In section 5.2.3 we will see that phase-separation can be a severe problem when using low-molecular weight hole-transporting materials (HTMs), such as ST 1163, as dopant for polyimide. From a certain doping concentration, the alignment ability of the HTAL is affected and the degree of alignment is substantially decreased. One approach to overcome this problem is the replacement of the low-molecular compounds by *polymers*.

5.2.2.2.1 Polymer Triphenyldiamine-Derivatives

Triphenylamine derivatives, such as (N,N'-biphenyl-N,N'-bis-(3-methylphenyl)-[1,1'-biphenyl]-4,4'-diamine) (TPD), as low-molecular weight compounds have been shown to be a suitable material for HTMs.¹⁶¹⁻¹⁶³ Therefore, polymers on the base of such triphenylamine derivatives were considered as promising candidates for polymer-HTMs. We investigated poly-TPD (triphenyldiamine), poly-NPD (naphthyl phenylamino-biphenyl) and poly-TPD with an additional (CH₂)₆-spacer unit in the main chain (p-HeO-TPD).

The polymers were blended into PI at a concentration of 13 wt.% at each case. In addition, it was tested if rubbed layers of the pure polymers – without the use of PI – could serve as HTALs. The alignment as well as the performance in electroluminescence were tested in devices with the structure ITO/ST 1163/(PI+ 13wt.%) *poly-TPD*/PF26am4/LiF/Ca.

The investigations showed that none of the three tested polymers – p-TPD, p-NPD and p-HeO-TPD – was suitable as *pure* alignment layer. Due to the lacking stiffness of these layers, all of them were partly removed after rubbing and mechanical traces produced by the rubbing were clearly visible. In all cases, the emissive layer of PF26am4 (section 6.2) was not aligned. When blended into PI, the alignment in photoluminescence was promising for all polymers, with polarization ratios between 8 and 12. However, in electroluminescence, the alignment behavior differed substantially. The samples with (PI+ HeO-TPD) and with (PI+ p-TPD) emitted isotropic light, and the polarization ratio in the case of (PI+ p-NPD) was lower than 10. Only the latter samples showed no rubbing traces, whereas the other two alignment layers were severely damaged. Moreover, the performance in EL was highly unsatisfying: the emitted color was greenish rather than blue, and the luminance was less than 30 cd/m² at 18 V, resulting in low power and luminous efficiency. Finally, the device stability was poor.

These results demonstrate that the polymer HTMs do not serve as alternatives to low-molecular weight compounds for the use in polarized LEDs. Therefore, they will not be further discussed in this work.

5.2.2.2 Polyaniline as Hole-Transporting Material in Polyimide

In section 6 we will see that the onset and operating voltages of isotropic LEDs are in general remarkably lower than the ones of polarized LEDs containing the different hole-transporting alignment layers discussed in the previous sections. This is due to the usage of polyimide as alignment matrix within polarized LEDs, which is only conducting after doping. Consequently, the performance of the resulting devices strongly depends on the nature of the dopants. So far, the minimum value of the onset voltage was obtained using a bilayer hole injection structure containing low-molecular weight compounds. In the following, we report on attempts to replace these compounds by the polymer polyaniline (PAni).

Polyaniline (PAni) is known to be highly conductive after doping with functionalized protonic acids like camphorsulfonic acid (CSA).^{164,165} We blended PAni-CSA with polyimide at different concentrations to obtain hole conducting alignment layers after conversion, similar to the ones reported for the low-molecular weight compounds.

In a first step, we tested if rubbed films of blends of PAni-CSA and PI are suited for serving as alignment layer. Our experiments showed that the alignment strength of these layers on top of glass substrates were extraordinary high. Endcapped polyfluorene PF2/6am2 (section 6.2)

was aligned on top of rubbed layers of blends of PI and 40 wt.% PAni-CSA, yielding dichroic ratios in absorption of $D > 20$, which are among the highest values reported so far (Figure 5.13). It should be noted that for very well-aligned samples, the determination of the dichroic ratio can be difficult. As shown in the Figure, the background correction might be problematic, especially in the region of very short wavelengths. In case of high degrees of alignment, the absorption perpendicular to the molecular orientation is very low, and the error in the dichroic ratio caused by the baseline adjustment can be up to 25 %. Therefore, to be on the safe side, values larger than 20 are not quoted explicitly in the following.

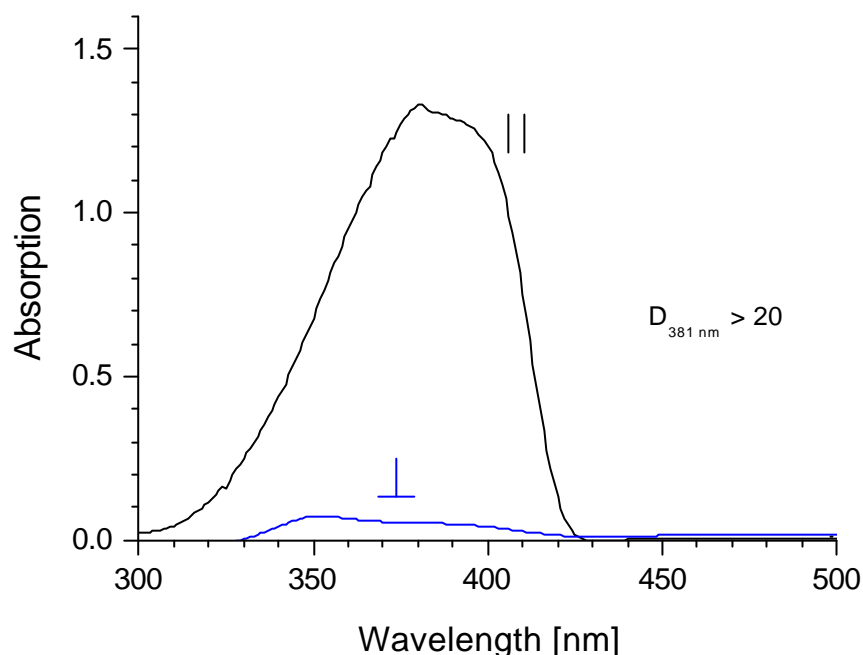


Figure 5.13. Polarized absorption spectra of PF2/6am2 (section 6.2) aligned on top of rubbed 40% PAni-CSA in PI on glass substrates. For very low absorption values in perpendicular direction, the error due to background direction in the dichroic ratio is up to 25 %, explaining why only the order of the value is given.

However, the performance of PAni-CSA+ PI blends within polarized light-emitting devices was not very satisfying. For all the tested devices, the polarization ratios in electroluminescence did not exceed values of $P \sim 10$. Moreover, these layers showed very poor hole-injection characteristics in connection with polyfluorene. The consequential imbalance of charge carrier injection and oversupply of electrons led to high currents resulting in very low efficiencies. In paragraph 6 we will see that the overall performance of devices, which contained low-molecular weight compounds as dopants in the HTALs was superior in all respects. As illustrated in Figure 5.14, devices with comparable efficiencies showed more than doubled polarization ratios of 22 instead, and the efficiency of devices with polarization ratios of ~ 10 was more than one order of magnitude higher. Therefore, blends containing PAni-CSA will not be discussed in further detail.

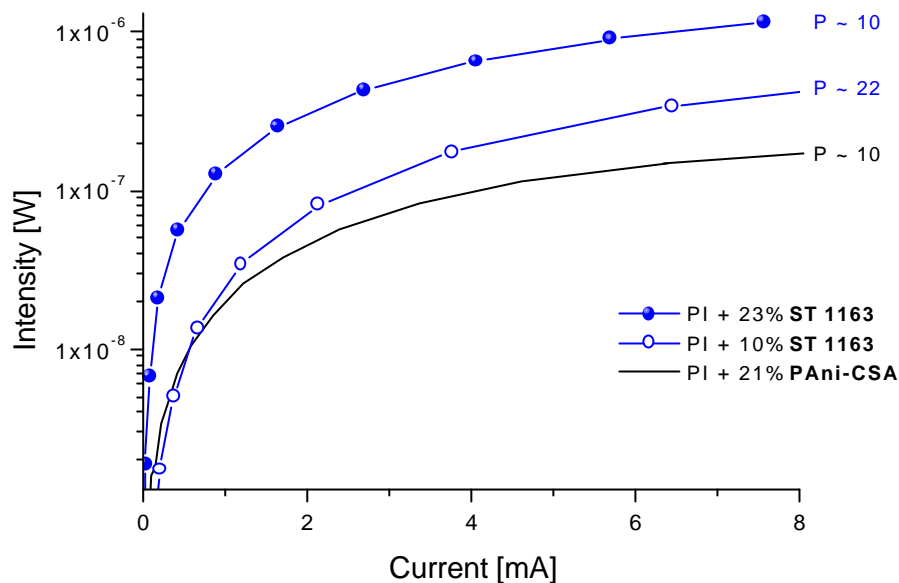


Figure 5.14. Photometric efficiencies for comparable polarized LEDs with alignment layers of PI doped with PAni-CSA (no symbols) and ST 1163 (circles), respectively. The polarization ratios of the respective devices are also given.

5.2.3 Influence of Doping on the Alignment and on Electroluminescence

The concentration of the low-molecular weight HTMs, which were introduced in section 5.2.2.1 within the PI matrix was found to have an influence both on the electroluminescence and on the alignment behavior of the respective devices. It turned out that increasing the filler content up to a certain value had a positive effect on the brightness and onset/operating voltages, but that the alignment ability of the doped HTALs continuously decreased with augmenting filler contents.

In section 6.2.2 we will report on polarized light-emitting diodes of the structure ITO/ST 1163/(PI+ x wt.%ST 1163)/PF26am9 /Ca. We will see that the luminance *increased* (at decreasing onset voltage) from 200 to more than 800 cd/m² when the concentration of the HTMs in PI was increased from 10 wt.% to 30 wt.%, whereas the polarization ratio *decreased* from 22 to 5 (Figure 6.13). These findings demonstrate that the concentration has to be carefully balanced for electroluminescence performance and alignment strength. However, devices with 20 wt.% doping yielded the best overall EL performance and showed the highest power efficiency, and therefore higher concentrations are not of interest for device applications. An explanation for the observed decrease of order parameters with increased dopant concentrations will be given in the next paragraph.

5.2.4 Influence of Doping on the Morphology of Hole-Transporting Alignment Layers

In the following, we will show that the influence of the dopant concentration on the achievable degree of alignment can be explained by severe changes in the morphology of the hole-transporting alignment layers due to phase-separation, an inherent problem when blending polymers with low-molecular weight compounds.⁸ Films with different concentrations of ST 1163 in PI were investigated by means of low-voltage scanning electron microscopy (LVSEM) and atomic force microscopy (AFM). The results obtained show an optimized doping concentration balancing between best possible alignment strength and electroluminescence performance.

For all the layers described below, blends of precursor-PI and different concentrations of ST 1163 were spincoated on top of ITO-covered glass substrates to obtain hole-transporting layers of approximately 40 nm thickness after conversion. To investigate the influence of the rubbing treatment on the film morphology, unrubbed and rubbed layers were compared for different filler contents.

Figure 5.15 shows scanning electron microscope pictures of unrubbed layers with doping concentrations of ST 1163 in PI increasing from 10 to 40 wt.%. Looking at the pictures for low filler contents, we find that the appearance of the respective layers is comparatively homogeneous. However, at higher filler contents, the surface is covered with increasing density by round spots of increasing size. The concentration dependence suggests that these spots correspond to hole-transporting molecules, which phase-separate within the polyimide blends.

As shown in the Figure, the phase-separated structures are almost not noticeable for dopant concentrations of 10 wt.%, and the layer surface is rather flat with a root-mean-square (RMS) roughness of 1.4 nm. At a concentration of 15 wt.%, dark spots with a diameter of 60 to 130 nm can be faintly perceived. When the concentration reaches 20 wt.%, the degree of phase-separation starts to become considerably, and the diameter of these areas varies from 100 to 220 nm. Comparison of the different pictures reveals that the appearance of the nanophase-separated structures changes with the concentration of the HTMs. While at very low contents, the HTMs were noticed as dark spots, these marks are encircled by bright edges for a content of 20 wt.%. The latter indicates that they form crater-like depressions within the PI film, which are surrounded by protruding fringes. According to AFM measurements, the depth of these craters is between 3 and 6 nm (Table 5.2). When the filler contents further increases to 30 and 40 wt.%, the form of the nanophase-separated structures changes from depressions to globules with a height between 10 and 15 nm and diameter between 180 and 400 nm. The RMS increases to 4 nm (30 wt.%) and 6-8 nm (40 wt.), respectively.

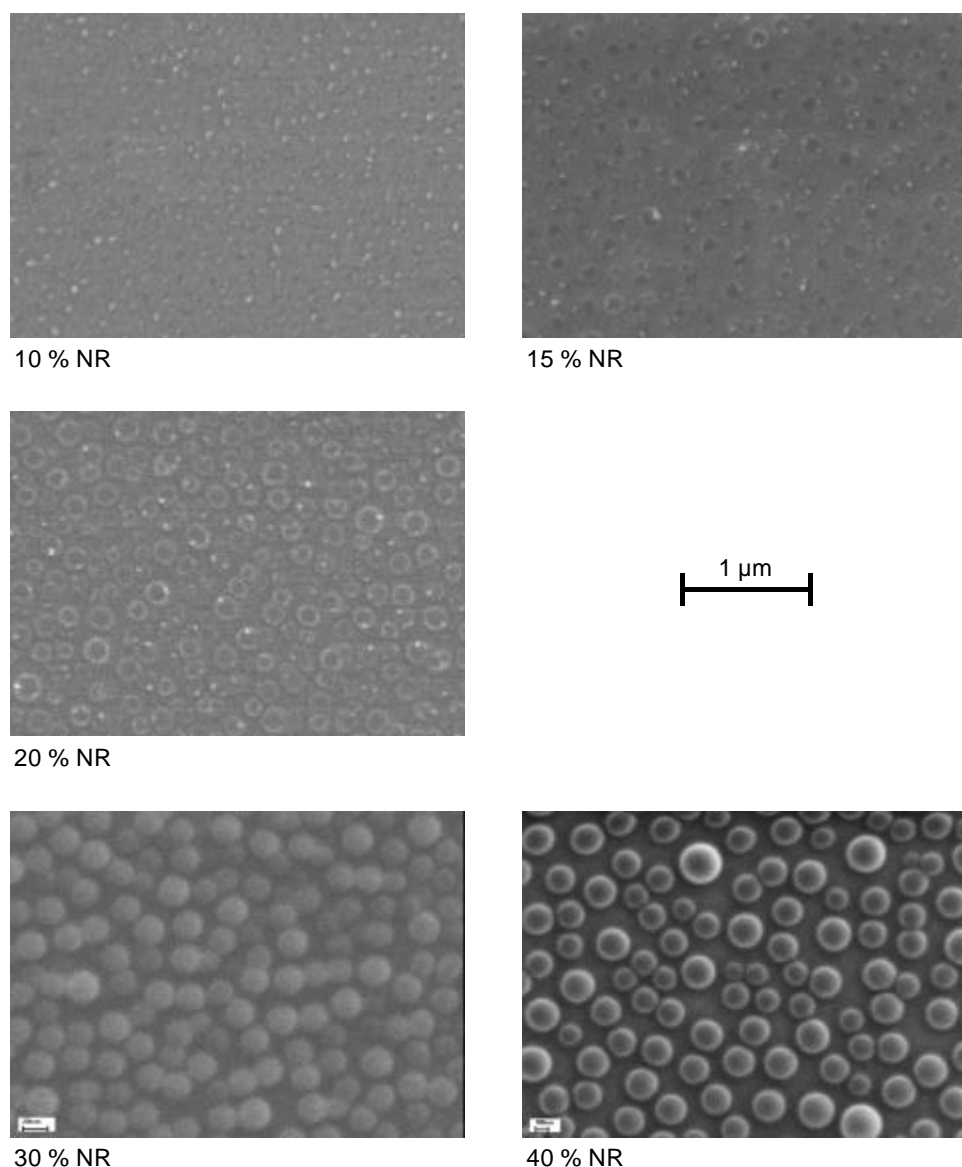


Figure 5.15. Low-voltage scanning electron microscope (LVSEM) pictures of unrubbed layers (NR) of PI doped with ST 1163 at different concentrations (in wt.%).

In addition to these nanophase-separated structures, one observes bright spots of comparatively large size dispersed all over the samples. This can be seen when looking at the film at lower magnification (Figure 5.16, left column). The diameters of these spots increase with augmenting filler content from ~ 700 nm for 10 wt.% to ~ 1650 nm for 40 wt.% (Table 5.2). Due to this concentration dependence, they are interpreted as accumulations of hole-transporting molecules. AFM investigations reveal a blister-like shape of these microdomains with height increasing from 25 nm for 10 wt.% to 60 nm for 40 wt.% doping.

These observations suggest that the hole-transporting molecules tend to diffuse out of the layers to the surface, and starting from a certain concentration, the PI matrix might be too severely degraded to incorporate or keep them inside of the film. Excessing HTMs start to well out of the PI matrix and form nanophase-separated structures with a size of 180 to 400 nm

arching over the PI film. Furthermore, microphase-separated agglomerates with diameters in the range of $\sim 1 \mu\text{m}$ are formed on top of the layers, which are not incorporated into the polyimide matrix at all. These interpretations will be further supported by the following discussion of the layer morphology after rubbing.

Figure 5.16 shows LVSEM pictures of unrubbed and rubbed layers of PI doped with ST 1163 at different concentrations. The effects of the rubbing procedure on the morphology of the alignment layers are evaluated regarding to the appearance of (i) the rubbed layers as a whole, (ii) the nanophase-separated structures of HTMs, and (iii) the agglomerates on top of the layers.

As can be seen from the pictures, the extent to which the film morphology is influenced by the rubbing, strongly depends on the concentration of the hole-transporting moieties. Figure 5.16 and 5.17 show that for low concentrations of 10 and 15 wt.% the matrix of the layers is not noticeably disturbed by the rubbing, and the films are very homogeneous. The layers only show very few single fissures produced by the rubbing procedure. On the contrary, for filler contents of 30 and 40 wt.%, the entire film is covered with rubbing grooves (Figure 5.20). For 10 wt.% doping, the few microgrooves are approximately 50 nm wide and 5 nm deep, and for filler contents of 40 wt.% these values increase to 140 nm and 15 nm, respectively.

These findings suggest that with higher doping concentrations, the ratio of PI to dopant molecules within the matrix is too low to arrive at a sufficient degree of imidization and to yield the stiffness inherent to fully imidized polyimide. This assumption is in agreement with Han and Im¹⁹³ who noticed a lower degree of imidization for higher dopant and lower polyimide contents in comparable conductive polyaniline/polyimide blends. As a consequence, we observe a significant increase both of the number and the size of the rubbing traces.

The finding mentioned in section 5.2.3 that the layers with low doping concentrations yield the highest polarization ratios (see Figure 6.13) demonstrates that alignment on top of rubbed PI is due to molecular alignment rather than to microgrooves, which are created by the rubbing. This is consistent with previous studies (section 2.2.5.2).^{116,117,120,122,194,195} Furthermore, hole-transporting characteristics of the doped PI layers, characterized by a percolation-type transport threshold, indicates that a large fraction of the HTMs is still incorporated into the layer matrix. Thus, the alignment layers doped at moderate concentrations, are stiff *and* conducting.

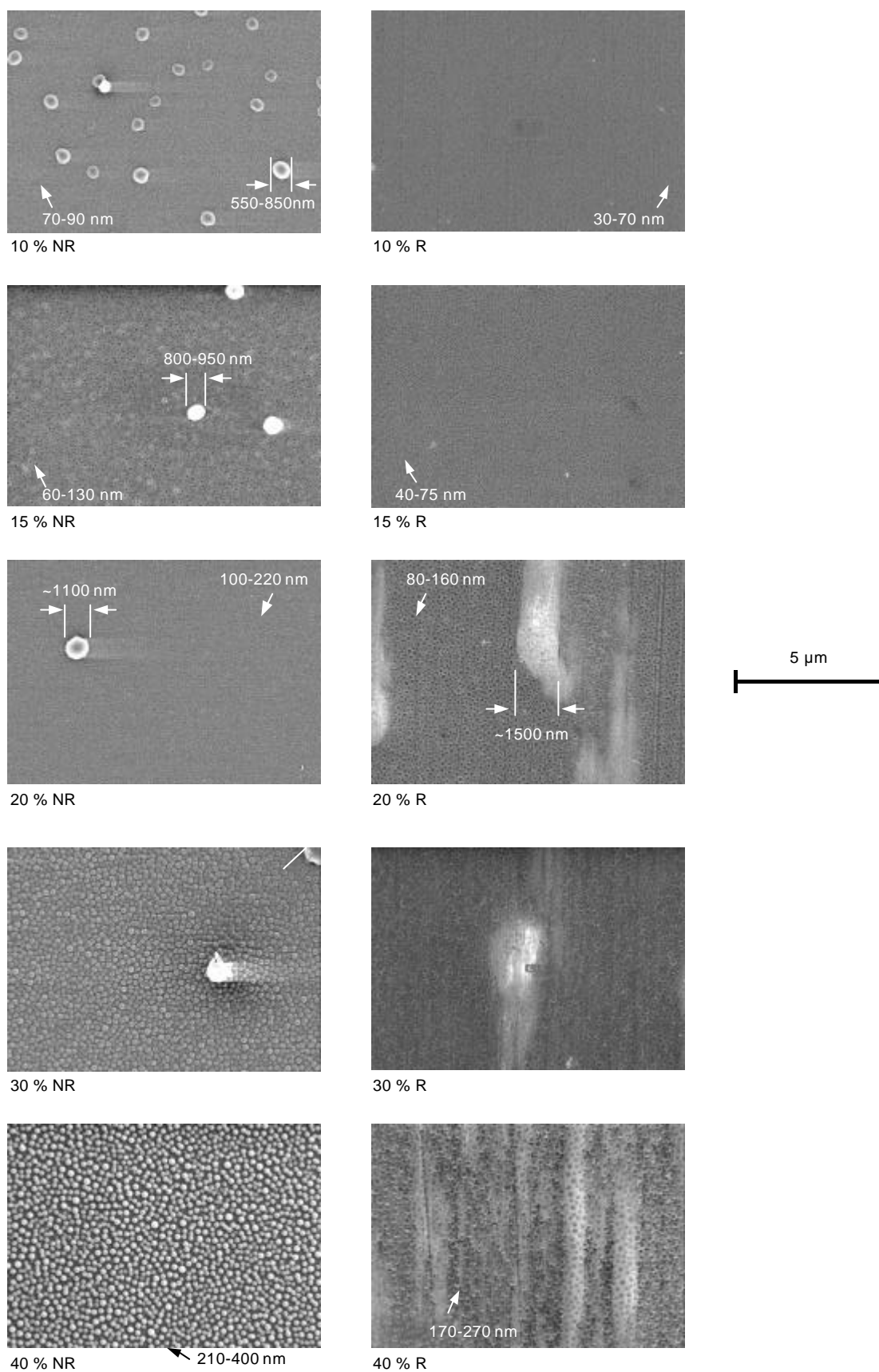


Figure 5.16. LVSEM pictures, showing the comparison of unrubbed (NR) and rubbed (R) layers of PI doped with ST 1163 at different concentrations (in wt.%). The size of the nanostructures inside the layers and of the agglomerates on top, respectively, is also shown (as evaluated from LVSEM and AFM measurements). The direction of rubbing was vertical.

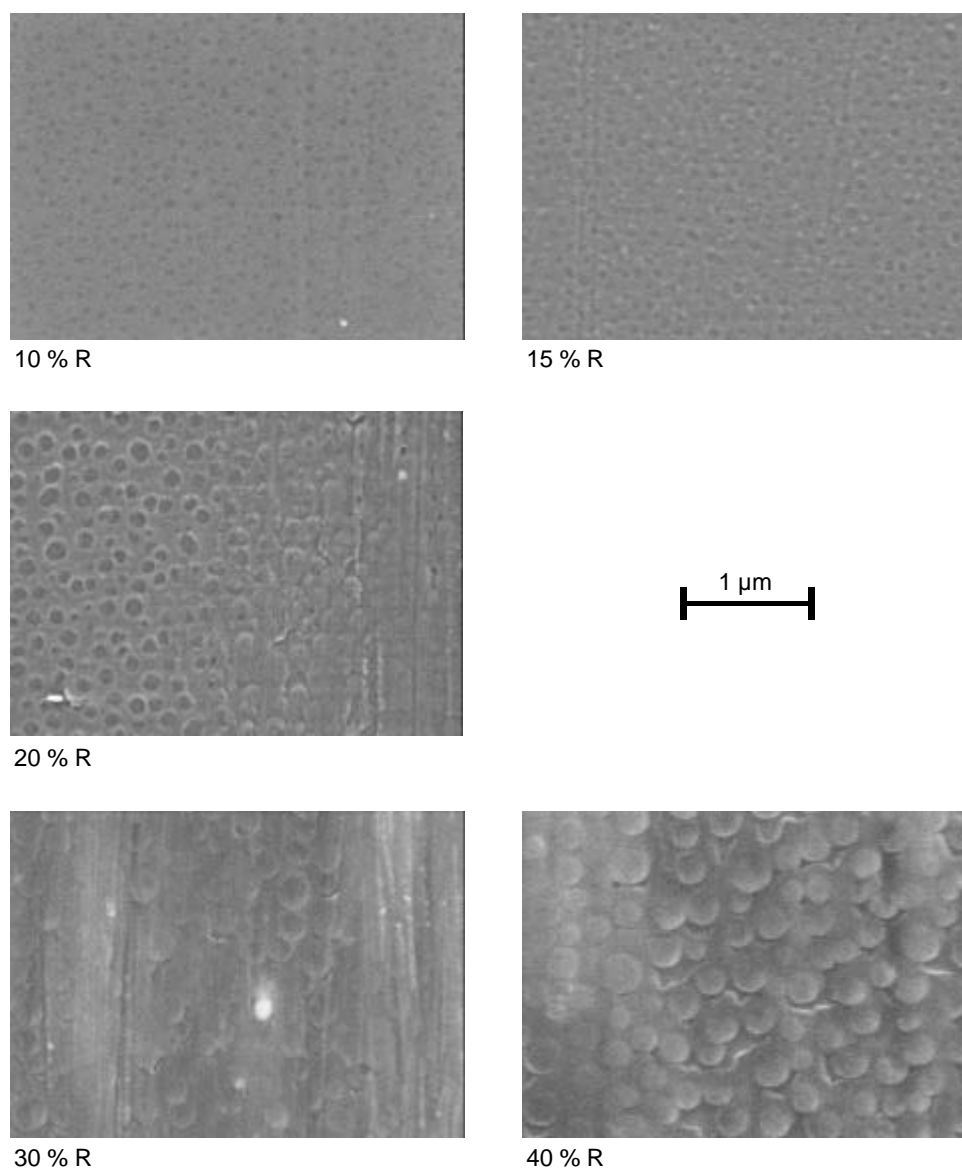


Figure 5.17. LVSEM pictures showing the comparison of rubbed (R) layers of PI doped with ST 1163 at different concentrations (in wt.%). The direction of rubbing was vertical.

Concerning the nano-size features, which are attributed to microphase-separation of HTMs *inside* the polyimide, the rubbing procedure has even a positive effect on the morphology of the layers. Evaluation of the size of these phase-separated HTMs demonstrates that the latter are partially covered by this procedure, and for all concentrations their average diameter decreases by rubbing by approximately one third to one fourth (Table 5.2).

Table 5.2. Diameter and depth of phase-separated clusters of HTMs inside of the layer and on top of the layer, respectively, for unrubbed (NR) and rubbed (R) films of PI doped with ST 1163 at different concentrations. The values for the diameter were determined both from LVSEM and from AFM measurements, and the height (positive val.)/depth (negative val.) was obtained from AFM studies.

Dopant concentr in PI [wt %]	HTMs <i>inside</i> of PI film		HTMs <i>on top</i> of PI film	
	Diameter [nm] (SEM/AFM)	Height [nm] (AFM)	Diameter [nm] (SEM/AFM)	Height [nm] (AFM)
10 % NR	70-90	-4 to -6	550-850	+25
R	30-70	-4 to -6	Not observed	Not observed
15 % NR	60-130	(No data)	800-950	(No data)
R	40-75	(No data)	Not observed	(No data)
20 % NR	100-220	-3 to -6	1000-1350	+40 to +45
R	80-160	-4 to -6	1200-1950	+20 to +30
30 % NR	180-360	+9 to +11	1200-1500	+50 to +60
R	120-270	-8 to -10	2000-2150	+20 to +25
40 % NR	210-400	+8 to +15	1300-2000	+55 to +60
R	170-270	Not measurable	1300-1550	+15 to +20

To be more precise, the rubbing has two different effects on the incorporated HTMs, depending on the filler content of the dopant materials. In case of moderate doping, where the HTMs form crater-like depressions within the film, the surroundings are removed by the rubbing, partly covering the depressions and reducing their overall size. However, for high dopant concentrations, where the HTMs form blister-like globules, this treatment has another consequence. Figure 5.16 reveals that the appearance of the microphase-separated features changes from bright marks to dark spots surrounded by bright fringes. Comparison of surface scans of unrubbed and rubbed samples clarifies this observance. Figure 5.18 shows AFM pictures of samples with dopant concentrations of 30 wt.%, together with horizontal and vertical scans over the surface along the black lines. In fact, the scans demonstrate that in the case of the un-rubbed sample – as mentioned above – the features arch over the surface and form globules of about 10 nm height (for visualization, each area belonging to a single dopant is marked with blue in the line-scan picture). Contrary, after rubbing, the features remain as crater-like holes with a depth of ~ 8 nm in the layer, surrounded by fringes, which protrude few nanometers over the surface.

This observation might be understood assuming that the rubbing procedure cuts off a part of the blisters, which then seems to crack – indicating that also in the case of high concentra-

tions, microphase separation causes depressions in the PI layer, which yet are covered by a thin outside layer. This coating is stripped off during rubbing and the released material then partly covers the hole. Thus, for the higher dopant concentrations, craters remain after the rubbing procedure, in contrast to the observations for low filler contents.

One could also suppose that the features at higher filler contents are *completely* filled by hole-transporting material. That would also imply that rubbing removes the dopants as a whole. The following considerations disprove this hypothesis, however. Estimations of the layers with 30 wt.% (Figure 5.15) show that under the assumption of massive blobs, 25 wt.% of the hole-transporting material would be incorporated into the microphase-separated features.* Thus, less than 5 wt.% would be integrated into the bulk of the layer. Since the globules are completely removed during the rubbing procedure, the film should be almost non-conductive after rubbing. However, the electrical performance of such films is not considerably affected by the rubbing treatment, as already mentioned (section 5.2.1 and Figure 6.13).

* In Figure 5.15, approximately 110 blisters with an average diameter of ~ 250 nm and an average height of ~ 10 nm are perceived on the area of $\sim 10^{-7}$ cm². Assuming massive blisters, they take a volume of $\sim 10^{-13}$ cm³ corresponding to a mass of $\sim 10^{-13}$ g. The mass of the 40 nm thick polyimide on this area can be estimated to $\sim 4 \cdot 10^{-13}$ g. Hence, the concentration of the observed dopant globules – which are only on the surface of the layer – is 25 wt.%.

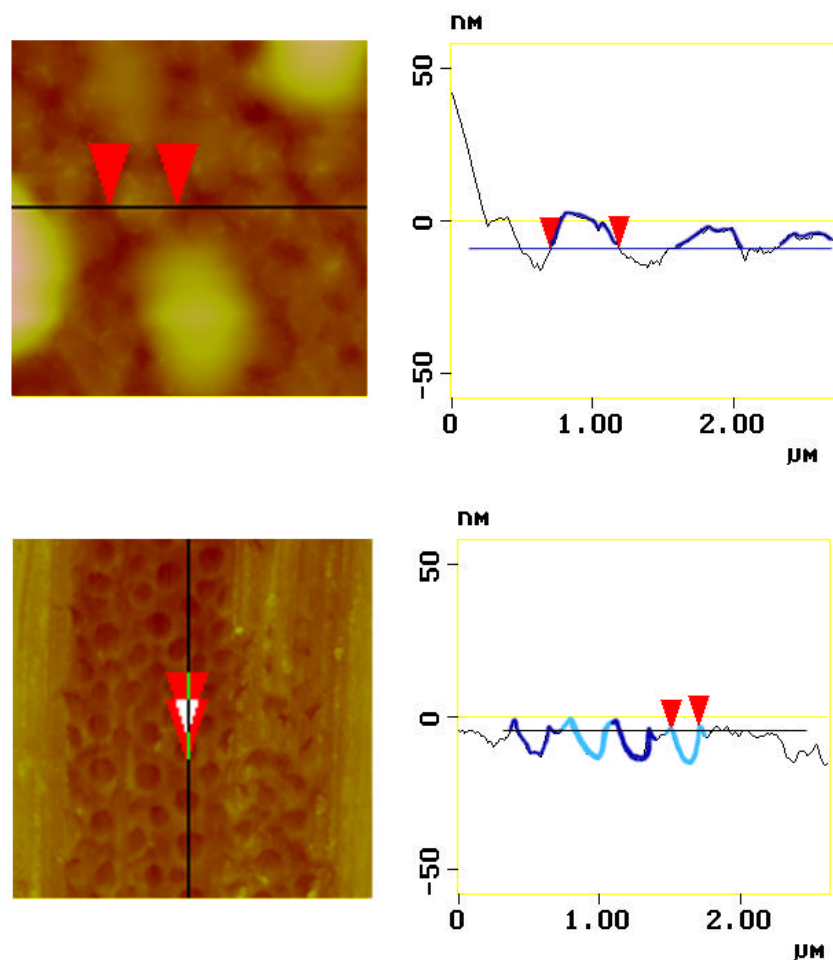


Figure 5.18. AFM pictures and Line-scans of unrubbed (NR) and rubbed (R) films of PI doped with 30 wt.% ST 1163. Line-scans are along the black lines shown in the AFM pictures in horizontal and vertical direction, respectively, and the arrows denote the respective positions in the pictures. For clarity, areas belonging to a single dopant island are marked with blue lines (dark and bright by turns). The black horizontal line in the line-scan pictures indicates the layer surface. The direction of rubbing was vertical.

The effect of rubbing and concentration on the above mentioned large agglomerates lying *on top* of the films becomes evident from the results both of LVSEM and of AFM measurements (Figure 5.16, Figure 5.19 and Figure 5.20). For filler contents of 10 and 15 wt.%, these particles – being present before rubbing – are completely removed by the rubbing treatment. In contrary, in the case of dopant concentrations of 20 wt.% and more, these agglomerates are smeared to smudgy bands covering the layer surface to a large extent. To some extent the latter consist of the material from the cut-off blisters, but mainly this material originates from the large agglomerates of HTMs, which lie on top of the matrix without being incorporated into it at all. The increase in diameter and decrease in height, respectively, of the smeared bands relative to the pristine agglomerates is between 40 and 50 % (Figure 5.19 and Table 5.2).

Obviously, the observed behavior is determined by the stiffness and roughness of the layer surface. In case of low dopant contents, the degree of imidization is high enough to yield a stiff layer, and the surface is relatively even. Both the unrubbed and the rubbed layers then resemble

an homogeneous PI film without dopants on top of the layer. However, for higher concentrations, the layers are softer, and instead of being removed by the rubbing, the agglomerates might stick at the protruding blisters caused by the nanophase-separated structures. The resulting blurred areas of soft HTMs lying on top of the films do not fulfill the essential requirement for serving as alignment layer, i.e. building a stiff matrix with high mechanical stability withstanding the rubbing treatment, like polyimide does. Particularly Figure 5.19 and Figure 5.20 show the large extent to which these smeared areas dominate the characteristics of the layer as a whole for concentrations larger than 20 wt.%.

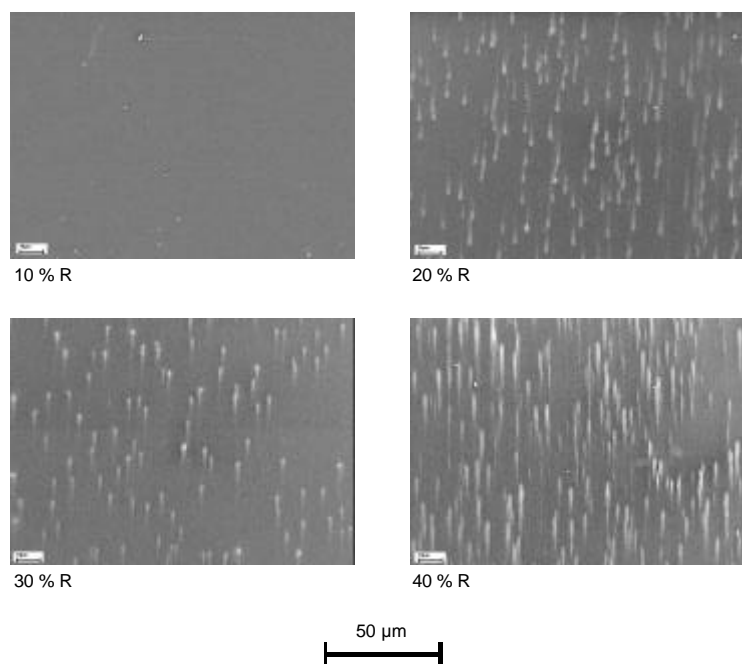


Figure 5.19. Comparison of rubbed (R) layers of PI doped with ST 1163 at different concentrations (in wt.%). The direction of rubbing was vertical.

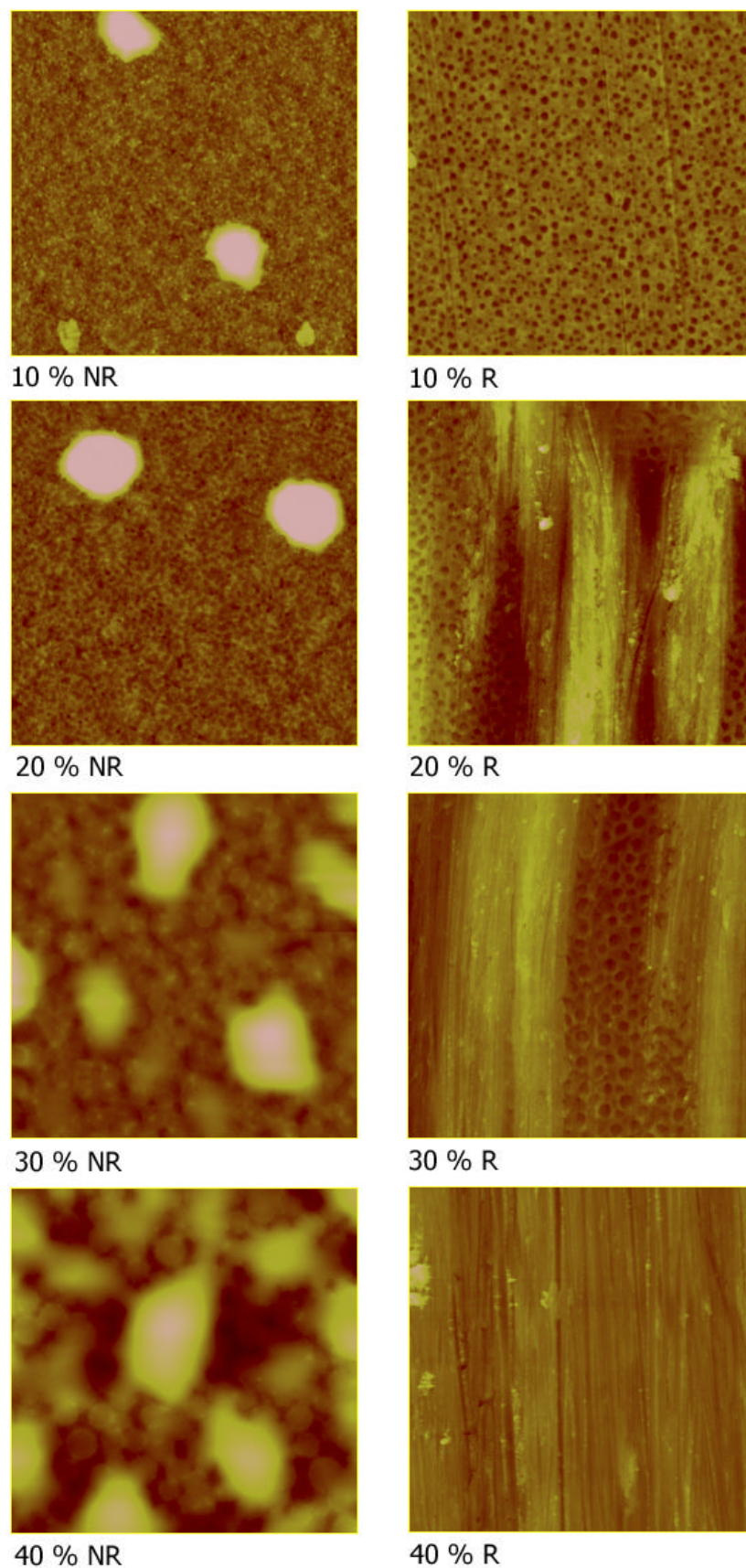


Figure 5.20. AFM pictures of unrubbed (NR) and rubbed (R) films of PI doped with hole-transporting material ST 1163 at different concentrations. The direction of rubbing was vertical. The length of the square area shown is 5 μm at each case.

It should be noted that the impact both of the dopant concentration and of the rubbing procedure on the morphology are surface effects. Neither the holes induced by microphase-separation nor the traces produced by the rubbing penetrate the film deeper than approximately 10 nm (Table 5.2). These findings are also confirmed by cyclovoltammetric data of the films.

Based upon our findings that a big fraction of the phase-separated HTMs lies as large clusters on top of rather than being incorporated into the films, it was tested if they could be removed by washing the samples in toluene. Since the hole-transporting alignment layers are reasonably inert to toluene after conversion⁴¹ this should only remove the excessing dopants, which are not included into the matrix and which therefore do not contribute to the hole-transport. The influence of such a treatment was investigated both on unrubbed and on rubbed layers. Figure 5.21 shows two samples with different concentrations of dopants before and after being stirred in a toluene bath for 3 hours and 3 minutes, respectively. As can be clearly seen from the pictures, the films in both cases initially showed a high density of the large agglomerates, which were completely removed after washing. The removal of the particles is complete already after 3 minutes, indeed disproving their incorporation into the matrix. Note, that these clusters are entirely removed also if the toluene treatment is done after the rubbing procedure. This suggests that the agglomerates might also be partly removed by the subsequent spincoating of an emissive layer from toluene solution.

Further investigations revealed that the alignment power of layers with dopant concentrations of 30 wt.% and higher was considerably lower than for layers with moderate filler contents even after the toluene treatment. This indicates that the remaining layer surface is still too rough and too soft to serve as appropriate alignment layer, attributable to the effects caused by the nanophase-separated HTMs inside of the matrix. Thus, simply removing the large agglomerates does not allow for an incorporation of layers with higher doping concentrations into polarized LEDs, with the aim to obtain enhanced EL performance without any reduction of alignment power.

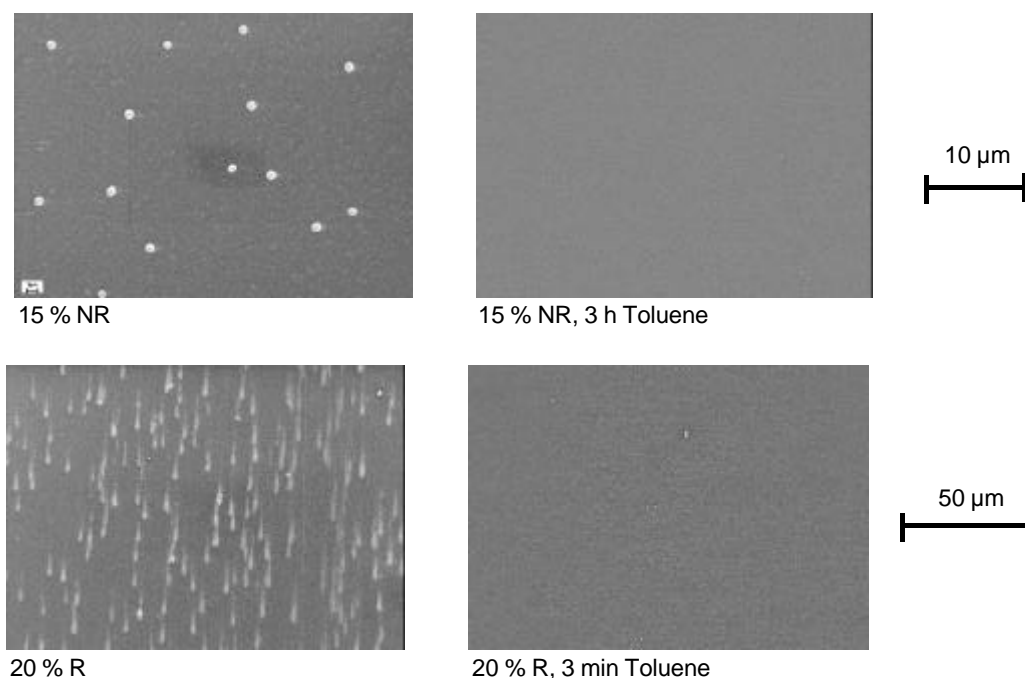


Figure 5.21. Unrubbed (NR) and rubbed (R) films of PI doped with ST 1163 at different concentrations without (left) and with (right) additional bathing in toluene. The direction of rubbing was vertical.

To summarize, the observed decrease of alignment with increasing dopant concentration was explained by LVSEM and AFM studies of unrubbed and rubbed layers of PI doped with ST 1163 at different concentrations. Investigation of the hole-transporting alignment layers showed that phase-separation is negligible for filler contents of 10 wt.% and starts at 15 wt.% doping. At these concentrations, the degree of imidization appears to be sufficient and the layer characteristics are dominated by the stiff polyimide, resulting in films with high alignment strength after rubbing and without any remarkable damage by microgrooves. The morphology is substantially modified by the dopants for concentrations higher than 20 wt.%, and phase-separation becomes more and more severe. Moreover, HTMs tend to well out of the matrix and form globules arching over the entire surface. However, these nanophase-separated structures are covered by a coating rather than being massive, and after rubbing the blisters are cut off without the conductivity of the film being affected. For all concentrations, there are excessing HTMs, which agglomerate into large clusters lying on top of the layers. For low concentrations, they are removed during rubbing, whereas at higher filler contents, they appear as blurred stripes covering the whole layer and leading to a decrease in alignment. It was shown that for layers with very high dopant concentrations, these clusters are entirely removed by a short toluene treatment, but that the resulting alignment power of such layers was still considerably lower than for lower concentrations.

5.2.5 Other Factors Influencing the Alignment

In the previous sections we described that the achievable degree of alignment strongly depends on the characteristics of the alignment layer and of the layer to be aligned. For instance, we ascertained that the obtainable polarization ratios are governed by the concentration of the dopants in the polyimide alignment layer and the concomitant changes in the layer morphology or, likewise, by the molecular weight of the polyfluorene. However, there are additional, external parameters, which influence the alignment behavior of the samples as well as their appearance. The most important ones will be shortly discussed now.

a) Rubbing Speed

We found that a high degree of homogeneity of the rubbed films requires a large mean number of fibers passing a position of unit width. This was accomplished by means of a fairly low translating speed of the substrate beneath the roller of 2.2 mm/s and a large number of 23 revolutions/s of the rotating cylinder, yielding a high velocity of the rubbing cloth relative to the sample of 510 cm/s. With a number of translations under the roller of $N = 2$ the obtained homogeneity was very satisfying and mechanical damage of the samples was not noticeable. A higher number of reruns was not necessary, as this did not lead to higher order parameters.

b) Rubbing Contact Pressure

The homogeneity of the films after rubbing depends on the bending depth of the cloth fibers due to contact pressure.¹⁷¹ The latter should be chosen to such a degree that all fibers just touch the surface of the respective samples. Conversely, if not all of the fibers are in contact with the sample, not all of the molecules in the alignment layer will be aligned and the resulting alignment will not be homogeneous. Extremely high contact pressures were found to result in mechanical damage of the alignment layers, again resulting in inhomogeneous alignment. Furthermore, the degree of orientation, which was obtained with moderate contact pressure was *not* enhanced by further increasing the rubbing pressure. These findings are partly in agreement with Kim *et al.* who perceived a minimum alignment strength required for the onset of any liquid crystal alignment, but partly also in contradiction to their observation of monotonic increase of the obtained LC order parameters with rubbing strength.¹⁹⁶ This difference might be explained by the fact that their LC systems under study showed average surface order parameters in the range of $S = 0.25$ only,* whereas the respective values for our systems are supposed to be substantially larger and possibly closer to a principally achievable limit of order.

* Kim *et al.* calculated the *average surface order parameter* in dependence of parameters, such as the rubbing strength and the order parameter of the polyimide. We did not determine the latter value and could only estimate our surface order parameter.

c) Rubbing Cloth

The nature of the rubbing cloth was also found to be relevant for the alignment procedure. Therefore, different types of rubbing clothes were investigated: the standard cotton pile cloth typically used in the rubbing experiments presented so far, a slightly smoother one, and two very smooth ones. The smoothness of the clothes is hereby mainly determined by the length, the diameter, and the resulting density of the fibers. A smooth cloth is characterized by short, thin fibers enabling a high density of fibers per unit area. The different clothes were tested with samples of the configuration Glass/PI (rubbed)/PF26am9 and in diodes of the structure ITO/ST 1163/ PI+ 15%ST1163 (rubbed)/PF26am9. Our experiments revealed that the standard cloth yielded the best results. Using this cloth, the high dichroic ratio $D > 20$ was obtained. For the slightly smoother one, the dichroic ratio was almost similar ($D = 18$), but for the two smoothest clothes the ratios were noticeably lower with values of 14 and 11. These results indicate that an extremely smooth cloth with short and thin rubbing fibers does not produce better alignment layers, even though it possesses better homogeneity of the fibers. Instead, rubbing with too smooth clothes lowers the degree of alignment when PI or PI doped with ST 1163 is used as alignment layer. As described in section 2.2.5.2, either frictional heating or direct mechanical forces (or both)⁵⁰ are responsible for the alignment of the polyimide. Obviously, a certain length and diameter of the rubbing fibers is required to provide this necessary intensity of interaction.

d) Reproducibility

An important concern in the rubbing process are attrition effects of the rubbing cloth. After the treatment of about 50 samples, the expected and observed degrees of alignment did not match anymore. We attributed this behavior to attrition of the rubbing fibers. Caused by the repeated use of the rubbing cloth, the nature of the fibers might approach the characteristics of the shorter and thinner rubbing fibers discussed above, for which lower degrees of alignment were observed, too. As a result of these findings, the rubbing cloth was changed after the treatment of 50 samples.

e) Humidity

Temperature and humidity effects are also thought to play a role in the alignment procedure. We noticed that the first 2–4 samples after the very beginning of a rubbing cycle (after not having used the rubbing machine for more than one day) never yielded any degree of orientation. This might be understood by assuming that after storage, the rubbing cloth has a certain degree of humidity, which is eliminated by the first rubbing cycles. The humidity might plasticize and soften the fibers, reducing the interaction with the polyimide surface. As a conse-

quence, the rubbing was performed in a fume-hood under constant nitrogen flow in order to ensure the dryness of the fibers.

f) Annealing Conditions

We found that there is no alignment of the LC polymer, if the annealing is done in air. We attribute this behavior to the negative influence of both oxygen and humidity on the alignment process. Therefore, the annealing was always done under inert atmosphere.

6 Electroluminescence from Polyfluorene

6.1 (Undoped) Polyfluorene

In chapter 4 we established that the alignment of polyfluorenes in liquid crystalline state on top of alignment layers is an appropriate (and so far the only) method to orient these polymers. Furthermore, we found that the highest degrees of alignment were obtained from polyfluorenes, which were substituted with ethylhexyl side-chains. In chapter 5 we gained detailed information about the morphology and other essential properties both of the polyfluorene and of the required hole-transporting alignment layers. The following paragraph finally covers the electroluminescence of devices with polyfluorene emissive layer. In the first part, we describe the establishment of the most favorable device architecture and the optimization of the respective layers on the way from isotropic towards polarized LEDs. In the second part, we will see that the performance of the LEDs was drastically enhanced in every respect by chemical modification of the polyfluorene, which was accomplished by endcapping of the main chains with hole-transporting moieties.

The work presented in the following chapter was performed in close collaboration with Dr. Tzenka Miteva who worked at the Max Planck-Institute for Polymer Research in Mainz from 1998 until 2001.

6.1.1 Optimization of the Device Architecture in Isotropic LEDs

The fabrication of advanced polarized light-emitting devices, requires detailed knowledge of the essential parameters, which determine the performance of isotropic LEDs. For that reason, we first established the architecture and layer configuration, which yielded the best performance for isotropic devices, followed by the investigation, which of these results could be translated into the polarized case. From the previous sections we know that highly satisfying device performance implies a multilayer instead of a single-layer LED structure. In general, the goal of designing a multilayer structure is the minimization of the injection barrier heights and the balance of charge carrier injection, respectively. Thus, we have to establish a layer configuration, which harmonizes the barriers between the emissive layer and the electrodes. As discussed in section 3.1.1.1 the HOMO level of the polyfluorene under study, PF2/6, is at

~ 5.9 eV and the LUMO level at ~ 2.6 – 2.9 eV.⁴² Due to the need for a transparent material the work function of the anode is fixed to the value of the commonly used ITO of 4.8–5.0 eV,^{13,14} whereas the appropriate cathode material can be selected with respect to the LUMO level of the emitter. Usually, the cathode material to be evaporated is chosen among the low work-function metals aluminum (4.3 eV), magnesium (3.7 eV) and calcium (2.9 eV).

The electronic properties of PF2/6 suggest the usage of a hole-injection layer due to the large barrier from the ITO-anode. As stated in section 3.1.6, a commonly used hole-injection layer is PEDOT-PSS, increasing the work function of the resulting anode combination up ~ 5.2 – 5.3 eV.¹³ On the cathode side, calcium is an appropriate material. Possibly, the device performance might be enhanced by the use of an ultrathin LiF-layer between the polyfluorene and the cathode, as reported by several groups.¹⁷⁰ In Figure 6.1, a scheme of a typical isotropic multi-layer LED as well as a schematic energy level diagram are shown.

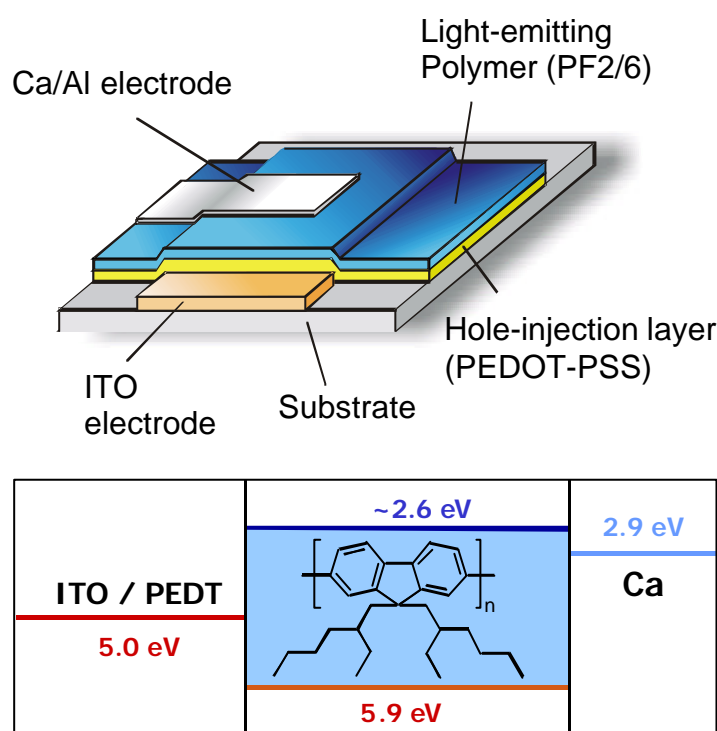


Figure 6.1. Schematic picture of a light-emitting device with a hole-injection layer of PEDOT-PSS below the emissive layer PF2/6. The energy levels of such a device are sketched in the lower drawing.

We compared devices with a 90 nm thick PF2/6 emissive layer and the mentioned cathode materials, and we simultaneously investigated the effect of 30 nm PEDOT-PSS hole-injection and 1 nm LiF electron-blocking layers, respectively. The thickness of Al and Mg cathodes was ~ 100 nm, and in case of the reactive calcium cathodes, a 20 nm thick Ca layer was covered

with a 100 nm Al protection layer in order to prevent from oxidation.* The device fabrication was done according to the procedure described in section 3.2.

As illustrated in Figure 6.2, the addition of PEDOT-PSS led to a dramatic increase both in the device brightness and in efficiency (see also Figure 6.3). As expected, the use of Ca yielded the lowest onset voltage of ~ 5 V. For all the cathode materials, the incorporation of an LiF layer led to enhanced device performance. The best isotropic diode structure with PF26 as emitting layer was shown to be ITO/PEDT/PF26/LiF/Ca, showing an onset voltage of ~ 4 V. For comparison, an isotropic diode with the multilayer architecture of a polarized LED is also shown. It contains a hole-transporting layer of polyimide doped with ST 638, as discussed in the next section. In this special case, the emissive polymer was not aligned on top of this diode.

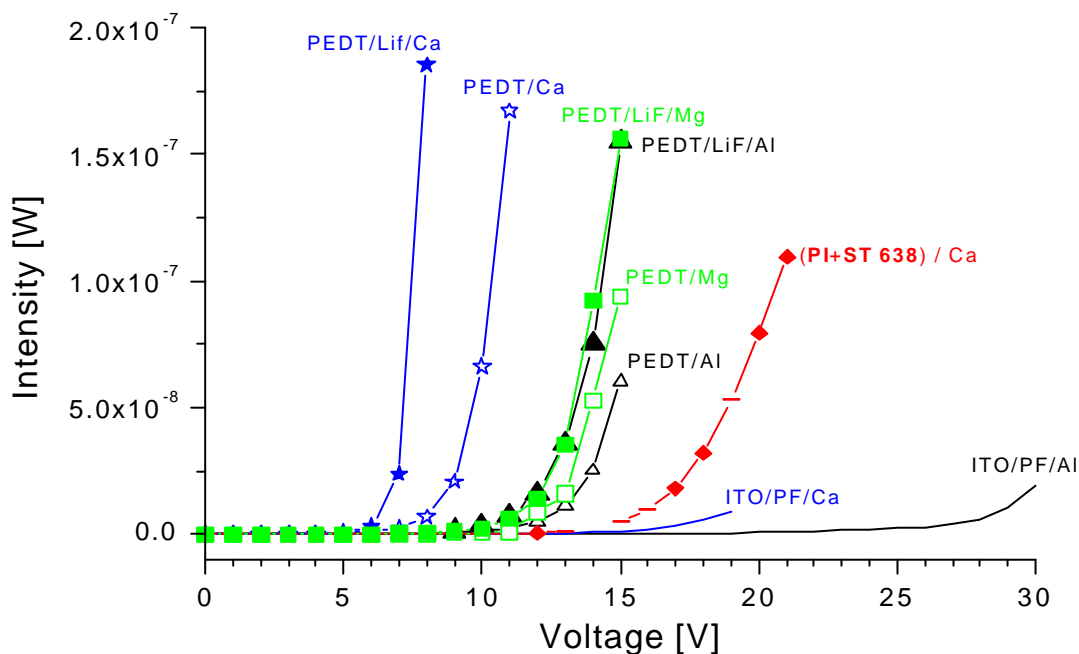


Figure 6.2. Intensity–voltage characteristics for diodes with isotropic PF2/6 emitting layer and different cathode materials, showing the effect of including a 30 nm PEDOT-PSS hole-injection layer and an 1 nm layer of LiF. For comparison, an isotropic diode with the structure of a polarized LED is also shown (PI + ST 638). 1 nW corresponds to approximately 1 cd/m² at this color.

* If we mention Ca cathodes in the following, it is always implied that they are covered by the Al protection layer.

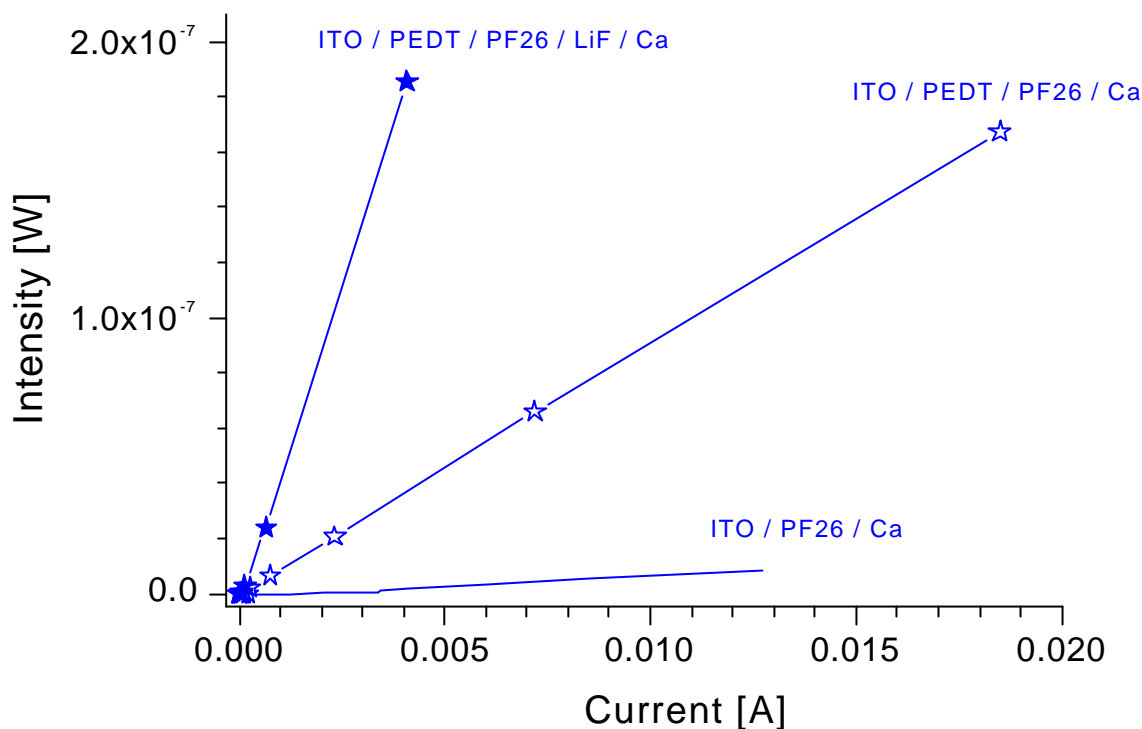


Figure 6.3. Intensity–current characteristics for diodes with isotropic PF2/6 emitting layer and different cathode materials, showing the effect of including a 30 nm PEDOT-PSS hole-injection layer and an 1 nm layer of LiF.

The EL performance is known to depend on the thickness of the emissive layer. Therefore, we investigated devices with PEDOT-PSS injection layer and Ca cathode and varied the thickness of the emitting layers from 70 to 200 nm (in this case, PF8C2/6 was used as emissive polymer). Figure 6.4 shows that the highest brightness and device efficiency was achieved for an active layer thickness of 70 nm. The devices with 95–100 nm thick emissive layers of PF8C2/6 had the same onset fields as those with 70 nm thick emissive layers, but the former were significantly more stable. It should be noted that the devices with 200 nm thick emissive layers had much lower onset voltages and higher brightness than those with 150 nm emissive layers. We believe that this irregular dependence of the device performance on the emissive layer thickness can be partly attributed to the reflection of the emitted light at the mirror-like metal electrodes. Depending on the thickness and the refractive index of the active layer, characteristic interference maxima and minima are generated, which might explain the observed behavior.¹⁵

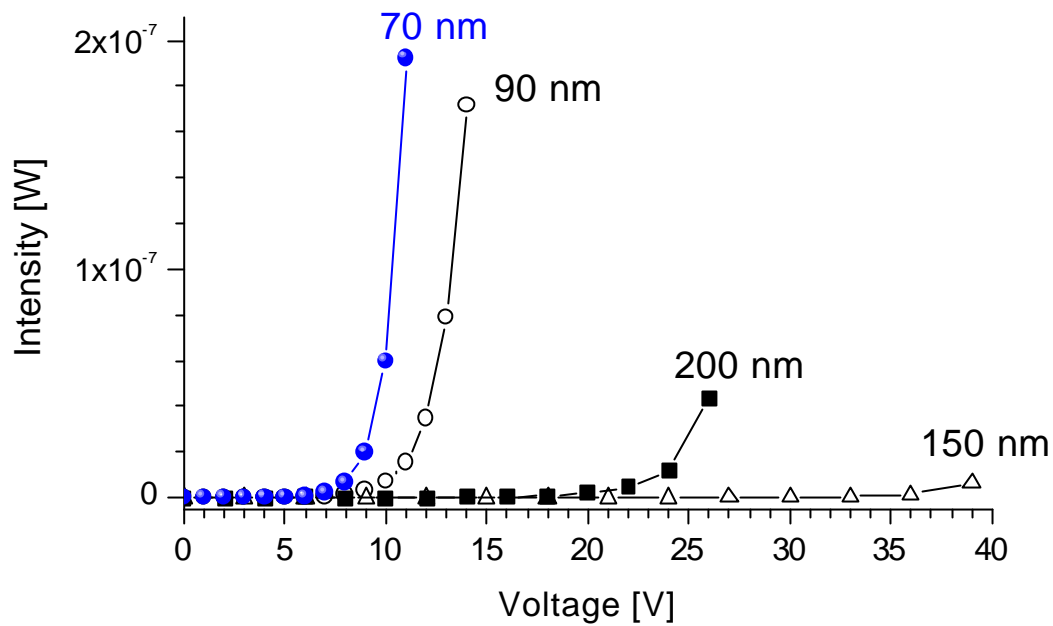


Figure 6.4. Influence of the thickness of the emissive layer on the device performance. The plot shows the intensity–voltage characteristics of isotropic devices of the structure ITO / PEDOT-PSS / PF8C2/6 / Ca.

In synthesis, we found that in the case of isotropic polyfluorene LEDs, the best results are obtained for a multilayer structure comprising an ITO anode and Ca cathode, and an emissive layer of thickness between 70 and 90 nm, which is sandwiched between a 30 nm PEDOT-PSS hole-injection layer and a 1 nm LiF-layer. Such devices have an onset voltage of ≈ 4 V, and the luminance at an operating voltage of 9 V is ≈ 200 cd/m² with CIE color coordinates of (0.21, 0.25), when using PF2/6 as the emitting material. The intensity–voltage characteristics together with the current–voltage curves and typical electroluminescent spectra are shown in Figure 6.5. The spectral characteristics will be discussed in section 6.1.3.

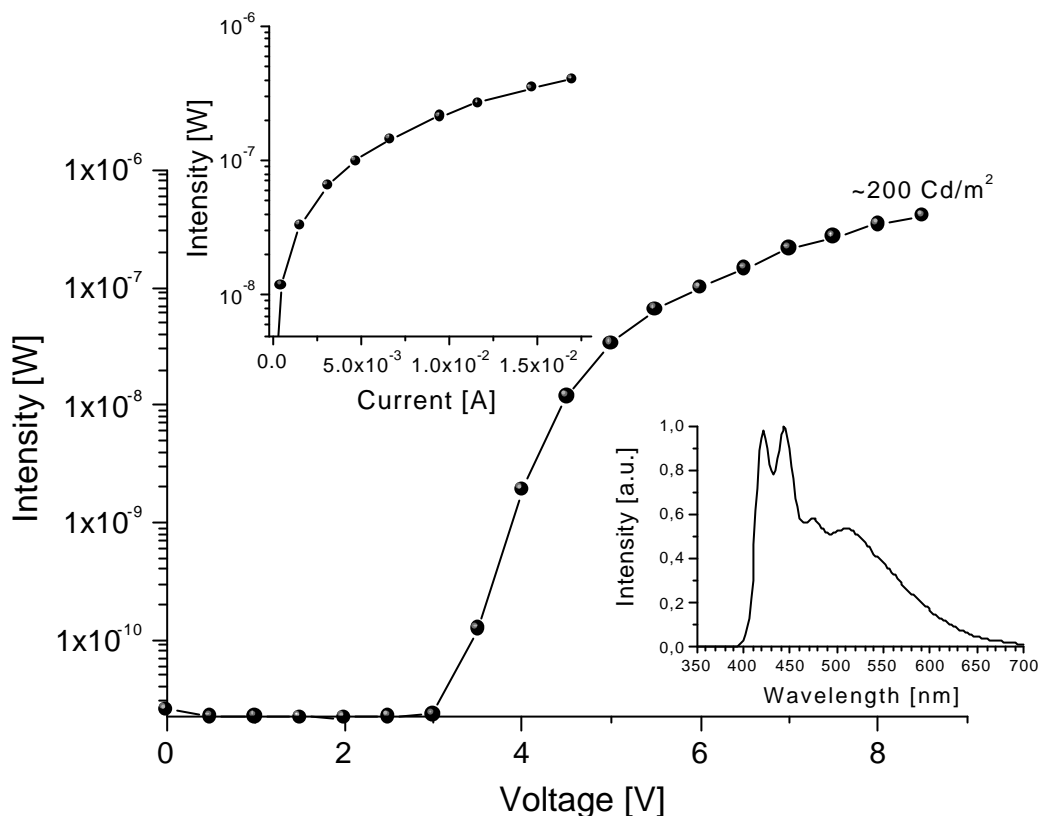


Figure 6.5. Intensity-voltage curves for devices with PF2/6 emissive layers. Insets: Intensity-current curves and electroluminescence spectra for the same devices (PEDOT-PSS hole-injection layers, Ca cathodes).

6.1.2 Polarized Electroluminescence from Undoped Polyfluorene

The results obtained in the last section can be transferred to the case of polarized LEDs, as far as the emissive layer thickness and the cathode side is concerned. Accordingly, the upper section of the multilayer structure also consists of a 70–90 nm thick PF2/6 layer, which is covered by a thin LiF layer and a Ca cathode. However, the alignment of PF2/6 requires the incorporation of an hole-transporting alignment layer of doped polyimide. For the polarized LEDs described in this work, PEDOT-PSS cannot be used as hole-injection layer, as it is not stable at temperatures higher than 200 °C, at which the HTALs have to be converted (see chapter 3).

In a first step, we tested polarized LEDs with only one HTAL between the ITO and the emissive layer. We shortly mentioned these devices in section 5.2.3. The respective LED structure resembled the one shown in Figure 6.1, with the only difference that the PEDOT-PSS was replaced by a rubbed HTAL of polyimide blended with 17 wt.% ST 638. The luminescence-voltage curve of such an aligned ITO/(PI+ 17%ST 638)/PF2/6/Ca device measured without polarizer is shown in Figure 5.10. An onset voltage of 12 V and luminance of 200 cd/m² at 18 V are typical for these devices. The emission appears blue with maxima at 425, 451 and

typical for these devices. The emission appears blue with maxima at 425, 451 and 477 nm and a shoulder at 505–510 nm for the light emitted with polarization parallel to the direction of rubbing. The maxima of the emission perpendicular to the rubbing are blue-shifted by approximately 5 nm. The electroluminescence spectra were very similar to the ones shown in Figure 6.7. The emission was highly anisotropic with a polarization ratio of 15 at the emission peak at 451 nm.

In a next step we obtained, as demonstrated in section 5.2.2.1, enhanced device performance using a *bilayer* HTL structure, i.e. a rubbed HTAL of polyimide doped with a low molecular hole-transporting material on top of a pure hole-injection layer, as shown in Figure 6.6.

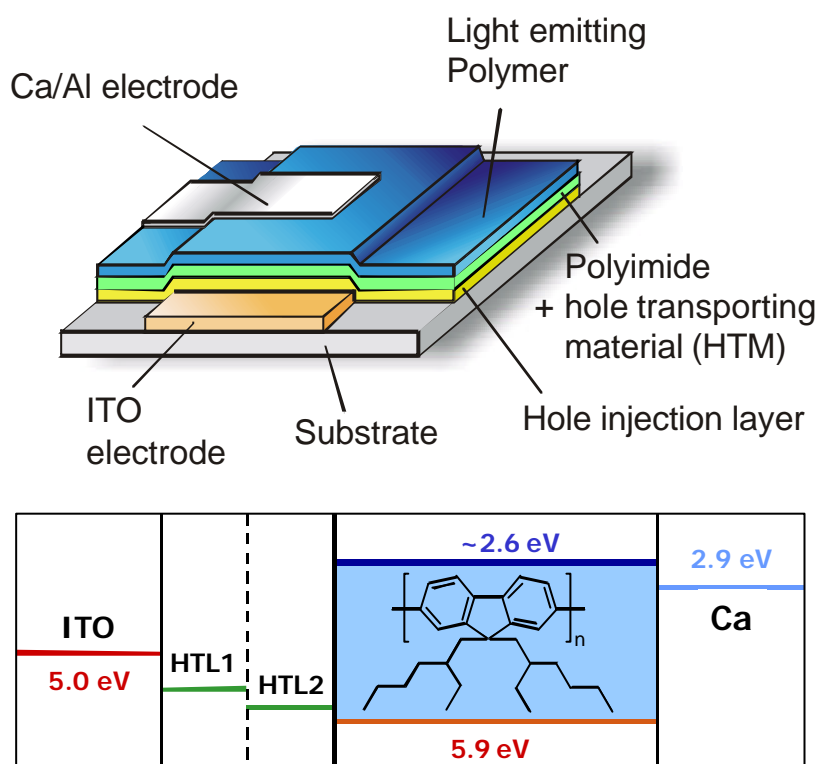


Figure 6.6: Schematic picture of a polarized light-emitting device with a rubbed hole-transporting alignment layer of doped PI and an additional hole-injection layer (consisting of a hole-transporting material) below the emissive layer. The energy levels of such a device are sketched in the lower drawing.

In section 5.2.2.1 we demonstrated that the insertion of a pure layer of ST 638 below a rubbed layer of (PI+ 20 wt.% ST 16-7) allowed for a device operation at considerably lower fields than in the case of devices without additional hole-injection layer below the HTAL (Figure 5.11). The degree of alignment was significantly increased by doping the PI with ST 16-7 instead of ST 638, while the spectral characteristics were unchanged. As shown in Figure 6.7, the emission parallel to the rubbing again peaked at 450 nm and the respective polarization ratio was as high as 21. The typical luminance of these devices was 100 cd/m² at 18 V.¹⁴²

Comparing the spectra of isotropic and aligned LEDs reveals obvious differences of the characteristic shape. We attribute this to thermal effects, which are caused by the annealing procedure rather than to order effects.

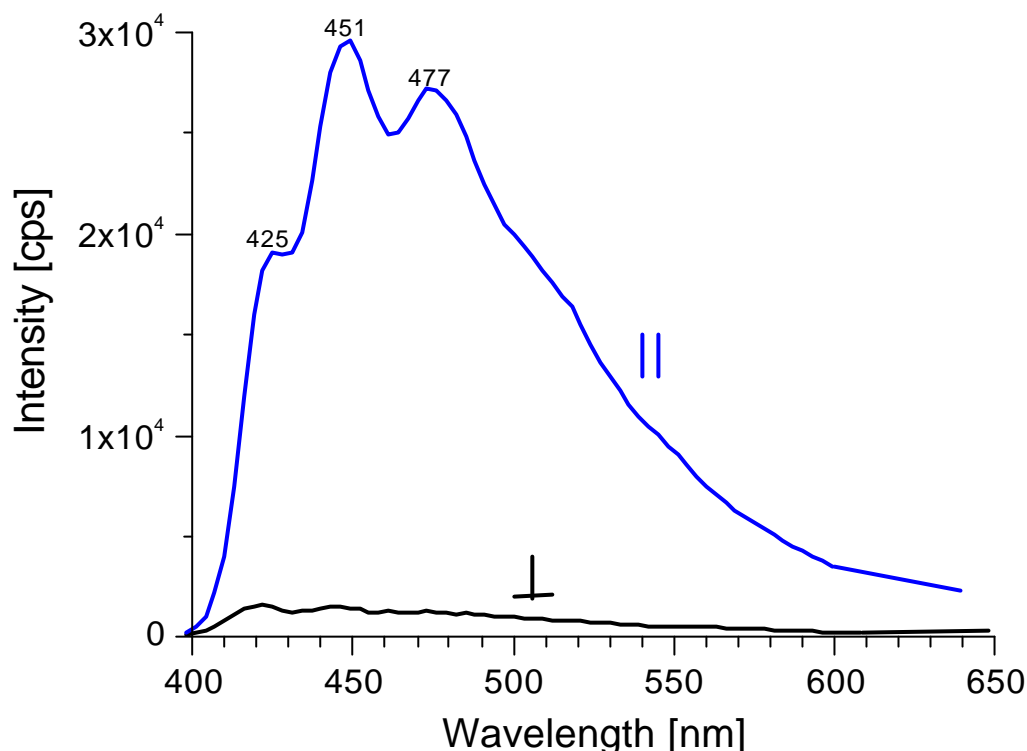


Figure 6.7. Electroluminescence spectra parallel and perpendicular to the direction of rubbing for devices of the structure ITO/ST 638/(PI+ 20% ST 16-7)/PF2/6/Ca. The polarization ratio at the peak at 451 nm was 21.

6.1.3 Problems with the Use of Undoped Polyfluorene

Although both the isotropic and polarized LEDs discussed above showed comparatively bright and blue emission, with the polarized LEDs reaching very high polarization ratios in excess of 20, all the devices based on non-aligned and aligned PF2/6 homopolymers displayed a red-shifted emission contribution in the electroluminescence spectrum. The intensity of this long-wavelength tail was found to vary for different batches of PF2/6 with different molecular weights. Furthermore, the device efficiency did not remarkably exceed values of ≈ 0.5 cd/A for the isotropic and 0.1 cd/A for the polarized LEDs. In section 3.1.1.1 we learned that the red-shifted emission tail is assigned to interchain interactions, which do form in films of conjugated polymers, such as aggregates and excimers.¹⁴⁷⁻¹⁴⁹ In general, interchain interactions imply a delocalization of the excited state wave function, which lowers the energy of this state relative to a

single-chain exciton, explaining the red-shift of interchain luminescence relative to the standard exciton emission. Likewise, also the low efficiency is attributed to aggregates and excimer forming sites, since they are known to provide nonradiative relaxation pathways, which lead to reduced emission efficiency relative to exciton luminescence.^{42,53,114,148,149}

Sainova *et al.* demonstrated that the simple physical addition of a small amount of low-molecular HTMs to the PF2/6 led to an effective suppression of the red-shifted emission contribution and an considerable increase in the luminance efficiency.¹⁶⁸ This was attributed to hole-trapping effects, which are explained as follows. The species responsible for the green emission contribution, which are believed to be already present in the ground state are predominantly populated due to charge carrier trapping. Thanks to the low ionization potential of the HTMs they also act as very efficient hole-traps, and compete with the aggregate sites for holes. The latter might actually become detrapped from the HTM and recombine with an electron on a nearby polyfluorene chain instead, provided that the HTMs are molecularly dispersed in the blend (Figure 6.8).

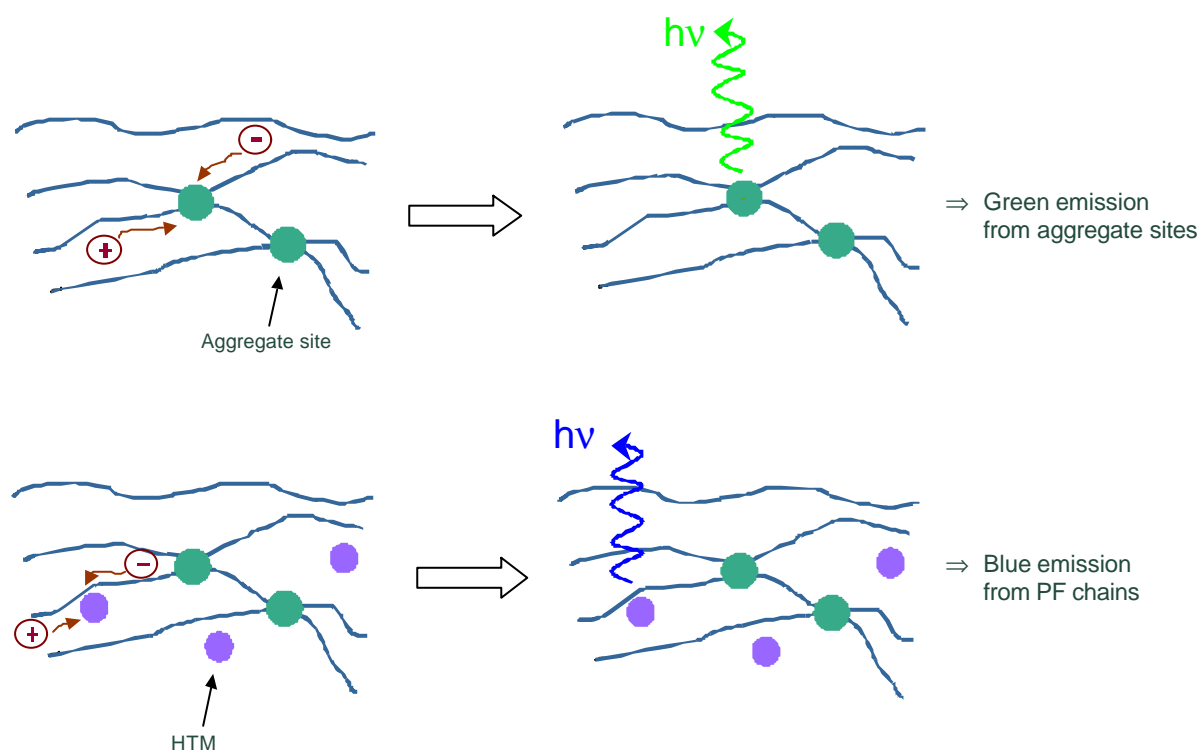


Figure 6.8. Cartoon explaining the blue emission in case of doping the PF2/6 layer with HTMs with low-oxidation potential. Due to hole-trapping at the HTM sites, recombination occurs predominantly along the chain rather than on aggregate sites.

However, the concept of doping the polyfluorene with low-molecular weight HTMs implies the possibility of phase-separation. As a consequence, the long-term device stability is severely affected and the LC properties of the polymer may be disturbed or even destroyed by the presence of the HTMs. In the next section, we demonstrate that a successful approach to over-

come this problem was the chemical attachment of the HTMs by endcapping the polyfluorene main chains.

6.2 Endcapped Polyfluorene

In the following, we show that endcapping of the polyfluorene main chain with low-molecular weight hole-transporting moieties is a concept, which extends the positive effects obtained for simply doping these HTMs into polyfluorene while simultaneously avoiding the observed problem of phase-separation.

6.2.1 Isotropic Electroluminescence from Endcapped Polyfluorene

6.2.1.1 Influence of the Endcapping on the Charge-Transporting Properties

In section 3.1.1.2 we investigated the chemical and electronic properties of PF2/6 endcapped with two types of HTMs. In the first case, PF2/6 was endcapped with bis(4-methylphenyl)(4-bromophenyl)amine, resulting in PF2/6am-X, where 'X' denotes the endcapper/monomer feed ratio in mol%. The second end-group was (4'-bromo-biphenyl-4-yl)naphthalen-2-yl-phenyl-amine, and the corresponding polymer is referred to as PF2/6nap-X. The chemical structures of these polyfluorenes are shown in Figure 3.6.

By means of cyclic voltammetry (Figure 3.7) we found that the end-groups act as independent electroactive moieties and that they form traps for holes within the PF matrix. In order to investigate the effect of the terminal HT moieties on the charge-transporting and emissive properties of the endcapped polyfluorenes, single layer sandwich devices were fabricated with either hole-injecting gold or with electron-injecting Ca/Al top electrodes.

Hole-only devices with PF2/6am-X active layer and a 50 nm Au top electrode reveal a pronounced effect of the endcapper on the current-voltage characteristics (Figure 6.9a). The current for devices with 2 mol% endcapper content is substantially lower than in the case of the non-endcapped PF2/6, whereas with increasing endcapper content, the values approach the characteristics of the pure material. The inset in Figure 6.9a shows that the current density j through the hole-only device increases gradually for higher endcapper concentrations after a sharp initial drop at low concentrations. The overall dependence of j on the endcapper concentration agrees qualitatively with the change of hole mobility in polymers doped with hole-

transporting molecules with increasing dopant concentration.¹⁹⁷ For the latter system, Pai *et al.* explained the sharp decrease at low concentrations by severe *hole-trapping* on the dopant molecules, while the gradual increase at higher concentrations was attributed to *charge transport* by hopping via the dopant molecules. The latter opens a new channel for charge carrier transport and explains the increased current density. In addition, at higher endcapper concentrations the hole-injection into the polymer is further expected to be facilitated in case of the hole-only devices discussed here.

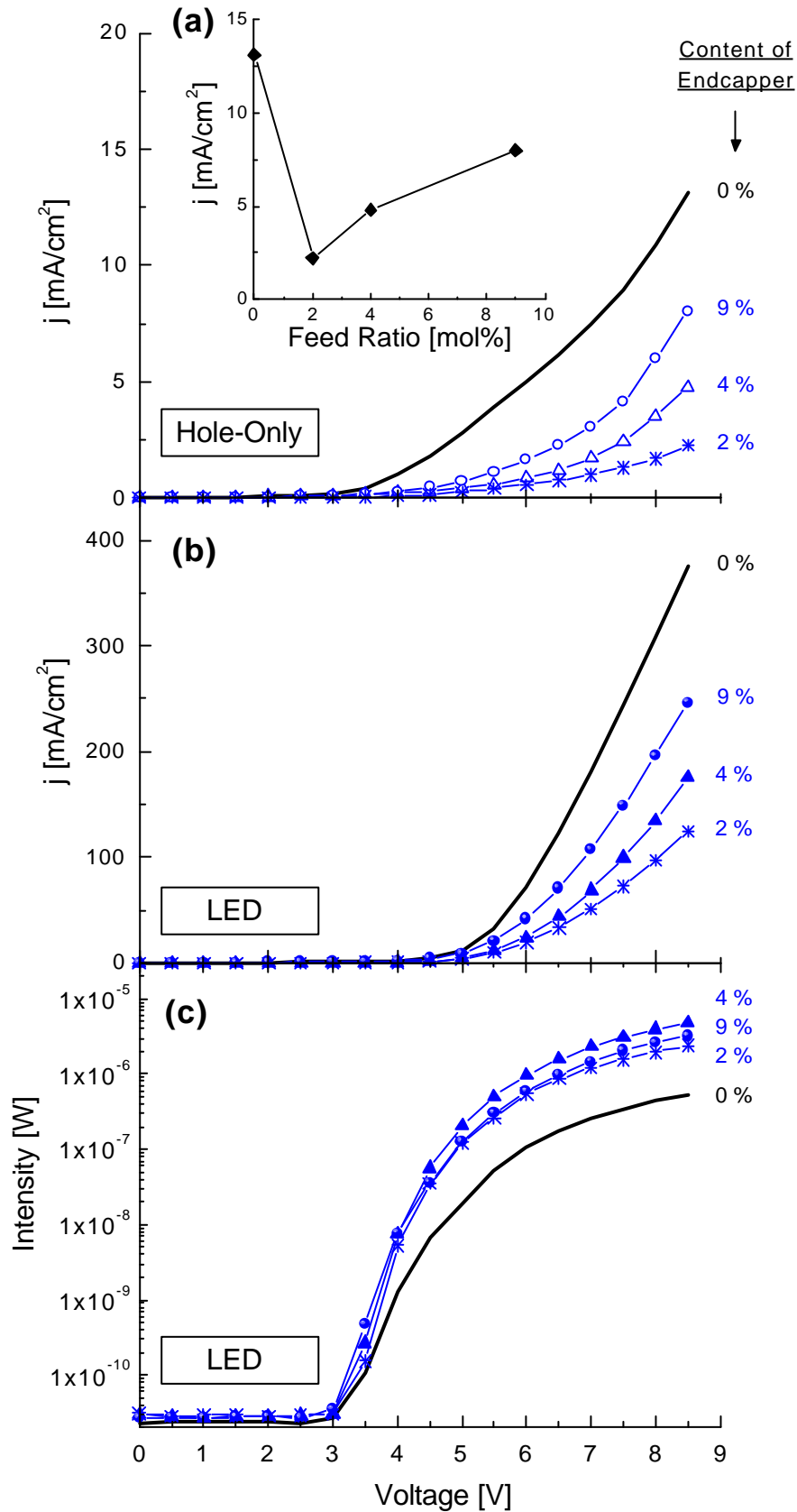


Figure 6.9. Current–voltage characteristics of (a): hole-only devices: ITO/PEDOT-PSS/PF2/6am-X/Au (open symbols) and (b) the corresponding LED devices: ITO/PEDOT-PSS/PF2/6am-X/Ca (solid symbols): PF2/6 (no symbols); PF2/6am2 (stars); PF2/6am4 (triangles); PF2/6am9 (circles). The inset shows the current density through the hole-only devices at 8.5 V as a function of the endcapper feed ratio (in mol%). (c): Intensity–voltage characteristics of the LEDs on a logarithmic scale. At the emissive color of the endcapped polyfluorene, 1 nW corresponds to ~ 0.3 cd/m².

6.2.1.2 Influence of the Endcapping on the Emission Characteristics

When electron injection is enabled through a 20 nm Ca-top electrode, the current in forward bias increases significantly (Figure 6.9b). This indicates that electrons rather than holes dominate the current through these bipolar devices (see also section 7.2.3.2). Figure 6.9 and 6.11 show that the attachment of HT moieties significantly raises the emitted light intensity compared to the non-endcapped PF2/6, whereas a further increase of the endcapper concentration itself does not lead to considerable changes. Most notably, the green emission tail peaking at ca. 515 nm, which was observed for the non-endcapped PF2/6, decreases continuously with increasing endcapper concentration, and is finally completely suppressed in the emission from the devices with a PF2/6am9 emitting layer.

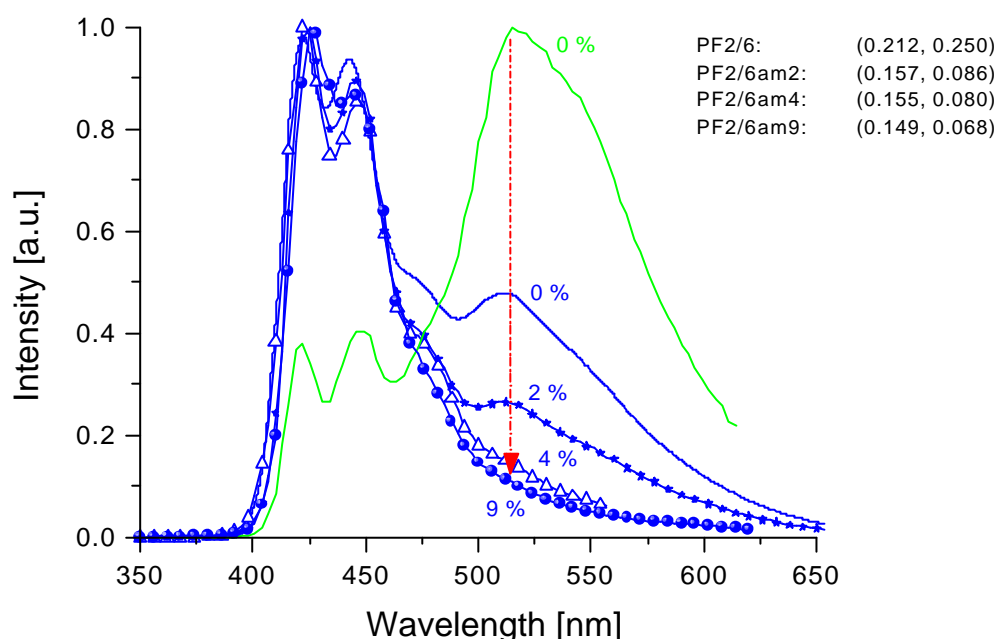


Figure 6.10. Emission spectra of the LEDs based on endcapped polyfluorene PF2/6am-X, and on pure PF2/6, respectively. PF2/6 (no symbols; the two spectra shown correspond to batches with molecular weights of $M_n = 195\,000$ g/mol (green line) and $M_n = 111\,000$ g/mol (blue line)); PF2/6am2 (stars); PF2/6am4 (triangles); PF2/6am9 (circles). The suppression of the red-shifted emission contribution with increasing endcapper content becomes evident. The spectra were recorded at a driving voltage between 4.5 V and 5 V. The CIE-coordinates of the respective devices are also given.

These results confirm the assumption made in section 6.1.3 that in case of the non-endcapped PF2/6 a certain fraction of the electron-hole-recombinations takes place at sites, which are less efficient emitters, such as aggregates or excimer forming sites.^{53,147-149,168} On the contrary, in the layers of the endcapped polyfluorenes, the predominant fraction of holes might be guided to the chain ends via charge-trapping, followed by recombination with an electron on the polyfluorene main chain, as sketched in Figure 6.8.

Strong evidence that the observed changes in device performance are related to the endcapper moieties rather than to the change in the molecular weight comes from the comparison of the two different endcappers. As illustrated in Figure 6.10 and Figure 6.11, the device performance is drastically improved when the endcapper bis(4-methylphenyl)phenylamine with the lower oxidation potential (Figure 3.7) is attached to the PF2/6. In this case, we noticed the suppression of the red-shifted emission as well as a substantial increase in the EL intensity at a given voltage. On the other hand, the (N-(biphenyl-4-yl)-N-naphth-2-yl-N-phenylamine) endcapper also leads to a suppression of the red-shifted emission, but the increase in device efficiency is only weak.

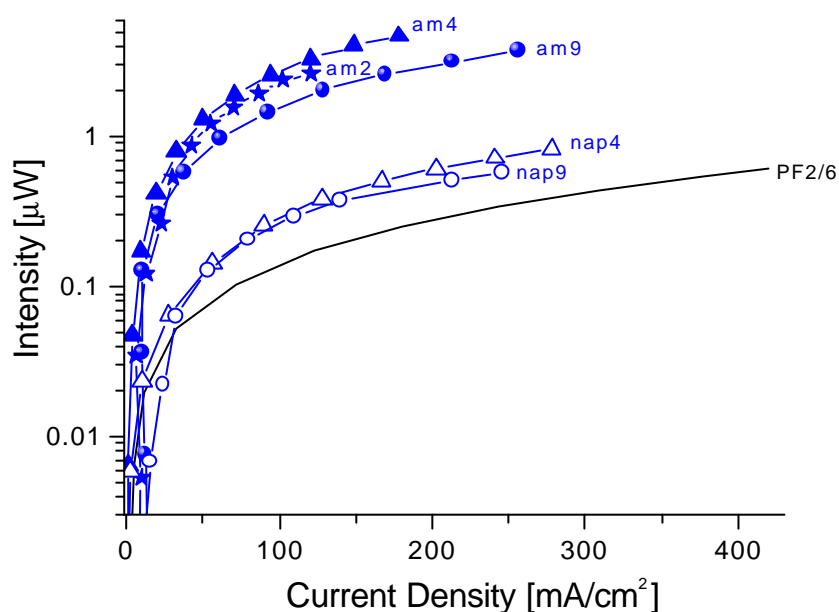


Figure 6.11. Comparison of intensity–current characteristics for LEDs based on endcapped and on pure polyfluorene, respectively. PF2/6 (no symbols), PF2/6napX (open symbols), and PF2/6am-X (filled symbols).

6.2.1.3 Performance of Isotropic LEDs from Endcapped Polyfluorene

The best diode performance was obtained for devices with PF2/6am4 with an endcapper feed ratio of 4 mol%. They exhibited an onset voltage of 3.5 V, a maximum luminance of 1600 cd/m² with a luminance efficiency of 1.1 cd/A, and CIE-color coordinates (0.150, 0.080) at 8.5 V, which is a deep blue. These values correspond to a luminous efficiency of 0.40 lm/W. At this concentration, the red-emission contribution is almost completely suppressed, but the concentration is still too low to allow for predominant charge transport by hopping via the endcapper groups (see also discussion in Pai *et al.*¹⁹⁷). Compared to the device with the non-

endcapped PF2/6, an improvement in efficiency of more than one order of magnitude is achieved, without disturbing the electronic and chemical structure of the backbone.

Figure 6.12 shows that the photometric efficiencies of all devices with PF2/6am-X emission layers depend only very weakly on the emission brightness for luminance higher than 200 cd/m^2 . Moreover, there is a complete color stability during the device operation for a given operation voltage. Interestingly, the emission color changes significantly from greenish-blue with coordinates (0.220, 0.217) to blue with increasing the bias beyond $\approx 4 \text{ V}$, and remains deep blue at higher voltages. This behavior is completely reversible. The greenish-blue emission color of the devices with all PF2/6am-X polymers at voltages below 4 V (corresponding to current levels of ca. $1\text{--}10 \text{ mA/cm}^2$) resembles the emission of the pure non-endcapped PF2/6. This indicates that the traps introduced by the endcapper moieties are not yet occupied at lower voltages.

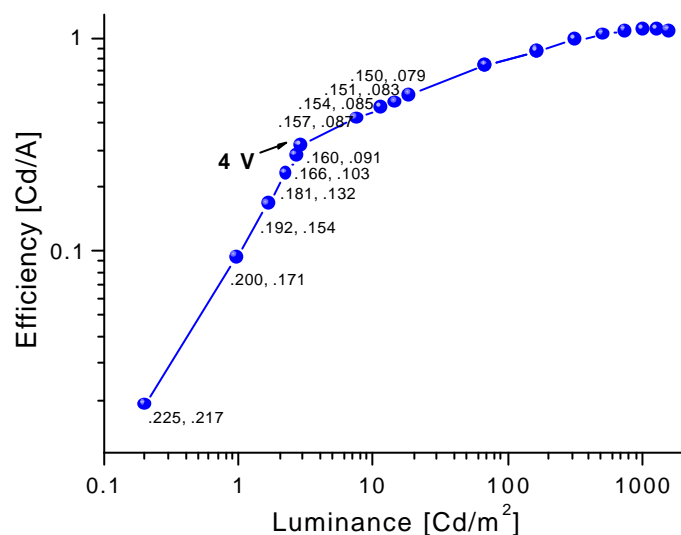


Figure 6.12. Efficiency–luminance–curve for an isotropic LED based on PF2/6am4. The numbers along the curve are the CIE-coordinates at the corresponding luminance levels.

Our results are better than $\approx 0.75 \text{ cd/A}$ at 1500 cd/m^2 which have been reported for optimized ITO/PEDOT-PSS/PFO/Ca devices.⁵³ For these devices a much lower content of the less efficient aggregate sites in their PF8 layers was achieved by narrowing the molecular weight distribution of the polymers, but the high sensitivity on morphological changes during the device operation was still present. On the contrary, aggregation seems not to be a critical issue in case of endcapped polyfluorenes. As described above the endcappers are believed to compete with the aggregate sites with respect to charge carrier trapping. Thus, aggregate sites, even though present in the material, will not be occupied by a large fraction of the overall number of injected charge carriers, and the contribution of the aggregates to the emission will be minor (see also the discussion in the following sections).

The luminous efficiency at high luminance compares well with that reported for an optimized three-layer device with a thermally-crosslinked polyfluorene emission layer at a comparable luminance.¹⁹⁸ An even higher efficiency of 2.7 cd/A at 100 cd/m² has recently been achieved using a PF2/6am2 emission layer and three crosslinked hole-injection layers (“graded injection”). For a luminance of 1000 cd/m² the efficiency dropped only slightly to 2.4 cd/A.¹⁹⁹

6.2.2 Polarized LEDs from Endcapped Polyfluorene

We confirmed that endcapping the polyfluorene with HT moieties maintained the LC properties and alignment abilities of the pristine polyfluorene. This is in contrast to, for example, the approach of the incorporation of hole-transport moieties into the polymer backbone,²⁰⁰ resulting in purely amorphous layers, which are not suitable for alignment. Another important finding with respect to polarized electroluminescence was that endcapping allowed for the tuning of the molecular weight, which has significant influence both on the transition temperatures and on the alignment behavior of the respective polymer (section 5.1.1). Consequently, all endcapped polyfluorenes showed similar or even higher alignment ability on rubbed alignment layers than their non-endcapped counterpart, and additionally, the annealing could be performed at lower temperatures. As shown in Table 5.1 and Figure 5.13, dichroic ratios of more than 20 were achieved for endcapped PF2/6am-X.

Polarized LEDs have been fabricated following the procedure as described in section 3.3 using a polyimide alignment layer doped with hole-transporting molecules ST 1163 at various concentrations. Generally, the best performance was observed for devices with a PF2/6am9 emission layer. We believe that due to the rather poor hole-transporting properties of the doped polyimide, the hole-current in these multilayer devices is limited by the alignment layer rather than by the emissive polymer layer. This was demonstrated both for non-aligned and aligned diodes and for different concentrations of ST 1163. As shown in Figure 6.13, the peak polarization ratio of the electroluminescence intensity reached values of 22 for an ST 1163 concentration of 10 wt.%, and 15 for a concentration of 15 wt.%. In the first case, the luminance was up to 200 cd/m² at 19 V, and the latter devices attained up to 800 cd/m² at 18 V with an efficiency of 0.25 cd/A. At comparable polarization ratios and brightness levels, the efficiencies of our polarized light emitting devices are more than doubled compared to the values reported by Whitehead *et al.* for PF8 based devices¹¹² and by Jandke *et al.* for devices based on rubbing-aligned PPV.⁸⁶

The Figure also shows that raising the concentrations of the dopant within the polyimide matrix from 10 to 30 wt.% led to drastically enhanced brightness of the devices, but at the same

time the polarization ratios dropped from values of 22 down to 5. Reasons for this behavior are given in section 5.2.4.

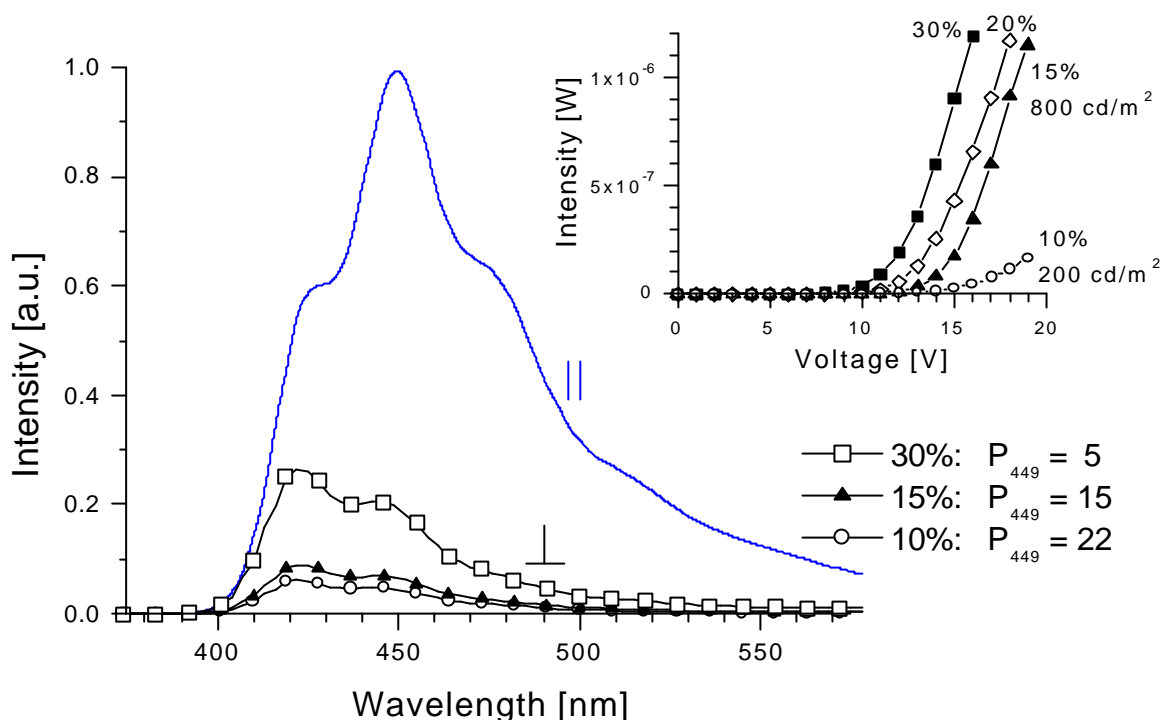


Figure 6.13. Polarized emission spectra for devices with 80 nm PF26am9 emissive layer and different concentrations of ST 1163 in the 30 nm HT alignment layer, normalized to identical parallel emission. The polarization ratios P of the respective devices are also given. (Hole-injection layer: 25 nm ST 1163, Ca cathodes). Inset: Intensity–voltage characteristics for the same devices.

In conclusion, we have seen that endcapping of the main chain of a polyfluorene homopolymer with hole-transporting moieties opened a way to blue LEDs with clearly enhanced efficiency and high color stability, without altering the electronic properties of the conjugated polymer backbone. Furthermore, we demonstrated that endcapping did neither disturb the LC properties nor the orientational abilities of the polyfluorene. Highly anisotropic LEDs with polarization ratios of 22 reaching luminance of 200 cd/m^2 at operating voltage of 19 V have been realized. LEDs with a polarization ratio of 15 showed a luminance of even 800 cd/m^2 .

7 Doping of Charge-Trapping Dyes into Polyfluorene

7.1 Green Emissive Thiophene Dyes

7.1.1 Isotropic Electroluminescence

As mentioned in section 2.1.4, blue emitters are of great interest, since full color displays can be realized by down-conversion from blue to green and red light. From the mentioned variety of blue-emitting conjugated polymers – such as derivatives of poly(*p*-phenylenevinylene)s (PPVs),²⁰¹ poly(*p*-phenylene)s (PPPs)^{202,203} and the poly(alkylfluorene)s^{42,53,55,56,204} – color tuning can be easily achieved by doping with lower band gap materials. For example, it was shown that doping a small amount of a fluorescent dye into an OLED can lead to significant changes in the color of luminescence.^{166,167}

In the following, we report on the effect on the emission color and on the device performance upon doping a low-molecular weight fluorescent thiophene dye S2_3 (inset Figure 7.1) into polyfluorene. With the aim to realize polarized emission, we chose this rod-shaped green-emitting dye, with photoluminescence peaking at 527 nm (not shown) and with absorption spectra as plotted in Figure 7.1. Due to its highly satisfying performance we used PF2/6am4 as the emissive host (section 6.2).

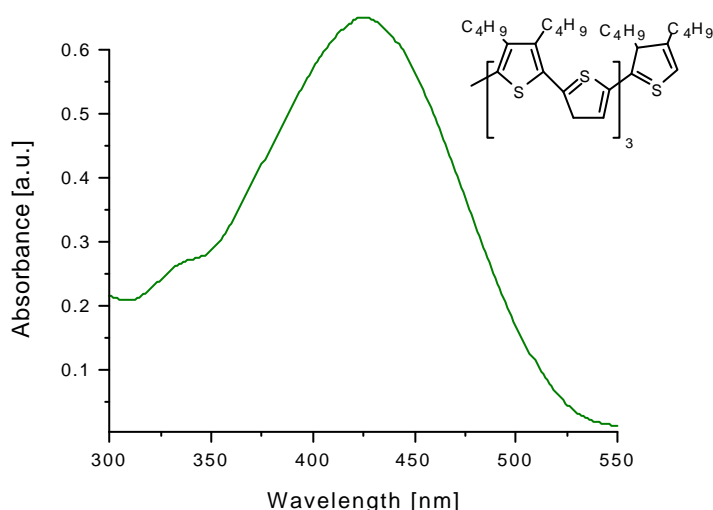


Figure 7.1. Absorption spectrum of a drop-casted layer of the thiophene dye S2_3, the chemical structure of which is also shown.

In Figure 7.2 we compare the electroluminescence spectra obtained from a device of the structure ITO/PEDOT-PSS/(PF26am4 + 1 wt.% S2_3)/LiF/Ca with a corresponding device of pure PF2/6am4 as emissive layer. In case of doping, we clearly observe emission from the dye. The peaks in the blue region of the spectrum are almost completely suppressed and the emission is dominated by the inherent peak of the dye at 527 nm. Considering the absorption characteristics of the dye and the emission properties of the polyfluorene suggests the energy transfer to occur via Förster transfer^{4,205} between energy donor (polyfluorene) and acceptor (dye) (see also section 7.2.3.1).

The performance of the doped device was highly satisfying. The recorded luminance was up to 5100 cd/m² at 13 V with an efficiency of 3.1 cd/A for emission peaking at 530 nm (Figure 7.3). The dopant concentration of 1 wt.% was low enough to prevent any phase-separation.

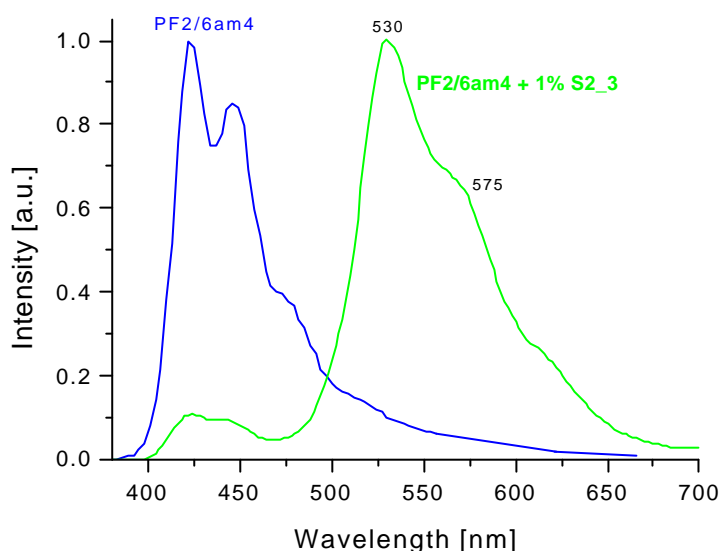


Figure 7.2. Emission spectra of LEDs with an emissive layer of PF26am4 (80 nm) doped with 1 wt.% of the low molecular emitter thiophene dye S2_3. PEDOT-PSS was used as hole-injection layer and LiF/Ca/Al as cathodes.

The light power intensity of the doped LEDs was almost one order of magnitude lower, but the luminance was more than three times higher (Figure 7.3).^{*} Since the current in the doped devices was 2–3 times lower (not shown here), the luminance efficiency was dramatically enhanced by the addition of S2_3, which is also attributable to the greener emission color. The intense color change suggests that the generation of excitons and subsequent recombination occurs directly on the dye. The different mechanisms of Förster energy transfer^{4,205} and charge carrier trapping, leading to the emission from guest molecules, which are blended into a host matrix, will be addressed in section 7.2.3.

^{*} This is due to the dependence of the photometric quantities on the selective spectral responsivity of the human eye (Appendix A.1, Figure A.1).

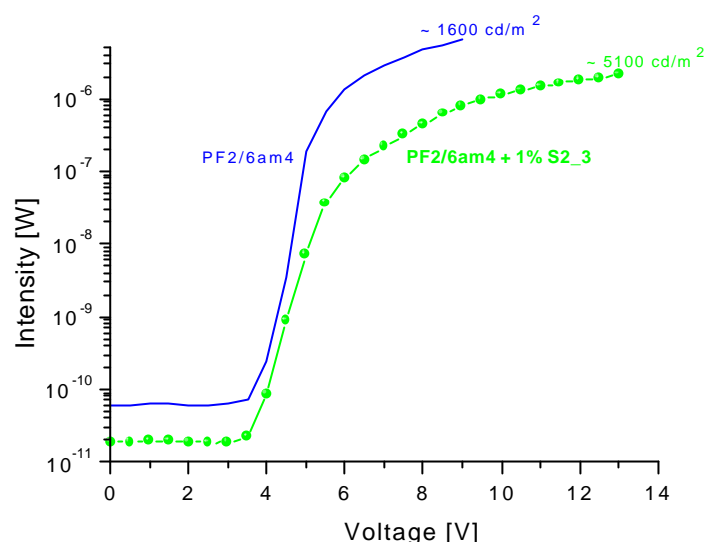


Figure 7.3. Intensity–voltage curves of LEDs with emissive layer of PF26am4 (80 nm) doped with 1 wt.% of the low molecular emitter thiophene dye S2_3. PEDOT-PSS was used as hole-injection layer and the combination of LiF/Ca/Al as cathodes.

7.1.2 Polarized Electroluminescence

The rod-like structure of the low-molecular thiophene dye suggested that the addition to polyfluorene should not affect the alignment behavior known from the undoped polymer. We investigated whether the potential of S2_3 for color tuning and efficiency improvement could be used in polarized emitting LEDs.

We doped PF2/6am4 with S2_3 at different concentrations and fabricated polarized LEDs of the structure ITO/ST 1163/(PI + 15 wt.% ST 1163)/(PF26am4 + x wt.% S2_3)/LiF/Ca. The influence of the doping on the alignment and on the device performance was studied by comparing the doped devices with corresponding LEDs of pure PF2/6am4.

The intensity–voltage and current–voltage characteristics of the respective devices are plotted in Figure 7.3. Except for the device with the highest dye content of 1 wt.%, the overall dependence of the current on the filler concentration is similar to the one observed for the end-capped devices, as discussed in section 6.2.1.1. The sharp decrease at low concentrations is attributed to severe *hole-trapping* on the dye molecules, while the gradual increase at higher contents is explained by *charge transport* by hopping via the dye molecules. The current characteristics of the devices with 0.3 wt.% dye concentration are comparable to the undoped devices, which might point to additional hopping via dye *and* endcapper moieties due to the increased proximity of the two species. The drop in the current of the device with 1 wt.% S2_3 is not unambiguously clear, but might be a symptom of phase-separation and aggregation.

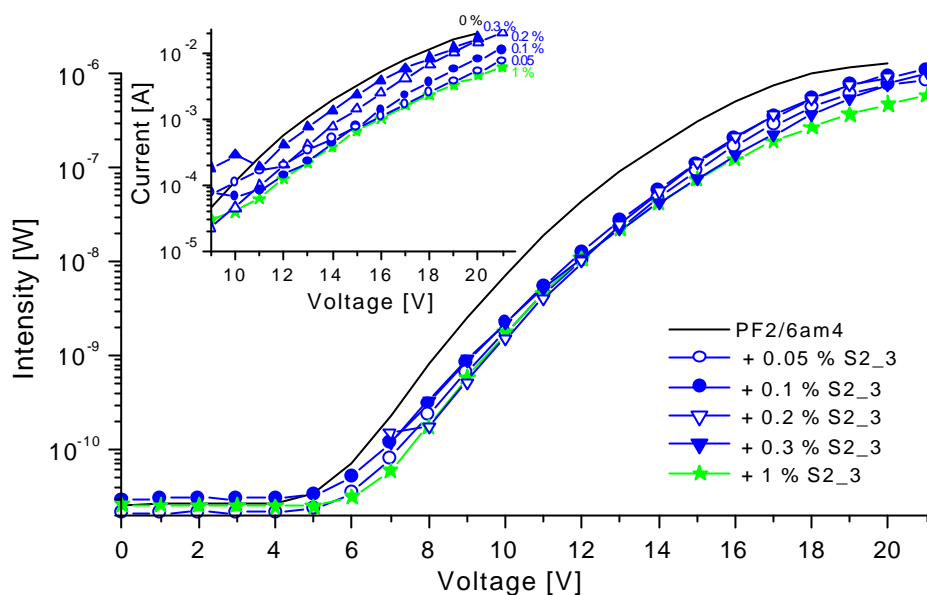


Figure 7.4. Intensity–voltage curves of polarized LEDs with the following structure ITO/ST 1163/(PI + 15 wt.% ST 1163)/(PF26am4 + x wt.% S2_3)/LiF/Ca. The inset shows the current–voltage characteristics of the corresponding devices.

The polarized electroluminescence spectra of the investigated LEDs are shown in Figure 7.5. First, we notice that all devices are highly anisotropic. As summarized in Table 7.1, the polarization ratio of the LED with a dopant concentration of 0.3 wt.% is 23 at the peak at 450 nm, and as high as 30 at 510 nm. The recorded luminance was 600 cd/m^2 and the efficiency was 0.30 cd/A . These are the highest values reported for polarized OLEDs so far. In case of 0.1 wt.% filler content, the degree of anisotropy is only slightly lower, while the luminance reaches 720 cd/m^2 at 0.50 cd/A . For the devices with 1 wt.% S2_3 in the blend, which display the highest contribution of green emission, the polarization ratio at 510 nm is 20 at a luminance of 500 cd/m^2 and an efficiency of 0.50 cd/A .

The spectra for doping concentrations of 0.1 and 0.3 wt.% resemble the ones recorded for the isotropic devices with pure PF2/6 emissive layers and PF2/6am2, respectively (section 6.2.1.2). One might assume that the green emission contribution could be attributed to aggregates rather than to the S2_3 dye. The remarkable difference to the spectra of pure PF2/6 layers shown in Figure 7.5, however, disproves this assumption.

Comparing the spectra of the polarized devices with the corresponding isotropic LEDs (Figure 7.2), reveals that in the case of anisotropic devices, the contribution of the dye to the emission is much less pronounced. The suppression of the blue emission contribution from the polyfluorene is considerably weaker and the peak at 450 nm is still higher than the peak of the dye at 527 nm. We assign this difference to the thermal treatment during the alignment procedure rather than to effects of the alignment.

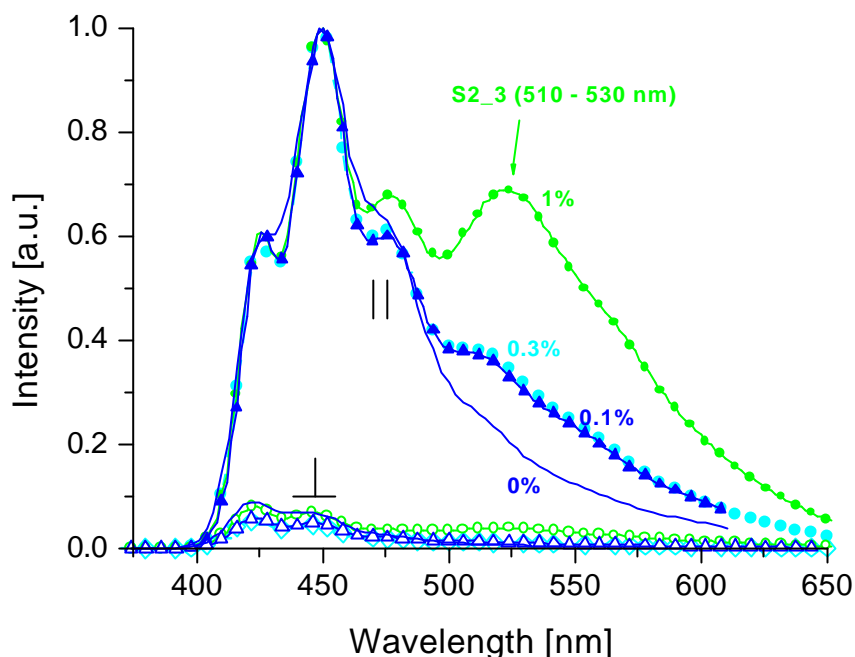


Figure 7.5. Polarized EL spectra of LEDs with the following structure ITO/ST 1163/(PI + 15 wt.% ST 1163)/(PF26am4 + x wt.% S2_3)/LiF/Ca/Al. The numbers at the curves correspond to the content of S2_3.

The high polarization ratios of the doped devices at 510 nm and the increase of anisotropy for increasing (moderate) dye concentrations might be explained by the assumption that the dopant molecules are situated in the better aligned domains of PF2/6am4. Due to efficient charge-trapping and the increased hole density, the EL emission then predominantly occurs from these better aligned polyfluorene domains. Moreover, the high degrees of orientation point to an alignment of the rod-like dye molecules themselves. This assumption is supported by the polarized absorption spectra shown in Figure 7.6. The spectra reveal enhanced degrees of alignment after doping and further increases for increasing dopant concentration. The contribution of the dye (absorption peak at 425 nm (Figure 7.1)) to the absorption spectra of the doped devices at high wavelengths is clearly noticeable.

Table 7.1. Performance of the polarized LEDs with structure ITO/ST 1163/(PI + 15 wt.% ST 1163)/(PF26am4 + x wt.% S2_3)/LiF/Ca.

S2_3 content [wt.%]	P at 450nm	P at 510nm	Luminance [cd/m ²]	Efficiency [cd/A]
0	15	23	800	0.25
0.1	21	27	720	0.50
0.3	23	30	600	0.30
1.0	15	20	500	0.50

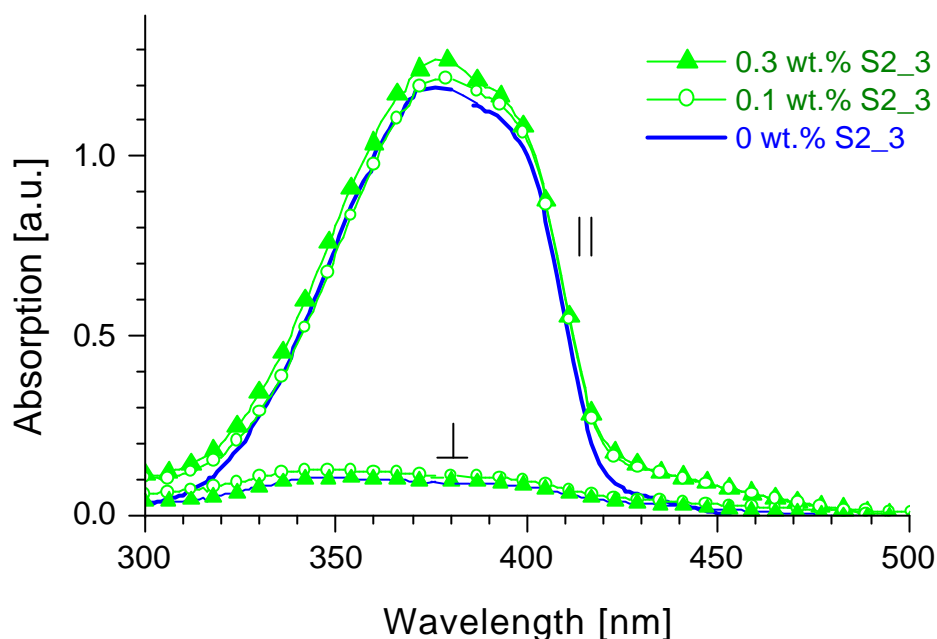


Figure 7.6. Polarized absorption spectra for devices with PF2/6am4 emissive layers and PF2/6am4 doped with S2_3 at different concentrations, respectively.*

The investigations presented above showed that doping polyfluorene at low concentrations with the green-emitting dye S2_3 leads to significant changes in the emission spectrum, and allows for the realization of green emission. The dopant was shown to act as active charge-trap, causing the exciton generation and recombination to occur primarily on the dye. Due to a decrease in the current and the high luminance values, the luminance efficiency was remarkably enhanced by the doping. Moreover, we realized highly polarized electroluminescence from blends of PF2/6am4 and S2_3 with polarization ratios of up to 30 and a luminance of 600 cd/m² at an efficiency of 0.30 cd/A. The high degrees of anisotropy were attributed to the

* Due to experimental reasons, the dichroic ratios are not evaluated for these polarized samples. In this special case, the absorption spectra were recorded *after* the cathode deposition and after operation in electroluminescence. To avoid reflections during the measurements, the mirror-like Ca/Al-cathodes have been removed by hydrochloric acid. The spectra are shown for comparison of the different samples, but the absolute dichroic ratios are expected to be considerably higher.

dye predominantly being located in the highly ordered regions of the polyfluorene. For devices with stronger pronunciation of the green emission contribution, the polarization ratio was 20 at 500 cd/m² and 0.50 cd/A. It should also be noted that the addition of the dye yields a controlled broadening of the spectra, without disturbing the high degrees of anisotropy. This is an important step towards the realization of 'white' polarized electroluminescence.

7.2 Red Light-Emitting Diodes Based on Dendronized Perylenes

The concept of color tuning and color down-conversion via doping a blue emissive polymer with lower bandgap materials was also applied to obtain red emission. This opens the way towards the realization of full color red-green-blue (RGB) emission starting off from a single blue emissive polymer. For example, the addition of tetraphenylporphyrin to PF8⁴⁵ yielded red emission from an originally blue emitting matrix, as well as doping ladder-type PPP with a polymer, which contained a perylene derivative in the main chain.²⁰⁶ However, this concept implies one major drawback, namely the tendency of this kind of small molecule emitters to phase-separate, which leads to lack of long-term device stability.

One approach to overcome these problems is the dendronization of small molecule chromophores. Dendrimers are monodisperse, highly ordered, hyperbranched three-dimensional nanostructures, which are built up in a stepwise synthesis. The finding that the core, the scaffold and the surface functionalization can be selected and varied independently makes dendrimers very attractive for the application in LEDs.²⁰⁷⁻²¹⁰

Furthermore, in the previous sections, we found that the addition of dopants to polyfluorene led to remarkable changes both of the current and the emission characteristics. This was partly attributed to the trapping of charge carriers at the dopants, followed by exciton generation and recombination directly on the dye. However, it remained to be clarified, whether the changes in the emission spectra are also due to Förster energy transfer from the host matrix to the guest molecules. The use of dendrimers should be a promising approach to address this question. The adjustable size of the scaffold opens a way to control the transfer mechanisms, since the Förster transfer scales with the transfer distance according to R^{-6} (Equation 1.3), whereas tunneling is proportional to e^{-kR} .

7.2.1 Dendrimers and Electroluminescence

Our aim was to realize and then to optimize EL emission from polyphenylene dendrimers with perylene diimide as luminescent core. Here, the emphasis lay on the separation and isolation of the emitter molecules resulting in the prevention of aggregation and crystallization. Perylene diimide derivatives have been successfully used as functional dyes in fluorescent solar collectors,²¹¹ photovoltaic cells,²¹² optical switches,²¹³ lasers²¹⁴ and in light emitting diodes²¹⁵⁻²¹⁷ because of their excellent chemical, thermal and photochemical stability.²¹⁸ However, this class of chromophores shows a high tendency to π -stacking because of its extended aromatic core.

To overcome this problem, we shielded this luminophor with polyphenylene dendrons consisting of tetraphenyl benzene repeat units. The dense packing of the benzene rings and the inherent stiffness of the phenyl-phenyl-bond provide a shape-persistent dendritic shell, which is also characterized by thermal and chemical stability. The synthesis of the fourfold ethynyl substituted tetraphenoxy perylene diimide derivative, which serves as a core molecule and the subsequent build-up of three generations of dendrimers via repetitive Diels-Alder reaction with tetraphenylcyclopentadienone building blocks is described elsewhere.²¹⁹ In the same work it was shown by optical characterization of these dendrimers that aggregation in solid state is effectively prevented already from the first generation on.

Subject of this investigation were the polyphenylene dendrimers of the first (G1) and second (G2) generation, as well as the non-dendronized tetraphenoxyperylene diimide model compound (M) (Figure 7.7). From these compounds two different kinds of LEDs were investigated. In a first approach, the active layers of the devices consisted of the pure materials M, G1 and G2 with the aim to show the prevention of aggregation for the dendritic structures. Next, these materials were doped as guest-molecules into a blue-emitting polyfluorene host (PF1/1/1/6, Figure 7.8).

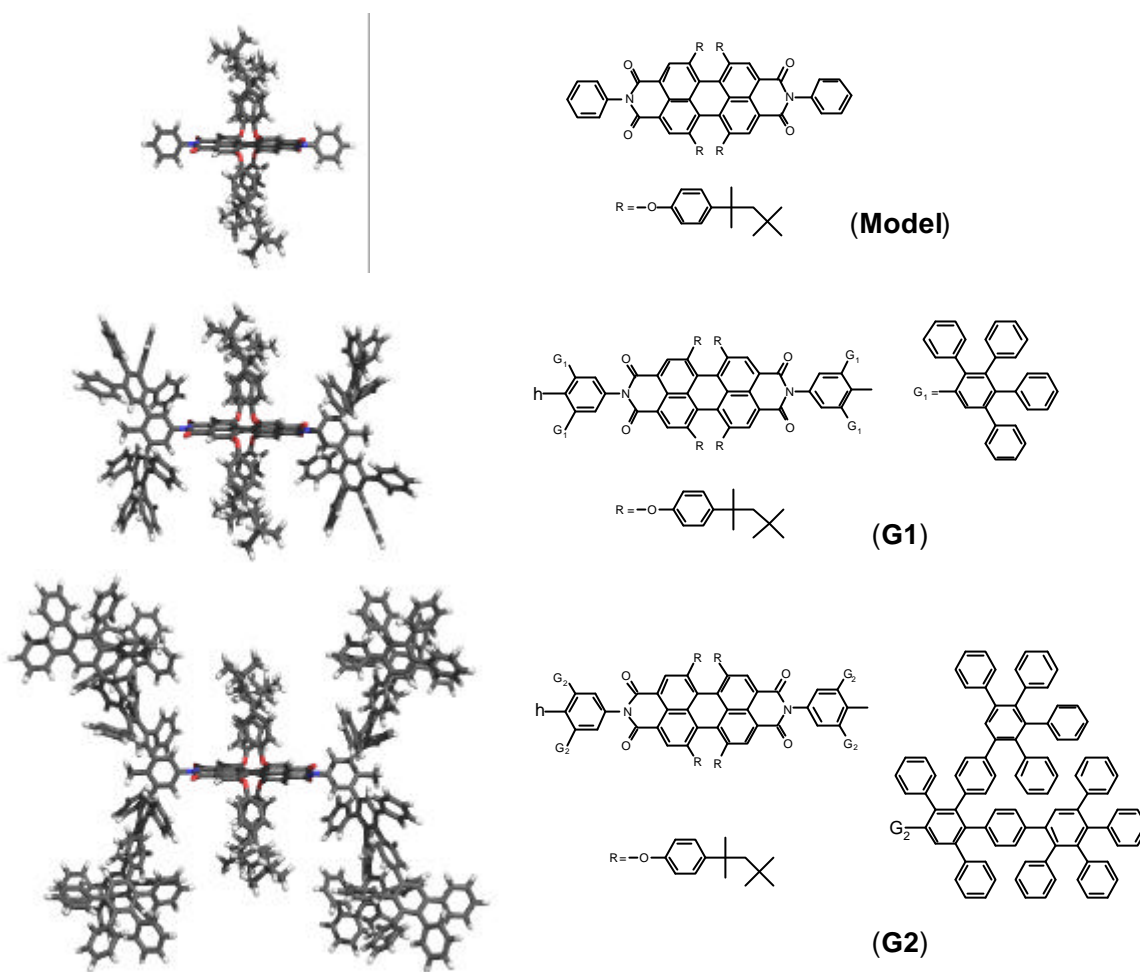


Figure 7.7. Structure of non-dendronized tetraphenoxypyrene diimide model compound (M) and the polyphenylene dendrimers of the first (G1) and second (G2) generation. On the left, simulations of the molecular structures are shown.²²⁰

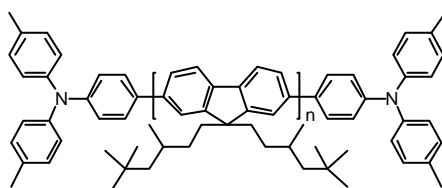


Figure 7.8. Structure of *a,w*-bis[N,N-di(4-methylphenyl)aminophenyl]-poly(9,9-bis(3,5,5-trimethylhexyl)fluorene-2,7-diyl) (PF1/1/1/6).

According to the procedure described in section 3.2, for all devices described in the following, a 20 nm hole-injecting layer from polyethylenedioxythiophene doped with poly(styrene sulfonate) (PEDOT-PSS, section 3.1.6) was spincoated on top of an ITO anode. The respective emissive layers were sandwiched between this PEDOT-PSS-layer and a LiF/Ca cathode (0.8 nm LiF and 20 nm Ca). Finally, a 100 nm aluminum protection layer was evaporated on top.

7.2.2 LEDs with Model Compound and Dendrimers as Active Layer

Figure 7.9 contains the electroluminescence spectra of the devices with M, G1 and G2 as active layers. The spectra of the non-dendronized and dendritic materials substantially differ from each other, whereas the spectra of G1 and G2 are almost identical. The characteristics of the spectrum of M with a 95 nm full-width at half-maximum (FWHM) and its additional shoulder clearly evidence closely packed chromophores. On the contrary, the narrow spectra of the dendrimers G1 and G2 indicate that already from the first generation on the π -stacking is completely suppressed. These results demonstrate that the shielding of the central dye with four space-filling, stiff dendrons effectively prevents any chromophore-chromophore interaction of the perylene molecules so that the luminophores behave like isolated emitters.

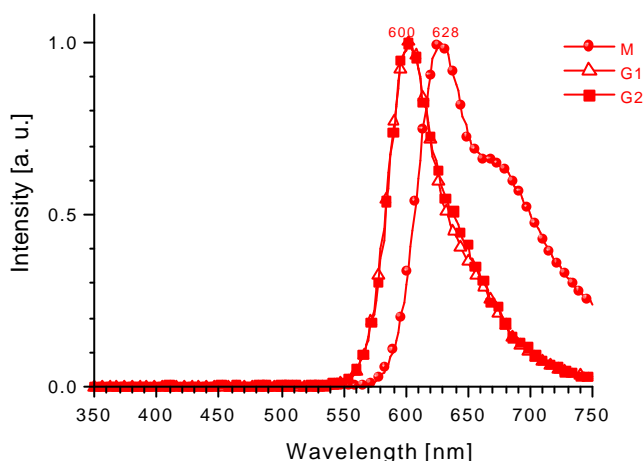


Figure 7.9. Electroluminescence spectra of devices with M (circles), G1 (triangles) and G2 (squares) as emissive layers.

The onset voltages of the devices with the pure materials as active layers were rather low with 4 V in the case of M and G1 and 7 V for G2. For single layer devices with the non-dendronized compound M, the luminance was 11 cd/m^2 at 18 V, only. In contrast, bright red EL with a luminance of 120 cd/m^2 at 11 V was obtained for pure G1. The CIE color coordinates were (0.627, 0.372). Compared to the results by Virgili et al. on poly(dioctylfluorene) layers doped with tetraphenylporphyrin, the driving voltage for reasonable brightness is 3 times lower.⁴⁵ They reported a luminance of 90 cd/m^2 at 33 V with an efficiency of 0.18 cd/A , but the X-color coordinate was 0.65, which is slightly more in the red. For G2, the luminance is only 13 cd/m^2 at 18 V, which we attribute to the isolating effect of the scaffold. Note, that the spin-coated films of all the pure materials were very inhomogeneous resulting in large currents. As a result, luminance efficiencies of all LEDs were quite low, with values of approx. 0.03 cd/A for the best devices.

7.2.3 Doping of M, G1, and G2 into Polyfluorene

To overcome the problem of the poor film qualities and still maintain the red emission from the perylene chromophores, M, G1 and G2 were blended into *a,w*-bis[N,N-di(4-methylphenyl)aminophenyl]-poly(9,9-bis(3,5,5-trimethylhexyl)fluorene-2,7-diyl) (PF1/1/1/6, Figure 7.8). This polymer is comparable to the endcapped polyfluorenes discussed in section 3.1.1.2 which were shown to yield very bright and highly efficient electroluminescence. The type of polyfluorene described here was used, since it showed good compatibility with M, G1 and G2. The focus of this studies was centered on investigating the influence of the degree of dendronization on the EL color, brightness and efficiency, and for the blended devices on the mechanisms leading to the emission from host molecules. The approach makes use of the excellent film forming properties of these polymers and provides further possibilities for device optimization. The two concentrations of the perylene-containing M, G1 and G2 dopants studied were 3 and 10 wt.% in PF1/1/1/6. Actually, due to the size of the scaffold and the resulting higher molecular weights of the dendrimers G1 and G2 the concentrations in wt.% are not identical with the effective concentrations of the active perylene chromophore molecules (Table 7.2).

Table 7.2. Concentration of respective dye in PF1/1/1/6 and the corresponding effective concentration of perylene chromophores (in wt.%).

Dopant material and concentration [wt.%]	Effective content of perylene dyes [wt.%]
10 % M	10.0
10 % G1	4.7
10 % G2	2.3
3 % M	3.0
3 % G1	1.4
3 % G2	0.7

7.2.3.1 Energy Transfer in Photoluminescence

As mentioned, one major goal for doping the polyfluorene was to achieve an emission contribution of the perylene host dye at dopant concentrations, which still allow for the preparation of homogeneous layers. Figure 7.10 shows the normalized photoluminescence spectra of films of pure PF1/1/1/6 and of the blends of PF1/1/1/6 and 3 wt.% of the respective dyes M, G1 and G2. On all cases, the excitation wavelength was 340 nm, close to the wavelength of minimum absorption of the dopant. Therefore, the contribution by excitons generated directly on the perylene dye should be small. As can be seen from the spectra, the emission from the

dopants decreases in the series M, G1 and G2. Doping with the non-dendronized M yields the most efficient energy transfer from the PF1/1/1/6 host molecules, the peak in the high wavelength region is located at 616 nm and reaches 80 % of the height of the strongest PF1/1/1/6 emission peak at 421 nm. From the spectra and by using the CIE color matching functions²²¹ color coordinates of $(X, Y) = (0.39, 0.19)$ were calculated. For the dendrimer G1 the contribution in the red is shifted to 603 nm and still reaches 60 % of the PF1/1/1/6 peak height, yielding CIE values of $(0.35, 0.18)$, whereas for G2 the peak in the red is at 598 nm and weak compared to the blue emission of the PF1/1/1/6. The corresponding color coordinates are $(0.19, 0.08)$.

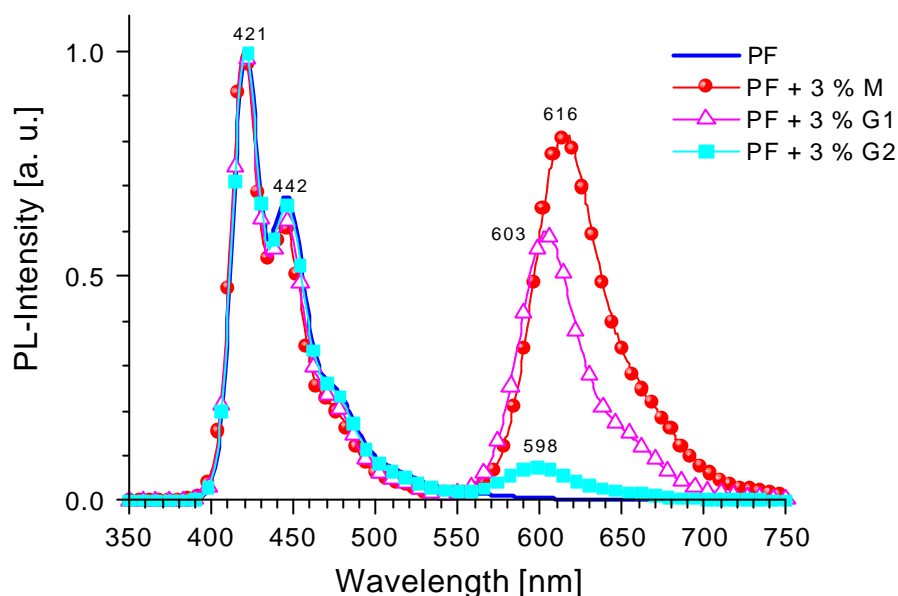


Figure 7.10. Photoluminescence spectra (normalized to the peak at 421 nm) of blends of PF1/1/1/6 and 3 wt.% of M (circles), of G1 (triangles) and of G2 (squares), respectively. For comparison, the spectrum of the pure PF1/1/1/6 (no symbols) is also shown. The excitation wavelength was 340 nm.

We believe that in the event of energy transfer, dipole-dipole Förster interaction is the dominating factor.^{4,205} This is the through-space resonant interaction of the transition dipole moments of excited PF1/1/1/6 donor (of energy) molecules and chromophore acceptor molecules. The rate of energy being transferred depends on various factors one of which is the distance between donor and acceptor. Therefore, the observation of the energy transfer decreasing in the series M, G1 and G2 can be well understood. Compared to the non-dendronized M, the spatial extent of the dendrimers is larger and increases from G1 to G2, resulting in a decrease in the Förster energy transfer rate.

An important measure for a quantitative estimation of the probability of energy transfer is the Förster radius (R_0) of the respective guest-host system. It mainly depends on the relative overlap of the donor fluorescence and the acceptor absorption bands and assesses the energy matching of the donor and acceptor excited states. This radius gives the distance between donor and acceptor at which an intermolecular energy transfer is equally probable as the depopulation

of the excited state via fluorescence, internal conversion or intersystem crossing. The probabilities of exciton energy transfer to a chromophore molecule and of recombination on the polyfluorene main chain are then the same.

The PL-emission of PF1/1/1/6 at excitation wavelength of 340 nm and the absorption spectra of M, G1 and G2 are shown in Figure 7.11. It is evident that the spectrum of PF1/1/1/6 with its two maxima at 421 and 442 nm overlaps strongly with the short-wavelength absorption bands of M, G1 and G2, which are located at 450 and 443 nm, respectively. (In addition, the absorption spectra of M, G1 and G2 demonstrate again the already described prevention of aggregation in solid-state for the dendronized compounds. The maximum of the non-dendronized M appears at 585 nm and is shifted to the red by 19 nm in comparison to the maxima of the dendrimers G1 and G2 at 566 nm.)

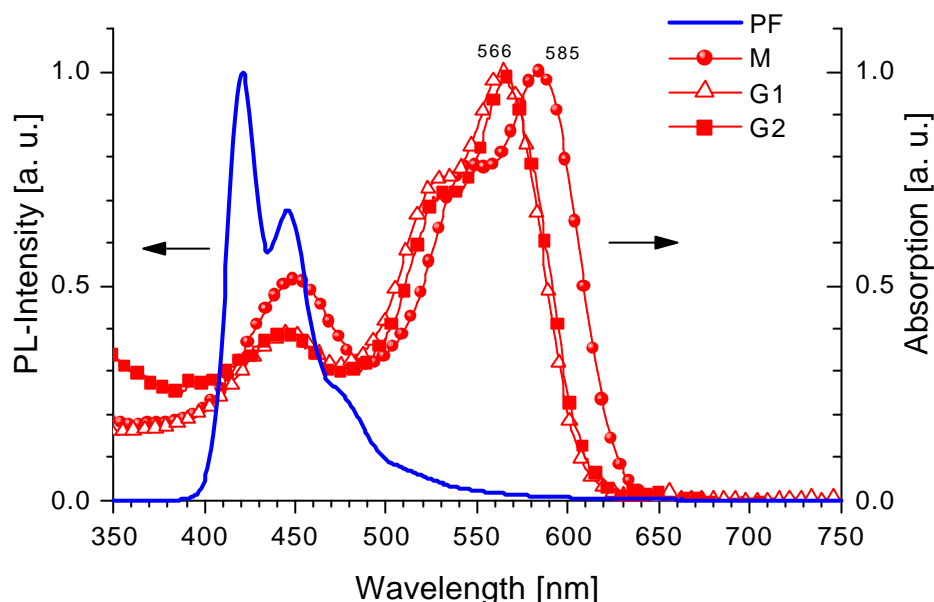


Figure 7.11. Fluorescence spectra of pure PF1/1/1/6 (no symbols) and absorption spectra of M (circles), of G1 (triangles) and of G2 (squares), respectively. All spectra are normalized to their respective emission maxima.

The Förster radii (R_0) for the respective guest-host systems were calculated according to the relation^{4,205}

$$(R_0)^6 = \frac{9(\ln 10)}{128\pi^5 N_A'} \frac{k^2 \Phi_f}{n^4} \cdot J \quad (7.1)$$

where k^2 is an orientation factor ($2/3$ for random orientations of donor and acceptor), Φ_f the fluorescence quantum yield of the donor in the absence of the acceptor (ca. 50 % for PF1/1/1/6), N_A' the number of molecules per millimole (Avogadro's constant $\times 10^{-3}$), and n is the refractive index of the host system ($n_{\text{PF1/1/1/6}} = 2$). J is the mentioned overlap integral between the donor fluorescence spectrum and the acceptor absorption spectrum (cm^6/mmol) defined by

$$J = \int_0^{\infty} F_m(\mathbf{n}) \cdot \mathbf{e}_Q(\mathbf{n}) \frac{d\mathbf{n}}{n^4} \quad (7.2)$$

where F_m is the spectral distribution of donor fluorescence ($\int F_m(\mathbf{n})d\mathbf{n} = 1$), $\mathbf{e}_Q(\mathbf{n})$ the molar decadic extinction coefficient spectrum of the respective acceptor (cm^2/mmol), and \mathbf{n} is the energy in wavenumbers in inverse centimeters. For all the blends of PF1/1/1/6 and M, G1 and G2, respectively, we calculate Förster radii of $R_0 = 29 \text{ \AA}$ (with $J_M = 5.0 \times 10^{-14} \text{ cm}^6\text{mmol}^{-1}$ and $J_{G1,G2} = 4.9 \times 10^{-14} \text{ cm}^6\text{mmol}^{-1}$). This value should be compared to the minimum distance between the conjugated PF1/1/1/6 main chain and the core of the dendrimer. In section 5.1.2 we showed that the comparable but slightly less bulky PF2/6 adopts a helical structure with the main chains surrounded by the side-chains and that the diameter of such a helix is in the range of 16 \AA .¹⁸⁰ Assuming that the shape of the dendrimers G1 and G2 is coffer-like with a box diameter of about 30 \AA for G1 and more than 44 \AA for G2,²²⁰ the minimal possible center-to-center distance R between the transition dipole moments of donor and acceptor can be estimated to approximately 22 to 24 \AA for G1 and 30 to 34 \AA for G2. The finding that only for G1 (and certainly for the smaller M, too), but not for G2 these values lie well below R_0 explains the good energy transfer for doping with M and G1 and the less pronounced transfer for G2.

A more quantitative description can be based on the assumption that the ratio V_i of fluorescent intensity from the dendrimer G_i and from the polyfluorene is proportional to the Förster energy transfer rate k_{ETi} which is given by^{4,205}

$$k_{ET} = \frac{9(\ln 10)k^2\Phi_f J}{128\pi^5 N_A n^4} \frac{1}{tR_i^6} = \frac{R_0^6}{tR_i^6}. \quad (7.3)$$

Here, t is donor fluorescent lifetime in the absence of the acceptor, R_0 is the Förster radius, and R_i is the donor-acceptor center-to-center distance for the respective dendrimer ($i = 1$ for G1, $i = 2$ for G2). If energy is indeed exchanged via Förster energy transfer, the ratio $V = V_1/V_2$ should equal the ratio $k = k_{ET1}/k_{ET2}$. From the PL intensities shown in Figure 7.10 we calculate $V = 0.6/0.08 = 7.5$. For comparison, we calculate $k \approx 7 \pm 4$ using the values of R_0 and the mean values of R_i obtained above (the large variation results from sixth power of the radii). This rather good agreement supports our interpretation, that the excitons generated on the PF1/1/1/6 chains are indeed transferred to the perylene dye via Förster energy transfer. It should be noted that our estimate completely neglects the migration of the exciton within the host as discussed recently for m-LPPP doped with a fluorescent polymer at low concentrations (below 5 wt.%).²²² Also, the effective volume concentration of the fluorescent perylene core was approximately three times smaller for G2 compared to G1 (Table 7.2). On the other hand, the comparison of results for the same mass ratio (in this case 3 wt.%) ensures that the volume fraction occupied by the matrix and the dopant is the same (provided that the mass densities of

G1 and G2 are comparable). Therefore, the total interfacial area as well as the average distance excitons have to travel in the host before they are transferred to the guest are comparable.

7.2.3.2 Charge-Transport Properties of the Layers

In order to study the effect of doping on the charge-transport properties of the blended active layers, hole-only devices with 50 nm hole-injecting gold top electrodes were fabricated. Even though the position of the HOMO-level of PF1/1/1/6 with respect to the work function of ITO/PEDOT or Au suggests, that the current through such a sandwich structure is injection-limited, investigations of these hole-only devices reveal a pronounced effect of the dopants on the current–voltage (I – V) characteristics (Figure 7.12, open symbols). For voltages lower than 10 V, the current of the devices with the non-dendronized M as dopant is almost one order of magnitude lower than for pure PF1/1/1/6. This indicates that neither the injection of holes from the PEDOT-PSS hole injection layer nor their transport through the emission layer are facilitated by the dopants. The obvious decrease in the hole current reveals that the non-dendronized M behaves as a shallow hole trap instead. Note that the oxidation potential of M as determined from cyclic voltammetry (CV) in solution is only 0.1 V lower than that of PF1/1/1/6 (E_{ox}^0 (M) = 1.0 V, E_{ox}^0 (PF1/1/1/6) = 1.1 V vs. Ag/AgCl). Due to aggregation, the oxidation potential for M in films is, however, expected to be even smaller. Layers doped with G1 and G2 show higher currents than pure PF1/1/1/6 for smaller bias, but larger currents for voltages above ca. 11 V. This effects in not yet understood, but one might suppose that the addition of the dopant to the PF1/1/1/6 alters e.g. the morphology of the layer or the PF1/1/1/6 chain orientation at the interfaces, thus affecting injection of holes or their transport in the blended layer.

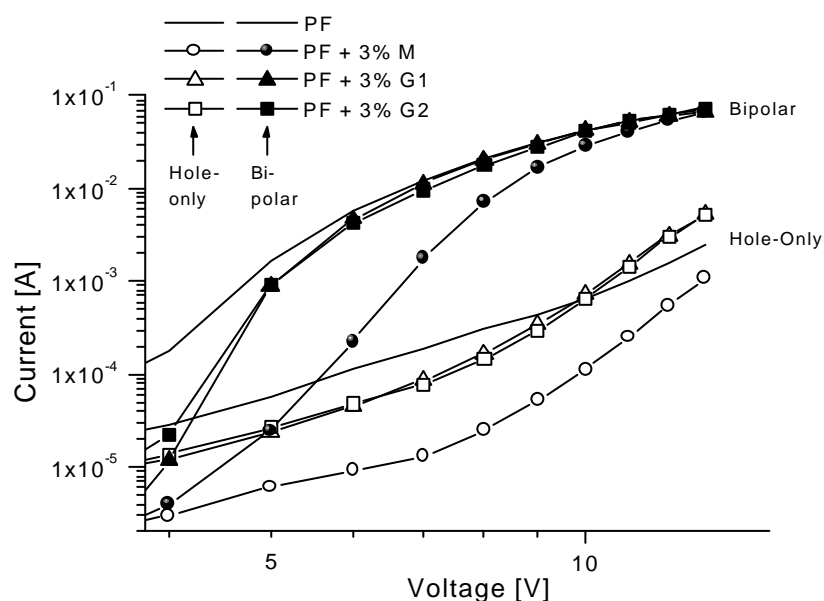


Figure 7.12. Current–voltage characteristics of hole-only devices (open symbols) and the corresponding bipolar LED devices (filled symbols). At each case, blends of PF1/1/1/6 with 3 wt.% of M (circles), of G1 (triangles) and of G2

(squares), respectively, are compared with pure PF1/1/1/6 devices (no symbols). Due to fluctuations in the low voltage region, the results are plotted only for voltages higher than 3.5 V for which the values were reproducible.

In comparison to the hole-only devices a significant rise in the current under forward bias is observed when electrons are injected from a LiF/Ca top electrode (Figure 7.12, closed symbols). This gives evidence that electrons are the majority carriers in PF1/1/1/6, as it is believed to be the case in other polyfluorenes (see also section 6.2.1.1).^{52,143}

At low bias, the current through the bipolar devices drops upon doping, similar to the hole-only devices. Comparison of the CV data for PF1/1/1/6 and for M, G1 and G2 shows that all of them behave as active electron traps, since the reduction peak potentials E_{red}^0 of the dopants (E_{red}^0 (M) = -0.8 V, E_{red}^0 (G1, G2) = -1.0 V are considerably less negative compared to E_{red}^0 (PF1/1/1/6) = -1.9 V vs. Ag/AgCl). For higher voltages, the current of all the blend devices approaches the values for those with pure PF1/1/1/6, but for the model compound this occurs only at remarkably higher voltages than in the case of the dendrimers G1 and G2. The I - V curves recorded for the higher doping concentrations of 10 wt.% (not depicted in Figure 7.12) show that the drop in the current is even more pronounced than it is for 3 wt.%, especially in the region of low voltages. Note, that for both the hole-only and the bipolar devices, the current does not noticeably depend on the generation, i.e. is not significantly influenced by the size of the dendritic scaffold. This indicates that the predominant fraction of charges are travelling within the PF1/1/1/6 matrix and only few are captured on the dendrimer cores at larger applied fields.

7.2.3.3 Electroluminescence – Intensity

Figure 7.13 shows the intensity–current characteristics of the LEDs with pure and doped PF1/1/1/6 emission layers. The intensity of the light emitted at a given current level from devices with M doped PF1/1/1/6 layer is at least an order of magnitude lower than the one emitted from the devices with pure PF1/1/1/6. This can be explained with charge carriers trapped at, most probably, aggregate sites of M, which serve as centers for recombination, since radiative recombination from aggregates is presumed to be rather inefficient.^{147-149,168} Increasing the dopant concentration from 3 to 10 wt.% leads to a further decrease by one order of magnitude in light intensity when M is used as a dopant (Figure 7.13), thus again suggesting the nature of the quenching sites to be aggregated perylene molecules. The light intensity at the same current level is noticeably higher for the devices with emission layer doped with dendrimer G1 and the emission onsets decreases to 4 V (Figure 7.14). Finally, with G2 as a dopant, the emission onset and intensity values are similar to the ones obtained for the pure PF1/1/1/6 devices. The de-

crease of the emitted light intensity with increasing dopant concentration is much less pronounced for the dendrimer G1, and for G2 the intensity changes only slightly when the concentration is raised.

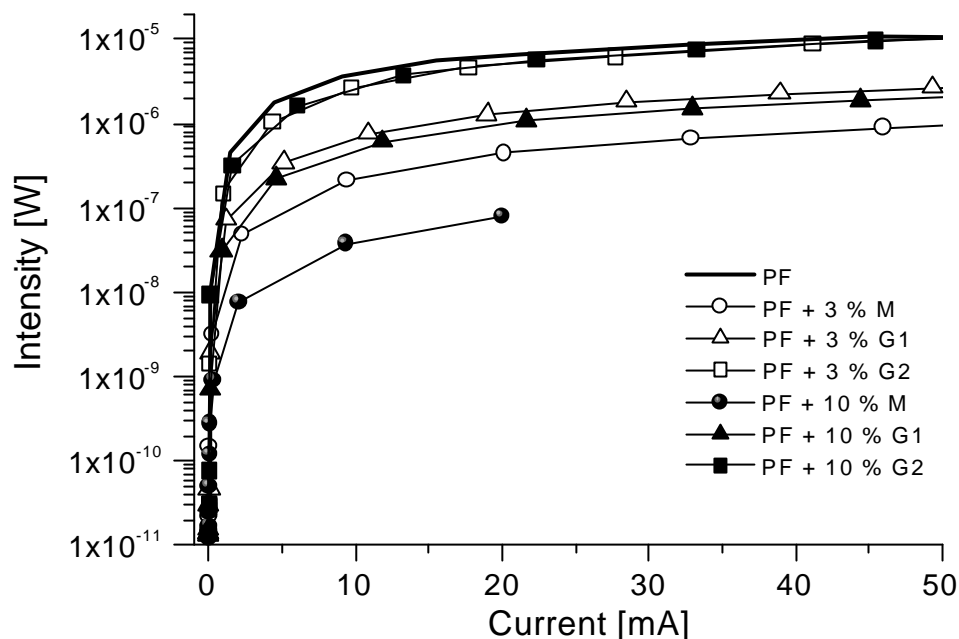


Figure 7.13. Emission intensity as a function of current for blends of PF1/1/1/6 and 3 wt.% (open symbols) and 10 wt.% (closed symbols) of M (circles), of G1 (triangles) and of G2 (squares), respectively. For comparison, the curve of the pure PF1/1/1/6 (no symbols) is also shown.

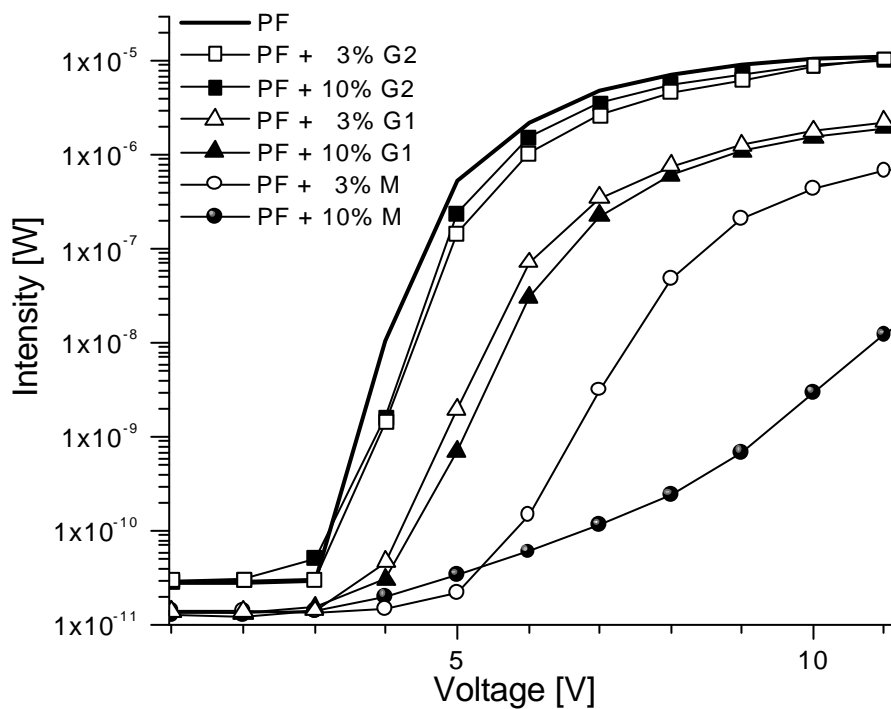


Figure 7.14. Intensity-voltage characteristics for PF1/1/1/6 (no symbols) and PF1/1/1/6 blended with 3 wt.% (open symbols) and 10 wt.% (closed symbols) of M (circles), of G1 (triangles) and of G2 (squares), respectively.

7.2.3.4 Emission Characteristics in Electroluminescence

Figure 7.15 shows that the EL spectrum of non-dendronized M in PF1/1/1/6 is dominated by the red emission from the dye at 612 nm with a very weak contribution by the PF1/1/1/6 inherent peak at 421 nm. Predominant emission from the chromophore is still registered for the dendrimer G1 showing a maximum at 600 nm and a smaller peak in the blue. The influence of doping on the spectral characteristics is, however, strongly reduced when doping with G2. In this case, the relative intensity of the red emission is only one third of that of the PF1/1/1/6 emission at 421 nm (at ca. 20 cd/m²).

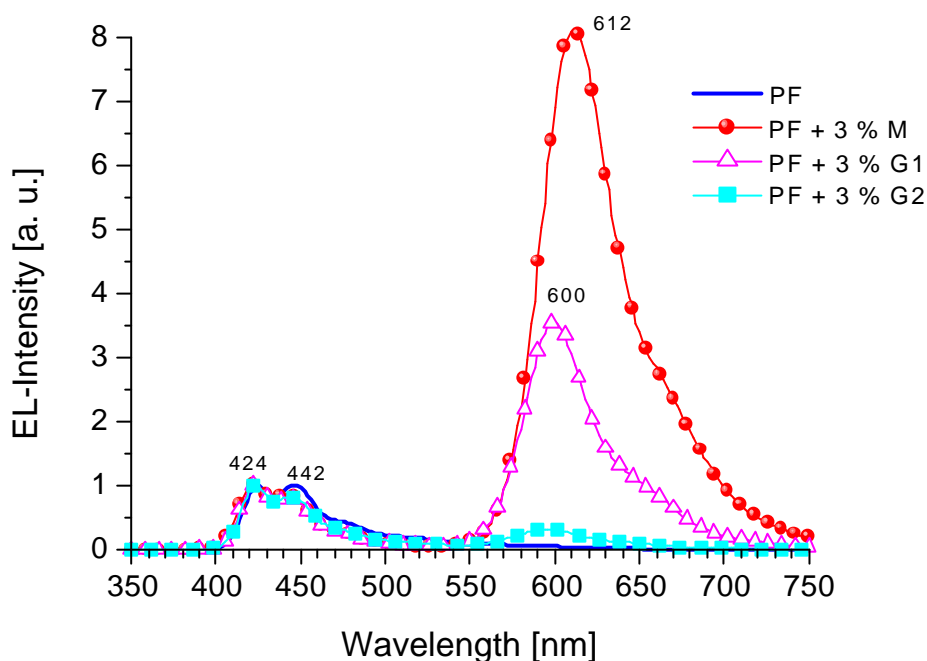


Figure 7.15. Electroluminescence spectra (normalized to the peak at 424 nm) for blends of PF1/1/1/6 and 3 wt.% of M (circles), of G1 (triangles) and of G2 (squares), respectively. For comparison, the spectrum of the pure PF1/1/1/6 (no symbols) is also shown. Due to the sensitivity of the photomultiplier, the spectra were recorded at luminance of about 20 cd/m². At higher values the emission characteristics changes (see Figure 7.16).

Comparing the electroluminescence spectra with the respective photoluminescence spectra shown in Figure 7.10 reveals that the emission from the dye is generally much more pronounced in EL than it is in PL, indicating that a significant fraction of excitons is generated directly on the perylene dye rather than in the PF1/1/1/6 matrix. This can be explained by the trapping of electrons on the dye. As discussed above, the chromophore sites are energetically more favorable for electrons than the PF1/1/1/6 sites. The resulting trapping of electrons – enabled by the suitable energy levels of the dopants – increases the probability for hole capture and subsequent recombination taking place on a chromophore. Consequently, in EL the red emission is much more pronounced than in PL, where excitons are predominately generated on the polyfluorene host and only partially transferred to the dendrimer core via energy transfer.

As documented above, the energy transfer in PL is strongly dependent on both the presence of a dendritic scaffold and on its size, since the polyphenylene dendrons increase the distance between donor and acceptor molecules. In the case of the scaffold being too large, recombination barely takes place at the guest molecules and the emission predominantly comes from the PF1/1/1/6 sites. Similarly, in electroluminescence the contribution of the red emission becomes smaller with increasing size of the scaffold, since the ability for trapping is largely decreased for the dendrimers compared to M. In accordance with this interpretation, the observed decrease of the red emission contribution when increasing the width of the scaffold is far more pronounced in EL than in PL. In the former case, tunneling of the charges through the scaffold is the rate-limiting step, which decreases exponentially with the width of the isolating scaffold according to quantum mechanics tunneling theories.

7.2.3.5 Color and Efficiency

Figure 7.16 shows the dependency of the emissive color on the applied voltage for PF1/1/1/6 blended with 3 and 10 wt.% of M, G1 and G2, respectively. It is shown that for all the samples the color coordinates change with higher voltages to lower values, i.e. into the bluish region. For the blend of PF1/1/1/6 and M, this color change is, however, quite small. For the lower dopant content, the difference in the CIE-coordinates (X , Y) between the color at 6 V and 11 V is (0.08, 0.04) only, and for 10 wt.% there is almost no color change. For doping with G1, this difference is (0.13, 0.09) for both concentrations, whereas it is (0.15, 0.13) when using G2 as the dopant.

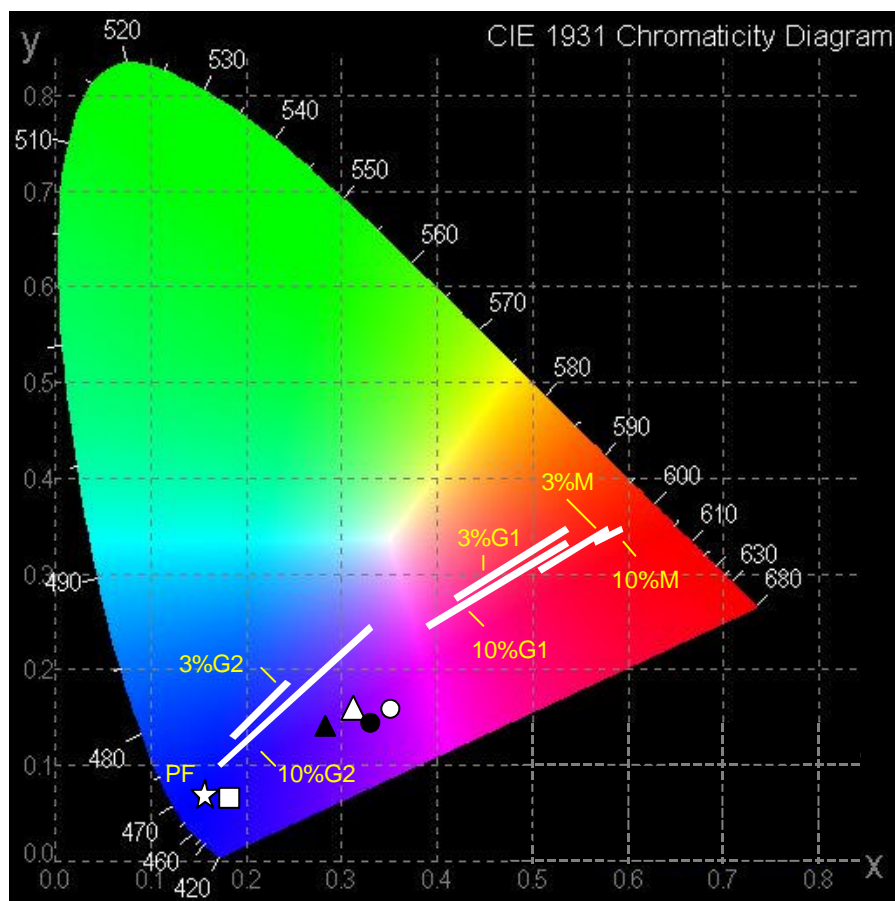
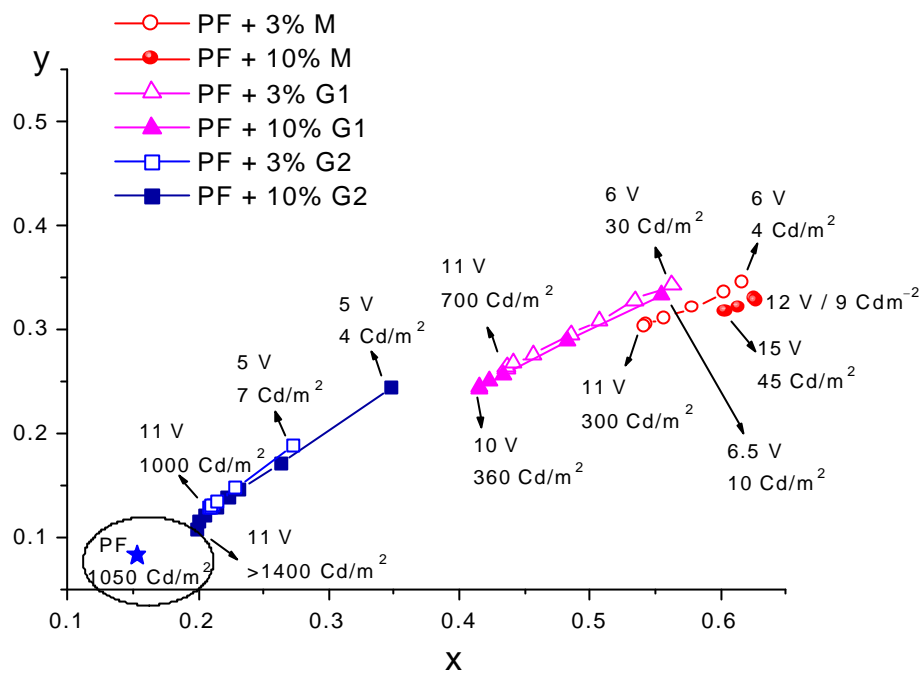


Figure 7.16. Upper graph: Voltage dependent color change of blends of PF1/1/1/6 and 3 wt.% (open symbols) and 10 wt.% (closed symbols) of M (circles), of G1 (triangles) and of G2 (squares), respectively, plotted in CIE-coordinates. The value of pure PF1/1/1/6 is also shown (star). Lower graph: For illustration, the values are drawn into the complete CIE-chromaticity diagram.²²³ Also shown are the calculated color coordinates of the emission in photoluminescence as single points with the same nomenclature as in the legend of the upper graph.

Interestingly, the color coordinates of electroluminescence and photoluminescence (the latter are shown in Table 7.3) for the blend of PF1/1/1/6 and M are very different, even at the largest driving voltage (the most bluish emission) (Figure 7.16, lower graph). This effect is still evident for G1, while for G2 the emission in EL at 11 V and in PL are almost identical. This is fully consistent with the statements made in the section above, according to which the similarity between EL and PL should increase with decreasing ability of the dopants to trap charges. The pronounced blue shift with higher degree of dendronization and larger driving voltages further indicates that charge trapping on the chromophore is kinetically hindered, as for higher current (higher charge carrier concentration) and for higher voltage (shorter transit time of the charge carriers) the emission from the dye becomes less significant.

Table 7.3. CIE color coordinates (X , Y) of blends of PF1/1/1/6 and M, G1 or G2, respectively, calculated from the PL spectra shown in Figure 7.10.

Dopant material	3 wt.% conc.	10 wt.% conc.
M	(0.35, 0.16)	(0.33, 0.14)
G1	(0.31, 0.16)	(0.28, 0.13)
G2	(0.18, 0.07)	(0.18, 0.07)

Concluding the results of the investigations of the spectral characteristics in PL and EL, improving the brightness and efficiency in the series M, G1 and G2, i.e. introducing and increasing a dendritic shell, implies at the same time a reduction of the red chromophore contribution to the emission. Therefore, a compromise has to be found between the improvement of device performance and a maintenance of red emission. When non-dendronized perylene M (3 wt.%) is used, the emission onset voltage is 6 V, and the luminance reaches 300 cd/m² at 11 V with a luminous efficiency of 0.05 cd/A and CIE-color coordinates (X , Y) = (0.56, 0.31). Blending PF1/1/1/6 with 3 wt.% G1 increases both the maximum luminance and the efficiency. The maximum brightness is 700 cd/m² at 11 V and 0.1 cd/A, respectively, but the EL spectrum at this voltage shows a strong blue emission contribution attributed to recombination on PF1/1/1/6 chains. Nevertheless, orange-red emission with a luminance of 100 cd/m² is achieved at a voltage of 6.5 V with the dominant emission by the guest (color coordinates: 0.49, 0.30). Obviously, an ideal compromise is realized in G1 with a complete prevention of aggregation and a sufficiently large charge transfer from the PF1/1/1/6 host to the perylene core. Using the second generation dendrimer G2, the brightness further increases to more than 1400 cd/m² at 11 V with an efficiency of 0.2 cd/A (for 10 wt.% G2), but the color is in the bluish region even at the lowest bias tested and for a dopant concentration of 10 wt.%. At 100 cd/m² the color coordi-

nates are (0.230, 0.140) for 3 wt.% G2 and (0.236, 0.145) for 10wt.% and the emission color is white-bluish.

7.2.3.6 Closing Remarks

In conclusion, the emission properties of perylene dendrimers doped at small concentrations into a polyfluorene host are shown to be significantly affected by the thickness of the dendritic scaffold. In photoluminescence, the energy transfer of excitons from the PF1/1/1/6 host to the perylene core can be satisfactorily explained by Förster transfer through the isolating scaffold. In electroluminescence, the red emission contribution from the perylene dye is, however, significantly stronger than in photoluminescence, and it increases for smaller driving currents. These results give strong evidence that the excitons in EL are generated directly on the perylene dye via charge carrier trapping and that the transfer of excitons generated on the PF1/1/1/6 host only gives a minor contribution to the perylene emission. This is in clear contrast to frequently given interpretations of electroluminescence and electrophosphorescence spectra of dye-doped polymer emission layers, which completely neglected direct exciton generation on the dopant.^{10,11,224,225} In fact, only few papers have pointed out the importance of charge carrier trapping by the dopant for controlling color and efficiency of doped emission layers in EL.^{45,226} In this respect, dendrimers in which the active chromophore is surrounded by an isolating shell represents an ideal model system for studying energy and charge carrier transfer processes. This is particularly evident in the extent of color shift as a function of driving voltage for different thickness of the scaffold. The shift is most pronounced for blends with the second generation dendrimer but almost absent in case of the model compound, for which charge carrier transfer from the host to the dye is not kinetically hindered.

8 Summary

The work described in this thesis concerns the steps on the way to the realization of blue polarized electroluminescence from aligned films in polymer light-emitting diodes. Polarized light-sources on the basis of highly ordered polymers have notable potential as backlight in liquid crystal displays. In this regard, the alignment of liquid crystalline polyfluorene, a blue-emitter known for outstanding performance, was tailored with regards to an application in LEDs. Therefore, alignment layers based on rubbed polyimide were modified for hole-conduction. Additionally, attention was directed towards the characterization of both highly aligned polyfluorene films and of hole-transporting alignment layers. Finally, results of tuning the emission color from blue to green and red by the doping of polyfluorene with fluorescent dyes are presented, combined with studies on the mechanisms leading to these color changes.

Chapter 2 provides insight into the theory relevant to this thesis. The first part gives an introduction into the fundamental principles of electroluminescence from conjugated polymers. *Polarized* electroluminescence requires a high degree of anisotropy in the emissive layer, therefore, the most common techniques for alignment of polymers are discussed, focusing on the orientation of liquid crystalline polymers by means of additional alignment layers.

A brief introduction of the materials and experimental methods used in this study is given in *Chapter 3*. Two blue emitting polymers, which are favorable for the employment as active layers in LEDs are compared, namely polyfluorene as the central emitter in this work as well as poly(phenyleneethynylene) (PPE). The essential chemical and physical properties of poly(dialkylfluorene)s in general are described, complemented by specific characteristics of polyfluorene endcapped with low-molecular weight hole-transporting moieties. Following a short description of the materials used for alignment and for doping, respectively, details about the preparation of isotropic and of polarized light-emitting diodes are presented. Finally, the techniques for the investigation of optical, electrical, and structural properties are introduced.

In *Chapter 4* different alignment techniques are applied to polyfluorene and to PPE, respectively, and considered with regards to the attained degrees of orientation. In the case of polyfluorene, alignment in liquid-crystalline state by means of additional alignment layers based on rubbed polyimide was shown to be the only appropriate technique to induce orientation of this polymer. It was established that the non-conducting polyimide can be modified for hole conduction by the addition of suitable hole-transporting moieties at moderate concentrations, without significantly affecting the alignment ability known from pristine polyimide. This enabled the incorporation of such modified alignment layers into light-emitting devices. Besides, the side-chain patterns were found to severely influence the alignment behavior of polyfluoro-

rene. The highest degree of order was observed for polyfluorene with branched ethylhexyl side-chains (PF2/6). This was explained by the assumption that branching of side-chains increases the persistence ratio of the polyfluorene, which increases the attainable order parameter of a liquid crystalline polymer. The degrees of alignment were observed to decrease with increasing side-chain length. According to investigations of the absorption characteristics, this was attributed to a planar, board-like backbone conformation, which goes along with stronger interchain interactions, unfavorable for alignment. In contrast to polyfluorene, PPE was incapable of aligning in the liquid crystalline state. DSC investigations revealed high similarity of the liquid crystalline and crystalline states, the latter of which is characterized by extremely high stiffness and planar backbone conformation. However, PPE was successfully aligned in the crystalline state by means of direct rubbing. The stiffness of the molecules enabled the transformation of the applied rubbing force to the rigid backbone and resulted in well-aligned samples. By this technique, polarized LEDs with PPE as the emissive layer were realized.

Both polyfluorene and the required hole-transporting alignment layers are investigated in *Chapter 5* by means of optical and electron microscopy, electron- and X-ray diffraction, yielding detailed information about the morphology, structure, and other essential properties. In the first part, the decrease of alignment ability with increasing molecular weight, which was observed for polyfluorene in general, was clarified by means of electron diffraction experiments. As maintained by TEM studies, the morphology of highly aligned PF2/6 films was shown to be characterized by highly ordered lamellae, which are disturbed by disordered regions. Within the ordered lamellae the wormlike molecules segregate with respect to their chain lengths, and in the disordered regions preferentially the end groups of the chains are assembled. The structure investigations revealed that the individual polymer chains of PF2/6 have a cylindrical rather than planar shape with hexagonal packing, in conjunction with a backbone conformation of almost linear structure of a $5/2$ -helix. The wormlike backbone is surrounded by a cylindrical shell of disordered side-chains, which act similarly to solvent between the chains. The consequential low viscosity gives an explanation to the enhanced alignment behavior of PF2/6 in comparison to PF8 or PPE.

The second part of *Chapter 5* gives details on the investigations of alignment layers. The effect of doping polyimide with HTMs on mechanical, charge injection and -transport properties was studied. Both, polymeric and low-molecular weight hole-transporting compounds were investigated concerning the obtainable degrees of alignment and performance in electroluminescence, but only the latter were found to be satisfying in both respects. The best results were obtained for LEDs where the emissive layer was spincoated on top of a bilayer structure consisting of a hole-injection layer of pure low-molecular HTM covered by a rubbed hole-transporting alignment layer of polyimide doped with such an HTM. Variations of the dopant

concentrations in the polyimide revealed that the luminance increased while the polarization ratio decreased with augmenting filler contents. According to SEM and AFM investigations of the influence of the dopant concentration on the morphology of the hole-transporting alignment layers, this observation was attributed to growing phase-separation and layer damage for filler contents higher than 20 wt.%.

Chapter 6 reports on the electroluminescence from devices using polyfluorene as the emissive layer. After optimization of the respective layers in blue-emitting isotropic LEDs, the realization of highly anisotropic electroluminescence from aligned PF2/6 was accomplished. Blue emission peaking at 450 nm with a polarization ratio of 21 was obtained from devices showing a luminance of 100 cd/m² at an operating voltage of 18 V. Furthermore, it was demonstrated that the performance of both isotropic and polarized LEDs was drastically enhanced by chemical modification of the polyfluorene, accomplished by endcapping of the main chains with hole-transporting moieties. The green emission contribution, which was observed for all devices with non-endcapped PF2/6 and attributed to interchain interactions, was effectively suppressed in the case of endcapping, and very good color stability was obtained. The efficiency of the devices was enhanced by more than an order of magnitude when PF2/6 was replaced by its endcapped counterpart. Both phenomena are explained by the finding that the end groups act as active charge-traps, causing the generation of excitons and the recombination to occur predominantly close to the chain ends rather than at less efficient aggregates or excimer forming sites, as observed for non-endcapped PF2/6. Moreover, the endcapping did not disturb the LC properties and alignment ability of the polyfluorene, and highly anisotropic LEDs with polarization ratios of 21 reaching a luminance of 200 cd/m² at an operating voltage of 19 V were realized. Devices showing a polarization ratio of 15 achieved a luminance of up to 800 cd/m². The efficiency of 0.25 cd/A of these devices at comparable polarization ratios and brightness levels was enhanced more than 2-fold compared to the values thus far reported.

Color tuning, accomplished by doping polyfluorene with lower bandgap materials, is described in *Chapter 7*. It was demonstrated that the addition of a *green* emitting thiophene dye resulted in significant changes in the emission spectrum and allowed for the realization of green emission. Similar to the non-emissive HTMs used for endcapping, the dye, too, was shown to act as active charge-trap, resulting in drastically enhanced device efficiencies. Moreover, polarized electroluminescence with peak polarization ratios of up to 30 and luminance of 600 cd/m² at an efficiency of 0.30 cd/A was realized.

To achieve *red* electroluminescence, dendronized perylene dyes, both as pure layers and as dopant for polyfluorene, were investigated in LEDs. Two generations of polyphenylene dendrimers with a perylene diimide core were compared with a non-dendronized model compound. Single layer devices with the first and second generation dendrimers as active layers

emitted pure red light (CIE color coordinates: 0.627, 0.372) with a luminance of up to 120 cd/m² at 11 V, but the efficiency was only 0.03 cd/A. To study the respective contributions of energy transfer and charge carrier trapping to the dopant emission, these materials were blended into polyfluorene, and the effect of dendronization on the emission color and electroluminescence intensity was studied. In photoluminescence, higher degrees of dendronization led to a reduction of the Förster transfer rate from the polyfluorene host to the perylene, resulting in a larger contribution of the host blue emission in the PL spectra. In electroluminescence, the dopants appeared to act as active traps for electrons, resulting in predominant recombination on the dye. Therefore, the contribution of red emission in electroluminescence was remarkably stronger than in photoluminescence where energy is exchanged exclusively via Förster transfer. A pronounced color change from red to blue with higher degree of dendronization and larger driving voltages was explained by the kinetic hindrance of electron transfer from the polyfluorene host to the dendrimer core. A perfect compromise between red color and bright emission was obtained for a blend of polyfluorene and the first generation dendrimer yielding 100 cd/m² at 6.5 V with the emission maximum at 600 nm.

A Appendix

A.1 Luminous Intensity and Luminance of OLEDs

When measuring light, one has to distinguish between radiometric and photometric quantities. Radiometric measurements do not consider the wavelength of the radiation. They are derived from the base unit of all light measurement, the *radiant flux* which measures the power of the radiation and describes the rate of energy flow in joules per second (watt). On the contrary, the photometry provides the respective psychophysical analog of any radiometric quantity by relating it to the selective spectral responsivity of the human eye. In general, this is done by the relative luminous efficiency functions,²²¹ $f(I)$, introduced by the 'Commission Internationale de L'Eclairage' (CIE).³⁷ They give the ratio of the energy of a spectral light of the wavelength I_{max} , to which the eye is most sensitive, to the energy of a spectral light of wavelength I , at which the two lights generate equivalent luminous sensations:

$$f(I) = \frac{E(I_{max})}{E(I)} \quad (\text{A.1})$$

The relative luminous efficiency function for bright light conditions (cones active) is the *photopic* curve $f(I)$ which peaks in the yellow-green at $I_{max} = 555$ nm, whereas for dark light conditions (rods active) the *scotopic* curve with a peak at 507 nm is used (Figure A.1). Convention dictates that unless otherwise stated, all photometric units are photopic quantities.

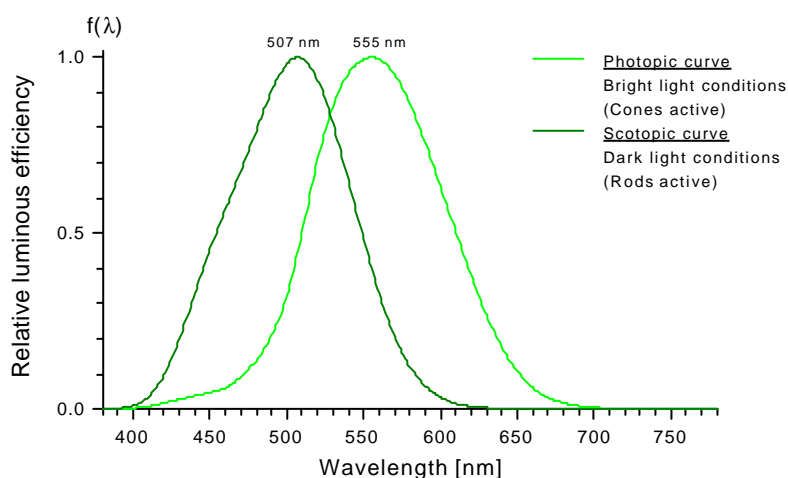


Figure A.1. The relative luminous efficiency function for bright light conditions (*photopic* curve; thick line) and for dark light conditions (*scotopic* curve; thin line) introduced by the CIE.²²¹

The photometric counterpart to the radiant flux and the base unit of the photometric quantities is the *luminous flux* F_v which is derived from weighting the radiant power with the photopic luminous function $f(I)$. It is expressed in lumens (lm), and per definition, $1 \text{ lm} = 1/683 \text{ W}$ at 555 nm.

The *luminous intensity* I is the luminous flux emitted from a point per unit solid angle in a particular direction. The SI unit of the luminous intensity is *Candela* (cd) and was defined in 1996 by the 'Conférence Générale des Poids et Mesures' as the luminous intensity in a given direction of a source that emits monochromatic radiation of frequency 540×10^{12} hertz and that has a radiant intensity in that direction of $1/683 \text{ Watt per steradian}$. Hence, a 1 candela light-source emits isotropically 1 lumen per steradian (lm/sr) in all directions and, since a steradian has a projected area of 1 m^2 at a distance of 1 meter, produces the *illuminance* E of 1 lumen per m^2 (1 lux) at a distance of 1 meter.

$$1 \text{ cd} = 1 \text{ lm/sr} = 1/683 \text{ Wsr}^{-1} \text{ at } 555 \text{ nm.} \quad (\text{A.2})$$

The physical measure of the photometric brightness of an LED is the *luminance* L . This is the luminous intensity per unit of projected area of any surface as measured from a given direction. The luminance is the amount of visible light leaving a point on a surface in a given direction. This surface can be a physical surface or an imaginary plane, and the light leaving the surface can be due to reflection, transmission, and/or emission. The standard unit of the luminance L is candela per square meter (cd/m^2), and thus:

$$1 \text{ cd/m}^2 = 1 \text{ lm}/(\text{m}^2\text{sr}). \quad (\text{A.3})$$

For the calculation of the *luminous efficiency* of an electrically driven light source, the power efficiency (Equation 2.7) is multiplied by the eye sensitivity curve $f(I)$:

$$\mathbf{h}_{lum} = \mathbf{h}_{pow} \cdot f(I) \cdot K_m \quad (\text{A.4})$$

with $K_m = 683 \text{ lm/W}$ for photopic vision and $K_m = 1699 \text{ lm/W}$ for scotopic vision.³⁸

A measure of the *luminance efficiency* \mathbf{h}_{lum} of light-emitting devices is the ratio of the obtained luminance L to the current density j in the device:

$$\mathbf{h}_{lum} = \frac{L}{j} \quad (\text{A.5})$$

the unit of the luminous efficiency is candela per ampere (cd/A).

For convenience, all radiometric and photometric concepts and units are summarized in Table A.1.

Table A.1. Radiometric and the respective photometric concepts and units. K_m in the equation of the luminous flux is $K_m = 683 \text{ lm/W}$ for photopic vision and $K_m = 1699 \text{ lm/W}$ for scotopic vision.

	Term	Symbol	Defining Equation	Remarks	SI Unit
Radiometry	<i>Radiant Flux</i>	Φ_r	$\Phi_r = \frac{dQ}{dt}$	Total quantity of light emitted from a source.	W = J/s
	<i>Radiant Intensity</i>	I_r	$I_r = \frac{d\Phi_r}{d\omega}$	Total quantity of light emitted by a point source, in a given solid angle.	W/sr
	<i>Irradiance</i>	E_r	$E_r = \frac{d\Phi_r}{dA}$	Density of light incident on a surface or in a given plane.	W/m ²
	<i>Radiance</i>	L_r	$L_r = \frac{dI_r}{dA \cos \theta}$	Amount of light emitted or reflected from an extended source in a given direction.	W/(m ² sr)
Photometry	<i>Luminous Flux</i>	Φ	$\Phi = K_m \int \Phi_r(\mathbf{I}) \cdot f(\mathbf{I}) d\mathbf{I}$	Total quantity of light emitted from a source.	lumen [lm]
	<i>Luminous Intensity</i>	I	$I = \frac{d\Phi}{d\Omega}$	Total quantity of light emitted by a point source, in a given solid angle.	candela [cd] (lumens/sr)
	<i>Illuminance</i>	E	$E = \frac{d\Phi}{dA}$	Density of light incident on a surface or in a given plane.	lumens/m ² [lux]
	<i>Luminance</i>	L	$L = \frac{dI}{dA \cos \theta}$	Amount of light emitted or reflected from an extended source in a given direction.	cd/m ² (lumens/m ² sr)

A.2 Chromaticity

Human night-time vision depends on sensitive rod photoreceptors, whereas human day-time color vision depends on the three types of cone photoreceptors. Each type of the cone has its maximum sensitivity at a different position of the visible spectrum; one type is long-, another middle- and the last one is short-wavelength sensitive. Therefore, they are commonly referred to as red (R), green (G) and blue (B). Any spectral light that is observed can be matched to a mixture of these three fixed-color *primary lights*. The three functions relating the matching intensities of the three primary lights to the respective wavelength of the spectral light are termed as the color matching functions $r(\lambda)$, $g(\lambda)$ and $b(\lambda)$ (CMFs). These functions apply to *real* red, green and blue matching lights, but in some cases they can be negative (in case this primary light has to be removed from the mixture and added to the monochromatic light to realize the match). To overcome this problem, they are commonly linearly transformed to *imaginary* matching lights, such as the *XYZ-primaries* defined by the CIE (Figure A.2). They can be used to match – with only positive weights – all visible colors. The $Y(\lambda)$ primary light is intentionally defined to have a color-matching function that exactly matches the photopic luminous efficiency function $f(\lambda)$ (section A.1).²²¹

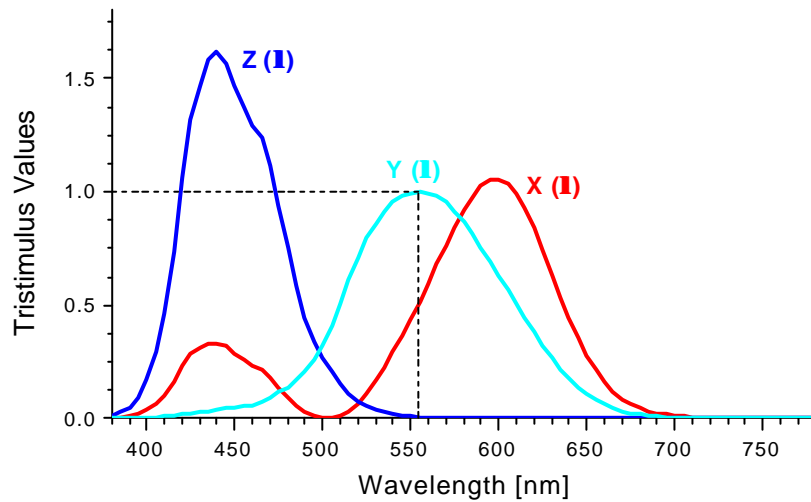


Figure A.2. The XYZ color matching functions defined by the CIE in 1931, modified by Judd and Vos in 1978.²²¹

The *chromaticity coordinates* x , y , z are derived from the relative magnitude of the tristimulus values X , Y , Z and describe the essential color attributes. They are calculated as follows:

$$x = \frac{X}{X + Y + Z}; \quad y = \frac{Y}{X + Y + Z}; \quad z = \frac{Z}{X + Y + Z} \quad (\text{A.6})$$

and hence:

$$x + y + z = 1. \quad (\text{A.7})$$

It is sufficient to give the x and y chromaticity coordinates since the remaining one can be calculated from these two variables. Commonly, they are plotted in the two-dimensional *chromaticity diagram* (Figure A.3). The horseshoe curve represents all pure colors, i.e. colors with only one wavelength in their spectral distribution (sine wave at the appropriate frequency). As all visible colors are made from combinations of these pure colors, they must be inside the area delimited by the curve. If two colors are given, any color connecting these two points can be obtained by mixing these colors, and in the case of three colors (e.g. E , F , G in Figure A.3), all colors in the triangular volume can be represented. White light (a blackbody radiating at 6447 Kelvin) corresponds to the point C with coordinates $(x = y = 1/3)$. For a point E , the dominant wavelength is obtained by the intersection of the line through E and C with the horseshoe curve.

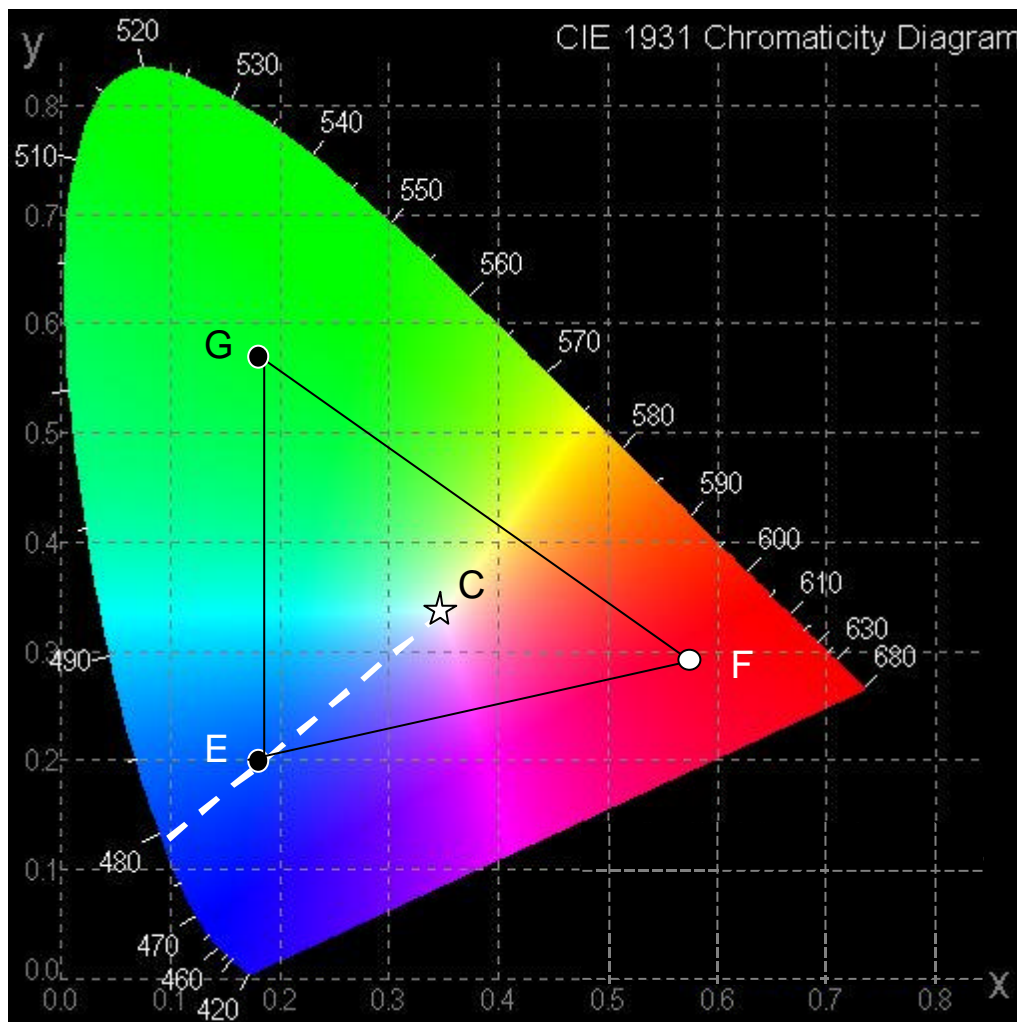


Figure A.3. Chromaticity diagram²²³ defined by the CIE in 1931.

A.3 Properties of Polyfluorenes with Different Side-Chain Patterns

Table A.2. Essential properties and chemical structures of polyfluorenes with different side-chain patterns. The fractions of PF2/6 were obtained from the batch of plain PF2/6, which is marked with a star. The full names of the polymers are given in the Appendix of abbreviations.

		M_n [g/mol]	M_w [g/mol]	PD	$T_{c@LC}$ [°C]	D	Chemical structure
Fractionated	PF2/6	373 000	455 000	1.22	174	1	
		253 000	308 000	1.22	174	1	
		154 000	212 000	1.38	172	2	
		101 000	165 000	1.63	168	16	
		62 000	138 000	2.22	164	17	
Plain PFs	PF2/6	195 000	320 000	1.66	172	10	
		127 000	210 000	1.65	169	13	
		111 000	247 000	2.22	169	~15*	
		106 000	233 000	2.19	167	16	
	PF3/5	32 000	66 000	2.05	195	12	
	PF8	150 000	300 000	2.0	174	9	
Endcapped PFs	PF2/6am2	103 000	146 000	1.41	165	>20	
	PF2/6am4	48 000	75 000	1.55	157	>20	
	PF2/6am9	12 000	31 000	2.57	135	>20	
	PF2/6nap3	59 000	89 000	1.5	151	>20	
	PF3/5am6	30 000	54 000	1.84	192	13	
PF Copolymers	PF8/1/1C2/6	173 000	288 000	1.66	149	13	
	PF4C12	129 000	213 000	1.65	152	3	

Zusammenfassung

Ziel im Rahmen der vorliegenden Dissertation war die Realisierung der polarisierten Elektrolumineszenz blau emittierender flüssigkristalliner Polyfluorene. Polymere Leuchtdioden, die aufgrund hoher Orientierung der Moleküle in der aktiven Schicht polarisiert emittieren, sind für eine Anwendung beispielsweise als Hintergrundbeleuchtung in Flüssigkristallanzeigen (LCDs) von Interesse. Es wurde gezeigt, dass sich mit der Ausrichtung von Polyfluoren auf Orientierungsschichten auf der Basis von geriebenem Polyimid hohe Ordnungsgrade erzielen lassen. Die Dotierung mit lochleitenden Materialien erlaubte erstmals den Einbau solcher Orientierungsschichten in Leuchtdioden und ermöglichte die Realisierung polarisierter Elektrolumineszenz. Die Morphologie und Struktur sowohl der hoch orientierten Polyfluorenfilme als auch lochleitender Orientierungsschichten wurden eingehend untersucht. Die Elektrolumineszenz-Eigenschaften von isotropen sowie polarisierten Leuchtdioden wurden ausführlich analysiert und anschließend durch chemische Modifizierung des Polyfluorens entscheidend verbessert. Zusätzlich wurde Polyfluoren mit fluoreszierenden Farbstoffen dotiert, um ausgehend von blauem Licht grüne und rote Emission zu erhalten. Hierbei wurde untersucht, in welchem Maß Förster-Energietransfer sowie Ladungsträgereinfang für die Emission der eingemischten Farbstoffe verantwortlich sind.

Eine Einführung in die Grundlagen der Elektrolumineszenz konjugierter Polymere findet sich in Kapitel 2 dieser Arbeit. Da polarisierte Elektrolumineszenz ein hohes Maß an Anisotropie der emittierenden Schicht erfordert, werden anschließend verschiedene Methoden zur Ausrichtung von Polymeren besprochen, wobei besondere Betonung auf der Orientierung flüssigkristalliner Polymere liegt.

Kapitel 3 behandelt die signifikanten Eigenschaften der Polymere sowie die experimentellen Methoden, die im Rahmen dieser Arbeit verwendet wurden. Neben Polyfluoren wird ein weiteres blau emittierendes Polymer, Polyphenylenethynylen (PPE), eingeführt. Bei der Charakterisierung der Polyfluorene wird im Anschluss an die Beschreibung der reinen Polymere insbesondere der positive Einfluss des Anbringens von lochleitenden Endgruppen an die Hauptkettenenden auf wesentliche Eigenschaften bezüglich der Elektrolumineszenz aufgezeigt. Außerdem werden die wesentlichen Merkmale von Polyimid, welches die Matrix der Orientierungsschicht bildet, sowie von verschiedenen Polymeren, die der Lochleitung und der Lochinjektion dienen, besprochen. Die Beschreibung der Methoden zur Präparation isotroper und polarisierter Leuchtdioden sowie zur Untersuchung der optischen, elektrischen und morphologischen Eigenschaften der Polymerfilme bilden den Abschluss dieses Abschnitts.

Im vierten Kapitel dieser Arbeit werden unterschiedliche Verfahren zur Ausrichtung der Polymermoleküle auf Polyfluoren sowie auf PPE angewandt und hinsichtlich der erreichbaren Ordnungsgrade verglichen und beurteilt. Im Falle von Polyfluoren wurde gezeigt, dass eine Orientierung im flüssigkristallinen Zustand mit Hilfe zusätzlicher Orientierungsschichten, welche auf geriebenem Polyimid basieren, die einzige geeignete Methode zur Orientierung dieses Polymers ist. Durch den Zusatz von niedrigmolekularen leitenden Materialien in geeigneter Konzentration in die Polyimid-Matrix konnte das nicht-leitende Polyimid so modifiziert werden, dass es sich in Leuchtdioden einbinden ließ, ohne dass die Orientierungseigenschaften der Schichten verloren gingen. Vergleiche unterschiedlicher Polyfluorene ergaben, dass die Länge und Struktur der Alkyl-Seitenketten das Orientierungsverhalten entscheiden beeinflussen. Hierbei wurde gezeigt, dass sich für verzweigte Seitenketten deutlich höhere Ordnungsgrade erreichen lassen als für solche mit linearen Seitenketten. Dies wurde mit dem vergrößerten Verhältnis aus Persistenzlänge und Polymerdurchmesser erklärt, was gemäß der Theorie der flüssigkristallinen Polymere zu einer Zunahme des erreichbaren Ordnungsparameter führt. Außerdem wiesen die Absorptionsspektren der Polyfluorene mit langen Seitenketten auf eine planare Konformation der Polymerrückgrate hin, welche aufgrund der starken Wechselwirkung zwischen den einzelnen Ketten eine Orientierung im flüssigkristallinen Zustand verhindert. Von allen untersuchten Polyfluoren ließ sich Poly(di-ethylhexylfluoren) (PF2/6) am besten orientieren.

Im Gegensatz zu Polyfluoren scheiterte der Versuch, PPE im flüssigkristallinen Zustand auf Orientierungsschichten auszurichten. Kalorimetrische DSC-Untersuchungen machten deutlich, dass sich die Struktur von PPE in flüssigkristalliner und kristalliner Phase nur unwesentlich voneinander unterscheiden. In beiden Phasen deuteten Absorptionsuntersuchungen auf eine planare Konformation der PPE-Rückgrate. Die Viskosität des als sehr steif bekannten Polymers PPE ist daher auch in flüssigkristallinem Zustand zu hoch, um eine Umordnung der Moleküle zu verursachen, welche allein durch Wechselwirkung mit einer Orientierungsschicht hervorgerufen wird. PPE konnte jedoch im kristallinen Zustand orientiert werden, indem anstatt einer zusätzlichen Orientierungsschicht der Polymerfilm selbst gerieben wurde. Die hohe Steifigkeit von PPE erlaubte die Übertragung der Kräfte, die durch das Reiben verursacht werden, auf das starre Polymerrückgrat und ermöglichte eine homogene Ausrichtung der Moleküle. Mit Hilfe dieser Methode konnten Leuchtdioden mit PPE in der aktiven Schicht verwirklicht werden, die polarisiert emittierten. Die bestmöglichen Methoden zur Ausrichtung der Moleküle unterschieden sich demnach für die beiden flüssigkristallinen Polymere Polyfluoren und PPE, und für beide Polymere wurden Verfahren gefunden, die die Herstellung von polarisierten Leuchtdioden ermöglichten.

In Kapitel 5 dieser Arbeit werden die Morphologie, die Struktur sowie weitere wesentliche Eigenschaften sowohl orientierter Polyfluorene als auch der zur Ausrichtung benötigten lochleitenden Orientierungsschichten aus dotiertem Polyimid besprochen. Hierfür wurden die Filme mit Hilfe von Licht- und Elektronenmikroskopie sowie von Elektronen- und Röntgenbeugungsexperimenten untersucht. Im ersten Teil wird die beobachtete Abnahme der Orientierbarkeit von Polyfluoren mit zunehmendem Molekulargewicht durch Elektronenbeugungsuntersuchungen näher beschrieben. Ergebnisse aus Transmissions-Elektronenmikroskopie Untersuchungen zeigten, dass sich die Morphologie orientierter PF2/6-Filme durch hochgeordnete Lamellen auszeichnet, welche in regelmäßigen Abständen von ungeordneten Regionen unterbrochen werden. Innerhalb der orientierten Lamellen sortieren sich die Moleküle nach ähnlicher Kettenlänge, wohingegen in den ungeordneten Gebieten vornehmlich die Endgruppen der Ketten vorzufinden sind. Strukturuntersuchungen ergaben, dass die einzelnen Polymerketten von PF2/6 zylindrisch sind und eine hexagonale Packung aufweisen, wobei die Polymerrückgrate eine 5/2-Helixstruktur bilden. Das wurmähnliche Rückgrat ist dabei zylinderförmig von einer Hülle aus ungeordneten Seitenketten umgeben, die ähnlich wie ein Lösungsmittel zwischen den einzelnen Ketten wirken. Die hieraus folgende geringe Viskosität des Polymers dient als Erklärung für die beobachtete bessere Orientierbarkeit von PF2/6 im Vergleich zu Polyfluoren mit linearen Oktyl-Seitenketten oder zu PPE.

Im zweiten Teil des fünften Kapitels werden Ergebnisse von Untersuchungen der lochleitenden Orientierungsschichten vorgestellt. Der Einfluss der Zugabe von lochleitenden Materialien zu Polyimid auf mechanische sowie auf elektrische Eigenschaften wurde untersucht. Bei moderater Lochleiter-Konzentration war die mechanische Stabilität der Filme ausreichend, um nach dem Reiben keine merklichen Unterschiede zu undotierten geriebene Filmen aufzuweisen. Vergleiche entsprechender Filme hinsichtlich Ladungsinjektion und -transport zeigten, dass erst durch die Dotierung eine Verwendung von Polyimid-Orientierungsschichten in Leuchtdioden ermöglicht wird. Sowohl polymere als auch niedrig-molekulare lochleitende Materialien wurden hinsichtlich der erreichbaren Orientierungsgrade sowie der resultierenden Elektrolumineszenz-Eigenschaften verglichen, wobei nur letztere in beiden Belangen zugleich zu vorteilhaften Ergebnissen führten. Es wurde gezeigt, dass sich die besten Resultate mit polarisierten Leuchtdioden erzielen ließen, bei denen die emittierende Schicht auf eine Doppelschicht-Struktur aufgebracht war, die der Lochinjektion und der Orientierung diente. Hierbei befand sich oberhalb einer *Lochinjektions*-Schicht aus reinem Lochleitermaterial eine weitere lochleitende *Orientierungsschicht* aus dotiertem Polyimid. Variation der Lochleiterkonzentrationen in Polyimid ergaben, dass die Helligkeit mit zunehmender Konzentration zunahm, wohingegen die erreichten Polarisationsverhältnisse gleichzeitig abnahmen. SEM- und AFM-Untersuchungen über den Einfluss der Lochleiterkonzentration auf die Schichtmorphologie ergaben, dass diese Beobachtun-

gen durch Phasenseparation und mechanische Beschädigung der Filme zu erklären ist, welche bei Konzentrationen oberhalb 20 Gewichtsprozent eintreten.

Im Kapitel 6 wird schließlich die Elektrolumineszenz von Leuchtdioden mit Polyfluoren als emittierende Schicht diskutiert. Zuerst wurde in isotropen Leuchtdioden die günstigste Diodenarchitektur ermittelt sowie die Optimierung der verwendeten Schichten vorgenommen. Die Ergebnisse wurden mit den Kenntnissen kombiniert, die im Rahmen der oben beschriebenen Untersuchungen erworben wurden, um die Herstellung von Leuchtdioden mit hoch-polarisierter Emission zu verwirklichen. Blaue Elektrolumineszenz mit einem Emissionsmaximum von 450 nm und einem Polarisationsverhältnis von 21 wurden erzielt, wobei die Leuchtdichte bei einer angelegten Spannung von 18 V etwa 100 cd/m^2 betrug, was der typischen Helligkeit eines Computermonitors entspricht. Alle Elektrolumineszenz-Eigenschaften ließen sich durch Endfunktionalisierung des Polyfluorens weiter deutlich verbessern, indem lochleitende Triarylamin-Derivate an die Enden der Hauptketten angebracht wurden ('Endcapping'). Der unerwünschte Beitrag zur Emission bei höheren Wellenlängen, welcher im Falle des reinen Polyfluorens beobachtet wurde und gemeinhin aggregierten Polymermolekülen zugeschrieben wird, wurde durch das Konzept der Endfunktionalisierung wirksam unterdrückt. Außerdem war die Farbstabilität wesentlich verbessert und die Effizienz der Leuchtdioden um mehr als eine Größenordnung höher als bei der Verwendung des reinen Polyfluorens. Diese Beobachtungen wurden mit den elektrochemischen Eigenschaften der Endgruppen erklärt. Letztere wirken als anziehende Fallen für Ladungsträger, was dazu führt, dass die Erzeugung von Exzitonen und die anschließende Rekombination vorwiegend in der Nähe der Kettenenden stattfindet, anstatt wie im Falle des reinen Polyfluorens an weniger effizienten Aggregaten oder Exzimer-erzeugenden Stellen. Es wurde gezeigt, dass die Endfunktionalisierung weder das Verhalten des Polymers im flüssig-kristallinen Zustand, noch dessen Orientierbarkeit beeinträchtigte. Die Verwendung des modifizierten Polyfluorens erlaubte die Herstellung von polarisierten Leuchtdioden mit einem Polarisationsverhältnis von 22 und einer Leuchtdichte von 200 cd/m^2 bei 19 V, wobei die Schwellspannung auf 7,5 V gesenkt wurde. Dioden mit einem Anisotropiefaktor von 15 erreichten Leuchtdichten von bis zu 800 cd/m^2 . Die Effizienz dieser Leuchtdioden war mit $0,25 \text{ cd/A}$ bei ähnlichem Polarisationsverhältnis und Leuchtdichte um mehr als doppelt so hoch wie die bisher berichteten Werte.

Die Veränderung der eigentlich blauen Emissionsfarbe durch die Zugabe von Materialien mit niedrigerer Bandlücke in eine Polyfluorenmatrix wird im Kapitel 7 beschrieben. Es wurde gezeigt, dass der Zusatz bereits geringer Konzentrationen eines grün emittierenden Thiophen-Farbstoffes das Emissionsspektrum des Polyfluorens entscheidend veränderte und die Realisierung *grüner* Emission ermöglichte. Genau wie im Falle der nicht-emittierenden Lochleiter, die für die Endfunktionalisierung des Polyfluorens verwendet wurden, wirken auch die Thiophen-

Farbstoffe als effektive Ladungsträgerfallen, was neben der Farbveränderung eine drastische Verbesserung der Leuchtdiodeneffizienzen zur Folge hatte. Darüber hinaus konnte mit Hilfe des dotierten Polyfluorens polarisierte grüne Elektrolumineszenz verwirklicht werden, wobei die Polarisationsverhältnisse Werte von bis zu 30 erreichten, bei einer Leuchtdichte von 600 cd/m^2 und einer Effizienz von $0,3 \text{ cd/A}$.

Im Hinblick auf rote Elektrolumineszenz wurden Leuchtdioden mit dendronisierten Perylenfarbstoffen in der emittierenden Schicht untersucht, zum einen in reiner Form und zum anderen in Mischungen mit Polyfluoren. Hierfür wurden zwei Generationen von Dendrimeren, bestehend aus zentralem Perylendiimid-Chromophor und Polyphenylen-Gerüst, mit einer nicht-dendronisierten Modellverbindung verglichen. Leuchtdioden mit reinen Filmen der ersten und zweiten Dendrimergeneration emittierten rotes Licht mit CIE-Koordinaten $(0,627/0,372)$ und einer Leuchtdichte von bis zu 120 cd/m^2 bei 11 V , wobei die Effizienz allerdings nur $0,03 \text{ cd/A}$ betrug. Um die unterschiedlichen Mechanismen zu klären, die zur Emission der Farbstoffmoleküle führen, wurden die Farbstoffe in Polyfluoren beigemischt, und der Einfluss der Dendronisierung auf die Emissionsfarbe und die Intensität der Elektrolumineszenz wurde untersucht. In Photolumineszenz wurde mit zunehmender Dendronisierung eine Abnahme des Förster-Energieübertrags vom Polyfluoren-Wirt zu dem Perylenfarbstoff-Gast verzeichnet, was zu einem höheren blauen Anteil im Emissionsspektrum führte. Hingegen wurde gezeigt, dass in Elektrolumineszenz die Farbstoffe als Elektronenfallen wirken und die Rekombination der Ladungsträger zu Exzitonen somit vorwiegend auf den Farbstoff- anstatt auf den Polyfluorenmolekülen statt findet. Aus diesem Grund war die Betonung der roten Emission in Elektrolumineszenz ungleich stärker als in Photolumineszenz, bei der die rote Emission ausschließlich durch Energieübertrag via Förstertransfer zu Stande kommt. Die Verstärkung einer Farbverschiebung von rot nach blau, die mit zunehmender Dendronisierung und ansteigender Betriebsspannung beobachtet wurde, konnte qualitativ mit der kinetischen Beeinträchtigung des Elektronenübertrags vom Polyfluoren-Wirt auf den Perylendiimid-Chromophor erklärt werden. Der bestmögliche Kompromiss aus roter Farbtiefe und Helligkeit wurde für die Mischung aus Polyfluoren und dem Farbstoff der ersten Dendrimergeneration erzielt. Bei angelegter Spannung von $6,5 \text{ V}$ lag die Leuchtdichte bei 100 cd/m^2 und bei 11 V bei 700 cd/m^2 , wobei die Emission bei 600 nm ihr Maximum hatte.

Abbreviations

AFM	Atomic force microscopy
Ca	Calcium
Cd	Candela
CIE	Commission Internationale de L'Eclairage
CV	Cyclovoltammetry
D	Dichroic ratio in absorption
DSC	Differential scanning calorimetry
E_{ox}^0 (E_{red}^0)	Onset potential for oxidation (reduction)
E_a	Electron affinity
EL	Electroluminescence
G1	Polyphenylene dendrimer of the first generation
G2	Polyphenylene dendrimer of the second generation
HOMO	Highest occupied molecular orbital
HT	Hole-transporting
HTAL	Hole-transporting alignment layer
HTM	Hole-transporting moiety
I_p	Ionization potential
ITO	Indium tin oxide
$I-V$	Current-voltage
j	Current Density
LC	Liquid crystal
LCD	Liquid crystal display
LCP	Liquid crystalline polymer
LED	Light-emitting diode
LiF	Lithiumfluoride
l_k	Kuhn length
lm	Lumen
l_p	Persistence length
LUMO	Lowest unoccupied molecular orbital
LVSEM	Low-voltage scanning electron microscopy
M	Non-dendronized tetraphenoxyperylene diimide model compound

M_n	Number average molecular weight
M_w	Weight average molecular weight
n	Refractive index
OLED	Organic Light-Emitting Diode
P	Polarization ratio in emission
p	Persistence ratio
PAni-CSA	Polyaniline doped with camphor sulfonic acid
PD	Polydispersity
PEDOT-PSS	Poly(3,4-ethylenedioxythiophene) doped with poly(styrene sulfonic acid)
PF	Polyfluorene
PF2/6	Poly(9,9-bis(2-ethylhexyl)fluorene-2,7-diyl)
PF2/6am-X	Poly(9,9-bis(2-ethylhexyl)fluorene-2,7-diyl) endcapped with X mol% bis(4-methylphenyl)(4-bromophenyl)amine
PF2/6napX	Poly(9,9-bis(2-ethylhexyl)fluorene-2,7-diyl) endcapped with X mol% (4'-bromo-biphenyl-4-yl)-naphthalen-2-yl-phenyl-amine
PF3/5	Poly(9,9-bis(2-propylpentyl)fluorene)
PF4C12	Poly(2,7-(9,9-bis(2-butyl))co-(9,9-bis(dodecyl))fluorene)
PF8/1/1C2/6	Poly(2,7-(9,9-bis(2-ethylhexyl))co-(9,9-bis((3S)-3,7-dimethyloctyl))fluorene)
PI	Polyimide
PL	Photoluminescence
PPE	Hexyl-dodecyl copoly(phenyleneethynylene)
PPV	Poly(<i>p</i> -phenylene-vinylene)
S	Order Parameter
SCLC	Space-charge limited current
SEM	Scanning electron microscopy
S2_3	Thiophene dye
ST 1163	N,N'-diphenyl-N,N'-bis(4'-(N,N-bis(naphth-1-yl)-amino)-biphenyl-4-yl)-benzidine
ST 16-7	4,4'-bis{N-(1-naphthyl)-N-phenylamino}-biphenyl
ST 638	4,4',4''-tris(1-naphthyl)-N-phenyl-amino)-triphenylamine
ST 755	1,1-bis-(4-bis(4-methyl-phenyl)-amino-phenyl)-cyclohexane
T	Temperature
$T_{C@LC}$	Temperature for transition from crystalline to liquid crystalline state
TEM	Transmission electron microscopy

T_g	Glass transition temperature
T_m	Melting temperature
U	Voltage
UV/Vis	Ultraviolet/Visible Light
DE	Barrier to charge injection
ϵ	Dielectric constant
ϵ_0	Vacuum permittivity
f_M	Metal work function
h	Quantum efficiency
l	Wavelength
n	Frequency

Bibliography

- ¹ M. Pope, H. P. Kallmann, P. Magnante. *J. Chem. Phys.* **1963**, *38*, 2042.
- ² C. W. Tang, S. A. VanSlyke. 'Organic electroluminescent devices'. *Appl. Phys. Lett.* **1987**, *51(12)*, 913.
- ³ J. H. Burroughes, D. D. C. Bradley, A. R. Brown, R. N. Marks, K. Mackay, R. H. Friend, P. L. Burns, A. B. Holmes. *Nature* **1990**, *347*, 539.
- ⁴ T. Förster. *Ann. Phys. (Leipzig)* **1948**, *2*, 55.
- ⁵ D. L. Dexter. *J. Chem. Phys.* **1953**, *21*, 836.
- ⁶ A. A. Lamola, N. J. Turro, *Energy Transfer and Organic Photochemistry*, Interscience Publishers, New York **1969**.
- ⁷ Bergmann-Schaefer, *Lehrbuch der Experimentalphysik, Band 6, Festkörper*, edited by W. Raith, Walter de Gruyter, Berlin, New York **1992**.
- ⁸ U. Mitschke, P. Bäuerle. 'The Electroluminescence of Organic Materials'. *Journal of Materials Chemistry* **2000**, *10(7)*, 1471.
- ⁹ J. L. Bredas, J. Cornil, A. J. Heeger. 'The Exciton Binding Energy in Luminescent Conjugated Polymers'. *Adv. Mat.* **1996**, *8*, 447.
- ¹⁰ M. A. Baldo, D. F. O'Brien, Y. You, A. Shoustikov, S. Sibley, M. E. Thompson, S. R. Forrest. 'Highly efficient phosphorescent emission from organic electroluminescent devices'. *Nature* **1998**, *395*, 151.
- ¹¹ V. Cleave, G. Yahiolu, P. Le Barny, R. H. Friend, N. Tessler. 'Harvesting singlet and triplet energy in polymer LEDs'. *Adv. Mat.* **1998**, *11(4)*, 285.
- ¹² E. H. Roderick, W. R. Frensley, M. P. Shaw, *Device Physics in Handbook on Semiconductors; Vol. 4*, edited by C. Hilsum, North-Holland, New York **1993**, 1.
- ¹³ T. M. Brown, J. S. Kim, R. H. Friend, F. Cacialli, R. Daik, W. J. Feast. 'Built-in field electroabsorption spectroscopy of polymer light-emitting diodes incorporating a doped poly(3,4-ethylene dioxythiophene)-hole injection layer'. *Applied Physics Letters* **1999**, *75*, 1679.
- ¹⁴ S. Janietz, D. D. C. Bradley, M. Grell, C. Giebeler, M. Inbasekaran, E. P. Woo. 'Electrochemical Determination of the Ionization Potential and Electron Affinity of Poly(9,9-Dioctylfluorene)'. *Applied Physics Letters*. **1998**, *73(17)*, 2453.
- ¹⁵ W. Graupner, S. Tasch, G. Leising, *Sollid-state Aspects of Conjugated Semiconductors in Semiconducting Polymers*, edited by G. Hadziioannou, P. F. v. Hutten, WILEY-VCH, Weinheim **2000**, 259.
- ¹⁶ Y. N. Gartstein, E. M. Conwell. 'Field-Dependent Thermal Injection into a Disordered Molecular Insulator'. *Chem. Phys. Lett.* **1996**, *255*, 93.
- ¹⁷ R. H. Fowler, L. Nordheim. *Proc. R. Soc.* **1928**, *A119*, 173.
- ¹⁸ H. Bässler, *Charge Transport in Random Organic Semiconductors in Semiconducting Polymers*, edited by G. Hadziioannou, P. F. v. Hutten, WILEY-VCH, Weinheim **2000**, 365.
- ¹⁹ D. V. Khramtchenkov, V. I. Arkhipov, H. Bassler. 'Charge Carrier Recombination in Organic Bilayer Electroluminescent Diodes. (I) Theory'. *Journal of Applied Physics*. **1997**, *81(10)*, 6954.
- ²⁰ Y.-H. Tak, H. Bassler. 'Charge Carrier Recombination in Organic Bilayer Electroluminescent Diodes. (II) Experiment'. *Journal of Applied Physics*. **1997**, *81(10)*, 6963.
- ²¹ T. K. Däubler. 'Photophysical Characterization of Photorefractive Polymers'. Ph.D.-Dissertation Thesis, University of Potsdam **1999**.
- ²² M. Pope, C. E. Swenberg, *Electronic Processes in Organic Materials*, Oxford Univ. Press (Clarendon), New York **1982**.
- ²³ J. C. Scott, G. G. Malliaras, *The Chemistry, Physics and Engineering of Organic Light-Emitting Diodes in Semiconducting Polymers*, edited by G. Hadziioannou, P. F. v. Hutten, WILEY-VCH, Weinheim **2000**, 411.
- ²⁴ G. Horowitz, *Physics of Organic Field-Effect Transistors in Semiconducting Polymers*, edited by G. Hadziioannou, P. F. v. Hutten, WILEY-VCH, Weinheim **2000**, 365.
- ²⁵ I. H. Campbell, D. L. Smith, *Physics of Polymer Light-Emitting Diodes in Semiconducting Polymers*, edited by G. Hadziioannou, P. F. v. Hutten, WILEY-VCH, Weinheim **2000**, 333.
- ²⁶ H. Bässler. *Physica Status Solidi B* **1993**, *175*, 15.
- ²⁷ P. M. Borsenberger, D. S. Weiss, *Organic Photoreceptors for Electrophotography*, Marcel Dekker, New York **1998**.

- 28 M. Redecker, D. D. C. Bradley, M. Inbasekaran, E. P. Woo. 'Non-dispersive hole transport in an electroluminescent polyfluorene'. *Appl. Phys. Lett.* **1998**, *73*, 1565.
- 29 G. Hadziioannou, P. F. van Hutten (Eds.), *Semiconducting Polymers*, WILEY-VCH, Weinheim **2000**.
- 30 P. Langevin. *Ann. Chem. Phys.* **1903**, *28*, 289.
- 31 J. Scott, S. Karg, S. A. Carter. 'Bipolar Charge and Current Distributions in Organic Light-Emitting Diodes'. *J. Appl. Phys.* **1997**, *82(3)*, 1454.
- 32 H. Bässler. *Poly. Adv. Tech.* **1996**, *9*, 402.
- 33 T. Tsutsui, S. Saito. *Intrinsically Conducting Polymers: An Emerging Technology; NATO ASI Series E: Appl. Sciences* **1993**, *246*, 123.
- 34 R. H. Friend, R. W. Gymer, A. B. Holmes, J. H. Burroughes, R. N. Marks, C. Taliani, D. D. C. Bradley, D. A. Dos Santos, J. L. Bredas, M. Logdlund, W. R. Salaneck. 'Electroluminescence in conjugated polymers'. *Nature*. **1999**, *397(6715)*, 121.
- 35 S. Tasch, W. Graupner, G. Leising, L. Pu, M. W. Wagner, R. H. Grubbs. 'Red-Orange Electroluminescence with New Soluble and Air-Stable Poly(naphthalene-vinylene)s'. *Adv. Mater.* **1995**, *7*, 903.
- 36 T. Kawase, D. J. Pinner, R. H. Friend, T. Shimoda. 'Grazing emitted light from films of derivative polymer of polyfluorene'. *Synth. Met.* **2000**, *111*, 583.
- 37 <http://www.cie.co.at>.
- 38 F. Pedrotti, L. Pedrotti, W. Bausch, H. Schmidt, *Optik*, Prentice Hall, München **1996**.
- 39 D. Kalinowski. 'Electroluminescence in Organics'. *Journal of Physics D Applied Physics* **1999**, *32(24)*, R179.
- 40 A. Meisel, T. Miteva, G. Glaser, V. Scheumann, D. Neher. 'Influence of dopant concentration on morphology of hole-transporting alignment layers based on a polyimide matrix'. *In preparation* **2000**.
- 41 M. Grell, W. Knoll, D. Lupo, A. Meisel, T. Miteva, D. Neher, H. G. Nothofer, U. Scherf, A. Yasuda. 'Blue polarized electroluminescence from a liquid crystalline polyfluorene'. *Advanced Materials* **1999**, *11(8)*, 671.
- 42 T. Miteva, A. Meisel, W. Knoll, H. G. Nothofer, U. Scherf, D. C. Müller, K. Meerholz, A. Yasuda, D. Neher. 'Improving the performance of polyfluorene-based organic light-emitting diodes via endcapping'. *Advanced Materials* **2001**, *8(13)*, 565.
- 43 A. Kraft, A. C. Grimsdale, A. B. Holmes. 'Electroluminescent Conjugated Polymers – Seeing Polymers in a New Light'. *Angew. Chem. Int. Ed.* **1998**, *37*, 402.
- 44 A. Meisel, A. Herrmann, T. Miteva, H.-G. Nothofer, U. Scherf, K. Müllen, D. Neher. 'High brightness light-emitting diodes based on dendronized perylene'. *To be submitted to Phys. Rev. B*.
- 45 T. Virgili, D. G. Lidzey, D. D. C. Bradley. 'Efficient energy transfer from blue to red in tetraphenylporphyrin-doped poly(9,9'-dioctylfluorene) light-emitting diodes'. *Adv. Mater.* **2000**, *12(1)*, 58.
- 46 D. Y. Kim, H. N. Cho, C. Y. Kim. 'Blue Light Emitting Polymers'. *Progr. Polym. Sci.* **2000**, *25*, 1089.
- 47 S. Komaba, A. Amano, T. Osaka. 'Electroluminescence Properties of Electropolymerized Poly(p-phenylene) Films by means of Electrochemical Oxidation and Reduction'. *Journal of Electroanalytical Chemistry* **1997**, *430*, 97.
- 48 R. E. Gill, G. G. Malliaras, J. Wildeman, G. Hadziioannou. 'Tuning of photo- and electroluminescence in alkylated polythiophenes with well-defined regioregularity'. *Adv. Mater.* **1994**, *6(2)*, 132.
- 49 D. D. Gebler, Y. Z. Wang, J. W. Blatchford, S. W. Jessen, L.-B. Lin, T. L. Gustafsson, H. L. Wang, T. M. Swager, A. G. MacDiarmid, A. J. Epstein. 'Blue electroluminescent devices based on soluble poly(p-pyridine)'. *J. Appl. Phys.* **1995**, *78(6)*, 4264.
- 50 J. H. Kim, C. Rosenblatt. 'Temperature effect on a rubbed polyimide alignment layer'. *Journal of Applied Physics* **2000**, *87(1)*, 155-158.
- 51 M. Gross, D. C. Muller, H. G. Nothofer, U. Scherf, D. Neher, C. Bräuchle, K. Meerholz. 'Improving the performance of doped pi-conjugated polymers for use in organic light-emitting diodes'. *Nature* **2000**, *405*, 661.
- 52 M. Inbasekaran, E. Woo, W. S. Wu, M. Bernius, L. Wujkowski. 'Fluorene homopolymers and copolymers'. *Synthetic Metals* **2000**, *111*, 397.
- 53 K. H. Weinfurter, H. Fujikawa, S. Tokito, Y. Taga. 'Highly efficient pure blue electroluminescence from polyfluorene: Influence of the molecular weight distribution on the aggregation tendency'. *Applied Physics Letters* **2000**, *76(18)*, 2502.
- 54 M. Grell, D. D. C. Bradley, M. Inbasekaran, G. Ungar, K. S. Whitehead, E. P. Woo. 'Intrachain ordered polyfluorene'. *Synthetic Metals* **2000**, *111*, 579.
- 55 A. W. Grice, D. D. C. Bradley, M. T. Bernius, M. Inbasekaran, W. W. Wu, E. P. Woo. 'High Brightness and Efficiency Blue Light-Emitting Polymer Diodes'. *Applied Physics Letters*. **1998**, *73(5)*, 629.

- 56 Y. Yang, Q. Pei. 'Efficient blue-green and white light-emitting electrochemical cells based on poly[9,9-bis(3,6-dioxaheptyl)-fluorene-2,7-diyl]'. *J. of Appl. Phys.* **1997**, *81*(7), 3294.
- 57 M. Ranger, D. Rondeau, M. Leclerc. 'New Well-Defined Poly(2,7-Fluorene) Derivatives – Photoluminescence and Base Doping'. *Macromolecules*. **1997**, *30*(25), 7686.
- 58 M. Fukuda, K. Sawada, K. Yoshino. 'Synthesis of fusible and soluble conducting polyfluorene derivatives and their characteristics'. *J. Polym. Sci., Part A: Polym. Chem.* **1997**, *31*, 2465.
- 59 Y. Ohmori, M. Uchida, K. Muro, K. Yoshino. 'Blue electroluminescent diodes utilizing poly(alkylfluorene)'. *Jpn. J. Appl. Phys.* **1991**, *30*(12B), 1941.
- 60 A. Kraft, A. C. Grimsdale, A. B. Holmes. 'Electroluminescent Conjugated Polymers – Seeing Polymers in a New Light'. *Angewandte Chemie (International Edition in English)* **1998**, *37*, 402.
- 61 J. Kido, *Organic Electroluminescent Materials and Devices*, edited by S. Miyata, H.-S. Nalwa, Gordon and Breach, Amsterdam **1997**.
- 62 M. Grell, D. D. C. Bradley. 'Polarized luminescence from oriented molecular materials'. *Advanced Materials*. **1999**, *11*(11), 895.
- 63 X. J. Zhang, S. A. Jenekhe. 'Electroluminescence of multicomponent conjugated polymers. 1. Roles of polymer/polymer interfaces in emission enhancement and voltage-tunable multicolor emission in semiconducting polymer/polymer heterojunctions'. *Macromolecules* **2000**, *33*(6), 2069.
- 64 P. W. M. Blom, M. Vissenberg. 'Charge transport in poly(*p*-phenylene vinylene) light-emitting diodes'. *Materials Science & Engineering R Reports* **2000**, *27*(3-4), 53.
- 65 R. E. Martin, F. Geneste, A. B. Holmes. 'Synthesis of Conjugated Polymers for Application in Light-Emitting Diodes'. *Comptes Rendus de l'Academie des Sciences Serie IV Physique Astrophysique* **2000**, *1*(4), 447.
- 66 R. H. Friend, N. C. Greenham, *Electroluminescence in Conjugated Polymers in Handbook of Conducting Polymers*, 2nd ed., edited by T. A. Skotheim, R. L. Elsenbaumer, J. R. Reynolds, Marcel Dekker, Inc., New York **1998**, 823.
- 67 A. Greiner. 'Design and Synthesis of Polymers For Light-Emitting Diodes'. *Polymers for Advanced Technologies*. **1998**, *9*(7), 371.
- 68 J. L. Segura. 'The Chemistry of Electroluminescent Organic Materials'. *Acta Polymerica*. **1998**, *49*(7), 319.
- 69 P. E. Burrows, S. R. Forrest, M. E. Thompson. 'Prospects and Applications For Organic Light-Emitting Devices'. *Current Opinion in Solid State & Materials Science*. **1997**, *2*(2), 236.
- 70 D. Bradley. 'Electroluminescent Polymers – Materials, Physics and Device Engineering'. *Current Opinion in Solid State & Materials Science*. **1996**, *1*(6), 789.
- 71 J. Salbeck. 'Electroluminescence with Organic Compounds'. *Ber. Bunsenges. Phys. Chem.* **1996**, *100*, 1667.
- 72 L. M. Landau, E. M. Lifshitz, L. P. Pitaevskii, *Statistical Physics, Part 1*, 3rd ed., Pergamon, Oxford **1980**.
- 73 M. Doi. *J. Polym. Sci., Polym. Phys. Ed.* **1981**, *19*, 229.
- 74 G. Marrucci, P. L. Maffettone. 'Description of the Liquid-Crystalline Phase of Rodlike Polymers at High Shear Rates'. *Macromolecules* **1989**, *22*, 4076.
- 75 V. N. Tsvetkov. *Acta Physicochim. USSR* **1942**, *16*, 132.
- 76 T. Sauer, T. Arndt, D. N. Batchelder, A. A. Kalachev, G. Wegner. 'The Structure of Langmuir-Blodgett Films from Substituted Phthalocyaninato-Polysiloxanes'. *Thin Solid Films* **1990**, *187*, 357.
- 77 P. Dyreklev, M. Berggren, O. Inganäs, M. R. Andersson, O. Wennerstrom, T. Hjertberg. 'Polarized Electroluminescence From an Oriented Substituted Polythiophene in a Light Emitting Diode'. *Advanced Materials*. **1995**, *7*(1), 43.
- 78 T. W. Hagler, K. Pakbaz, K. F. Voss, A. J. Heeger. 'Enhanced order and electronic delocalization in conjugated polymers oriented by gel processing in polyethylene'. *Phys. Rev. B* **1991**, *44*, 8652.
- 79 P. Smith, P. J. Lemstra. 'Ultra-high-strength polyethylene filaments by solution spinning/drawing'. *J. Mater. Sci* **1980**, *15*, 505.
- 80 D. D. C. Bradley, R. H. Friend, H. Lindenberger, S. Roth. 'Infra-red characterization of oriented poly(*p*-phenylene vinylene)'. *Polymer* **1986**, *27*, 1709.
- 81 U. Lemmer, D. Vacar, D. Moses, A. J. Heeger, T. Ohnishi, T. Noguchi. 'Electroluminescence from Poly(phenylenevinylene) in a Planar Metal-Polymer-Metal Structure'. *Appl. Phys. Lett.* **1996**, *68*, 3007.
- 82 J. Cognard. *Mol. Cryst. Liq. Cryst. Suppl. Ser.* **1982**, *Supplement 1*, 53.
- 83 M. Hamaguchi, K. Yoshino. 'Polarized Electroluminescence From Rubbing-Aligned Poly(2,5-Dinonyloxy-1,4-Phenylenevinylene) Films'. *Applied Physics Letters*. **1995**, *67*(23), 3381.

- 84 L. Kloppenburg, D. Song, U. H. F. Bunz. 'Alkyne Metathesis with Simple Catalyst Systems – Poly(*p*-phenyleneethynylene)s'. *J. Am. Chem. Soc.* **1998**, *120*, 7973.
- 85 T. Miteva, A. Meisel, M. Grell, H. G. Nothofer, D. Lupo, A. Yasuda, W. Knoll, L. Kloppenburg, U. H. F. Bunz, U. Scherf, D. Neher. 'Polarized electroluminescence from highly aligned liquid crystalline polymers'. *Synthetic Metals* **2000**, *111*, 173.
- 86 M. Jandke, P. Strohriegl, J. Gmeiner, W. Brütting, M. Schwoerer. 'Polarized electroluminescence from rubbing-aligned poly (*p*-phenylenevinylene)'. *Synthetic Metals* **2000**, *111*, 177.
- 87 D. Neher. 'Substituted Rigid Rod-Like Polymers – Building Block for Photonic Devices'. *Adv. Mater.* **1995**, *7(8)*, 691.
- 88 V. Cimrová, M. Remmers, D. Neher, G. Wegner. 'Polarized light emission from LEDs prepared by the Langmuir-Blodgett technique'. *Adv. Mater.* **1996**, *8*, 146.
- 89 J. C. Wittmann, P. Smith. 'Highly oriented thin films of poly(tetrafluoroethylene) as a substrate for oriented growth of materials'. *Nature* **1991**, *352*, 414.
- 90 Y. Yoshida, N. Tanigaki, K. Yase, S. Hotta. 'Color-Tunable Highly Polarized Emissions from Uniaxially Aligned Thin Films of Thiophene/Phenylene Co-oligomers'. *Adv. Mater.* **2000**, *12(21)*, 1587.
- 91 K. Wakita, S. Hotta, N. Sonoda, Y. Yang. *US Patent 5 546 889* **1996**.
- 92 K. Pichler, R. H. Friend, P. L. Burn, A. B. Holmes. 'Chain alignment in poly(*p*-phenylene vinylene) on oriented substrates'. *Synth. Met.* **1993**, *55*, 454.
- 93 B. Winkler, S. Tasch, E. Zojer, M. Ungerank, G. Leising, F. Stelzer. 'Synthesis and Characterization of a Novel Side-Chain Liquid Crystalline Poly(*p*-phenylenevinylene)'. *Synth. Met.* **1996**, *83*, 177.
- 94 X. L. Chen, Z. N. Bao, B. J. Sapjeta, A. J. Lovinger, B. Crone. 'Polarized electroluminescence from aligned chromophores by the friction transfer method'. *Advanced Materials* **2000**, *12(5)*, 344.
- 95 C. E. Stroog. *J. Polym. Sci.* **1976**, *11*, 161.
- 96 A. M. Donald, A. H. Windle, *Liquid Crystalline Polymers*, edited by R. W. Cahn, E. A. Davis, I. M. Ward, Cambridge University Press, Cambridge **1992**.
- 97 B. Winkler, S. Tasch, E. Zojer, M. Ungerank, G. Leising, F. Stelzer. 'Synthesis and characterization of a novel side-chain liquid crystalline poly(*p*-phenylenevinylene)'. *Synth. Met.* **1996**, *83*, 177.
- 98 A. H. Windle, *Structure of Thermotropic Main-Chain Polymers in Liquid Crystalline Polymers*, edited by R. W. Cahn, E. A. Davis, I. M. Ward, Cambridge University Press, Cambridge **1992**.
- 99 A. Ciferri, *Rigid and Semirigid Chain Polymeric Mesogens in Polymer Liquid Crystals*, edited by A. Ciferri, W. R. Krigbaum, R. B. Meyer, Academic Press, Inc., New York **1982**.
- 100 P. J. Flory, *Advances in Polymer Science*, edited by M. Gordon, Springer-Verlag, Berlin **1984**.
- 101 W. Maier, A. Z. Saupe. *Naturforsch.* **1960**, *A13/A14/A15*, 564/882/287.
- 102 A. H. Windle, *Structure of Thermotropic Main-Chain Polymers in Liquid Crystalline and Mesomorphic Polymers*, edited by V. P. Shibaev, L. Lam, Springer-Verlag, Inc., New York **1994**.
- 103 P. G. de Gennes, J. Prost, *The Physics of Liquid Crystals*, 2nd ed., Clarendon Press, Oxford **1993**.
- 104 J. Oberski, R. Festag, C. Schmidt, G. Lüssem, J. H. Wendorff, A. Greiner, M. Hopmeier, F. Motamedi. 'Synthesis and Structure-Property Relationships of Processable Liquid Crystalline Polymers with Arylenevinylene Segments in the Main Chain for Light-Emitting Applications'. *Macromolecules* **1995**, *28*, 8676.
- 105 G. Lüssem, F. Geffarth, A. Greiner, W. Heitz, M. Hopmeier, M. Oberski, C. Unterlechner, J. H. Wendorff. 'Polarized Electroluminescence of Light Emitting Liquid Crystalline Polymers'. *Liquid Crystals*. **1996**, *21(6)*, 903.
- 106 M. Ballauff. 'Kettensteife Polymere – Struktur, Phasenverhalten und Eigenschaften'. *Angew. Chem.* **1989**, *101*, 261.
- 107 M. Ballauff. 'Phase Equilibria in rod-like systems with flexible chains'. *Macromolecules* **1986**, *19*, 1366.
- 108 H. Martelock, A. Greiner, H. Heitz. *Macromol. Chem.* **1991**, *192*, 967.
- 109 L. Yu, Z. Bao. 'Conjugated polymers exhibiting liquid crystallinity'. *Adv. Mater.* **1994**, *6*, 156.
- 110 M. Grell, D. D. C. Bradley, M. Inbasekaran, E. P. Woo. 'A Glass-Forming Conjugated Main-Chain Liquid Crystal Polymer For Polarized Electroluminescence Applications'. *Advanced Materials*. **1997**, *9(10)*, 798.
- 111 K. S. Whitehead, M. Grell, D. D. C. Bradley, M. Inbasekaran, E. P. Woo. 'Polarized emission from liquid crystal polymers'. *Synthetic Metals* **2000**, *111*, 181.
- 112 K. S. Whitehead, M. Grell, D. D. C. Bradley, M. Jandke, P. Strohriegl. 'Highly polarized blue electroluminescence from homogeneously aligned films of poly(9,9-dioctylfluorene)'. *Applied Physics Letters* **2000**, *76(20)*, 2946.

- ¹¹³ P. M. Cotts, T. M. Swager, Q. Zhou. 'Equilibrium Flexibility of a Rigid Linear Conjugated Polymer'. *Macromolecules* **1996**, 29, 7323.
- ¹¹⁴ M. Grell, D. D. C. Bradley, X. Long, T. Chamberlain, M. Inbasekaran, E. P. Woo, M. Soliman. 'Chain Geometry, Solution Aggregation and Enhanced Dichroism in the Liquid-Crystalline Conjugated Polymer Poly(9,9-Diocyfluorene)'. *Acta Polymerica*. **1998**, 49(8), 439.
- ¹¹⁵ H. Lim, H. Park, J. G. Lee, Y. Kim, W. J. Cho, C. S. Ha. 'Polymeric light-emitting diodes utilizing TPD-dispersed polyimide thin film and organometallic complex'. *Proceedings of SPIE* **1998**, 3281, 345.
- ¹¹⁶ N. Ito, K. Sakamoto, R. Arafune, S. Ushioda. 'Relation between the molecular orientations of a very thin liquid crystal layer and an underlying rubbed polyimide film'. *Journal of Applied Physics* **2000**, 88(6), 3235-3241.
- ¹¹⁷ X. Liang, J. Liu, L. Han, H. Tang, S.-Y. Xu. 'Electric force microscopy study of the surface electrostatic property of rubbed polyimide alignment layers'. *Thin Solid Films* **2000**, 370, 238-242.
- ¹¹⁸ K. R. Brown, D. A. Bonnell, S. T. Sun. 'Atomic Force Microscopy of Mechanically Rubbed and Optically Buffed Polyimide Films'. *Liquid Crystals* **1998**, 25(5), 597-601.
- ¹¹⁹ R. Meister, B. Jérôme. 'The Conformation of a Rubbed Polyimide'. *Macromolecules* **1998**, 32, 480-486.
- ¹²⁰ H. Kikuchi, J. A. Logan, D. Y. Yoon. 'Study of local stress, morphology, and liquid-crystal alignment on buffed polyimide surfaces'. *Journal of Applied Physics* **1996**, 79(9), 6811-6817.
- ¹²¹ N. A. Van Aerle, M. Barmentlo, R. W. J. Hollering. 'Effect of Rubbing On the Molecular-Orientation Within Polyimide Orienting Layers of Liquid-Crystal Displays'. *Journal of Applied Physics* **1993**, 74(5), 3111-3120.
- ¹²² W. Chen, O. T. Moses, Y. R. Shen, K. H. Yang. 'Surface electroclinic effect on the layer structure of a ferroelectric liquid crystal'. *Phys. Rev. Lett.* **1992**, 68, 1547-1550.
- ¹²³ M. B. Feller, W. Chen, Y. R. Shen. 'Investigation of Surface-Induced Alignment of Liquid-Crystal Molecules By Optical 2nd-Harmonic Generation'. *Physical Review A* **1991**, 43(12), 6778-6792.
- ¹²⁴ H. Mada, T. Sonoda. *Japanese Journal of Applied Physics, Part 2* **1993**, 32(L1245),
- ¹²⁵ M. F. Toney, T. P. Russell, J. A. Logan, H. Kikuchi, J. M. Sands, S. K. Kumar. 'Near-Surface Alignment of Polymers in Rubbed Films'. *Nature* **1995**, 374(6524), 709-711.
- ¹²⁶ Y. J. Kim, Z. Zhuang, J. S. Patel. 'Effect of multidirection rubbing on the alignment of nematic liquid crystal'. *Appl. Phys. Lett.* **2000**, 77(4), 513-515.
- ¹²⁷ N. Ito, K. Sakamoto, R. Arafune, S. Ushioda. 'Relation between the molecular orientations of a very thin liquid crystal layer and an underlying rubbed polyimide film'. *Journal of Applied Physics* **2000**, 88(6), 3235.
- ¹²⁸ M. O'Neill, S. M. Kelly. 'Photinduced surface alignment for liquid crystal displays'. *J. Phys. D: Appl. Phys.* **2000**, 33, R67.
- ¹²⁹ W. M. Gibbons, P. J. Shannon, S. T. Sun, B. J. Swetlin. *Nature* **1991**, 351, 49.
- ¹³⁰ J.-H. Kim, S. Kumar, S.-D. Lee. 'Alignment of liquid crystals on polyimide films exposed to ultraviolet light'. *Phys. Rev. E* **1998**, 57(5), 5644.
- ¹³¹ M. Hasegawa, Y. Taira. *J. Photopoly. Sci. Technol.* **1995**, 8, 241.
- ¹³² J.-H. Kim, B. R. Acharya, S. Kumar, K. R. Ha. 'A method for liquid crystal alignment using in situ ultraviolet exposure during imidization of polyimide'. *Appl. Phys. Lett.* **1998**, 73, 3372.
- ¹³³ K. H. Yang, K. Tajima, A. Takenaka, H. Takano. 'Charge Trapping Properties of UV-Exposed Polyimide Films for the Alignment of Liquid Crystals'. *Japan. J. App. Phys.* **1996**, 35, L561.
- ¹³⁴ A. E. A. Contoret, S. R. Farrar, P. O. Jackson, S. M. Khan, L. May, M. O'Neill, J. E. Nicholls, S. M. Kelly, G. J. Richards. 'Polarized electroluminescence from an anisotropic nematic network on a non-contact photoalignment layer'. *Advanced Materials* **2000**, 12(13), 5.
- ¹³⁵ G. Klärner, R. D. Miller. 'Polyfluorene Derivatives - Effective Conjugation Lengths From Well-Defined Oligomers'. *Macromolecules*. **1998**, 31(6), 2007.
- ¹³⁶ M. Kreyenschmidt, G. Klaerner, T. Fuhrer, J. Ashenurst, S. Karg, W. D. Chen, V. Y. Lee, J. C. Scott, R. D. Miller. 'Thermally Stable Blue-Light-Emitting Copolymers of Poly(Alkylfluorene)'. *Macromolecules*. **1998**, 31(4), 1099.
- ¹³⁷ G. Klärner, M. H. Davey, W. D. Chen, J. C. Scott, R. D. Miller. 'Colorfast Blue-Light-Emitting Random Copolymers Derived From Di-N-Hexylfluorene and Anthracene'. *Advanced Materials*. **1998**, 10(13), 993.
- ¹³⁸ M. Inbasekaran, W. Wu, E. P. Woo. *US Pat.* 5.777.070 **1998**.
- ¹³⁹ M. Grell, M. Redecker, K. S. Whitehead, D. D. C. Bradley, M. Inbasekaran, E. P. Woo, W. Wu. 'Monodomain alignment of thermotropic fluorene copolymers'. *Liquid Crystals*. **1999**, 26(9), 1403.
- ¹⁴⁰ M. Ranger, M. Leclere. 'Optical and electrical properties of fluorene-based pi-conjugated polymers'. *Canadian Journal of Chemistry*. **1998**, 76(11), 1571.

- 141 M. Grell, W. Knoll, D. Lupo, A. Meisel, T. Miteva, D. Neher, H. G. Nothofer, U. Scherf, A. Yasuda. 'Blue polarized electroluminescence from a liquid crystalline polyfluorene'. *Advanced Materials* **1999**, *11(8)*, 671.
- 142 T. Miteva, A. Meisel, H.-G. Nothofer, U. Scherf, W. Knoll, D. Neher, M. Grell, D. Lupo, A. Yasuda. 'Polymeric light-emitting diodes with highly polarized blue emission'. *Proceedings SPIE* **1999**, *3797*, 231.
- 143 M. Bernius, M. Inbasekaran, E. Woo, W. S. Wu, L. Wujkowski. 'Fluorene-based polymers-preparation and applications'. *Journal of Materials Science: Materials in Electronics* **2000**, *11(2)*, 111.
- 144 D. V. Khramtchenkov, H. Bassler, V. I. Arkhipov. 'A Model of Electroluminescence in Organic Double-Layer Light-Emitting Diodes'. *Journal of Applied Physics*. **1996**, *79(12)*, 9283.
- 145 H.-G. Nothofer. 'Flüssigkristalline Polyfluorene'. Ph.D. Dissertation Thesis, University of Potsdam **2001**.
- 146 E. G. Mc Rae. *Austr. J. Chem.* **1961**, *14*, 354.
- 147 T. Q. Nguyen, R. C. Kwong, M. E. Thompson, B. J. Schwartz. 'Improving the performance of conjugated polymer-based devices by control of interchain interactions and polymer film morphology'. *Applied Physics Letters* **2000**, *76(17)*, 2454-2456.
- 148 V. N. Bliznyuk, S. A. Carter, J. C. Scott, G. Klarner, R. D. Miller, D. C. Miller. 'Electrical and photoinduced degradation of polyfluorene based films and light-emitting devices'. *Macromolecules*. **1999**, *32(2)*, 361.
- 149 R. Jakubiak, C. J. Collison, W. C. Wan, L. J. Rothberg, B. R. Hsieh. 'Aggregation quenching of luminescence in electroluminescent conjugated polymers'. *Journal of Physical Chemistry*. **1999**, *103(14)*, 2394-2398.
- 150 R. F. Mahrt, T. Pauck, U. Lemmer, U. Sieger, M. Hopmeier, R. Hennig, H. Bässler, E. O. Gobel, P. H. Bolivar, G. Wigmann, H. Kurz, U. Scherf, K. Müllen. 'Dynamics of optical excitations in a ladder-type pi -conjugated polymer containing aggregate states'. *Phys. Rev. B* **1996**, *54*, 1759.
- 151 J. Teetsov, M. A. Fox. 'Photophysical characterization of dilute solutions and ordered thin films of alkyl-substituted polyfluorenes'. *Journal of Materials Chemistry*. **1999**, *9(9)*, 2117-2122.
- 152 W. L. Yu, J. Pei, W. Huang, A. J. Heeger. 'Spiro-functionalized polyfluorene derivatives as blue light-emitting materials'. *Advanced Materials* **2000**, *12(11)*, 828.
- 153 M. Grell, D. D. C. Bradley, G. Ungar, J. Hill, K. S. Whitehead. 'Interplay of Physical Structure and Photophysics for a Liquid Crystalline Polyfluorene'. *Macromolecules* **1999**, *32*, 5810-5817.
- 154 www.syntec-synthon.com.
- 155 J. Pommerehne, H. Vestweber, W. Guss, R. F. Mahrt, H. Bässler, M. Porsch, J. Daub. 'Efficient Two Layer Leds on a Polymer Blend Basis'. *Advanced Materials* **1995**, *7(6)*, 551.
- 156 K. Meerholz, H. Gregorius, K. Müllen, J. Heinze. 'Voltammetric studies of solution and solid-state properties of monodisperse oligo(*p*-phenylenevinylene)s'. *Adv. Mater.* **1994**, *6*, 671.
- 157 S. F. Alvarado, P. F. Seidler. 'Direct Determination of the Exciton Binding Energy of Conjugated Polymers Using a Scanning Tunneling Microscope'. *Physical Review Letters* **1998**, *81(5)*, 1082.
- 158 L. Kloppenburg, D. Jones, J. B. Claridge, H.-C. zur Loye, U. H. F. Bunz. 'Poly(*p*-phenyleneethynylene)s are Thermotropic Liquid Crystalline'. *Macromolecules* **1999**, *32(13)*, 4460.
- 159 T. Miteva, L. Palmer, L. Kloppenburg, D. Neher, U. H. F. Bunz. 'Interplay of thermochromicity and liquid crystalline behavior in poly(*p*-phenyleneethynylene)s: Pi-Pi interactions or Planarization of the conjugated backbone?'. *Macromolecules* **2000**, *33(3)*, 652.
- 160 H. Fujikawa, S. Tokito, Y. Taga. 'Energy structures of triphenylamine oligomers'. *Synth. Met.* **1997**, *91*, 161.
- 161 Y. Qiu, J. Qiao. 'Photostability and morphological stability of hole-transporting materials used in organic electroluminescence'. *Thin Solid Films* **2000**, *372*, 265.
- 162 S. Tokito, H. Tanaka, K. Noda, A. Okada, Y. Taga. 'Thermal stability in oligomeric triphenylamine/tris(8-quinolinolato) aluminum electroluminescent devices'. *Appl Phys. Lett.* **1997**, *70*, 1929.
- 163 S. A. VanSlyke, C. W. Tang. *US Patent No. 5061569*, 29. Oct. **1991**.
- 164 M. G. Han, S. S. Im. 'Electrical and Structural Analysis of Conductive Polyaniline/Polyimide Blends'. *Journal of Applied Polymer Science* **1999**, *71*, 2169.
- 165 A. G. MacDiarmid, A. J. Epstein. 'Polyanilines – from solitons to polymer metal, from chemical curiosity to technology'. *Synth. Met.* **1994**, *69(1-3)*, 179.
- 166 A. A. Shoustikov, Y. J. You, M. E. Thompson. 'Electroluminescence Color Tuning by Dye Doping in Organic Light-Emitting Diodes'. *IEEE Journal of Selected Topics in Quantum Electronics* **1998**, *4(1)*, 3.
- 167 C. W. Tang, S. A. VanSlyke, C. H. Chen. 'Electroluminescence of doped organic thin films'. *Journal of Applied Physics* **1989**, *65*, 3610.

- 168 D. Sainova, T. Miteva, H. G. Nothofer, U. Scherf, I. Glowacki, J. Ulanski, H. Fujikawa, D. Neher. 'Control of color and efficiency of light-emitting diodes based on polyfluorenes blended with hole-transporting molecules'. *Applied Physics Letters* **2000**, 76(14), 1810.
- 169 L. Groenendaal, F. Jonas, D. Freitag, H. Pielartzik, J. R. Reynolds. 'Poly(3,4-ethylenedioxythiophene) and its Derivatives – Past, Present, and Future'. *Adv. Mater.* **2000**, 12(7), 481.
- 170 L. S. Hung, C. W. Tang, M. G. Mason. 'Enhanced electron injection in organic electroluminescence devices using an Al/LiF electrode'. *Appl. Phys. Lett.* **1997**, 70(2), 152.
- 171 D.-S. Seo, K. Muroi, S. Kobayashi. 'Generation of pretilt angles in nematic liquid crystal media alligned on polyimide films prepared by spincoating and rubbing'. *Mol. Cryst. Liq. Cryst.* **1992**, 213, 223.
- 172 <http://www.leo-em.co.uk/>.
- 173 Butler, Joy, Bradly, Krause. 'Low-voltage scanning electron microscopy of polymers'. *Polymer* **1995**, 36(9), 1781.
- 174 L. Reimer, *Scanning Electron Microscopy*, Springer-Verlag, **2000**.
- 175 <http://www.jeol.com/docs.html>.
- 176 D. L. Vezie, E. L. Thomas, W. W. Adams. 'Low-voltage, high resolution scanning electron microscopy: a new charcterisation technique for polymer morphology'. *Polymer* **1995**, 36(9), 1761.
- 177 <http://www.di.com>.
- 178 <http://www.siliconmdt.com>.
- 179 S. S. Sheiko, *Imaging of Polymers Using Scanning Force Microscopy in Advances in Polymer Science, Vol. 151* Springer-Verlag, Berlin **2000**.
- 180 G. Lieser, M. Oda, T. Miteva, A. Meisel, H.-G. Nothofer, U. Scherf, D. Neher. 'Ordering, graphoepitaxial orientation, and conformation of a polyfluorene derivative of the hairy-rod type on an oriented substrate of polyimide'. *Macromolecules* **2000**, 33, 4490.
- 181 D. Müller, M. Gross, K. Meerholz, T. Braig, M. S. Bayerl, F. Bielefeldt, O. Nuyken. 'Novel cross-linkable hole-transport monomer for use in organic light-emitting diodes'. *Synth. Met.* **2000**, 111, 31.
- 182 J. Teetsov, M. A. Fox. 'Photophysical characterization of dilute solutions and ordered thin films of alkyl-substituted polyfluorenes'. *Journal of Materials Chemistry*. **1999**, 9(9), 2117.
- 183 V. N. Tsvetkov, E. I. Rjuntsev, I. N. Shtennikova, *Intramolecular Orientational Order and Properties of Polymer Molecules in Liquid Crystalline Order in Polymers*, edited by A. Blumstein, Academic Press, Inc., New York **1978**.
- 184 J. Teetsov, D. A. Vanden Bout. 'Near-field scanning optical microscopy (NSOM) studies of nanoscale polymer ordering in pristine films of poly(9,9-dialkylfluorene)'. *Journal of Physical Chemistry B* **2000**, 104(40), 9378.
- 185 M. Grell, D. D. C. Bradley, G. Ungar, J. Hill, K. S. Whitehead. 'Interplay of Physical Structure and Photophysics for a Liquid Crystalline Polyfluorene'. *Macromolecules* **1999**, 32, 5810.
- 186 C. Albrecht, G. Lieser, G. Wegner. *Prog. Colloid Polym. Sci.* **1993**, 92, 111.
- 187 M. W. Geis, D. C. Flanders, H. J. Smith. *Appl. Phys. Lett.* **1979**, 35, 71.
- 188 M. Oda, G. Lieser, H.-G. Nothofer, U. Scherf, D. Neher. 'Torsional potential, bond angle and conformational characteristics of polyfluorene'. *submitted to J. Chem. Phys.*
- 189 D. Stauffer, *Introduction to Percolation Theory*, Taylor&Francis, London **1985**.
- 190 A. J. Bard, L. A. Faulkner, *Electrochemical Methods - Fundamentals and Applications*, WILEY, New York **1984**.
- 191 C. Giebeler, H. Antoniadis, D. D. C. Bradley, Y. Shirota. 'Space-charge-limited charge injection from indium tin oxide into a starburst amine and its implications for organic light-emitting diodes'. *Appl. Phys. Lett.* **1998**, 72(19), 244.
- 192 C. Giebeler, H. Antoniadis, D. D. C. Bradley, Y. Shirota. 'Influence of the hole transport layer on the performance of organic light-emitting diodes'. *Journal of Applied Physics* **1999**, 85(1), 608.
- 193 M. G. Han, S. S. Im. 'Electrical and Structural Analysis of Conductive Polyaniline/Polyimide Blends'. *Journal of Applied Polymer Science* **1999**, 71, 2169-2176.
- 194 K. R. Brown, D. A. Bonnell, S. T. Sun. 'Atomic Force Microscopy of Mechanically Rubbed and Optically Buffed Polyimide Films'. *Liquid Crystals*. **1998**, 25(5), 597-601.
- 195 M. F. Toney, T. P. Russell, J. A. Logan, H. Kikuchi, J. M. Sands, S. K. Kumar. 'Near-Surface Alignment of Polymers in Rubbed Films'. *Nature*. **1995**, 374(6524), 709-711.
- 196 J.-H. Kim, C. Rosenblatt. 'Rubbing Strength Dependence of Surface Interaction Potential and Surface-Induced Order above the Nematic-Isotropic Transition'. *Journal of Applied Physics* **1998**, 84(11), 6027-6032.

- 197 D. M. Pai, J. F. Yanus, M. Stolka. *Journal of Chemical Physics* **1984**, *88*, 4414.
- 198 J. P. Chen, G. Klaerner, J. I. Lee, D. Markiewicz, V. Y. Lee, R. D. Miller, J. C. Scott. 'Efficient, blue light-emitting diodes using cross-linked layers of polymeric arylamine and fluorene'. *Synthetic Metals*. **1999**, *107(2)*, 129.
- 199 C. D. Müller, T. Braig, H.-G. Nothofer, M. Arnoldi, M. Groß, U. Scherf, O. Nuyken, K. Meerholz. 'Efficient blue organic light-emitting diodes with graded hole-transport layers'. *Chem. Phys. Chem.* **2000**, *1(4)*, 207.
- 200 M. Redecker, D. D. C. Bradley, M. Inbasekaran, W. W. Wu, E. P. Woo. 'High Mobility Hole Transport Fluorene-Triarylamine Copolymers'. *Adv. Mater.* **1999**, *11(3)*, 241.
- 201 C. Zhang, H. v. Seggern, K. Pakbaz, B. Kraabel, H. W. Schmidt, A. J. Heeger. *Synth. Met.* **1994**, *62*, 35.
- 202 G. Grem, G. Leising. *Synth. Met.* **1993**, *55-57*, 4105.
- 203 G. Grem, G. Leditzky, B. Ullrich, G. Leising. *Adv. Mater.* **1992**, *4*, 36.
- 204 Q. B. Pei, Y. Yang. 'Efficient Photoluminescence and Electroluminescence From a Soluble Polyfluorene'. *Journal of the American Chemical Society*. **1996**, *118(31)*, 7416.
- 205 T. Förster. *Discuss. Faraday Trans.* **1965**, *27*, 7.
- 206 S. Tasch, E. J. W. List, C. Hochfilzer, G. Leising, P. Schlichting, U. Rohr, Y. Geerts, U. Scherf, K. Müllen. *Phys. Rev. B* **1997**, *56(8)*, 4479-4483.
- 207 Y. Kuwabara, H. Ogawa, H. Inada, N. Noma, Y. Shirota. *Adv. Mater.* **1994**, *6(9)*, 677-679.
- 208 P.-W. Wang, Y.-J. Liu, C. Devadoss, P. Bharathi, J. S. Moore. *Adv. Mater.* **1996**, *8(3)*, 237-241.
- 209 M. Halim, J. N. G. Pillow, I. D. W. Samuel, P. L. Burn. *Adv. Mater.* **1999**, *11(5)*, 371-374.
- 210 T. Sato, D.-L. Jiang, T. Aida. *J. Am. Chem. Soc.* **1999**, *121*, 10658-10659.
- 211 A. Goetzberger, W. Greubel. *Appl. Phys.* **1972**, *14*, 123.
- 212 D. Schlettwein, D. Wöhrle, E. Karmann, U. Melville. *Chem. Mater.* **1994**, *6*, 3.
- 213 M. P. O'Neil, M. P. Niemczyk, W. A. Svec, D. Gosztola, G. L. Gaines, M. R. Wasielewski. *Science* **1992**, *257*, 63.
- 214 R. Gvishi, R. Reisfeld, Z. Burshtein. *Chem. Phys. Lett.* **1993**, *213*, 338.
- 215 H. Murata, C. D. Merritt, H. Mattouossi, Z. H. Kafafi. *SPIE Conference on Organic Light-Emitting Materials and Devices II* **1998**, *3476*, 88-95.
- 216 J. Kalinowski, P. D. Marco, V. Fattori, L. Giuletti, M. Cocchi. *J. Appl. Phys.* **1998**, *83(8)*, 4242-4248.
- 217 X. Z. Jiang, Y. Q. Liu, S. G. Liu, W. F. Qiu, X. Q. Song, D. B. Zhu. *Synthetic Metals* **1997**, *91*, 253-256.
- 218 H. Zollinger, *Color Chemistry*, VCH Verlagsgesellschaft, Weinheim **1987**.
- 219 A. Herrmann, V. Sinigersky, T. Weil, U.-M. Wiesler, T. Vosch, J. Hofkens, F. C. D. Schryver, K. Müllen. *Chem. Eur. J.* **2000**, *submitted*,
- 220 A. Herrmann. 'Rylenfarbstoffe in Nanoskopischen Systemen – Synthese, Charakterisierung und Anwendung'. Ph.D. Dissertation Thesis, Johannes Gutenberg-Universität Mainz **2000**.
- 221 <http://www-cvrl.ucsd.edu/>.
- 222 E. J. W. List, C. Creely, G. Leising, B. Schlicke, A. D. Schlütter, U. Scherf, K. Müllen, W. Graupner. *Chem. Phys. Lett.* **2001**, *accepted*.
- 223 <http://www.efg2.com/Lab/Graphics/Colors/Chromaticity.htm>.
- 224 M. D. McGehee, T. Bergstedt, C. Zhang, A. P. Saab, M. B. O'Reagan, C. G. Bazan, V. I. Srdanov, A. J. Heeger. 'Narrow bandwidth luminescence from blends with energy transfer from semiconducting conjugated polymers to europium complexes'. *Advanced Materials* **1999**, *11(16)*, 1349.
- 225 C.-L. Lee, K. B. Lee, J.-J. Kim. 'Polymer phosphorescent light-emitting devices doped with tris(2-phenylpyridine) iridium as a triplet emitter'. *Applied Physics Letters* **2000**, *77*, 2280.
- 226 S. Berleb, W. Brütting, M. Schwoerer, R. Wehrmann, A. Elschner. 'Effect of Majority Carrier Space Charges on Minority Carrier Injection in Dye Doped Polymer Light-Emitting Devices'. *Journal of Applied Physics* **1998**, *83*, 4403.
- 227 A. Montali, P. Smith, C. Weder. 'Poly(*p*-phenylene ethynylene)-based light-emitting devices'. *Synth. Met.* **1998**, *97(2)*, 123.

List of Figures

Figure 1.1. Schematic picture of a very simple LED with a polymer layer sandwiched between two electrodes.	9
Figure 1.2. Schematic picture of a polarized LED.	11
Figure 2.1. Typical energy level diagram of organic molecules.	13
Figure 2.2. Schematic energy level diagram for a single-layer LED with structure ITO/polymer/metal cathode	17
Figure 2.3. Cartoon of a conventional liquid crystal display (LCD).	23
Figure 2.4. Principles of the molecular design of liquid-crystalline polymers	30
Figure 3.1. Structure of substituted polyfluorene homopolymer.	35
Figure 3.2. Three-dimensional model of polyfluorene.	35
Figure 3.3. Various substitution patterns for the synthesis of polyfluorenes.	37
Figure 3.4. Calorimetric characterization of a film of PF2/6	37
Figure 3.5. UV/Vis absorption and photoluminescence spectra of PF2/6 in solution and in solid state.	38
Figure 3.6. Chemical structures of poly(9,9-bis(2-ethylhexyl)fluorene-2,7-diyl) endcapped with bis(4-methylphenyl)phenylamine (PF2/6amX) and with (N-(biphenyl-4-yl)-N-naphth-2-yl-N-phenylamine) (PF2/6napX), respectively.	40
Figure 3.7. Cyclic voltammograms for PF2/6am9 and PF2/6nap9. Inset: energy diagram for orbital levels	42
Figure 3.8. Chemical structure of poly(2,7-(9,9-bis(2-ethylhexyl))co-(9,9-bis((3S)-3,7-dimethyloctyl))fluorene)	42
Figure 3.9. Chemical structure of poly(2,7-(9,9-bis(2-butyl))co-(9,9-bis(dodecyl))fluorene) (PF4C12).	43
Figure 3.10. Chemical structure of hexyl-dodecyl copoly(phenyleneethynylene) (PPE).	43
Figure 3.11. Chemical structure of poly(phenoxyphenylimide) (PI).	43
Figure 3.12. Chemical structures of different hole-transporting materials (ST 638, ST 16-7, ST 755, ST 1163).	45
Figure 3.13. Cyclic voltammograms for ST 638, ST 16-7, ST 755 and 1163	45
Figure 3.14. Chemical structure of N,N'-biphenyl-N,N'-bis-(3-methylphenyl)-[1,1'-biphenyl]-4,4'-diamine (TPD).	46
Figure 3.15. Chemical structure of PAni-CSA.	46
Figure 3.16. Chemical structure of thiophene dye S2_3.	47
Figure 3.17. Chemical structures of PEDOT-PSS.	48
Figure 3.18. Picture of rubbing machine.	50
Figure 3.19. Picture of annealing setup with heating table under a glass cover	51
Figure 3.20. Computer-controlled setup for recording electroluminescence spectra.	52
Figure 4.1. Temperature-dependent powder X-ray diffraction of poly(9,9-bis(2-ethylhexyl)fluorene-2,7-diyl)	59
Figure 4.2. Polarized absorption spectra of PF2/6am aligned on top of photoaligned and rubbed PI, respectively ..	61
Figure 4.3. Chemical structures of PF2/6, PF3/5, PF8, PF4C12, and PF8/1/1C2/6.	63
Figure 4.4. Polarized absorption spectra of polyfluorenes with different alkyl side-chains aligned on rubbed PI	64
Figure 4.5. Chemical structure of hexyl-dodecyl copoly(phenyleneethynylene) (PPE).	66
Figure 4.6. DSC-traces of PPE	67
Figure 4.7. Polarized absorption spectra of PPE aligned by direct rubbing.	67
Figure 4.8. Directly rubbed films of PPE viewed under the polarization microscope	68

Figure 5.1. DSC-traces of PF2/6 fractionated into portions of different molecular weights.....	70
Figure 5.2. Electron diffraction patterns of different fractions of PF2/6 with varying molecular weights	72
Figure 5.3. A film of PF2/6 aligned on top of rubbed hole-transporting alignment layer of PI doped with ST 638 .	75
Figure 5.4. Electron micrographs of an oriented PF2/6 film	77
Figure 5.5. Polarized optical micrographs of PF2/6 films on top of rubbed polyimide alignment layers.....	79
Figure 5.6. Temperature dependent X-ray diffraction pattern of fibers of PF2/6.....	79
Figure 5.7. Electron diffraction pattern of PF2/6 oriented on top of rubbed polyimide	81
Figure 5.8. Molecular Modeling of oligo(25)-fluorene with 5/q helix	82
Figure 5.9. Current density–voltage characteristics for polyimide films with different content of ST638 filler.	85
Figure 5.10. Intensity–voltage characteristics of devices with doped, pristine and without alignment layer of polyimide between the ITO anode and an emissive layer of PF2/6.....	87
Figure 5.11. Intensity–voltage characteristics for diodes with PF2/6 and different combinations of HTMs.....	89
Figure 5.12. Intensity–voltage curves for diodes with HTALs of PI blended with ST 638 and ST 1163.	91
Figure 5.13. Polarized absorption spectra of PF2/6am2 aligned on top of rubbed 40% PAni-CSA in PI.....	93
Figure 5.14. Photometric efficiencies for polarized LEDs with alignment layers of PI doped with PAni-CSA and ST 1163, respectively.	94
Figure 5.15. Low-voltage scanning electron microscope (LVSEM) pictures of unrubbed layers of PI doped with ST 1163 at different concentrations.....	96
Figure 5.16. LVSEM pictures of unrubbed and rubbed layers of PI doped with ST 1163	98
Figure 5.17. LVSEM pictures of rubbed layers of PI doped with ST 1163 at different concentrations.....	99
Figure 5.18. AFM pictures and Line-scans of unrubbed and rubbed films of PI doped with 30 wt.% ST 1163	102
Figure 5.19. Comparison of unrubbed and rubbed layers of PI doped with ST 1163 at different concentrations....	103
Figure 5.20. AFM pictures of unrubbed and rubbed films of PI doped with ST 1163 at different concentrations...	104
Figure 5.21. Unrubbed and rubbed films of PI doped with ST 1163 without/with additional bathing in toluene.	106
Figure 6.1. Schematic picture of a light-emitting device with a hole-injection layer below the emissive layer.	111
Figure 6.2. Intensity–voltage characteristics for diodes with isotropic PF2/6 emitting layer and different cathode materials, showing the effect of including a 30 nm hole-injection layer and an 1 nm layer of LiF.	112
Figure 6.3. Intensity–current characteristics for diodes with isotropic PF2/6 emitting layer and different cathode materials, showing the effect of including a 30 nm PEDOT-PSS layer and an 1 nm layer of LiF.	113
Figure 6.4. Influence of the thickness of the emissive layer on the device performance.	114
Figure 6.5. Intensity-voltage curves for devices with PF2/6 emissive layers.....	115
Figure 6.6: Schematic picture of a polarized light-emitting device with bilayer HTAL structure	116
Figure 6.7. Electroluminescence spectra for polarized LEDs with aligned PF2/6	117
Figure 6.8. Cartoon explaining the blue emission in case of doping the PF2/6 layer with HTMs.....	118
Figure 6.9. Current–voltage characteristics of hole-only devices and of corresponding LEDs with PF2/6amX.....	121
Figure 6.10. Emission spectra of the LEDs based on endcapped polyfluorene PF2/6amX and on pure PF2/6	122
Figure 6.11. Comparison of intensity–current characteristics for LEDs based on endcapped and on pure PF2/6.	123
Figure 6.12. Efficiency–luminance-curve for an isotropic LED based on PF2/6am4.	124
Figure 6.13. Polarized emission spectra for devices with PF26am9 and different concentrations of ST 1163	126

Figure 7.1. Absorption spectrum of thiophene dye S2_3, the chemical structure of which is also shown.	127
Figure 7.2. Emission spectra of LEDs with emissive layer of PF26am4 doped with thiophene dye S2_3	128
Figure 7.3. Intensity–voltage curves of LEDs with emissive layer of PF26am4 doped with thiophene dye S2_3. ...	129
Figure 7.4. Intensity–voltage curves of polarized LEDs with emissive layer of PF26am4 doped with S2_3	130
Figure 7.5. Polarized EL spectra of LEDs with emissive layer of PF26am4 doped with S2_3	131
Figure 7.6. Polarized absorption spectra for devices with PF2/6am4 without/with doping with S2_3	132
Figure 7.7. Structure of non-dendronized model compound and polyphenylene dendrimers of two generations ..	136
Figure 7.8. Structure of PF1/1/1/6.	136
Figure 7.9. Electroluminescence spectra of devices with M, G1 and G2 as emissive layers.	137
Figure 7.10. Photoluminescence spectra of blends of PF1/1/1/6 and 3 wt.% of M, of G1 and of G2.	139
Figure 7.11. Fluorescence spectra of pure PF1/1/1/6 and absorption spectra of M, of G1, and of G2	140
Figure 7.12. Current–voltage characteristics of hole-only devices and corresponding bipolar LED devices of PF1/1/1/6 blended with 3 wt.% of M, of G1 and of G2	142
Figure 7.13. Emission intensity as a function of current for blends of PF1/1/1/6 and 3 wt.% and 10 wt.% of M, of G1 and of G2	144
Figure 7.14. Intensity–voltage characteristics for PF1/1/1/6 and PF1/1/1/6 blended with M, G1 and G2	144
Figure 7.15. Electroluminescence spectra for blends of PF1/1/1/6 and M, G1 and G2	145
Figure 7.16. Voltage dependent color change of blends of PF1/1/1/6 and M, G1 and G2, plotted in CIE-coordinates. For illustration, the values are drawn into the complete CIE-chromaticity diagram	147
Figure A.1. Relative luminous efficiency functions for bright (photopic) and dark (scotopic) light conditions	154
Figure A.2. The XYZ-color matching functions defined by the CIE in 1931, modified by Judd and Vos in 1978 ..	157
Figure A.3. Chromaticity diagram defined by the CIE in 1931	158

List of Tables

Table 3.1.	Influence of endcapper feed ratios on the molecular weight of endcapped polyfluorenes.....	40
Table 5.1.	Influence of the molecular weight on phase transition temperatures and on the dichroic ratios.....	73
Table 5.2.	Diameter and depth of phase-separated clusters of HTMs inside and on top of layers of unrubbed and rubbed films of PI doped with ST 1163	100
Table 7.1.	Summary of performance of polarized LEDs with emissive layers of PF26am4 doped with S2_3.	132
Table 7.2.	Relation between concentration of dendronized dyes in polyfluorene and the effective concentration of perylene chromophores	138
Table 7.3.	CIE color coordinates of PL emission of blends of PF1/1/1/6 and M, G1 or G2.	148
Table A.1.	Radiometric and respective photometric concepts and units	156
Table A.2.	Essential properties and chemical structures of polyfluorenes with different side-chain patterns.....	159

List of Publications

- [1] M. Grell, W. Knoll, D. Lupo, A. Meisel, T. Miteva, D. Neher, H. G. Nothofer, U. Scherf, A. Yasuda
Blue polarized electroluminescence from a liquid crystalline polyfluorene
Advanced Materials **1999**, *11*, 671.
- [2] T. Miteva, A. Meisel, H.-G. Nothofer, U. Scherf, W. Knoll, D. Neher, M. Grell, D. Lupo, A. Yasuda
Polymeric light-emitting diodes with highly polarized blue emission
Proceedings SPIE **1999**, 3797, 231.
- [3] G. Lieser, M. Oda, T. Miteva, A. Meisel, H.-G. Nothofer, U. Scherf, D. Neher
Ordering, graphoepitaxial orientation and conformation of a polyfluorene derivative of the "hairy-rod-type" on an oriented substrate of polyimide
Macromolecules **2000**, *33(12)*, 4490-4495.
- [4] T. Miteva, A. Meisel, M. Grell, H.-G. Nothofer, D. Lupo, A. Yasuda, W. Knoll, L. Kloppenburg, U. H. F. Bunz, U. Scherf, D. Neher
Polarized electroluminescence from highly aligned liquid crystalline polymers
Synthetic Metals **2000**, *111-112*, 173-176.
- [5] H.-G. Nothofer, A. Meisel, T. Miteva, D. Neher, M. Forster, M. Oda, G. Lieser, D. Sainova, A. Yasuda, D. Lupo, W. Knoll, U. Scherf
Liquid crystalline polyfluorenes for blue polarized electroluminescence
Macromolecular Symposia **2000**, *154*, 139-148.
- [6] C. Bauer, G. Urbasch, H. Giessen, A. Meisel, H.-G. Nothofer, D. Neher, U. Scherf, R. F. Mahrt
Polarized photoluminescence and spectral narrowing in an oriented polyfluorene thin film
ChemPhysChem **2000**, *3*, 142-146.
- [7] T. Miteva, A. Meisel, W. Knoll, H.-G. Nothofer, U. Scherf, D. C. Müller, K. Meerholz, A. Yasuda, D. Neher
Improving the performance of polyfluorene based organic light-emitting diodes via endcapping
Advanced Materials **2001**, *8(13)*, 565.
- [8] T. Miteva, A. Meisel, G. Nelles, H.-G. Nothofer, U. Scherf, W. Knoll, A. Yasuda, D. Neher
Highly polarized light-emitting diodes
Proceedings ITG, **2001**.
- [9] A. Meisel, A. Herrmann, T. Miteva, H.-G. Nothofer, U. Scherf, K. Müllen, D. Neher
High Brightness Light-Emitting Diodes Based on Dendronized Perylene
To be submitted to Physical Reviews B.
- [10] A. Meisel, T. Miteva, G. Nelles, D. Sainova, H.-G. Nothofer, U. Scherf, W. Knoll, A. Yasuda, F. C. Grozema, T. J. Savenije, B. R. Wegewijs, M. J. W. Vermeulen, L. D. A. Siebbeles, J. M. Warman, D. Neher
Anisotropy of Optical and Electrical Properties of Highly-Oriented Polyfluorenes
Proceedings Polytronic, **2001**.
- [11] F. C. Grozema, T. J. Savenije, M. J. W. Vermeulen, L. D. A. Siebbeles, J. M. Warman, A. Meisel, H.-G. Nothofer, U. Scherf, and D. Neher
Electrodeless measurement of the in-plane anisotropy in the photoconductivity of a rub-aligned polyfluorene film
Advanced Materials **2001**, *accepted for publication*.
- [12] A. Meisel, T. Miteva, G. Glaser, V. Scheumann, D. Neher
Influence of dopant concentration on the morphology of hole-transporting alignment layers based on a polyimide matrix
To be published.

List of Patents

- [1] W. Knoll, A. Meisel, T. Miteva, D. Neher, H.-G. Nothofer, U. Scherf, A. Yasuda, M. Grell, D. Lupo
Polyimide layer comprising functional material, device employing the same and method of manufacturing same device
Sony Ref. S98P5134WO00; Sony AZ: PAE98-094MSL / MPG AZ: GI 2669 GMK,
06/22/2000 (int. publ. date)
- [2] W. Knoll, A. Meisel, T. Miteva, D. Neher, H.-G. Nothofer, U. Scherf, A. Yasuda
End-capped polyfluorenes, films and devices based thereon
European Patent Application (Patent No. 00108877.2-2203), filed 04/26/2000 by Sony International (Europe) GmbH.
- [3] T. Miteva, A. Meisel, D. Neher, G. Nelles, A. Yasuda
Polarized light-emitting diodes based on aligned polyfluorene layers doped with anisotropic dyes for improved efficiency and higher polarization ratios
Submitted as patent by Sony International (Europe) GmbH.

Danke Schön

An erster Stelle möchte ich mich bei meinem Betreuer Herrn Prof. Dr. Dieter Neher bedanken. Das Arbeiten unter seiner Anleitung war nicht nur in wissenschaftlicher, sondern auch in persönlicher Hinsicht eine großartige Erfahrung und hat mir immer großen Spaß gemacht. Ich danke ihm für seine Fähigkeit, selbständiges Arbeiten durch entgegengebrachtes Vertrauen zu fördern und dennoch bei Fragen jederzeit mit Erklärungen, Vorschlägen oder Ideen weiter zu helfen. Ich konnte mir keine bessere Betreuung wünschen.

Ganz besonderen Dank möchte ich Herrn Prof. Dr. Wolfgang Knoll aussprechen. Seine gewinnende Persönlichkeit und die damit verbundene Art, eine Gruppe zu leiten, war für mich gleichbedeutend mit dem Aufbau einer Gemeinschaft, die aus viel mehr als nur aus der Summe ihrer Mitglieder bestand. Ich danke ihm für die uneingeschränkte Förderung meines wissenschaftlichen Arbeitens – nicht nur, indem er mir die Gelegenheit gab, unter besten Bedingungen am Max Planck-Institut für Polymerforschung arbeiten zu dürfen, sondern auch durch das Ermöglichen der Teilnahme an Konferenzen und Seminaren im Inland sowie im nahen und fernen Ausland.

My special thanks to Dr. Akio Yasuda. I greatly benefited from working in collaboration with SONY International. It always was a pleasure for me to meet him and to be a part of his group. I also deeply acknowledge the financial and scientific support he granted to me.

Bei Herrn Prof. Dr. Hartmut Roskos bedanke ich mich ganz herzlich dafür, dass er sich ohne zu zögern zur Betreuung dieser externen Doktorarbeit bereit erklärte. Trotz der Tatsache, dass dieses Projekt außerhalb seines täglichen Wirkens bearbeitet wurde, ermöglichte seine engagierte Teilnahme an dieser Arbeit anregende und fruchtbare wissenschaftliche Diskussionen. Außerdem danke ich ihm für die Einladungen zu Seminarvorträgen, in denen ich die Ergebnisse dieser Arbeit vorstellen konnte.

Mein größtmöglicher Dank gilt Frau Dr. Tzenka Miteva. Insbesondere die Bearbeitung des Gebiets der Elektrolumineszenz erfolgte in enger Zusammenarbeit mit ihr. Ich habe sehr vieles bei meiner täglichen Arbeit mit ihr und von ihr gelernt, wofür ich mich bedanken möchte – aber am allermeisten bedanke ich mich für die Freundschaft, die zwischen uns entstanden ist.

Außerdem danke ich Heinz-Georg Nothofer, der innerhalb des Projektes für die Synthese der Polyfluorene verantwortlich war. Mein Dank gilt außerdem der gesamten elektrooptischen Gruppe im weitesten Sinn. Das Arbeiten und das gemeinsame Zusammensein mit Thomas Däubler, Dr. Andreas Herrmann, Dr. Don Lupo, Dr. Gabi Nelles, Dessislava Sainova und Achmad Zen hat mir große Freude gemacht und wird mir immer in guter Erinnerung bleiben.

Bei Frau Dr. Véra Cimrová, Herrn Dr. John Warman und Dr. Masahiko Hara bedanke ich mich für die Einladung zu unvergesslichen Gast- und Forschungsaufenthalten in Prag, in Delft und in Tokio.

All die technischen Probleme hätten niemals gelöst werden können ohne die Hilfe der Servicegruppen am MPI. Ich danke den Glasbläsern, der Mechanikwerkstatt und dem Elektroniklabor. Ganz besonders danke ich Andi Scheller für seinen aufopferungsvollen Kampf gegen sämtliche Computerprobleme, die immer wieder auftraten.

Dass ich jeden Morgen wieder gerne ans MPI gefahren bin, lag nicht zuletzt an meinen fabelhaften Kollegen. Insbesondere möchte ich mich hier bei Volker bedanken, an erster Stelle für die entstandene Freundschaft, aber auch für das tägliche Leihen der Mensakarte sowie für unzählige Dinge, die ich von ihm lernen konnte. Martin G. aus LU hat mir meine Zeit am MPI auch ganz besonders verSCHÖNert. Ihm danke ich zusätzlich für die Mail-Korrespondenz nach seinem eigenen Ausscheiden ($> 10^6$ /yoctosec). Ralf danke ich für die *konstruktiven* Reibereien, Menno (I!mdf) für die gute Laune, und Thomas danke ich für die Pfeifkonzerte. Kirstin, Heike, Arrelaine, Gretl, Stefan, Bernhard, Sven, Christoph und all die anderen in der Gruppe haben mir die Zeit in- und außerhalb der Kaffee-Ecke zur Freude gemacht. Ich bin außerdem froh, dass ich mit dem gesamten Arbeitskreis-Knoll an der Organisation einer grandiosen Weihnachtsfeier teilnehmen durfte und den Zusammenhalt der gesamten Gruppe während der Vorbereitungen miterleben konnte.

Bei Tzenka, Arrelaine und Thorsten bedanke ich mich für das Durchlesens meines Manuskripts und die damit verbundenen Zeitopfer.

Für mentalen Ausgleich in meiner Zeit außerhalb des MPI sorgten meine Freunde. Außergewöhnlich ganz besonders sage ich Danke Schön zu Jörn für das Frischhalten des Körpers und des Geistes, zu Nils für die sporadischen Anrufe morgens, mittags, nachmittags und abends während der Zeit meines Schreibens, zu Matthias für seine Spontaneität, zu Rico für die Beantwortung *wirklich* schwieriger Fachfragen, zu Nico für gute Musiktipp und zu vielen anderen für manches mehr.

Elke und Werner danke ich sehr für ihre beständige Unterstützung während der ganzen langen Zeit bis hierhin. Sigrid, Sandra, Sophia und Eberhard bin ich unwahrscheinlich ganz besonders dankbar für die Basis zu allem.

Abschließend, aber dafür am allerliebsten, danke ich Ulli für ihre bedingungslose Liebe.

Curriculum Vitae

Name: Andreas Meisel
Address: Spessartstr. 19
D-60385 Frankfurt
Date of Birth: 16.11.1971
Place of Birth: Karlsruhe

School Education

1978–1982 Primary School in Gaggenau
1982–1991 Grammar School in Gaggenau

Civil Service

1991–1992 Deutsches Rotes Kreuz, Baden-Baden

University Education

1992–1998 Studies in Physics,
University of Frankfurt
1997 Final Thesis with Daimler-Benz AG, Ulm

Ph.D.-Program

Since 1998 Dissertation under Prof. Dr. Dieter Neher in the group of
Prof. Dr. Wolfgang Knoll at
Max Planck-Institute for Polymer Research, Mainz
in collaboration with SONY International (Europe) GmbH, Stuttgart
1998–2000 Scholarship of University of Mainz, Graduiertenkolleg

Additional Information:

09/95–11/95 Internship in the environment protection department with
Daimler-Benz AG, Stuttgart and in the optical measurement
department with Daimler-Benz AG, Ulm
08/96–10/96 Freelance in optical measurement department with Daimler-Benz AG,
Ulm
1998/1999/2000 Research visits:
Institute of Physical and Chemical Research (RIKEN) in Tokyo, Japan
Academy of Sciences of the Czech Republic, Prague, Czech Republic
Delft University of Technology, Delft, Netherlands.